RECOMBINANT GLYCINE RECEPTORS: STOICHIOMETRY AND KINETICS

By
Paraskevi Krashia

Submitted for the degree of Ph.D

University College London
Neuroscience, Physiology & Pharmacology

Supervised by
Prof. Lucia G. Sivilotti

'I confirm that the work presented in this thesis is my own. Where information has been derived from other sources, I confirm that this has been indicated in the thesis'.

Paraskevi Krashia
July 2009

Abstract

Glycine receptors (GlyR) are anion-permeable channels that belong to the pentameric ligand-gated ion channel family. Different GlyR subtypes are known. The main synaptic form is thought to be α1β heteropentamers which mediate fast synaptic inhibition in the adult spinal cord and brainstem. Data on recombinant receptors suggest two possible stoichiometries for this subtype, 2α1:3β and 3α1:2β. Evidence for the first comes from experiments on oocytes, whereas a study in mammalian cells favours the latter, raising the possibility that stoichiometry depends on the expression system. Here, we assess the stoichiometry of α1β GlyRs in *Xenopus* oocytes using two different electrophysiological approaches. The first involves the use of a reporter mutation at the conserved 9′ position of the pore-lining domain. In other receptors, this mutation shifts agonist sensitivity in proportion to the number of mutated subunits. Recordings from mutant receptors failed to point towards one or the other stoichiometry. The second approach involved single-channel recordings from conductance mutants. This approach was also inconclusive for stoichiometry. However, we provide evidence that oocytes are not a suitable expression system for the study of heteromeric glycine receptors as they are highly prone to contamination by homomers.

α2 homomeric GlyRs are predominant early in development and are replaced by α1 subunits in the first postnatal days. We investigated the activation mechanism of these channels in HEK293 cells by maximum likelihood fitting of single-channel data, at a wide range of glycine concentrations. The mechanism we propose suggests that α2 channels can open only when all binding sites are occupied by glycine, and only after the channel undergoes a conformational change (‘flip’) that links binding to gating. Macroscopic data favour a two binding site model. The scheme can describe adequately macroscopic currents from fast concentration jumps experiments when desensitization is included in the model.

Table of Contents

List of Tables

List of Figures

Abbreviations

AMPA	(RS)-α-amino-3-hydroxy-5-methyl-4-isoxazole propionic acid
ACh	Acetylcholine
AChBP	Acetylcholine binding protein
ATP	Adenosine tri-phosphate
CaMKII	Ca^{2+}/calmodulin-dependent kinase II
DNA	Deoxyribonucleic acid
CHO	Chinese hamster ovary
CMV	Cytomegalovirus
CNS	Central nervous system
cRNA	Coplementary ribonucleic acid

DMEM	Dulbecco's modified Eagle's medium
EGFP (e-GFP)	Enhanced green fluorescent protein
ELIC	*Erwinia chrysanthemi* ligand-gated ion channel
ER	Endoplasmic reticulum
GABA (R)	γ-amino butyric acid (receptor)
GLIC	*Gloeobacter violaceous* ligand-gated ion channel
GlyR	Glycine receptor
GlyT	Glycine transporter
5-HT_3R	5-hydroxytryptamine type-3 receptor
HBSS	Hank's buffered salt solution
HEK293	Human embryonic kidney cells (cell line 293)
HPLC	High performance liquid chromatography
IPSC	Inhibitory postsynaptic current
IPSP	Inhibitory postsynaptic potential
LGIC	Ligand-gated ion channel
mGluR	Metabotrobic glutamate receptor
MA	Membrane-associated
MR	Microscopic reversibility
NMDA (R)	N-methyl-D-aspartate (receptor)
nAChR	Nicotinic acetylcholine receptor
PCR	Polymerase chain reaction
PKA	Protein kinase A
PKC	Protein kinase C
pLGIC	Pentameric ligand-gated ion channel
P_{open}	Probability of (channel) opening
PTK	Protein tyrosine kinase
PTX	Picrotoxin
RMS	Root mean square
SCAM	Substituted cysteine accessibility method
SEM	Standard error of mean
TEVC	Two-electrode voltage clamp
TM	Transmembrane domain

TRP	Transient receptor potential
UTR	Untranslated region
UV	Ultra violet
VIAAT	Vesicular inhibitory amino-acid transporter
ZAC	Zinc-activated channel

Chapter 1: Introduction

1.1 Ion channels and the pLGIC family of receptors

The ability of neurons to generate electrical signals and respond to each other relies on both the selective permeability of the cell membrane and on the electrochemical gradient of different ions across it. Ion channels maintain the selective permeability of the membrane by controlling ion fluxes. Some of these channels are able to respond to changes in the membrane potential (voltage-gated), others can sense mechanical or thermal stimulation of the cell membrane (stretch and heat-activated channels), whereas others are gated by extracellular, or intracellular, signals (ligand-gated ion channels; LGICs).

Neurotransmitter receptors belong to the latter group; a neurotransmitter binds to its specific receptor, an ion channel opens and the resulting ion fluxes change the membrane potential of the cell. Whether the neurotransmitter is excitatory or inhibitory depends on the type of receptor activated and also by the permeant ion's concentration in and out of the cell. Fast synaptic transmission uses ionotropic receptors which give rise to fast events which typically last a few milliseconds (Purves *et al*., 3rd edition). Ionotropic LGICs can be divided into four superfamilies: (1) the pentameric LGICs (pLGIC), (2) glutamate receptors, (3) the ATP-gated channels and (4) the TRP channels (Le Novère and Changeux, 1999; http://www.ebi.ac.uk/compneur-srv/LGICdb/LGICdb.php). The pLGIC superfamily contains the group of cation-permeable channels that include the nicotinic acetylcholine receptor (nAChR), the serotonin type 3 receptor (5-HT_3R) and the zinc-activated channels (ZAC), cation selective GABA channels, the group of anion-permeable channels which are the receptors for glycine (GlyRs) and GABA ($GABA_A$Rs and $GABA_C$Rs), the bacterial GLIC and ELIC channels and finally the glutamate and histamine receptors of invertebrates (Beg and Jorgensen, 2003; Bocquet *et al*., 2009; Davies *et al.,* 2003; Gisselmann *et al.,* 2002; Hilf and Dutzler, 2008; Lynch, 2004).

The various subunits of pLGICs share a fairly high degree of similarity in their amino-acid sequence that points to a common evolutionary ancestor (Okamura *et al.,* 2005; Ortells and Lunt, 1995; Xue, 1998). All pLGICs share some basic features: they are pentameric proteins with multiple agonist and antagonist binding sites that are distinct from the channel gate but can interact with it at a distance by changing the quaternary structure of the receptor. They can take at least three functional states i.e. closed at rest, open channel in the presence of agonist

and closed channel in the presence of agonist (desensitized). When the agonist is absent, these receptors have a low probability of opening. Channel opening is initiated by the association of the agonist to the extracellular binding site of the receptor (binding). This leads to dramatic conformational changes of the receptor-agonist complex, causing the central ion pore to open (gating). Additional modulation of binding or gating can arise from the association of other molecules to distinct sites on the complex (e.g. antagonists, blockers). Also, the duration of the exposure to the agonist can determine the likelihood of access to open or desensitized states.

1.2 Glycine receptors

1.2.1 Background – glycine as a neurotransmitter

Glycine was first proposed as a neurotransmitter after a detailed analysis of its distribution and concentration in different spinal cord regions by Aprison and Werman (1965). Additional studies thereafter agreed that glycine is an inhibitory neurotransmitter: in the spinal cord, glycine was shown to be associated with interneurons (Davidoff *et al.*, 1967) and electrophysiological studies by both Curtis *et al.* (1967) and Werman *et al.* (1967) showed that glycine hyperpolarizes adult spinal motoneurons by an increase in the neuronal chloride conductance. Other studies showed that glycine can be synthesized in neurons, released after neuronal stimulation and taken up by spinal motoneurons and synaptosomes with a high-affinity transport (see Bowery and Smart, 2006; Rajendra *et al.,* 1997). The alkaloid strychnine is a potent blocker of spinal cord inhibitory neurotransmission (Curtis *et al.,* 1968; Young and Snyder, 1973) and its high-affinity binding sites are colocalized with endogenous glycine and glycine-mediated actions (Rajendra *et al.,* 1997).

In the adult nervous system hyperpolarisation mediated by glycine reduces the excitability and firing of neurons (mainly in the spinal cord and the brainstem) and controls coordination of spinal reflexes, locomotion, pain transmission and respiration. Glycine and GABA produce hyperpolarisation only in adult neurons where the equilibrium potential for Cl^- is similar or more negative than the cell's resting potential. In embryonic neurons the situation is reversed: the intracellular Cl^- concentration is high and the opening of a chloride-conducting channel depolarizes the cell membrane (see Stein and Nicoll, 2003). Thus, GlyRs and GABARs are excitatory in embryonic neurons and their activation can ultimately result in calcium influx and this, in turn, is important for the proper development of the cell (Ye, 2008).

1.2.2 Purification and cloning of GlyR subunits

Betz and co-workers succeeded in purifying the glycine receptor from the rat spinal cord by affinity chromatography, taking advantage of the fact that the receptor could irreversibly bind to radiolabelled strychnine after exposure to UV light (Pfeiffer and Betz, 1981; Pfeiffer *et al.*, 1982; reviewed in Bowery and Smart, 2006; Lynch 2004). Three polypeptides were purified, with masses of 48 kDa, 58 kDa and 93 kDa (Pfeiffer *et al.*, 1982). The 48 kDa peptide was shown to be associated with strychnine and glycine; the entire amino-acid sequence was resolved and cDNA clones obtained (Grenningloh *et al.*, 1987; see also Baker *et al.*, 1994). The high homology of this peptide with the amino-acid sequences of nicotinic AChR subunits let to the classification of the GlyR as a member of the pLGIC family (Langosch *et al.*, 1988). The 48 kDa protein therefore, was named the α subunit (now α1), in accordance with the naming of ligand-binding subunits of this superfamily. The 58 kDa polypeptide, on the other hand, did not associate with strychnine or glycine (Graham *et al.*, 1985). The amino-acid and the cDNA sequences corresponding to this peptide were analyzed and the protein was named the β subunit (Grenningloh *et al.*, 1990a). The third isolated polypeptide of 93 kDa was found to be a peripheral cytoplasmic protein interacting with the receptor. Cloning of this protein, now known as gephyrin, was also performed by Betz and colleagues (Schmitt *et al.*, 1987).

Subsequent molecular cloning studies revealed a number of different subunit isoforms in humans and rodents (Lynch 2004; Rajendra *et al.*, 1997). Two additional α subunit isoforms were identified in the rat, α2 (Akagi *et al.*, 1991; Kuhse *et al.*, 1990a) and α3 (Kuhse *et al.*, 1990b). Sequences corresponding to these have also been identified in humans and mice (Grenningloh *et al.*, 1990b; Rajendra *et al.*, 1997; see also Cummings *et al.*, 1998). An additional α4 isoform has been described in mice and chick (Harvey *et al.*, 2000; Matzenbach *et al.*, 1994). Further diversity of α subtypes arises from alternative splicing of subunit pre-mRNA or from gene polymorphisms. A variant of the α1 subunit ($\alpha1^{ins}$), with eight additional amino-acids in the cytoplasmic region, was described in the rat (Malosio *et al.*, 1991b). Two rat α2 cDNA variants, products of alternative splicing, were also described (α2A, α2B; Kuhse *et al.*, 1991). These variants, highly homologous to the human α2 cDNA (Grenningloh *et al.*, 1990b), differ due to two amino-acid substitutions in the N-terminal domain. Another α2 variant (denoted as $\alpha2^{*}$) is a result of a polymorphism in the rat α2 gene (Kuhse *et al.*, 1990a). Alternative splicing of the human α3 primary transcript generates two variants, denoted as α3K

and α3L, of which the α3L is identical to the rat α3 subunit (Kuhse *et al.,* 1990b; Nikolic *et al.,* 1998). The α3K variant lacks 15 amino-acids in the cytoplasmic loop. Adding to these, recently a new α3 subunit variant has been identified in rats (Meier *et al.,* 2005). This variant (α3-Pro185Leu) is a result of a single nucleotide polymorphism at position 554, due to a cytidine-to-uracil substitution during RNA editing (Meier *et al.,* 2005).

Non-mammalian GlyR subunits have been studied in detail in the zebrafish CNS. An α subunit variant (αZ1) is highly homologous to the mammalian α1 subunit but also shares some similarities, in the transmembrane and cytoplasmic domains, with the α2 subunit (David-Watine *et al.,* 1999). More recently a second variant of this subunit has been identified, with 15 additional amino-acids in the N-terminal domain (named αZ1L), likely to arise from alternative splicing of the zebrafish primary transcript (Devignot *et al.,* 2003). Imboden and colleagues cloned three other α subunits, which they named αZ2, αZ3 and αZ4; phylogenetic analysis and molecular characteristics of the αZ2 variant classify it as an α2-like subunit whereas αZ3 is more similar to the mammalian α3 (Imboden *et al.,* 2001a and b).

Despite the big diversity of α subunits, only one β subunit (the one originally cloned by Grenningloh *et al.,* 1990a; Handford *et al.,* 1996) is known today. The equivalent non-mammalian βZ subunit was found in zebrafish (Imboden *et al.,* 2001c). All the α subunits share a high sequence identity to each other (~80-90% homology; Rajendra *et al.,* 1997) whereas the β subunit only shares a similarity of ~47% with the α1 subunit (Grenningloh *et al.,* 1990a and b).

1.2.3 Distribution of GlyR subunits in the CNS

Soon after their cloning, *in situ* hybridization studies in the rat showed that α1 transcripts are found at high density in the spinal cord and the brainstem of adults and at lower levels in the superior and inferior colliculi, the cerebellar deep nuclei and the hypothalamus (García-Alcocer *et al.,* 2008; Malosio *et al.,* 1991a; Sato *et al.,* 1992) but are absent from cortical regions. Developmentally, α1 transcripts become detectable at approximately E15, reaching a peak at P15 (Malosio *et al.,* 1991a). Expression of the $\alpha1^{ins}$ mRNA represents ~30% of the total α1 mRNA and follows a similar pattern throughout development (Legendre, 2001; Malosio *et al.,* 1991b).

Transcripts for α2 are found mainly in the embryonic spinal cord and the brainstem; by contrast to α1, mRNA is also found in the cortex, hippocampus and the thalamus (Malosio *et al.,* 1991a; Sato *et al.,* 1992) and at high densities in the developing cerebellum (García-Alcocer *et al.,* 2008). In the adult, transcripts of α2 are still detectable at low levels, mainly in the auditory brainstem nuclei, the retina and certain regions of the cortex (Malosio *et al.,* 1991a; Piechotta *et al.,* 2001; Racca *et al.,* 1998). The α2A and α2B variants described in the rat have similar patterns of distribution during development. Both isoform mRNA levels are high early during development (higher for α2A) but drop quickly after maturation; the transcripts for α2A become undetectable whereas α2B is still present in the adult brain (Kuhse *et al.,* 1991; Legendre, 2001).

The decrease of α2 mRNA levels from embryogenesis to adulthood (by P20 in the rat) is accompanied by a postnatal increase in α1 and α3 transcripts (Malosio *et al.,* 1991a). The levels of α3 transcripts are generally lower than those of α1 throughout development. The mRNA for α3 has been mostly detected in the olfactory bulb, hippocampus and the cerebellar granule layer with lower signals present in the spinal cord (Malosio *et al.,* 1991a; see also Harvey *et al.,* 2004).

Transcripts of the α4 subunit are detected at very low levels in the adult rat spinal cord and retina and in the mouse adrenal glands (Matzenbach *et al.,* 1994). More recently, an *in situ* hybridization study performed in chick embryos localized α4 mRNA molecules in high densities in the spinal cord, dorsal root and sympathetic ganglia, suggesting that this subunit is an embryonic GlyR subunit isoform, similar to α2 (Harvey *et al.,* 2000; Legendre, 2001).

The distribution of the β subunit mRNA is much wider than that of any α, with transcripts in most regions of the embryonic and adult brain. These have low levels before birth, increase postnatally and remain like that throughout adulthood and are present also in areas that lack α subunits (Fujita *et al.,* 1991; Malosio *et al.,* 1991a). This is a puzzling finding as β subunits cannot form functional GlyRs without the presence of an α subtype in recombinant expression systems and it is reasonable to assume that the same occurs *in vivo* (Grenningloh *et al.,* 1990a).

Consistent with mammalian studies, mRNA for the αZ1, αZ2 and also the βZ subunits are detected in the zebrafish retina, spinal motoneurons and in posterior brain regions (Imboden *et*

al., 2001c). These results are in agreement with immunocytochemical studies performed on the goldfish Mauthner neuron using antibodies against the mammalian α1 subunit (Seitanidou *et al.*, 1988; Triller *et al.*, 1993).

1.2.4 Functional GlyRs in the nervous system

The distribution of functional glycine receptors has been studied by approaches that include *in vitro* autoradiography of [^{3}H]-strychnine or [^{3}H]-glycine (Zarbin *et al.*, 1981; Young and Snyder, 1973) to identify the localization of strychnine or glycine binding sites respectively, immunocytochemistry studies with monoclonal antibodies in combination with electron or light microscopy (Racca *et al.*, 1997; Triller *et al.*, 1985) and also studies on animals with targeted deletions of GlyR subunits or of glycine transporters (Betz *et al.*, 2006; Harvey *et al.*, 2004; McDearmid *et al.*, 2006; Young and Cepko, 2004; Young-Pearse *et al.*, 2006). This work broadly agrees with the results of the *in situ* hybridization: receptors for glycine are present at high levels in the spinal cord and the brainstem (pons and medulla) and at lower levels in the midbrain, thalamus, hypothalamus, the cerebellum, the hippocampus and in retinal ganglia (Legendre, 2001; Lynch, 2004; Rajendra *et al.*, 1997). In many of these regions, glycine-mediated neurotransmission has also been described, suggesting that these GlyRs are synaptic. Detailed studies have also been performed for the Mauthner neuron in the zebrafish hindbrain, characterizing the inhibitory glycinergic synapses present there (Triller *et al.*, 1997).

GlyRs are also involved in non-synaptic function. Early in development, the activation of glycine (and GABA) leads to cell depolarisation, resulting in the activation of voltage-gated Ca^{2+} channels, in a transient increase in intracellular Ca^{2+} and finally in the activation of cytoplasmic mechanisms that underlie development (Gao *et al.*, 1998; Flint *et al.*, 1998). GlyRs are also thought to facilitate transmitter release by a presynaptic depolarizing action (Jeong *et al.*, 2003; Turecek and Trussell, 2001, 2002).

GlyRs are often colocalised with receptors for GABA. Mixed presynaptic boutons containing both transmitters were shown to exist in the spinal cord (Schneider and Fyffe, 1992; Todd, 1990; Todd *et al.*, 1996), in the brainstem (Dumba *et al.*, 1998), in cerebellar Golgi cells (Dugué *et al.*, 2005; Ottersen *et al.*, 1988) and in the cerebellar cortex (Crook *et al.*, 2006). Mixed inhibitory interneurons in the spinal cord co-release GABA and glycine from individual vesicles that contain both transmitters (Chéry and de Koninck, 1999; Jonas *et al.*, 1998). The

presence of mixed synaptic terminals is usually correlated with the expression of both $GABA_AR$ and GlyRs in the postsynaptic membrane, as shown by immunocytochemistry (Todd *et al.*, 1996; Triller *et al.*, 1987) and electrophysiological studies (Hamill *et al.*, 1983), supporting the idea that some neurons can mediate both GABAergic and glycinergic transmission (Figure 1.1).

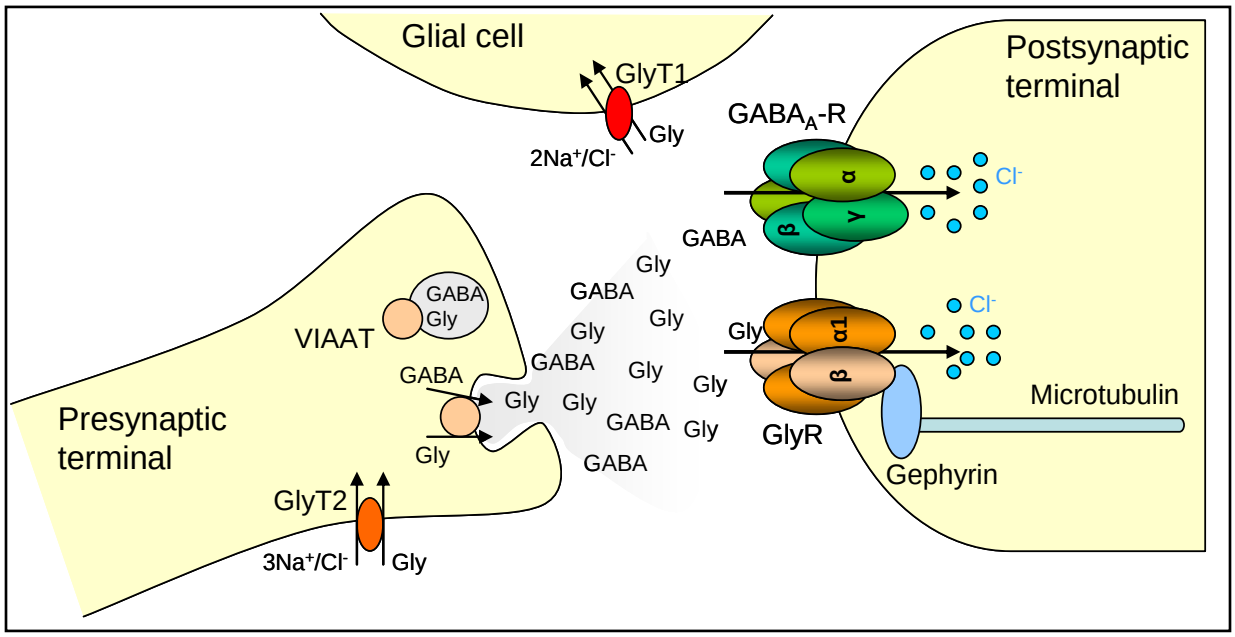

Figure 1.1 Features of glycine-mediated synaptic transmission
In the presynaptic cell the vesicular inhibitory amino-acid transporter (VIAAT) packs glycine into synaptic vesicles, often together with GABA. Excitation of the cell causes the fusion of synaptic vesicles with the presynaptic membrane and the release of glycine (and GABA) into the synaptic cleft. The neurotransmitters are then diffused in the cleft and bind to their receptors in the postsynaptic membrane, increasing the cell's Cl^- conductance. Glycinergic transmission is terminated by the uptake of glycine into adjacent nerve terminals or glial cells, mediated by glycine transporters (GlyTs).

It was recently shown that GABA, co-released with glycine, can act directly on GlyRs and modulate the decay of glycinergic transmission (Lu *et al.*, 2008; see also Singer, 2008). A GABAergic component in glycinergic transmission (distinguishable due to the slower time course of GABAergic currents) is important early in development, when both neurotransmitters depolarize neurons. Afterwards, transmission changes to glycine-dominant in most spinal and brainstem synapses (Baccei and Fitzgerald, 2004; Gao *et al.*, 2001; González-Forero and Alvarez, 2005). GABARs produce longer currents and the more sustained depolarizations may be needed by the embryonic neurons to increase the levels of

cytoplasmic Ca^{2+} (Gao and Ziskind-Conhaim, 1995, 1998; Gao *et al.,* 1998; see also Tapia *et al.,* 2001).

1.2.5 Structure

i. General features – models of structure

The ACh receptor at the neuromuscular junction is the most studied receptor in the pLGIC family. This receptor was the first ligand-gated channel to be characterized in detail. Most of the available information, therefore, concerning the structure of other members of the family, such as GlyRs which concern this study, is deduced from the knowledge concerning the ACh receptor.

Despite the fact that none of the pLGIC family members has been crystallized to date, a detailed knowledge of the structure of AChRs comes from very well defined models: the crystal structure of a soluble ACh binding protein from the *Lymnea stagnalis* snail (AChBP; Brejc *et al.,* 2001; Smit *et al.,* 2001), the cryo-electron microscopy structure of the *Torpedo* AChR (Miyazawa *et al.,* 2003; Unwin, 2005) and the recently resolved X-ray structures from two prokaryotic pLGICs, from *Gloeobacter violaceus* (GLIC; Bocquet *et al*., 2009) and from *Erwinia chrysanthemi* (ELIC; Hilf and Dutzler, 2008). The AChBP is a homolog of the N-terminal domain of the AChR, providing high resolution information on the extracellular domain (Karlin, 2002), whereas the other three models provide detailed information on the pore of the channel. The 4Å resolution image from Unwin's group has been essential for understanding the relations between the structure and the function of pore residues and for locating the position of the gate.

ii. Subunit topology

Characteristic sequence motifs in the secondary structure of pLGIC subunits include (Figure 1.2): (1) an extracellular N-terminal domain where agonists bind, (2) four α-helical transmembrane domains (TM1-TM4), (3) a large intracellular loop between TM3 and TM4 and (4) the extracellular C-terminal region (Karlin, 2002). All subunits have a conserved cysteine loop in the N-terminal domain. For the α1 GlyR subunit, this loop is between Cys138 and Cys152 (Rajendra *et al.,* 1997). In the case of GlyR subunits, there is a second Cys-loop, formed by a disulfide bond between residues Cys198 and Cys209 for the α1 subunit (Rajendra *et al.,* 1997). All pLGICs assemble as pentamers: as homomers of five identical subunits or as

heteromers of different subunits (Karlin, 2002; Langosch *et al.*, 1988). The wide variety of subtypes of the pLGICs found in the CNS arises from the big number of possible different combinations of subunits to compose heteromers (Sivilotti and Colquhoun, 1995).

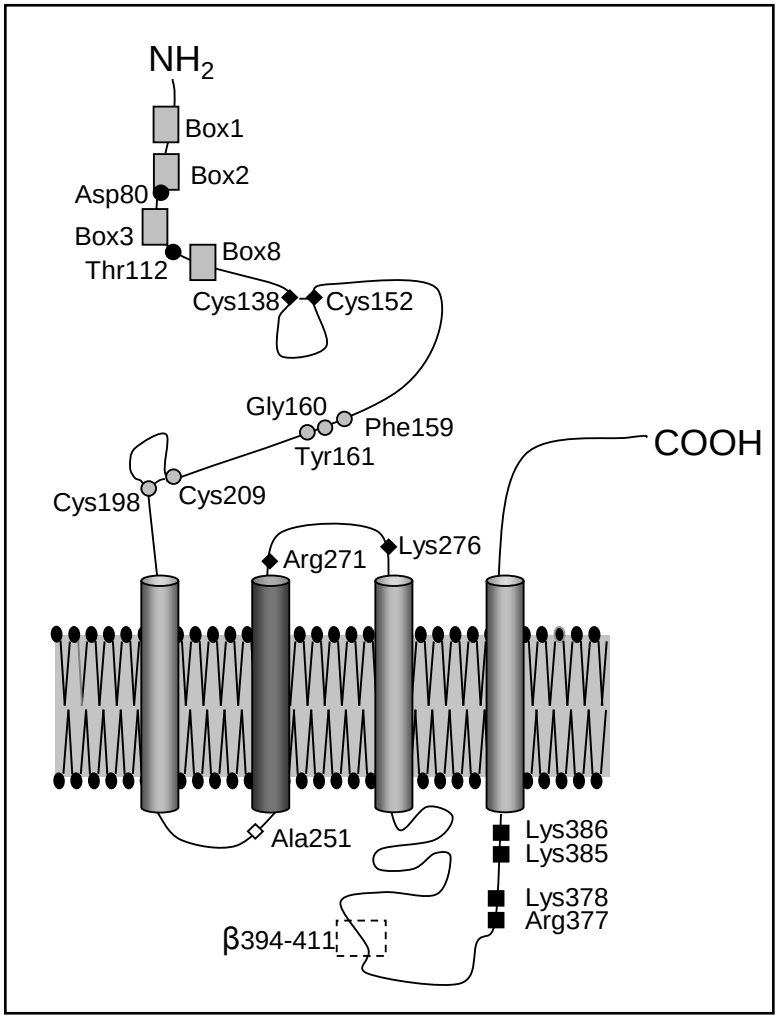

Figure 1.2 Membrane topology of a GlyR subunit
Representation of the human α1 subunit showing the extracellular N- and C-terminals and the four transmembrane domains, with the pore-lining TM2 highlighted in dark grey. Also shown are functionally important regions or residues involved in: assembly (grey boxes), zinc modulation (black circles), ligand binding (grey circles), ionic selectivity (white diamond), gating (black diamonds) and single-channel conductance (black squares). The dashed-lined box indicates the gephyrin binding domain (human β subunit numbering).

iii. N-terminal domain

The sequence of the snail's AChBP subunits shares ~20-24% similarity with the N-terminal region of muscle nAChR subunits and a ~15-18% homology with subunit sequences of the 5-

HT_3, $GABA_A$, $GABA_C$ and glycine receptors (Sixma, 2007; Sixma and Smit, 2003). It lacks the intracellular and transmembrane domains of a pLGIC but it can bind to agonists, toxins and competitive antagonists that are known to bind to the nACh receptor, making it an important model for the ligand binding region (Karlin, 2002; Sixma and Smit, 2003; Ulens *et al.*, 2006), even though it remains unclear whether the AChBP is in a resting, activated or desensitized state. The 2.7Å crystal structure of the AChBP (Brejc *et al.*, 2001) showed that each subunit has a sandwich-like structure of 10 β-sheets, following a short α-helix at the most distant part from the membrane, and forms a modified immunoglobulin structure. The pentamer is a cylinder with an external diameter of 80Å, an inner diameter of ~18Å and a height of 60Å (Sixma and Smit, 2003). A similar structure has also been described for the bacterial GLIC and ELIC, although the α-helix appears to be missing from the prokaryotic channels (Bocquet *et al.*, 2009; Hilf and Dutzler, 2008).

The agonist binding sites are located in pockets between the interfaces of neighbouring subunits, each pocket being formed by loops of residues from both subunits involved (Figure 1.3). Residues from α subunits contribute to loops A, B and C, whereas the neighbouring γ, δ or ε subunit forms loops D, E, F and G (reviewed in Arias, 2000; Corringer *et al.*, 2000; Sine, 2002; Sixma and Smit, 2003). By analogy with the muscle AChR, the principal binding subunit is termed α; the secondary binding subunit is a non-α peptide (Karlin, 2002; Sine, 2002; Sine and Engel, 2006).

A combination of studies (reviewed in Karlin, 2002; Sine, 2002; Sixma and Smit, 2003) resulted in the generation of several models of pLGICs (cfr. Figure 1.3 from Laube *et al.*, 2002). Modelling and mutagenesis studies on GlyRs were able to identify different amino-acids that are essential for glycine and/or strychnine binding (Breitinger and Becker, 2002; Laube *et al.*, 2002; Lynch , 2004). According to the terminology given for ACh receptors four equivalent loops (A, B, C, D) on the N-terminal part of GlyRs, immediately preceding the TM1, have been implicated in agonist/antagonist binding. Loops B and C are the most essential. Mutational studies surrounding the Phe159–Gly160–Tyr161 triplet in Loop B (α1 numbering; Schmieden *et al.*, 1993; Vandenberg *et al.*, 1992b) and the equivalent Gly167 on α2 (or Glu167 on α2*; Kuhse *et al.*, 1990a) suggest that the region containing the triplet forms a binding domain for strychnine and is probably involved in agonist binding (Figure 1.2). A similar triplet motif was found in $GABA_A$ (Amin and Weiss, 1993) and 5-HT_3 receptors (Spier

and Lummis, 2000), showing a conservation of this domain in pLGICs (Lynch, 2004). These are residues that constitute the "aromatic box" which is involved in cation-π interaction in the whole superfamily (Grudzinska *et al.*, 2005; Pless *et al.*, 2008). Loop C includes the second cysteine loop formed between residues Cys198 and Cys209 (α1 numbering) which is characteristic of GlyRs (Figure 1.2; Rajendra *et al.*, 1997). Disruption of the loop by point substitutions of either the Cys198 or the Cys209 abolishes the binding of glycine or strychnine (Rajendra *et al.*, 1995b). Other residues of the loop also affect glycine and/or strychnine binding (Rajendra *et al.*, 1995b; Vandenberg *et al.*, 1992a and b). Adding to these two regions, other residues found in loop A (Han *et al.*, 2001; Vafa *et al.*, 1999) and loop D (Schmieden *et al.*, 1992) have also been studied, but, as mutations of such residues have little effect in the sensitivity of GlyRs to ligands, it is questionable whether they are part of a ligand binding domain (Lynch, 2004).

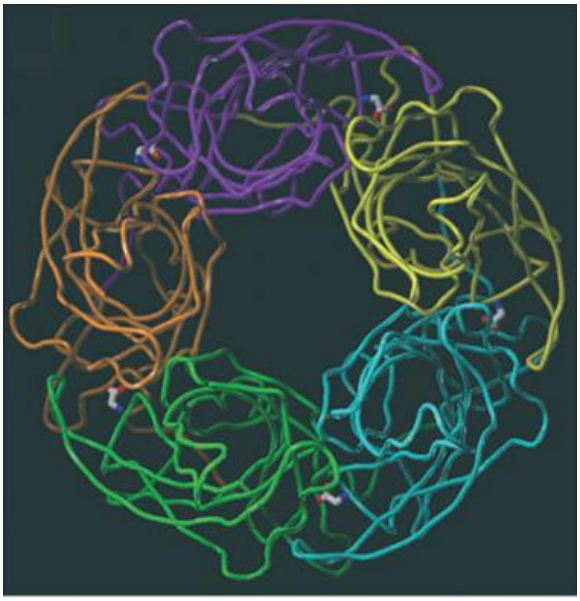

Figure 1.3 The N-terminal region of the α1 GlyR
This model, by Laube and colleagues (2002), is created by homology modelling based on the crystal structure of the AChBP from *Lymnea stagnalis* (Brejc *et al.*, 2001). The N-terminal regions of the five subunits, viewed from the top, are coloured separately. The model shows the five possible binding sites for glycine (ball and stick structure) located at the interfaces of adjacent subunits.

As most studies were performed on homomeric GlyRs, the role of the β subunit in binding has not been investigated thoroughly. A study on heteromeric α1β GlyRs however, concluded that

residues Arg86 (Loop D) and Glu180 (Loop B) of the β subunit are in direct interactions with glycine (Grudzinska *et al.*, 2005; see also Betz and Laube, 2006). Interestingly, a hyperekplexia mutation at residue Gly229 (Loop C) of the β subunit affects the glycine sensitivity of heteromeric receptors (Rees *et al.*, 2002).

A recent study investigated the role of the signature Cys-loop, formed between Cys138 and Cys152 (α1 subunit; Figure 1.2) and concluded that, although it is essential for modulation by anesthetics, it is unlikely to serve as a binding site for glycine (Schofield *et al.*, 2004; see also Vandenberg *et al.*, 1993). The loop appears to be important for receptor activation during gating (Schofield *et al.*, 2003).

Besides its contribution in ligand binding, the N-terminal domain of GlyR subunits contains residues that are important for the assembly of pentamers and also residues that are involved in the modulation of GlyR function by zinc (Figure 1.2). Both processes are discussed below.

iv. Transmembrane domains (TM)

Direct information on the structure of the membrane-spanning part of pLGICs comes from the bacterial GLIC and ELIC X-ray structures and also from Unwin's work on the *Torpedo* AChR. Note that the three models are in excellent agreement (Bocquet *et al*., 2009; Hilf and Dutzler, 2008). The resolution for Unwin's model has been progressively increased from the first description in 1995 to the latest 4Å model (Miyazawa *et al.*, 1999 and 2003; Unwin, 1995, 2005). The model shows the four TM domains of each subunit arranged symmetrically around the central ion pore. All TM domains are α-helical: the channel is lined mostly by the five TM2 helixes, whereas the other TM domains (arranged in a clockwise orientation) shield the channel from the membrane lipids (Miyazawa *et al.*, 1999). A number of mutagenesis and chemical labeling studies agree that the TM2 domains form the ion pore. In agreement, peptide fragments of M2 segments of α1 GlyR subunits can spontaneously adopt an α-helical secondary structure and assemble together to form chloride channels in lipid bilayers (Mitchell *et al.*, 2000).

Other indirect methods have been used to probe the structure of the membrane-spanning regions (reviewed in Cascio, 2004; Karlin, 2002; Lummis, 2004; Lynch, 2004). The most extensively used one is the substituted cysteine accessibility method (SCAM) described by Karlin and Akabas (1998) and recently used by Lynch and co-workers to identify residues on

the M2-M3 loop related to glycine binding and GlyR activation (Lynch *et al.,* 2001). SCAM studies agree with Unwin's data that most (at least 75%) of the segment of TM2 domains is an α-helix (Akabas *et al.,* 1994). Unwin's model predicts that each TM domain extents ~10Å over the membrane surface. In agreement with the hydrophobicity of these regions, charged amino-acids are present only at the beginning and end of each TM domain (Miyazawa *et al.,* 2003). The charged residues that frame each TM domain of the GlyR α1 subunit are: Arg218 and Asp247 (TM1), Arg252 (0′) and Arg271 (19′; TM2), Asp284 and Arg309 (TM3) and Lys389 and Lys411 for TM4.

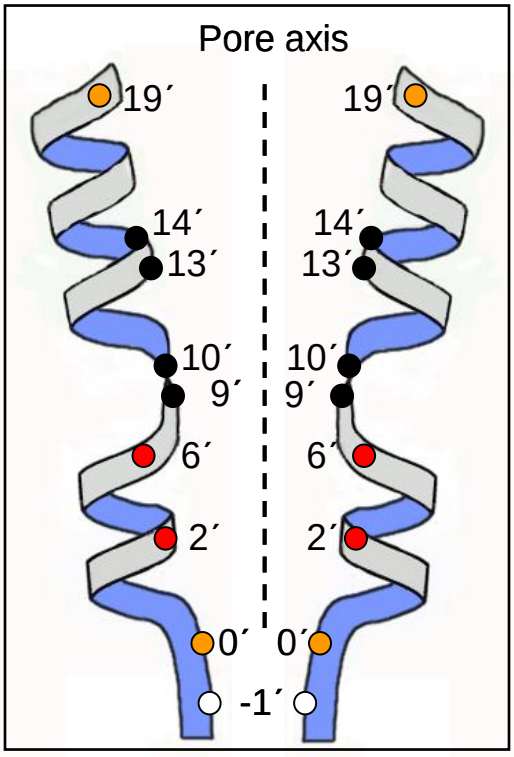

Figure 1.4 The ion channel pore of GlyRs
Schematic representation of two α1 subunit TM2 domains tilting inwards towards the pore axis, according to Unwin's model for the AChR. The highly conserved Leu (9′) in the middle of the domain and the adjacent 10′, 13′ and 14′ residues (shown in black) form the hydrophobic interactions that keep the pore closed. Other residues shown are the ones related to picrotoxin inhibition (red), ionic selectivity (white) and the charged residues that mark the limits of the TM2 (in orange). Numbering is as in Miller (1989).

When the pore is viewed from the synaptic cleft the five TM2 domains appear to tilt inwards towards the central axis. The highest density on the electron microscope appears near the middle of the ion pore, suggesting this is the gate of the channel (Miyazawa *et al.,* 1999, 2003;

Unwin, 2005). This area coincides with a highly conserved leucine at position 9′ of the TM2 (Figure 1.4). According to this model, the pore is highly symmetrical due to equal side-by-side hydrophobic interactions between the residues at 9′, 10′, 13′ and 14′, forming two levels of contacts: one between the side-chains of a 9′ leucine and the 10′ residue on its adjacent TM2 and the second between the side-chains of residues at positions 13′ and 14′ of neighbouring subunits. These interactions create a hydrophobic girdle that causes the TM2 domains to bend inwards, keeping the channel closed (Miyazawa *et al.*, 2003). The residues that line the pore of GlyRs (α1 subunit numbering) are Leu261 (9′), Thr262 (10′), Thr265 (13′) and Gln266 (14′). The location of the gate in the middle of the TM2 regions has also been suggested by molecular dynamics simulations on the AChR (Amiri *et al.*, 2005; Corry, 2006) and more recently by picrotoxin trapping experiments on the GABAR (Bali and Akabas, 2007). Earlier studies with SCAM suggested a different location deeper in the pore, between positions -2′ and 2′ (Wilson and Karlin, 1998; Xu and Akabas, 1996), but this may have been an artefact due to undetected spontaneous openings of the Cys-mutants (Bali and Akabas, 2007).

v. <u>The loops between TM domains</u>

The charged residue at position 247 (Asp247, α1 numbering) indicates the beginning of the TM1-TM2 loop, which is formed by only five amino-acids (TM1-Asp-Ala-Ala-Pro-Ala-TM2). It was suggested early on that this loop links the binding signals with the gate of the channel (Lynch *et al.*, 1997; see also Czajkowski, 2005). There is also evidence that the five residues lie in the ion-conducting pathway (Filippova *et al.*, 2004) suggesting a role of the loop in ionic selectivity (see also Galzi *et al.*, 1992; Imoto *et al.*, 1988; Keramidas *et al.*, 2000). This domain can influence the desensitization properties of GlyRs (Saul *et al.*, 1999) and might play a role in zinc potentiation (Lynch *et al.*, 1998).

The TM2-TM3 loop extents from Arg271 to Asp284 and according to Unwin's model it is formed by the helical parts of the domains that extend outside the membrane (Ma *et al.*, 2005; Miyazawa *et al.*, 2003). The best characterized residue is the charged Arg271 (Figure 1.2): mutations of this residue to Gln or Leu cause hyperekplexia (Shiang *et al.*, 1993) by reducing the channel sensitivity to glycine (by ~400–fold; Rajendra *et al.*, 1994). Other effects include transforming partial agonists to competitive antagonists (Rajendra *et al.*, 1995a) and converting picrotoxin from a competitive antagonist to an allosteric potentiator (Lynch *et al.*, 1995). Finally, these mutations also reduce single-channel conductance by abolishing the high

conductance state of the wild-type receptor (Langosch *et al.,* 1994). Together these effects suggest that the TM2-TM3 loop may mediate the transduction of binding into gating (Lynch *et al.,* 1997). Other mutations in this area cause hyperekplexia (Kwok *et al.,* 2001) and a single-channel study on one of these mutations, at position 276 (Lys276Glu; Figure 1.2), showed that indeed the mutation affects gating (Lewis *et al.,* 1998). Residues in the TM2-TM3 loop are also involved in the modulation of glycine and GABA receptors by alcohols and anesthetics (Dupre *et al.,* 2007; Mihic *et al.,* 1997), by zinc (Lynch *et al.,* 1998) and by protons (Li *et al.,* 2003; Wilkins *et al.,* 2005).

This large cytoplasmic loop (TM3-TM4) is the least conserved region, in length and sequence, across the pLGIC family members (Le Novère and Changeux, 1999). What information there is on the loop's structure comes from Unwin's study, which managed to resolve an α-helical segment (called the membrane-associated helix, MA) before the beginning of the TM4 (Unwin, 2005). In α1 the loop extends from Arg309 to Lys389 and is even longer in the β subunit (Asn333 to Leu463). Naturally the role of the cytoplasmic loop as a target for modulation by internal molecules has been intensively studied and has shown interactions with kinases and phosphatases and sites that undergo ubiquitination (Lynch, 2004). Residues in the MA stretch contribute to regulating the single-channel conductance of cationic channels (Gee *et al.,* 2007; Hales *et al.,* 2006; Kelley *et al.,* 2003; Peters *et al.,* 2004) and more recently the same has been shown for GlyRs (Carland *et al.,* 2009; see section 3.2.1). The TM3-TM4 loop of the β subunit contains the gephyrin binding domain (Figure 1.2), an 18 amino-acid motif required for interaction with gephyrin, and therefore receptor clustering and anchoring to synapses (Kneussel and Betz, 2000; Kneussel and Loebrich, 2007; Meyer *et al.,* 1995).

1.2.6 Function

i. Ionic selectivity

Permeability experiments on glycine and GABA receptors indicate pore diameters of 5.2 Å and 5.6 Å, respectively (Bormann *et al.,* 1987; Rundström *et al.,* 1994) and identical permeability sequences for both receptor types ($SCN^- > I^- > Br^- > Cl^- > F^-$; Bormann *et al.,* 1987). The conductance sequence for GlyRs is $Cl^- > Br^- > I^- > SCN^- > F^-$ and there are likely two binding sites for anions in the pore region (Bormann *et al.,* 1987).

Early work on AChRs has shown that rings of charged residues in the pore determine ionic selectivity and conductance (Imoto *et al.,* 1988; Imoto, 1993; Konno *et al.,* 1991). Mutation of the appropriate residues can convert a cation-selective receptor, like the α7 neuronal nAChR, into an anion-selective channel (Galzi *et al.,* 1992) and *vice-versa*. The ionic selectivity conversion was assessed for most members of the nicotinic superfamily (reviewed in Jensen *et al.,* 2005; Keramidas *et al.,* 2004). For anion-selective channels like $GABA_A$-Rs and GlyRs, conversion of selectivity can be achieved by reversing Galzi's mutations. Both a deletion of the proline at -2′ position and the Ala-1′Glu substitution are needed to create cationic ρ1 $GABA_A$ receptors (Wotring *et al.,* 2003; see also Jensen *et al.,* 2002) whereas the Ala-1′Glu mutation (Ala251) is sufficient by itself in the α1 GlyR homomer (Keramidas *et al.,* 2002; Figure 1.4).

In addition to that, uncharged residues within the TM2 domain (such as those at positions 2′, 6′ and 9′) also affect the ionic selectivity and conductance (Cohen *et al.,* 1992a, b; Imoto *et al.,* 1991; Villarroel *et al.,* 1991).

ii. Assembly and trafficking to the cell membrane

The first evidence that GlyRs are pentamers came from chemical cross-linking of purified spinal cord GlyR subunits. This gave rise to products of up to 260 kDa that contained the 48 kDa (α1 subunit) and 58 kDa subunits (β subunit) in varying ratios. Given that 260 kDa is approximately 5 times the mean subunit mass, it was concluded that the native GlyRs are pentamers (Langosch *et al.,* 1988, 1990).

Channel assembly takes place in the endoplasmic reticulum (ER) and involves many control points and the interference of various chaperone proteins (Millar and Harkness, 2008; Sarto-Jackson and Sieghart, 2008). The N-terminal region of GlyRs contains 'assembly boxes', i.e. determinants for heteromeric or homomeric assembly (Kuhse *et al.,* 1993). Mutations of β subunit residues in these boxes to the equivalent α1 residues makes β subunits behave like alphas and assemble as homomers. The minimum β-to-α1 mutations necessary for homomeric assembly were mutations in box1 and box3 or in box1, box2 and box8 (Griffon *et al.,* 1999; Kuhse *et al.,* 1993; Figure 1.2).

Exit from the ER occurs after the individual subunits have received the appropriate post-translational modifications and have been assembled into pentamers with the correct

composition (Connolly, 2008; Millar and Harkness, 2008; Sarto-Jackson and Sieghart 2008). Little is known about the subsequent steps and how receptors are trafficked to the cell-membrane, which chaperone proteins are involved or how the targeting at somatic, dendritic or axonal membrane occurs. There is evidence to suggest that after exiting the ER and *trans*-Golgi network, newly-formed GlyR pentamers are inserted into the plasma membrane via exocytosis (Meier *et al.,* 2000; Rosenberg *et al.,* 2001). The insertion is localized mainly in the soma, where the receptors form clusters of low density (microclusters) and is followed by lateral diffusion towards postsynaptic regions where GlyRs interact with gephyrin (Groc and Choquet, 2008; Meier *et al.,* 2000; Rosenberg *et al*., 2001).

iii. Retention to synapses – Interaction with gephyrin

Gephyrin is essential for long-term, stable anchoring of the receptors to the cytoskeleton of postsynaptic regions (Kneussel and Loebrich, 2007). *In situ* hybridization studies revealed different gephyrin isoforms throughout the nervous system and peripheral tissues, where they interact with polymerized tubulin (Kirsch *et al.,* 1991, 1993b; Prior *et al.,* 1992; Racca *et al.,* 1997) and immunocytochemistry studies detected gephyrin in CNS neurons containing high densities of GlyRs (Kirch and Betz, 1993; Triller *et al.,* 1985 and 1987; van den Pol and Gorcs, 1988). Betz and colleagues characterized the gephyrin binding motif on the cytoplasmic loop of β subunits (Meyer *et al.,* 1995; Figure 1.2). Until recently therefore the consensus has been that only β subunit-containing receptors can be localized in synapses and hence can have a role in synaptic transmission (but see Legendre, 2001). Treatment of cultured spinal neurons with antisense oligonucleotides against gephyrin is sufficient to block the postsynaptic clustering of GlyRs and similar results are obtained with drugs that disrupt the cytoskeleton or with targeted mutations of the gephyrin gene (Feng *et al.,* 1998; Kirsch *et al.,* 1993a; Kirsch and Betz, 1995).

Even after stabilization by gephyrin, GlyRs still can diffuse freely between subcompartments of the cell membrane (Dahan *et al.,* 2003; Kneussel and Loebrich, 2007; Meier *et al.,* 2001). Lateral diffusion of GlyRs is Ca^{2+}-dependent and can be driven by the activation of NMDARs, suggesting that the recruitment of GlyRs in synapses acts as a compensation for increased excitatory neurotransmission (Lévi *et al.,* 2008).

iv. Release and uptake of glycine – Characteristics of glycinergic transmission

In the neuron, glycine can either be newly synthesised or recycled by re-uptake after its release from synaptic terminals. The packaging of glycine in synaptic vesicles and their accumulation near the release site requires its active transport from the cytosol into the vesicles: the procedure requires an H^+/ATPase on the vesicular membrane (which provides the necessary energy for the transport) and also the vesicular inhibitory amino-acid transporter (VIAAT; Figure 1.1), which can also pack GABA into vesicles, in exchange for protons (Gasnier, 2000; McIntire *et al.,* 1997; Sagné *et al.,* 1997). The stoichiometry of this exchange is one proton per glycine molecule (Gasnier, 2000) and in mixed glycine/GABA neurons the two transmitters compete for their uptake into vesicles (Chaudhry *et al.,* 1998; Dumoulin *et al.,* 1999; Wojcik *et al.*, 2006).

The basic concept of classic neurotransmission is that the arrival of an action potential in a presynaptic terminal is followed by the simultaneous fusion and release of many synaptic vesicles carrying the transmitter (Katz and Miledi, 1965b). Like other transmitters, the release of glycine can be either evoked or spontaneous and is highly dependent on the extracellular calcium concentration and its entry through voltage-gated calcium channels (Borst and Sakmann, 1996; Clements, 1996; Katz and Miledi, 1965a; Reid *et al.,* 2003). Likewise, the release of glycine can be modulated by mGluRs that inhibit the actions of voltage-gated Ca^{2+} channels or activate presynaptic K^+ channels, interfering with the release machinery (Katsurabayashi *et al.,* 2004; Shoudai *et al.,* 2007). Other factors indirectly affecting the release of glycine and/or the frequency of glycinergic IPSCs are volative anaesthetics, neurotrophins and cell-stressing conditions (Bardoni *et al.,* 2007; Saransaari and Oja, 2009; Yamashita *et al.,* 2001). Presynaptic ligand-gated channels (nAChRs, $GABA_A$Rs, P2X ATP receptors and glycine receptors themselves) can also modulate the release of glycine (Jang *et al.,* 2002; Jeong *et al.,* 2003; Kiyosawa *et al.,* 2001; Takeda *et al.,* 2003; Wang *et al.,* 2001).

After its release in the cleft, glycine is cleared away by re-uptake into adjacent nerve terminals or glial cells (Figure 1.1). The process is mediated by a family of membrane proteins, named glycine transporters (GlyTs; Eulenburg *et al.,* 2005). Two different GlyTs have been identified, GlyT1 and GlyT2, which mediate glycine uptake in glial cells and neurons respectively (Gadea and Lopez-Cólomé, 2001; Jursky and Nelson, 1995; Zafra *et al.,* 1995a, b). The presence of GlyT2 on glycinergic neurons ensures the enrichment of synaptic terminals with glycine

needed for vesicular loading. The distinct localization and pharmacology of the two GlyTs (Mezler *et al.,* 2008; Supplisson and Roux, 2002) and the generation of GlyT knockout mice have been important tools for the identification of glycinergic synaptic transmission sites and neurotransmission deficiencies (Betz *et al.,* 2006; Eulenburg *et al.,* 2006).

v. Modulation of GlyR function

GlyR subunits carry a number of motifs on which modulatory molecules can act, including motifs for phosphorylation, ubiquitination and glycosylation and also binding sites for ions, cytoplasmic proteins and pharmaceutical compounds.

- Zinc: The most extensively studied modulation of GlyR function is the one mediated by zinc ions (Zn^{2+}). The modulation by zinc is biphasic: at low concentrations (<10 μM) zinc potentiates glycine-mediated currents whereas at higher concentrations it acts as an inhibitor (Bloomenthal *et al.,* 1994; Laube *et al.,* 1995; Miller *et al.,* 2005a, b; Smart *et al.,* 2004). These effects are mediated by two distinct binding sites for Zn^{2+} in the N-terminal domain of GlyRs (Figure 1.2): mutagenesis studies have highlighted residues Asp80 and Glu192 (α1 subunit) for the potentiating effect (Laube *et al.,* 2000; Lynch *et al.,* 1998; Miller *et al.,* 2005a) and His107, His109, Thr112 and Thr133 for inhibition (Harvey *et al.,* 1999; Laube *et al.,* 2000; Miller *et al.,* 2005b, 2008; Nevin *et al.,* 2003). Other divalent cations such as copper and nickel can also inhibit GlyRs (Chen *et al.,* 2006; Schumann *et al.,* 2009; Trombley and Shepherd, 1996; Wang *et al.,* 2002).
- Ca^{2+}: Changes in the levels of cytoplasmic Ca^{2+}, either by entry via Ca^{2+}-gated channels or via ionotropic glutamate channels, appear to modulate GlyR-mediated currents (Diana and Bregestovski, 2005; Fucile *et al.,* 2000; Mukhtarov *et al.,* 2005; Ragozzino and Eusebi, 1993; Xu *et al.,* 1999, 2000). The results of these studies are conflicting, arguing in favour of potentiation or inhibition depending on the preparation. In cultured spinal cord neurons, in brainstem motoneurons and in recombinant systems internal Ca^{2+} was shown to potentiate glycinergic responses (Fucile *et al.,* 2000; Mukhtarov *et al.,* 2005). This enhancement is associated with an increase in the apparent affinity of GlyRs for glycine and has been hypothesized to be mediated by the Ca^{2+}-dependent dissociation of a cytoplasmic factor from the GlyR (Diana and Bregestovski, 2005; Fucile *et al.,* 2000).
- Phosphorylation: Consensus sites for phosphorylation (by PKC, PKA, CaMKII and PTK) are present in the TM3-TM4 cytoplasmic loop; in addition to that kinases can modulate GlyR

function through other proteins such as gephyrin (Zita *et al.,* 2007). Modulation by phosphorylation appears to be tissue-dependent (Legendre, 2001; Lynch, 2004). For example, phosphorylation by PTK or PKC enhances glycine-induced currents in hippocampal neurons (Caraiscos *et al.,* 2002; Schönrock and Bormann, 1995) but PKC-mediated phosphorylation depresses glycinergic IPSCs in the spinal cord (Albarran *et al.,* 2001; Tapia *et al.,* 1997; Vaello *et al.,* 1994). Activation of PKA instead had opposite effects on the same preparation (Tapia *et al.,* 1997; Vaello *et al.,* 1994). Phosphorylation also appears to increase the rate of receptor desensitization and slow the recovery from desensitization and the deactivation of glycinergic currents (Gentet and Clements, 2002).

- G-proteins: βγ subunits enhance glycinergic currents in spinal neurons and recombinant systems via an increase in the apparent affinity of the receptors for glycine and an increase in the probability of channel opening. The interaction is mediated by two basic amino-acid motifs in the TM3-TM4 loop of the α1 subunit (Yevenes *et al.,* 2003, 2006).
- Protons: There is evidence that protons antagonize the binding of zinc to its inhibitory site: lowering the external pH inhibits glycine currents and also results in a reduced inhibition by zinc of recombinant GlyR (Harvey *et al.,* 1999). In the spinal cord reduction of the extracellular pH causes a reversible inhibition of both evoked and spontaneous GlyR-mediated currents, whereas the opposite occurs at high pH (Li *et al.,* 2003). Proton sensitive sites have been identified in the N-terminal domain of both the α1 and the β subunit and mutations on these residues cause a reduction in proton sensitivity to variable extents (Chen *et al.,* 2004; Chen and Huang, 2007).

Other substances are known to modulate GlyRs, but less is known of their mechanism of action: neurosteroids (Laube *et al.,* 2002; Maksay *et al.,* 2001), substance P (Wang *et al.,* 1999), melatonin (Wu *et al.,* 2000), tropeines (Maksay *et al.,* 2004), alcohol and anaesthetics (for reviews see Cascio, 2006; Laube *et al.,* 2002).

1.2.7 Pharmacology

i. Glycine and partial agonists

Irrespective of the expression system or the receptor subtype, glycine is a highly potent, full agonist for GlyRs (Legendre, 2001; Lynch, 2004). Other amino-acids acting on GlyRs are β-alanine, taurine and GABA, with the rank order of potency being: glycine > β-alanine > taurine

> GABA (Figure 1.5; de Saint Jan *et al.*, 2001; Fucile *et al.*, 1999; Horikoshi *et al.*, 1988; Lewis *et al.*, 1991).

The concentration of taurine in the developing CNS is approximately 5-fold higher than in the adult, reaching the millimolar range, making it a good candidate for the activation of GlyRs during development (Flint *et al.*, 1998; Mori *et al.*, 2002). The actions of taurine on GlyRs (and on GABARs) have been well documented in most brain regions including the spinal cord (Baev *et al.*, 1992), the retina (Balse *et al.*, 2006; Pan and Slaughter, 1995; Young and Cepko, 2004) and the brainstem (Kontro and Oja, 1987; Ren and Greer, 2006). Similarly to taurine, β-alanine can also act on $GABA_A$ receptors (Horikoshi *et al.*, 1988; Tokutomi *et al.*, 1989). Both taurine and β-alanine have high-affinity transporters in the mammalian brain (Liu *et al.*, 1992; Smith *et al.*, 1992). GlyRs can also be activated by GABA (David-Watine *et al.*, 1999; de Saint Jan *et al.*, 2001; Fucile *et al.*, 1999). Despite the wide distribution of taurine or β-alanine however, there is no evidence yet to show that either of them can mediate synaptic currents at GlyRs. On the other hand, a direct action on synaptic GlyRs of the rat auditory nucleus was recently shown for GABA (Lu *et al.*, 2008; Singer, 2008).

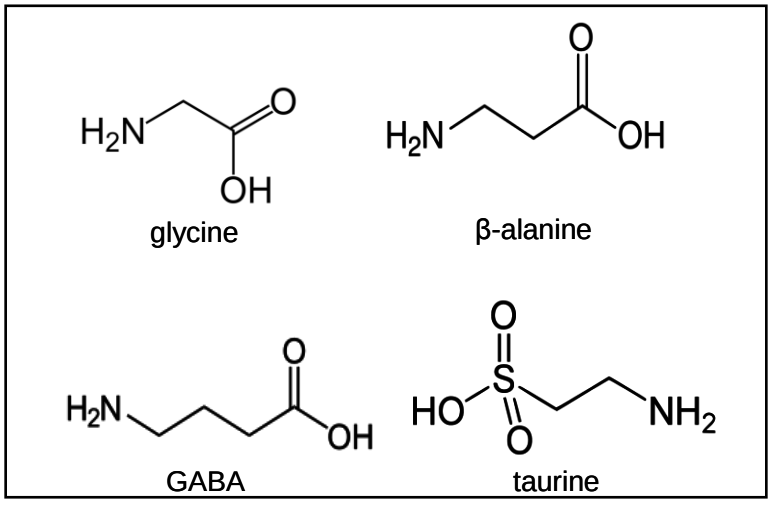

Figure 1.5 Glycine and partial agonists of GlyRs
The chemical structure of endogenous amino-acids acting on GlyRs.

The efficacy of GlyR agonists can vary depending on the expression system or the level of expression (see for example Taleb and Betz, 1994). Therefore, taurine behaves as a full agonist on α1 GlyRs in mammalian cells (Rajendra *et al*., 1995a) but as a partial agonist in oocytes (Schmieden *et al.* 1989, 1992). A recent study on the partial agonism of glycine receptors

showed that taurine is a partial agonist due to of its reduced ability to induce a conformational change in the channel that will lead to opening, compared with glycine (Lape *et al.,* 2008). Variations due to different expression systems have also been reported for the less studied α2 and α2β subtypes (Farroni and McCool, 2004).

ii. Picrotoxin

Picrotoxin (PTX) is a plant alkaloid that exerts its convulsant action by inhibiting $GABA_A$Rs, GlyRs and the invertebrate glutamate receptor chloride channel (Lynch, 2004). PTX is an equimolar mixture of picrotin and picrotoxinin, both of which can inhibit glycine-evoked currents in a manner that depends on receptor subtype (Lynch *et al.,* 1995; Yang *et al.,* 2007). Homomeric GlyRs are very sensitive to PTX (IC_{50} values of 5-10 μM) in difference to heteromeric channels which are less sensitive (Pribilla *et al.,* 1992). A series of side-directed mutations identified amino-acids within the TM2 region of the β subunit which confer resistance to PTX to heteromeric GlyRs (Pribilla *et al.,* 1992). Thereafter, a series of studies investigating the effects of PTX inhibition have tried to elucidate the location of the binding site and characterise the mechanism of action of this compound (Hawthorne and Lynch, 2005; Shan *et al.,* 2001; Wang *et al.,* 2006; Yang *et al.,* 2007). PTX inhibition is highly sensitive to point mutations at residues 2´ and 6´ of the TM2 (Figure 1.4; Shan *et al.,* 2001; Wang *et al.,* 1995; Xu *et al.,* 1995) and the initial hypothesis was that PTX binds in the channel pore and acts as an open-channel blocker (Cascio, 2006 Lynch, 2004). However, recent evidence suggests that the mechanism of action on GlyRs is more complicated and may differ across different anionic channels, ranging from channel block to an allosteric mechanism of inhibition (see Hawthorne and Lynch, 2005; Lynch *et al.,* 1995; Wang *et al.,* 2006; Yang *et al.,* 2007).

iii. Strychnine

Strychnine is a plant alkaloid acting as a high-affinity competitive antagonist of GlyRs. It can selectively antagonise both glycine and partial agonists with a dissociation constant of 2-15 nM (Lewis *et al.,* 1998; Legendre, 2001; Lynch, 2004). Due to its selective action on GlyRs, it is the only known tool, to date, to distinguish between Gly- and GABA-mediated inhibitory neurotransmission in the CNS. Based on this, it has been used extensively for the purification and localisation of GlyRs in the brain and spinal cord (see sections 1.2.2-1.2.4). Different strychnine analogs have also been developed and their actions tested (reviewed in Rajendra *et al*., 1997).

1.2.8 Glycine receptor-related diseases

Defects in GlyR function in humans, mice and cattle can lead to startle diseases. Human hyperekplexia is a neurological disorder characterised by excessive responsiveness to startle, usually accompanied by muscle rigidity and in severe cases by stiffness in the neonatal period. Many mutations in either the α1 or the β subunit of GlyR are known to cause hyperekplexia (Kwok *et al.,* 2001; Lynch, 2004), usually by reducing the expression of GlyRs or by impairing gating. This reduces the effectiveness of inhibitory neurotransmission during a reflex, which increases the frequency of excitation of motoneurons (Bakker *et al.,* 2006; Lynch, 2004). In humans these mutations can either be hereditary (major and minor phenotype), or sporadic (Bakker *et al.,* 2006). The most common cause of hereditary hyperekplexia is a point mutation at Arg271 (Figure 1.2) in α1 (Kwok *et al.,* 2001; Langosch *et al.,* 1994; Rajendra *et al.,* 1994; Shiang *et al.,* 1993). Most of the identified autosomal dominant mutations have been localized either in the TM1-TM2 or the TM2-TM3 loop (reviewed in Lynch, 2004; Zhou *et al.,* 2002) suggesting that hyperekplexia can be related with a distortion in the allosteric mechanism of gating (Lewis *et al.,* 1998; Lynch *et al.,* 1997). Sporadic cases of hyperekplexia, with similar symptoms as the hereditary forms, have also been identified, resulting from mutations in GlyR genes or from mutations in GlyR-related proteins such as glycine transporters or gephyrin (Bakker *et al.,* 2006; Eulenburg *et al.,* 2006; Rees *et al.,* 2003).

In mice, three naturally-occurring mutations result in startle syndromes with symptoms similar to those of human hyperekplexia. The *spastic* mutation is an insertion of a ~7 kb repeating element in the GlyR β gene, leading to inappropriate splicing and to reductions in the levels of the β subunit (Kingsmore *et al.,* 1994; Mülhardt *et al.,* 1994). This subsequently affects the ability of receptors to cluster in synapses. The *spasmodic* mouse results from a point mutation (Ala52Ser) in α1, which leads to a 6-fold reduction in glycine sensitivity (Graham *et al.,* 2006; Ryan *et al.,* 1994; Saul *et al.,* 1994). A detailed kinetic analysis showed that the mutation decreases the ability of the receptor to acquire a pre-opening conformation that enables the channel to open after glycine binding (Plested *et al.,* 2007; see also Steinbach, 2007). The third startle case is that of *oscillator* mice, caused by a frameshift mutation in the TM3-TM4 loop of the α1 subunit, resulting in a drastic reduction in the surface expression of GlyRs (Kling *et al.,* 1997; Buckwalter *et al.,* 1994). This is the only GlyR mutation with a lethal phenotype. Mutant mice differ from human hyperekplexia cases in that they have a normal phenotype for up to 3

weeks after birth, until the developmental switch from α2 to α1 subunit is complete at ~P20 (Malosio *et al.*, 1991a).

1.3 Kinetics of GlyRs

1.3.1 Activation mechanism of GlyRs

Studies on cationic pLGICs suggest that the structural link between the binding sites and the transmembrane regions is formed by the interactions between three domains (Figure 1.6): the pre-TM1 region (β-sheet 10), the loop 2 (which connects the first and second β-sheets) and the TM2-TM3 loop (Lee and Sine, 2005; Lummis *et al.*, 2005; Sine and Engel, 2006; Unwin *et al.*, 2002). Similar conclusions have been drawn for glycine and $GABA_A$ channels (Kash *et al.*, 2003 and 2004; Keramidas *et al.*, 2006; Crawford *et al.*, 2008).According to these studies the binding of the neurotransmitter triggers a wave of conformational changes through the membrane, which begins from the binding site and leads to the opening of the channel pore (Chakrapani *et al.*, 2004; Czajkowski, 2005).

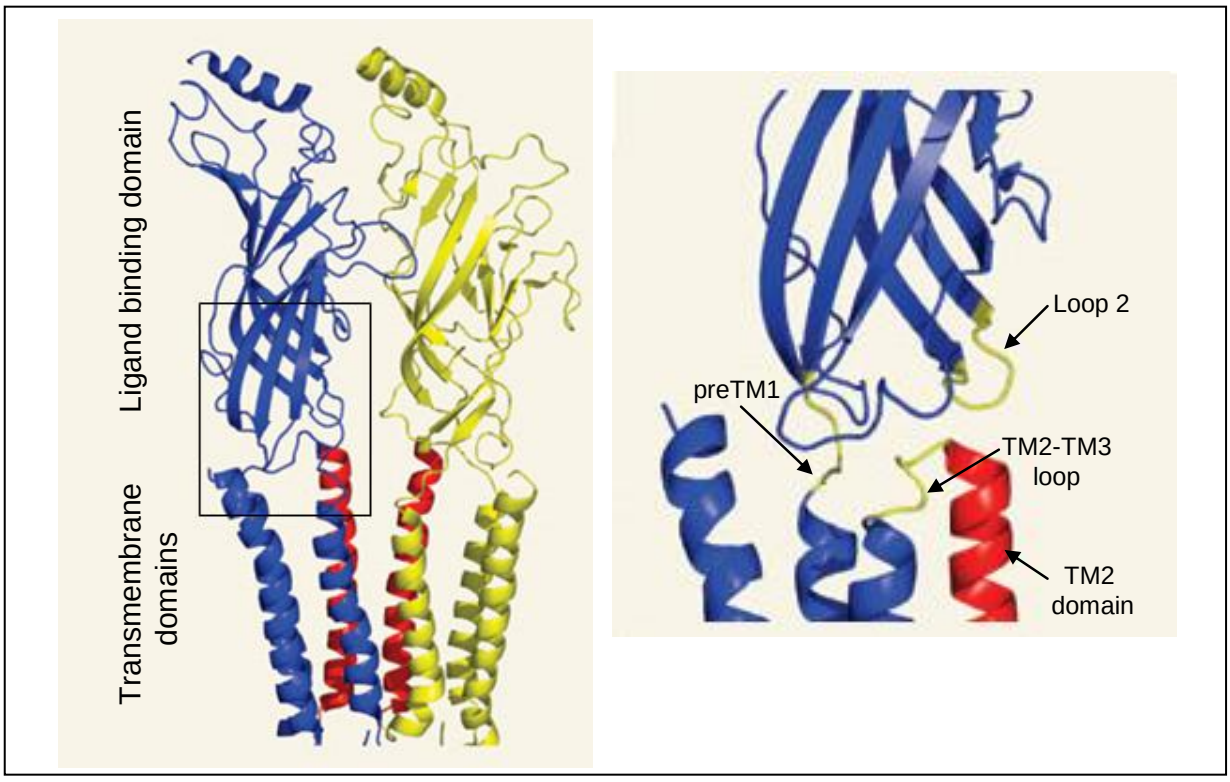

Figure 1.6 From agonist binding to channel gating
On the left is a structural model of two adjacent subunits of the muscle nicotinic receptor built from the AChBP (extracellular domain) and Unwin's model for the transmembrane regions (from Czajkowski, 2005). The TM2 domains are in red. The area in the box is enhanced on the right. In yellow are the three loops involved in the transitions from binding to gating.

Events such as binding, gating and channel activation are not easily discriminated by mere mutagenesis studies if these rely only on macroscopic measurements and the wild-type activation mechanism is poorly characterised (Colquhoun, 1998). Detailed studies have been performed for nicotinic receptors using linear-free energy relationships in combination with single point mutations and single-channel recording, to provide information about the sequence with which the activation wave spreads through the receptor (for examples see Cymes *et al.*, 2002; Grosman *et al.*, 2000).

Alternatively, the role of a residue can be studied by characterizing the channel activation mechanism by single-channel recording from wild-type and mutant receptors. The simplest mechanism of LGIC activation, shown in Figure 1.7, was introduced by del Castillo and Katz in 1957 (Colquhoun, 2006a). With kinetic models the events of binding and gating can be distinguished: binding is determined by the microscopic dissociation rate constant K_A (where $K_A = k_{off}/k_{on}$) and channel opening by the equilibrium constant for gating E ($E = \beta/\alpha$; Colquhoun, 1998).

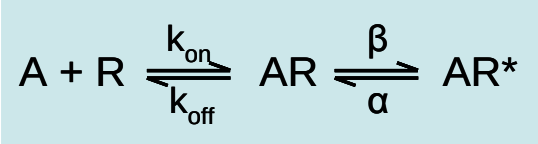

Figure 1.7 A simple mechanism of channel activation
This mechanism was introduced by del Castillo and Katz to describe the activation of muscle nicotinic receptors. It describes how the binding of an agonist (A) to the resting receptor (R) results in a complex (AR) that can undergo the conformational changes that lead to the open state (AR*). Both the equilibrium dissociation constant for binding ($K_R = k_{off}/k_{on}$) and the equilibrium constant for gating ($E = \beta/\alpha$) determine the sensitivity of the receptor for the agonist (Colquhoun, 1998).

The scheme in Figure 1.7 is an over-simplification of the real activation mechanism of any pLGIC, as it assumes a single binding step, a single bound shut state and a single open state and no desensitization.

At present, the most appealing mechanism for describing the activation of GlyRs in a single-channel level is the 'flip' model of Burzomato *et al.* (2004), shown in Figure 1.8. Channel openings can occur from any of three liganded shut states with the efficacy for gating (E) increasing as more glycine molecules bind. Binding of the ligand increases the probability that

the channel is in a higher-affinity shut form (flipped states). A plausible physical interpretation for the flipped states is that they represent the receptor at a point at which the extracellular domain has closed onto the agonist, but the wave of conformational change has not yet reached the channel gate. The 'flip' model describes well all the characteristics of the channel including the EC_{50} and Hill slope values obtained from macroscopic data for both the α1 and α1β channel subtypes (Beato *et al.,* 2004; Burzomato *et al.,* 2004). The model can describe well the behaviour of native GlyRs from spinal cord motoneurons (Beato and Sivilotti, 2007), is equally successful for describing data from mutant GlyRs bearing the spasmodic mouse mutation (Plested *et al.,* 2007) and can be used for describing the action of partial agonists for both glycine and muscle nicotinic receptors (Lape *et al.,* 2008).

The most recent activation mechanism for α2 homomeric GlyRs has been described by Mangin and colleagues (Mangin *et al.,* 2003). This is described more thoroughly in Chapter 3.3.

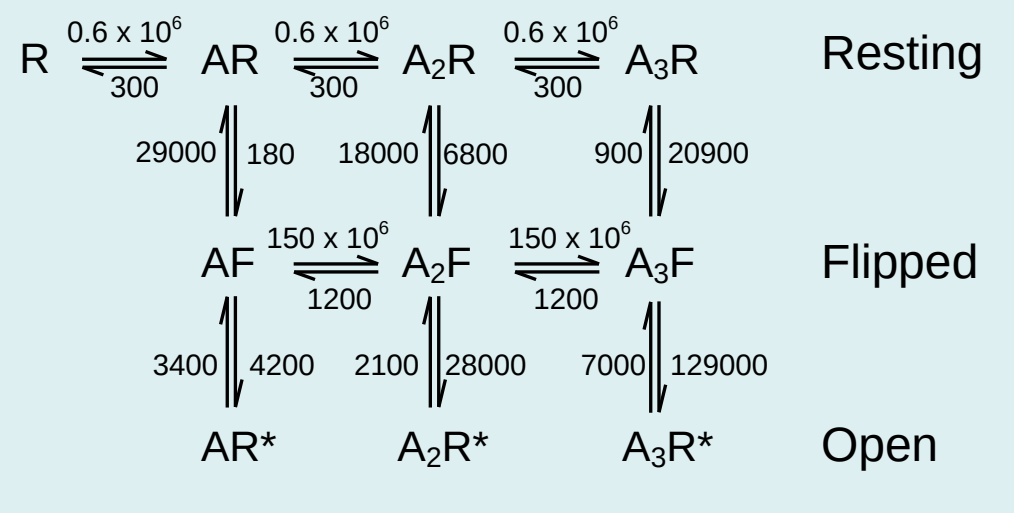

Figure 1.8 The 'flip' mechanism and the reaction rates for α1β GlyRs
This mechanism was suggested by Burzomato *et al.,* (2004) to describe the activation kinetics of α1β GlyRs. It describes the conformational changes that occur in the channel after the binding of up to three glycine molecules, that shift the receptor from the resting states (R) to higher affinity shut states (Flipped), hence enabling the channel to open (R*). For these reaction rates: K_R = 520 μM; K_F = 8 μM; *E*1 = 1.3; *E*2 = 13; *E*3 = 20. All reaction rates are in s^{-1} except the association rate constants for the R and F states, which are in $M^{-1}s^{-1}$ (Burzomato *et al.,* 2004).

1.3.2 Characteristics of glycinergic synaptic currents

The switch from α2 to the expression of α1 subunits at ~P20 in rats (Malosio *et al.,* 1991a) underlies the developmental changes in the time course of the IPSCs. Thus, glycinergic IPSCs progressively become faster (with faster decay rates) as the expression of α1 subunits increases (Ali *et al.*, 2000; Legendre and Korn, 1994; Singer *et al.*, 1998; Singer and Berger, 1999 and 2000). The time course of glycinergic IPSCs is usually characterised by a fast mono-exponential rising phase and a mono- or bi-exponential deactivation phase (Beato, 2008; Burzomato *et al.,* 2004; Legendre, 2001; Singer *et al.,* 1998; Singer and Berger, 1999). The deactivation time constant for spontaneous IPSCs are in the range of 6-10 ms (Burzomato *et al.*, 2004; Singer *et al.,* 1998). The time course of deactivation is now known to be affected by the intracellular chloride concentration (Pitt *et al*., 2008). Glycine is removed from the synaptic cleft with a time constant of 0.3-0.9 ms (Beato, 2008; Clements, 1996; Legendre, 2001; Suwa *et al.,* 2001).

A number of different studies have shown that the amplitude distribution of glycinergic mIPSCs is highly variable and skewed towards big currents but the deactivation kinetics of these currents do not differ, irrespective of amplitude (Legendre and Korn, 1994, 1995; Singer *et al.,* 1998). On the other hand, when responses to concentration jumps are considered, the current amplitude is correlated with differences in the desensitization properties of receptors, with at least two desensitization components being observed when the receptor density is high (Legendre *et al.,* 2002). Information concerning the kinetics of desensitization of GlyRs is still limited (but see Beato *et al.,* 2007; Pitt *et al.,* 2008; see also Mangin *et al.,* 2003).

1.4 Aim

As mentioned previously, adult synaptic GlyRs are α1β heteromers and their stoichiometry is still somewhat uncertain: data on recombinant receptors suggest two possible stoichiometries, 2α1:3β and 3α1:2β. Evidence for the first comes from experiments on oocytes (Grudzinska *et al.,* 2005), whereas a study in mammalian cells favors the latter (Burzomato *et al.,* 2003), raising the possibility that stoichiometry depends on the expression system. The primary aim of my work was to identify the stoichiometry of α1β heteromeric GlyRs in *Xenopus* oocytes. For this purpose I used two independent approaches. The first one involves recording from oocytes expressing heteromers with a reporter mutation in the TM2 domain, which shifts glycine

sensitivity in proportion to the number of mutated subunits in the pentamer. This approach was used for identifying the stoichiometry of many members of the pLGIC family, including α1β GlyRs in HEK293 cells (Burzomato *et al.,* 2003). The second approach involves single-channel recordings from conductance mutants, in a manner similar to that described by Béhé *et al.* (1995) and Cooper *et al.* (1991) for NMDA receptors and α4β2 nicotinic receptors, respectively.

The second objective of my project was to characterize the kinetics of α2 GlyRs in the same way as done for other GlyR subtypes (Beato *et al.,* 2004; Burzomato *et al.,* 2004; Lape *et al.,* 2008). The interest in the α2 subtype arises from the fact that it is likely to be the embryonic subtype in the spinal cord. The kinetic analysis of α2 homomers involved maximum likelihood fitting of a mechanism to single-channels from HEK293 cells. Macroscopic data from glycine concentration jumps were also considered. The model describes the transitions between open, shut and desensitized states of the channel, taking into account the conformational changes that lead from binding to channel opening and the number of functional agonist binding sites in the channel.

Chapter 2: Methods

2.1 Stoichiometry of α1β GlyRs in *Xenopus* oocytes – 9′ mutations

2.1.1 cRNA constructs for oocyte expression

cDNA constructs, containing the coding sequences for the rat GlyR α1 (GenBank accession number AJ310834) and β subunits (accession number AJ310839) and an added Kozak consensus sequence (GCCACC) upstream of the start codon (Groot-Kormelink and Luyten, 1997), were amplified and cloned as described previously (Beato *et al.*, 2002; Burzomato *et al.*, 2003). To facilitate their expression in oocytes the constructs were subcloned into the pSP64T.GL vector, the features of which are shown in Figure 2.1. The constructs were designed using the Vector NTI programme (Suite 5.5, Invitrogen, UK). The 9′ mutations ($\alpha1^{L289T}$, $\alpha1^{L289S}$, β^{L307T} and β^{L307S}; mutants shall be referred to as $\alpha1^{LT}$, $\alpha1^{LS}$, β^{LT} and β^{LS}) were introduced using the QuickChange^{TM} Site-Directed Mutagenesis Kit (Stratagene, UK) and the full-length sequence of each subunit was verified.

In order to proceed to synthesis of capped RNA (cRNA) for expression of the subunits in oocytes, it was first necessary to produce large amounts of stock plasmid DNA. This was done by transforming competent bacterial cells (DH5α *E.coli* cells, Invitrogen, UK) and thereafter purifying the produced plasmids (HiSpeed plasmid Maxi Kit, QIAGEN GmbH). Details of these procedures can be found in Appendix A.

The [insert]/pSP64T.GL constructs were linearized downstream of 3′ UTR (Figure 2.1) and cRNA was transcribed using the SP6 mMessage mMachine Kit (Ambion, UK; see Appendix A). The quality and quantity of each subunit cRNA were checked by RNA gel electrophoresis using the appropriate RNA markers.

2.1.2 *Xenopus laevis* oocyte preparation and cRNA injection

Mature female *Xenopus laevis* frogs (Figure 2.2*A*) were anaesthetized by immersion in ethyl m-aminobenzoate solution (tricaine, methanesulphonate salt, Sigma-Aldrich, UK; 0.2% solution w/v, brought to pH 7.2 by the addition of NaOH) for 30-40 min and were killed by decapitation and destruction of the brain and spinal cord (in accordance with Home Office regulations) before removal of the ovarian lobes. The ovarian lobes were washed thoroughly and clumps of stage V-VI oocytes (Figure 2.2*B*) were dissected in sterile, double-filtered modified Barth's solution consisting of (in mM): NaCl 88; KCl 1; $MgCl_2$ 0.82; $CaCl_2$ 0.77;

$NaHCO_3$ 2.4; Tris-HCl 15; with 50 units/ml of penicillin and 50 mg/ml of streptomycin (Invitrogen, UK) in HPLC water; pH 7.4 was adjusted with NaOH. During the dissection, immature, dead or dying cells were discarded. The remaining oocytes were treated with collagenase (type IA, Sigma-Aldrich; 245 collagen digestion units/ml in 5 ml Barth's solution; 10-12 oocytes/ml; this is a rather mild treatment that does not produce defolliculation on its own) for 50-65 min on an orbital shaker at 18 ^{o}C and 100 rpm, then rinsed several times with fresh Barth's solution and stored at 4 ^{o}C overnight. Prior to cRNA injection, the follicle layer (Figure 2.2*C*) was removed manually from collagenase-treated cells with watchmaker's forceps (Fine science tools, Interfocus).

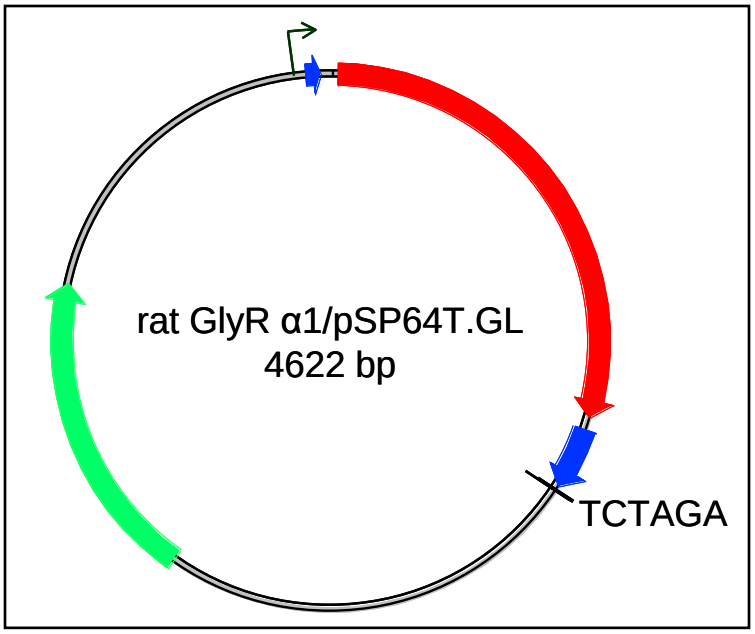

Figure 2.1 The rat α1/pSP64T.GL construct
Features of the pSP64T.GL vector used for oocyte expression of GlyRs. The vector contains 5′ and 3′ untranslated regions (UTRs; blue arrows) for the *Xenopus* β-globin gene (Akopian *et al*., 1996). The coding sequence for the rat α1 subunit (red arrow) is inserted between the two UTRs. The plasmid also contains a prokaryotic promoter (SP6; black arrow), recognized by a RNA polymerase during the *in vitro* transcription reaction and the coding sequence of a gene that provides resistance to ampicillin (green arrow). The linearisation of the construct for the *in vitro* transcription was performed using XbaI (the unique restriction site for the enzyme is indicated by the black line).

Oocytes chosen for injection were placed on a nylon mesh (24 x 15 mm with each square of the grid measuring 1 x 1 mm), glued to a 35 mm Petri dish (Figure 2.2*D*). Injection needles were produced from glass capillaries (3.5" Drummond #3-000-203-G/X, 88.9 x 1.14 x 0.053 mm, Drummond Scientific Co). These were pulled, broken to form a staggered tip of 12-16 µm

and finally forged into the shape of a hypodermic needle, to minimize damage to the oocyte membrane. The needles were backfilled with RNase-free mineral oil (Sigma-Aldrich, UK) and loaded from the tip with the appropriate cRNA combination (Table 2.1). The cRNA mixtures were injected into the cytoplasm (vegetal pole, Figure 2.2*D*) with a Nanoject automatic oocyte Injector (Drummond Scientific, Broomall, PA). The success of the injection was confirmed visually by a real-time increase in the cell diameter. All cRNA aliquots were freshly defrosted from -80 ºC and kept on ice during the procedure. The injections were done under sterile conditions in order to avoid cRNA degradation and/or infection of the injected cells.

Table 2.1 Wild-type and/or 9´ mutant cRNA combinations use for injections.

cRNA combination	**α1:β concentration for injection (ng/µl)**	**Oocyte batches (N)**
α1	0.5	2
α1+β	0.5:20	5
$\alpha1^{LT}$	0.5, 2, 5, or 8	2
$\alpha1^{LT}$+β	0.5:20, 1:40 or 2:80	2
α1+β^{LT}	0.5:20 or 2:80	6
$\alpha1^{LT}$+β^{LT}	0.5:20 or 1:40	2
$\alpha1^{LS}$	0.5, 5 or 8	2
$\alpha1^{LS}$+β	0.5:20	2
α1+β^{LS}	0.5:20	2
$\alpha1^{LS}$+β^{LS}	0.5:20 or 1:40	2

After injection the oocytes were incubated (in individual wells of a multiwell plate) for ~48-60 hrs at 18 ^{o}C in Barth's solution containing 5% heat-inactivated horse serum to improve oocyte health (Gibco BRL; Boorman *et al*., 2000) and then stored at 4 ^{o}C. Experiments were carried out at 18 ^{o}C between 2.5 and 5 days from injection. The total amount of cRNA injected per oocyte (in 46 nl of RNase-free water) was determined empirically, with the aim of achieving a maximum glycine-evoked current that would not exceed 1 µA (to contain the series resistance error to an acceptable size). For all α1+β combinations, the α1:β ratio of cRNA in a mixture

was kept constant at 1:40, in order to avoid contamination by α1 homomeric receptors, in the hope of forcing oocytes to express a predominantly heteromeric receptor population (this is successful in HEK293 cells, see Burzomato *et al.*, 2003).

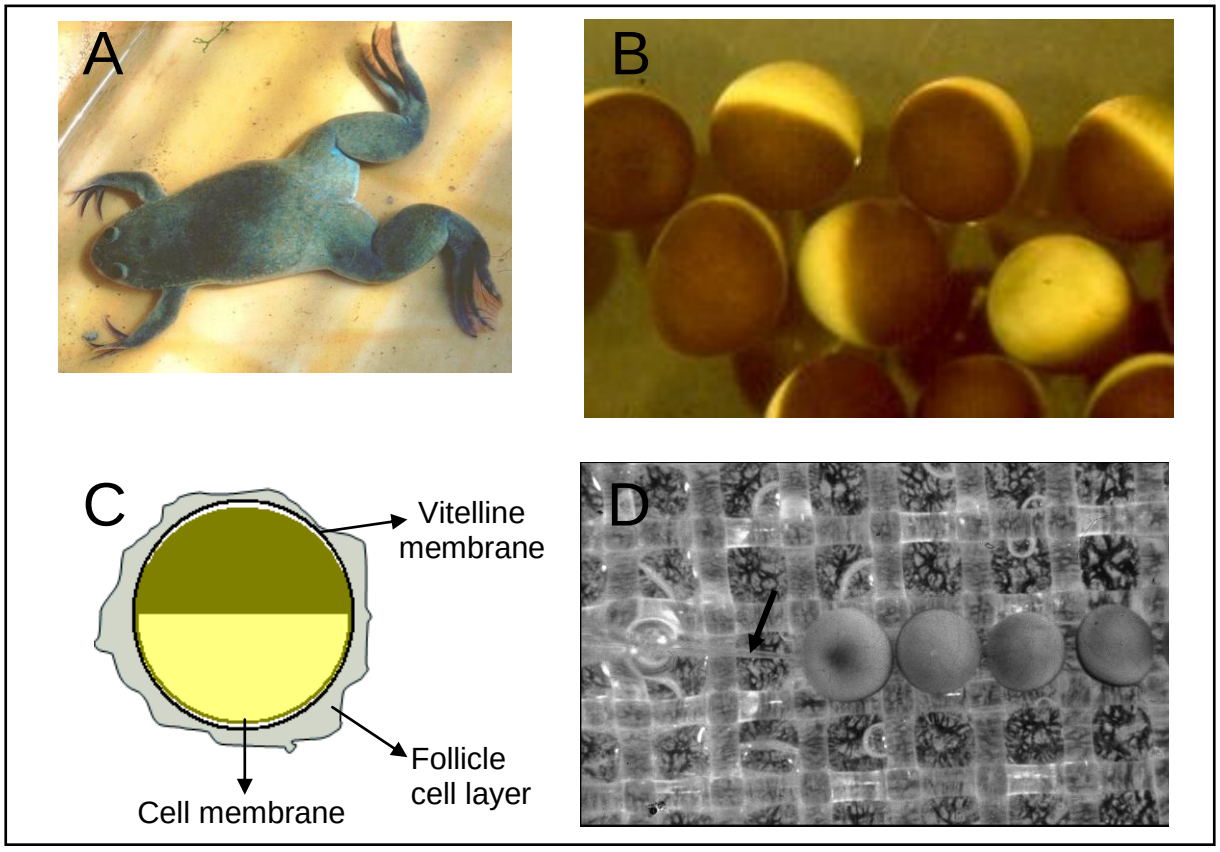

Figure 2.2 The *Xenopus laevis* oocyte as an expression system
A, The South African clawed frog, *Xenopus laevis*. *B*, Mature, stage V-VI oocytes with well-defined animal (dark green) and vegetal hemispheres (yellow). *C*, Representation of an oocyte with its surrounding layers: the vitelline layer surrounds the cell membrane and is removed prior to patching whereas the outer layer of follicle cells is removed manually after enzymatic treatment. *D*, Cytoplasmic injection of oocytes with cRNA: the cells are placed on a nylon mesh glued on a Petri dish. The arrow indicates the injection needle (from Sigel and Minier, 2005).

2.1.3 Electrophysiological recordings – TEVC

The collagenase treatment is performed for stripping off the follicle cells that surround the oocyte and are coupled with it via gap junctions (Figure 2.2*C*). This ensures that the electrical coupling does not interfere with the signal recorded from oocytes; also, the removal of the follicular layer allows an easier impalement with the electrodes. The large size of the oocyte (diameter ~1.2 mm) makes it ideal for two-electrode voltage clamp recording (TEVC). Each

cell used for recording was held in a circle of insect pins, positioned in a thick Sylgard® layer coating the floor of a 0.2 ml bath. Cells were continuously superfused (4.5-5 ml/min) with modified Ringer solution composed of (in mM): NaCl 150; KCl 2.8; $MgCl_2$ 2; $CaCl_2$ 1; HEPES 10; pH 7.2 adjusted with NaOH. All recordings were done at 18 ^oC. Cells were voltage-clamped at -70 mV with the TEVC mode of an Axoclamp 2B amplifier (Molecular Devices, CA). Electrodes were pulled from filamented, thin-walled borosilicate glass (GC150TF, Warner Instrument Corp.) and backfilled with 2 M potassium acetate. Their resistance did not exceed 1 MΩ on the current-passing side. Recordings were not started if the holding current exceeded -200 nA (in the absence of agonist). Such cells were discarded.

Concentration-response curves were obtained by decreasing the concentrations of glycine, freshly prepared from frozen stock aliquots with Ringer solution, and applied at 5 min intervals via the bath perfusion. These intervals were sufficient to ensure reproducible responses. Glycine (Fluka) was applied for a period sufficient to obtain a stable plateau response or the beginning of a sag after a peak (at low or high concentrations respectively). Currents were recorded on a flat bed chart recorder (Kipp & Zonen) and on a computer (Clampex 9 software, Molecular Devices, CA). To compensate for rundown throughout each experiment, a standard glycine concentration (~EC_{30} for each combination) was applied every third response. The experiment was started only after checking that this standard gave reproducible responses and was compensated for rundown only if this did not exceed ~30% from the first to the second standard; otherwise the experiment was stopped. For rundown corrections see Appendix B.

Picrotoxin (Sigma-Aldrich, UK) concentration-inhibition curves for cells injected with α1 or α1+β were obtained as follows: a standard glycine concentration (100 μM; ~EC_{50} of α1 GlyRs) was applied at the beginning of each experiment and then increasing concentrations of PTX were co-applied with the standard (PTX/Gly). Each PTX application started 5 minutes before each PTX/Gly application, to ensure PTX equilibration. The standard glycine (in the absence of PTX) was repeated every third response; this was done after 5 min perfusion with control Ringer solution, to wash out any remaining PTX. Experiments with more than a 30% (α1) and 40% (α1β) decrease in the current from the first to the second standard were discarded: in the experiments chosen for fitting, there was an average of 22.6% (for α1, n = 3) and 38.5% (for α1+β, n = 4) decrease from the initial control current. For all combinations data were obtained from more than one oocyte batch in order to ensure reproducibility of results.

2.1.4 Data Analysis – Curve fitting

Concentration-response curves were plotted using the responses to different glycine concentrations (after corrections for rundown). Each curve was then fitted to the Hill equation:

$$I = I_{\max} \frac{[A]^{n_H}}{[A]^{n_H} + EC_{50}{}^{n_H}} \qquad \text{[eq.3]}$$

where I is the measured current, I_{max} is the maximum current, [A] is the agonist concentration, n_H is the Hill coefficient and EC_{50} is the agonist concentration for 50% of the maximum response. Each experiment was fitted separately by equally weighted least squares, using the program CVFIT (Colquhoun and Vais; http://www.uc.ac.uk/pharmacology/dc.html). The curve parameters calculated by the program are I_{max}, n_H and EC_{50}. Numbers in the text are means ± standard deviation of the mean (SEM) from the individual fits of each experiment. For each experiment, responses were normalized to the fitted I_{max} of the same experiment; normalized responses from all experiments were then pooled, giving an average concentration-response curve. These were fitted again to the Hill equation, for the purpose of display in figures.

Concentration-inhibition curves to PTX were fitted to the Hill equation (eq.3). The curve parameters calculated by CVFIT in this case are I_{max}, n_H and IC_{50} (the concentration of picrotoxin at 50% of inhibition). The average parameters for each combination (Table 3.1, Chapter 3) and the plots of the pooled normalized values (Figure 3.2, Chapter 3) were obtained as above. PTX experiments from α1+β injected cells were also fitted with a two-component Hill equation:

$$I = r \frac{IC_{50_1}{}^{n_{H1}}}{IC_{50_1}{}^{n_{H1}} + [B]^{n_{H1}}} + (1-r) \frac{IC_{50_2}{}^{n_{H2}}}{IC_{50_2}{}^{n_{H2}} + [B]^{n_{H2}}} \qquad \text{[eq.4]}$$

where I is the normalized glycine current measured at its peak; [B] is the picrotoxin concentration; IC_{50_1} and IC_{50_2} are the antagonist concentrations (for 50% inhibition) for the first and second component, respectively; n_{H1} and n_{H2} are the Hill coefficients for the two components and r is the ratio between the amplitudes of two components. The two-component fits were done in order to check for contamination by α1 homomers. Two-component free fits gave poorly defined parameters. Each experiment was therefore re-fitted, by constraining the first component's parameters to be equal to those obtained from the free fits of the α1 receptor experiments. Even so, these fits were also poorly defined.

Significance tests were performed using Students' t test and a one-way nonparametric ANOVA followed by Bonferroni's post hoc multiple comparison test (GraphPad Prism 4, GraphPad Software).

2.2 Stoichiometry of α1β GlyRs - conductance mutations

2.2.1 Chimeric GlyR subunit constructs

Two chimeric subunits (Figure 2.3*A*) were chosen for the conductance experiments in oocytes: (i) the rat GlyR β subunit with the TM2 domain of the rat GlyR α1 (named β^{Ch}) and (ii) the rat GlyR α1 subunit containing the TM2 domain of the rat GlyR β subunit ($\alpha1^{Ch}$). Figure 2.3*B* shows the exact amino-acid residues that have been exchanged between the two subunits. The chimeric constructs were created by Dr. Fe Abogadie. Subcloning in the pSP64T.GL vector and cRNA production followed the procedure described in sections 2.1.1 and Appendix A.

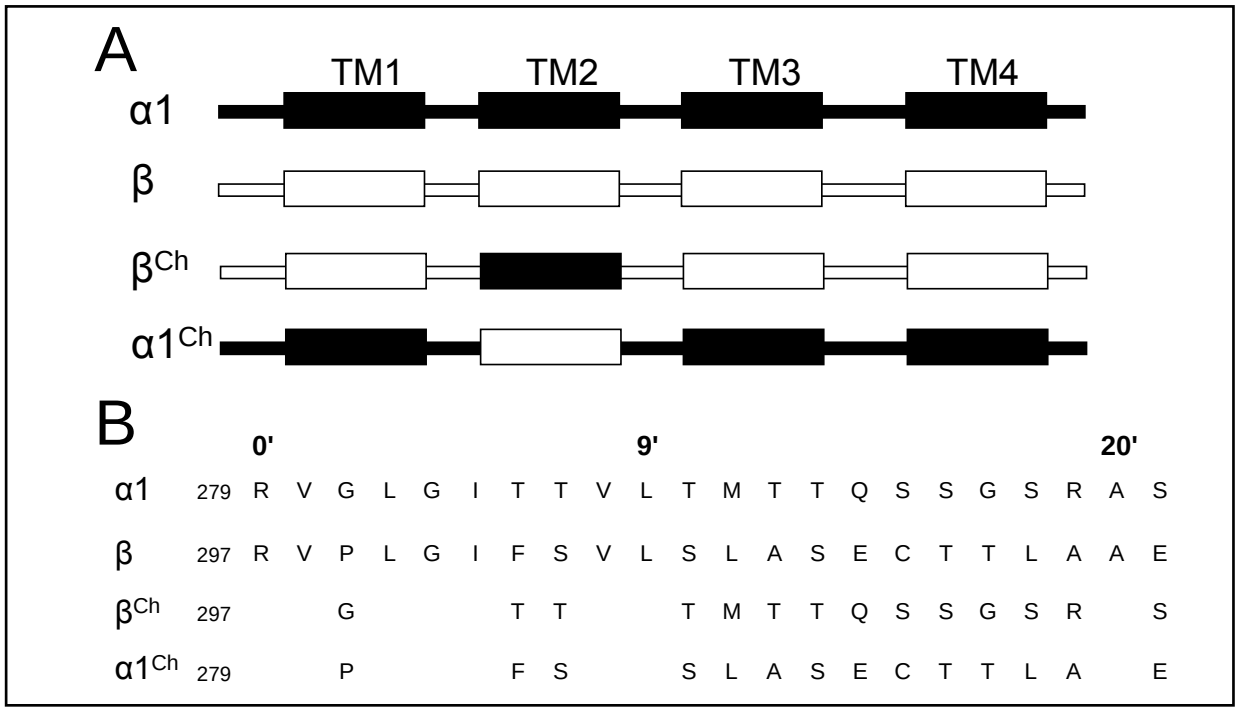

Figure 2.3 Chimeric GlyR subunit constructs
A, Structure of the chimeric constructs: the β^{Ch} is identical to the rat wild-type subunit but contains the TM2 domain of α1. Similarly, the $\alpha1^{Ch}$ contains the TM2 domain of β. *B*, The amino-acid sequence of the TM2 domain for the rat α1 and β subunits (top two lines). The bottom two lines show the amino-acids that were exchanged between the two subunits for the creation of the TM2 chimeras. Note that the last amino-acid (position 21′) was also exchanged, in agreement with Bormann *et al*. (1993).

For transient expression in human embryonic kidney cells (HEK293) the coding sequences for the rat GlyR α1, β, $\alpha1^{Ch}$ and β^{Ch} subunits, with the Kozak consensus sequence (GCCACC) added upstream of each codon, were cloned into the pcDNA3.1 vector. The features of a [insert]/pcDNA3.1 construct are described in Figure 2.4. The full-length sequence of each cDNA was verified by sequencing.

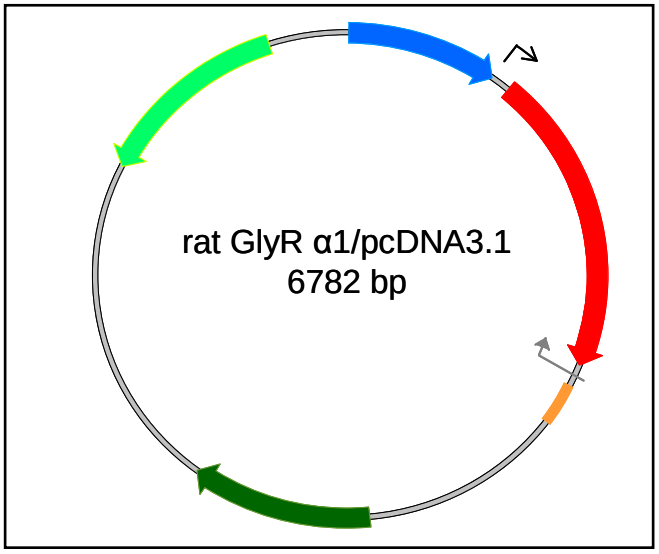

Figure 2.4 The rat α1/pcDNA3.1 construct
The pcDNA3.1 vector contains a viral promoter (cytomegalovirus promoter, CMV; blue arrow) which can drive the expression of the inserted α1 gene in HEK293 cells. The coding sequence for the rat α1 subunit (red arrow) is inserted immediately after the promoter. The plasmid also contains two prokaryotic promoters (T7 and SP6; black and grey arrows respectively), a polyA signal for the bovine growth hormone (orange line) and the coding sequences for genes that provide resistance to ampicillin (dark-green arrow) and neomycin (light-green arrow).

2.2.2 Oocyte injections with cRNA

Oocytes were prepared and injected as previously described in section 2.1.2. Table 2.2 summarizes the injected cRNA combinations. As mentioned previously I wanted to avoid the contamination of the experiments by homomeric receptors. The cRNA mixtures (in 46 nl of RNase-free water per oocyte) were therefore prepared by maintaining a ratio of 1:40 for α1+β combinations and 1:40:40 for $\alpha1+\beta+\beta^{Ch}$. For the latter combination I also tested a ratio of 1:10:10 and 1:20:20.

Table 2.2 Wild-type and/or TM2 chimeric cRNA combinations used for injections.

cRNA combination	α:β or α:β:β concentration (ng/μl)	Oocyte batches (N)
α1	2 or 3	4
α1+β	1:40 or 2:80	5
$\alpha1+\beta^{Ch}$	1:40, 2:80 or 3:120	8
$\alpha1^{Ch}$	2 or 10	2
$\alpha1^{Ch}+\beta$	2:80	2
β^{Ch}	2	1
$\alpha1+\beta+\beta^{Ch}$	1:40:40, 2:80:80, 3:30:30 or 2:40:40	7

2.2.3 Culture and transfection of HEK293 cells

Flasks of HEK293 cells (American Type Culture Collection-CRL-1573; LGC Promochen, Teddington, UK) were maintained in a humified incubator at 37 °C (95% air and 5% CO_2). Cells were cultured in Dulbecco's modified Eagle's medium (DMEM) supplemented with sodium pyruvate (0.11 g/l), heat-inactivated fetal bovine serum (10% v/v) and penicillin G (100 units/ml)/streptomycin sulphate (100 μg/ml), all purchased from Invitrogen, UK. Passaging of cells was performed every 2-3 days and up to 30 times (see Appendix A for a standard passaging protocol). Cells were plated on sterile glass coverslips (13 mm diameter, sterilized over flame) which were placed in 35 mm sterile Petri dishes containing 1.5-2 ml of DMEM. Plating was performed 4-6 hours before transfection to allow cells to attach. Transfection was by calcium phosphate-DNA co-precipitation (Groot-Kormelink *et al.*, 2002). Briefly: the cDNA mixture for each combination was added to $CaCl_2$ solution (340 mM in sterile water) at a volume ratio of 1:5 respectively. The DNA/$CaCl_2$ mixture was added drop-by-drop in an equal volume of 2x Hank's buffered saline (HBSS containing: 280 mM NaCl, 2.8 mM Na_2HPO_4, 50 mM HEPES, pH 7.2 with NaOH) to form the precipitate. The final mixture was then added dropwise over the plated cells.

The total amount of the cDNA mixture per plate was kept constant at 3 μg. The composition is shown in Table 2.3. For the transfection of the $\alpha1+\beta+\beta^{Ch}$ cDNA combination I used an overall

subunit cDNA ratio of 1:40 (α1: total β) to minimize the contamination by homomers (Burzomato *et al.,* 2003). The cDNA mixture also included a plasmid (pEGFP-c1; BD Biosciences, UK) which contains the coding sequence for the enhanced green fluorescent protein (e-GFP) with the added Kozak sequence immediately upstream of the start codon and the mammalian cytomegalovirus promoter (CMV). Expression of the fluorescent marker allowed the detection of transfected cells. After transfection the cells were incubated for at least 10 hours (37 ^{o}C, 95% air and 5% CO_2), then washed repetitively with HBSS (to remove the remaining precipitate) and finally were left to rest in 2 ml of DMEM. Recordings were performed 2-3 hours after washing and for not more than 3 days after transfection.

Table 2.3 Composition of the α1+β+β^{Ch} cDNA mixture for HEK293 cell transfection.

Plasmid DNA	**α1 + β + β^{Ch}**
[α1]/pcDNA3.1	2%
[β]/pcDNA3.1	40%
[β^{Ch}]/pcDNA3.1	40%
pEGFP-c1	18%

2.2.4 Test of expression – TEVC recordings from oocytes

Before proceeding to single-channel recording I checked whether the chimera-containing combinations produced sufficient current. I tested this by bath-applying 1 mM glycine (in Ringer solution) and measuring the macroscopic current using TEVC. Cells were held at -70 mV. The four combinations tested were: α1+β^{Ch}, β^{Ch}, $\alpha1^{Ch}$ and $\alpha1^{Ch}$+β. The concentrations of the cRNA mixtures for each combination are the lowest ones shown in Table 2.2, except in the case of $\alpha1^{Ch}$ where both concentrations were tested. In order to make sure that the very low or absent responses to glycine in the case of the $\alpha1^{Ch}$ and $\alpha1^{Ch}$+β combinations really mean that these receptors are not functional and are not a chance finding due to bad oocyte health or low expression efficiency for the given batch, these experiments were done in two different oocyte batches. In every batch I also injected a highly expressing combination (α1+β, 1:40 ng/μl, 46 nl per oocyte) to compare the expression levels with those from the four combinations.

2.2.5 Single-channel recordings from oocytes

Recordings were obtained in the cell-attached and in the outside-out configuration. For both cases, oocytes were stripped of their vitelline membrane (Figure 2.2*C*) immediately before patching to ensure a clean cell membrane and the formation of a gigaohm seal (Hamill *et al.*, 1981). Devitellinization was achieved by incubating the oocyte for 5-10 minutes in hyperosmotic Barth's solution (3-5 ml of Barth's solution and 1 ml of sucrose, 1 M), followed by manual removal of the vitelline membrane with sharp-tipped watchmaker's forceps. All recordings were performed at 18 ^{o}C.

i. Cell-attached single-channel recordings – current/voltage plots

Oocytes were bathed in a high potassium solution to drive the oocyte resting membrane potential to a consistent value, close to 0 mV. The solution contained (in mM): KCl 150; HEPES 10; EGTA 10; pH 7.2 adjusted with KOH.

Because I was interested in measuring single-channel conductances, I did not want to depend on the oocytes' internal concentration of chloride, which may vary between cells (or batches) and could be limiting the measured conductance of the channels. I therefore set up conditions that would allow the measurement of chloride currents without any limitations from the oocyte: 1. patches were held at a positive holding potential (i.e. negative pipette potential), which forces chloride ions to flow from the pipette to the cell. This current is not influenced by differences in internal chloride concentrations between different cells. 2. To increase the driving force for chloride, the pipette solution contained a high concentration of chloride. Bormann *et al.* (1987) reported a half-saturating chloride concentration of 108 mM for GlyRs in outside-out patches. Hence, electrodes were back-filled with (in mM): KCl 200; HEPES 10; EGTA 10; pH 7.2 adjusted with KOH. The pipette solution also contained 1 mM glycine; at this concentration channel openings occur in clusters. The pipette solution was freshly thawed from frozen aliquots. For the $\alpha1+\beta+\beta^{Ch}$ combination I also tested a glycine concentration of 50 μM (see results).

Patch pipettes were pulled from thick-walled, filamented borosilicate glass (GC150F, Harvard Apparatus) and coated near the tip with Sylgard^{TM} (Dow Corning) for improving their dielectric properties. Prior to use each electrode was fire-polished to maintain a clean tip for the formation of a giga-ohm seal. The final resistance of the electrodes was 4-10 MΩ.

For each current/voltage (I/V) plot single-channel currents were obtained at holding potentials ranging from 0 to +70 mV (ie. pipette potentials of 0 to -70 mV). As I increased the holding potential, in some patches I observed a high frequency of channel openings, attributable not to GlyRs but to endogenous stretch channels. These channels, well characterized by Yang and Sachs, (1990) and Methfessel *et al.* (1986) are easily distinguishable from GlyRs. Despite this, all patches in which these channels were detected were discarded.

ii. Outside-out single-channel recordings – chord conductance measurements

Oocytes were bathed in a modified Ringer's solution containing (in mM): NaCl 150; KCl 2.8; $MgCl_2$ 1; $CaCl_2$ 2; HEPES 10; pH 7.4 adjusted with NaOH; ~305 mOsm osmolarity. Glycine (1 mM in extracellular solution) was applied in the superfusant with exchange time of ~2 minutes. All outside-out experiments were performed at a holding potential of -100 mV. Electrodes were prepared as described for the cell-attached experiments. They had a resistance of 10-15 MΩ and were backfilled with (in mM): CsCl 120; TEA-Cl 20; $CaCl_2$ 1; $MgCl_2$ 2; HEPES 10; EGTA 11; pH 7.2 with CsOH; osmolarity was adjusted with sucrose to be equal or higher than the bath solution's (~310-315 mOsm) to increase the stability of the excised patch. Glycine was applied only after ensuring that no single-channel activity was detected when the patch was kept in bath solution for at least 1 minute. Due to the bigger membrane surface compared with cell-attached patches, often many channels were simultaneously open in outside-out patches. I did not record unless well separated clusters were detected.

All solutions used for single-channel recording (in both configurations) were prepared using HPLC-grade water (VWR, UK) to minimize contamination by glycine and were filtered through a 0.2 μm cyclopore™ track-etched membrane (Whatman International Ltd, Maidstone, UK) to remove impurities that can block electrodes or affect the quality of the seal. To ensure a high signal-to-noise ratio, the level of the bathing solution was kept as low as possible. In the case of outside-out recording the excised membrane patch was lifted to just under the surface of the solution, to minimize the pipette capacitance and to reduce noise. The quality of every patch was checked immediately after sealing, by observing the noise meter on the amplifier (I_{RMS}); patches were discarded if the noise on the meter exceeded 0.27 pA after the holding potential was applied. Single-channel currents were recorded with an Axopatch 200B amplifier, pre-filtered at 10 kHz using the amplifier's 4-pole Bessel filter (Molecular Devices, CA) and saved on a digital audio tape with a DRA-200 digital tape recorder (Bio-Logic

Science Instruments, Claix, France). For off-line analysis each record was replayed from the tape, filtered at 3 kHz with an 8-pole Bessel filter and digitized at 33 kHz with a Digidata 1322A using Clampex software (both from Molecular Devices, CA).

All single-channel data were analyzed by cursor measurement of amplitudes using the event detection mode of Clampfit 9.2 software (Molecular Devices, CA).

iii. Analysis of cell-attached recordings

Each cluster in a patch was analyzed individually. Events shorter than 10 ms (for 1 mM patches, both configurations) were ignored. During the scan dubious events (double openings, baseline breakdowns etc.) were rejected. At the end of the scan a list of all events per amplitude level is created. For all cell-attached experiments (1 mM Gly) there was always only one main level of opening for each cluster. Any other levels, attributed to 'subconductances', appeared rarely (<1% of events) and hence were excluded from the analysis (rejected during the scan). From the list of amplitudes measured by the software I calculated the average amplitude for each cluster. For each holding potential, clusters were separated into groups of similar mean amplitude. The average amplitude of each group represents a data point on the I/V plot. Data points were fitted to equation 5 (straight line):

$$I = A \times V + B \qquad \text{[eq.5]}$$

where A is the slope of the line, corresponding to the slope conductance of a channel, and B is the Y axis intercept (current at 0 mV).

In addition to the 1 mM patches obtained in the cell-attached configuration, I also had one patch with 50 μM glycine in the pipette solution. At this concentration I did not observe clusters of channel openings but only shorter groups of fewer openings, e.g. bursts. All bursts obtained at each holding potential were analysed together, with a continuous scan of the software.

iv. Analysis of outside-out recordings

The analysis of outside-out patches was also performed by cursor measurement. In this case I recorded only at one holding potential (-100 mV). Similar to before, each cluster was scanned individually, ignoring events shorter than 10 ms. By contrast to what is observed for cell-attached experiments, GlyRs open to several conductance levels in outside-out patches (Beato

et al., 2002; Beato and Sivilotti, 2007; Bormann *et al.,* 1993). For each level I calculated the average amplitude for the entire patch. In the average values I only included openings at the main conductance level of each cluster. These average current amplitudes were then converted into chord conductances, assuming a reversal potential of 0 mV and with no correction for junction potential. The junction potential formed between the bath and pipette solution was 3.8 mV (calculated in Clampex). This would mean a corrected membrane potential of -103.8 mV. The equilibrium potential for chloride, calculated from the Nernst equation is ~2 mV. The errors in the chord conductance estimations, therefore, are minimal: for example, what was reported as amplitude of 4 pA at -100 mV is truly 4.1 pA at -101.8 mV, when the corrections for junction potential and the equilibrium potential of 2 mV are considered.

2.2.6 Single-channel recordings from HEK293 cells

Recordings were obtained in the cell-attached configuration. The transfected cells were bathed in extracellular solution that contained (in mM): Na-gluconate 20; NaCl 102.7; KCl 2; $CaCl_2$ 2; $MgCl_2$ 1.2; HEPES 10; TEA-Cl 20; sucrose 15; glucose 14; pH 7.4 with NaOH). Solutions and electrodes were prepared as described for oocytes. Electrodes were back-filled with extracellular solution containing glycine at the required concentration (1 mM or 200 μM). Their resistance was 5-12 MΩ. The pipette solution was freshly thawed from frozen aliquots. For I/V plots all patches were held at a range of holding potentials (0 mV to -100 mV). Recordings, pre-filtered at 10 kHz, were obtained with an Axopatch 200B amplifier. For off-line analysis they were filtered at 3 kHz and digitized at 33 kHz.

Analysis was performed similarly to what was described for the oocyte cell-attached data. For 1 mM and 200 μM patches, at which clustered channel openings were observed, events that had a duration of less than 10 ms were excluded. Each cluster was analyzed individually. Unwanted events such as double openings or baseline breakdowns were rejected. After the scan, the average amplitude at each holding potential was plotted on an I/V plot and data were fitted to equation 5, in order to estimate the slope conductance for each patch.

Additional to Clampfit analysis, one recording from each concentration was also idealized by time course fitting, using the program SCAN, courtesy of David Colquhoun. The software converts the trace to a list of openings and shuttings, where the duration of each event and also the fitted amplitude values of each opening are listed. After choosing and imposing the

appropriate resolution (20 μs), stability plots and fitted amplitude diagrams for each holding potential were created using EKDIST. Only openings longer than twice the risetime of the filter (and equal to ~221 μs for 3 kHz) were used for the fitted amplitudes histograms in order to avoid the uncertainty of assigning amplitudes to short events. Each histogram was fitted by a single Gaussian component. The mean current amplitude at each holding voltage, corresponding to the peak of the Gaussian curve, was then plotted on the I/V plot, for estimating the slope conductance for that patch. All the programs used for analysis can be downloaded from http://www.ucl.ac.uk/Pharmacology/dc.html.

2.3 Kinetics of α2 GlyRs in HEK293 cells

2.3.1 GlyR α2 subunit cDNA construct, HEK293 cell culture and transfection

HEK293 cells were transiently transfected with the pcDNA3.1 vector containing the coding sequence for the rat GlyR α2 subunit (Isoform A; GenBank accession number AJ310837). The α2/pcDNA3.1 construct has a total size of 6815 bp and contains all the features shown in Figure 2.4. The full-length sequence of the cDNA was verified by sequencing PCR. HEK293 cells were cultured and transfected as described previously. The DNA mixture used for transfection contained 3-20% of α2/pcDNA3.1 and 18% pEGFP-c1; the mixtures were supplemented with the appropriate amount of pcDNA3.1 vector cDNA lacking the α2 coding sequence. Adding the empty vector ensured that the level of α2 GlyR homomer expression is kept optimal and the single-channel patches did not contain too many simultaneous channel openings. Cells used for concentration jumps (outside-out recordings) were plated onto coverslips coated with poly-L-lysine prior to transfection. Coating was performed by incubating the coverslips for ~40 minutes with poly-L-lysine (Sigma-Aldrich, UK), followed by thorough washing with autoclaved water and oven-drying at 60 °C.

2.3.2 Single-channel recordings – experimental procedure and data analysis

Recordings, performed at 19-21 °C, were obtained in the cell-attached configuration and at a holding potential of -100 mV (pipette potential of +100 mV) for all patches. Solutions and electrodes were prepared as described before in sections 2.2.5 and 2.2.6. The extracellular solution contained (in mM): Na-gluconate 20; NaCl 102.7; KCl 2; $CaCl_2$ 2; $MgCl_2$ 1.2; HEPES 10; TEA-Cl 20; sucrose 15; glucose 14; pH 7.4 with NaOH) and the electrodes (5-12 MΩ) were back-filled with extracellular solution containing glycine (at concentrations ranging from

20 μM to 10 mM). All recordings were filtered at 10 kHz and stored on a PC hard drive (sampling rate 100 kHz).

For off-line analysis the recordings were filtered at 5 or 7 kHz and sampled at 50 kHz or 71.43 kHz respectively, according to the signal-to-noise ratio of each recording. Amplitudes, open times and shut times were idealized with SCAN. More than 10000 transitions were used from each patch. Parts of records that included baseline changes or breakdowns, dubious channel openings etc. were excluded from the scan. After choosing and imposing the resolution (20 μs for both shut and open times), dwell-time distributions of shut times and open periods and also histograms of fitted amplitudes were created with EKDIST. For all patches the fitted amplitude histograms were fitted with a single Gaussian curve. Only fitted amplitudes longer than two filter risetimes (equal to twice the 10-90% risetime of the filter that is calculated as 0.3321/fc were fc is the cutoff frequency; risetime is 66 μs for 5 kHz or 47μs for 7 kHz) were used for the histograms.

The distributions of shut times and open periods were fitted with a mixture of exponential density functions. Each open period was defined as the duration of time at which the channel remained continuously open, regardless of amplitude; that is the time between two adjacent shut times longer than the imposed resolution. The true number of the channels in one patch is unknown but for kinetic analysis it is essential to isolate, within the idealised record, stretches of openings that are likely to arise from one individual channel. The reason for the initial fitting of shut-time distributions with EKDIST was to determine a critical shut time (t_{crit}) that would enable me to divide the record into true one channel stretches of openings. Fits to the distributions obtained at EKDIST are only descriptive and not mechanism dependent; hence parameters estimated by EKDIST were not used further in the analysis. The process of determining t_{crit} can be ambiguous but the conclusions do not depend critically on this choice.

For α2 receptors it was impossible to distinguish between clusters and bursts at different glycine concentrations (see Results). Hence, the P_{open} for each idealized record was calculated after considering all openings as clusters. The definition of a cluster is a group of openings that is separated by a gap that is longer than $t_{crit.}$ P_{open} for each cluster was the ratio between the cluster's total open time and cluster length. Dubious openings and clusters with a low number of open periods (<10) were excluded. The t_{crit} value I chose (7-10 ms) was different and higher

than the various t_{crit} values chosen for model fitting. This was done in order to have more accurate measurements of P_{open} since a low t_{crit} might result in breaking a cluster into several others. Two traces were idealised for each concentration and the P_{open} values for all clusters were pooled and averaged for the P_{open}-concentration curve. Fits of the P_{open} curve with the Hill equation were poorly defined.

For kinetic modeling the postulated mechanisms were evaluated using maximum likelihood fitting and the program HJCFIT (http://www.ucl.ac.uk/Pharmacology/dc.html). For this purpose the idealized data from all concentrations were grouped into sets, each set containing 2 or 3 patches at low, intermediate and high agonist concentrations. When only two patches were used, these were always of low and high concentration. A total of 12 patches were used, two of each of 20 μM, 30 μM, 50 μM, 100 μM, 1 mM and 10 mM glycine. All recordings from one set were input into the program together with a resolution of 20 μs (set as the duration of the fastest event that can be detected), a t_{crit} value for each patch and a mechanism and the data were fitted simultaneously with HJCFIT. The program calculates a likelihood value for the initial guesses for the rate constant values, taking into account the imposed resolution and by implementing a correction for missed events (Colquhoun *et al.*, 2003; Hawkes *et al.* 1992). The rate constant values are then adjusted in order to maximize the likelihood, until a maximum is reached.

The openings are separated into groups according to the t_{crit} so that all openings in a group are likely to derive from the same channel. Ideally, the groups would correspond to individual bursts at low agonist concentrations (20-100 μM) and to clusters (groups of bursts) at higher agonist concentrations (1 mM, 10 mM). In the case of low concentrations HJCFIT calculates the likelihood of each group using the initial and final vectors (CHS vectors) as described by Colquhoun *et al.,* (2003). These take into account that shut times longer than t_{crit} are excluded and the recording is divided into bursts that are separated by shut times longer than $t_{crit.}$ The true length of a shut time (deriving from one channel) has to be at least as long as the observed one. Similarly, for high agonist concentrations the likelihood is calculated with steady-state vectors. CHS vectors cannot be used in this case because the true duration of shut times is likely to be distorted by desensitization (Colquhoun *et al.,* 2003). For fitting I tested different values of t_{crit} combined with the use, or not, of CHS vectors for low concentrations (20-100

μM). This was done because I could not discriminate between clusters and bursts: at low concentrations openings were clustered, similar to high concentrations.

To test the quality of a fit, as a first step I refitted data using different initial guesses for the rate constant values. If the fit is good and the likelihood surface has only one well-defined maximum, changing the initial guesses should still converge to the same estimates for the rate constants. Additionally, fits that gave association rate constant values greater than 10^9 $M^{-1}s^{-1}$ were rejected since such values are physically impossible. As a second step, I compare the predictions of the mechanism and the rate constants obtained by HJCFIT with the experimental data. This is done using different data display: shut-time distributions, open-period distributions and the predicted P_{open} curve. All data are expressed as mean ± SEM.

2.3.3 Recordings of macroscopic currents and analysis

Concentration response curves for glycine (courtesy of L.Sivilotti; unpublished data) were performed in the whole-cell configuration at a holding potential of -60 mV. Glycine (concentrations ranging from 50 μM to 10 mM) was applied by means of a U-tube system, with exchange times lower than 6 ms. Experiments were carried out as in Burzomato *et al.* (2003). Current responses were compensated for rundown as described in Appendix B and the corrected responses for each experiment were fitted to the Hill equation (equation 3) using CVFIT. Individual experiments were normalized to their fitted maxima, then pooled and fitted again to give the plot in Figure 3.31*C*.

Fast concentration jumps were performed in outside-out patches with a theta tube (Hilgenberg, Malsfeld, Germany) cut to the tip to a final diameter of ~150 μm. The tube was driven by a piezo stepper (Burleigh Instruments, NY, USA). Glycine (0.1, 0.5, 1 and 10 mM), prepared in bath solution, was washed in and out through the double-barreled perfusion system. The exchange time was measured between normal and 30% diluted bath solution before each experiment (to optimize the position of the electrode) and after the end of the experiment and rupture of the patch.

The bath solution contained (in mM): Na-gluconate 20; NaCl 102.7; KCl 2; $CaCl_2$ 2; $MgCl_2$ 1.2; HEPES 10; TEA-Cl 20; sucrose 15; glucose 14; pH 7.4 adjusted with NaOH. For studying the effect of different Cl^- concentrations the pipettes (with a resistance of 8-15 MΩ) were

backfilled either with a 'high [Cl^-]' solution containing (mM) 107.1 KCl, 1 $CaCl_2$, 1 $MgCl_2$, 10 Hepes, 11 EGTA, 20 TEA-Cl and 2 MgATP or with a 'low [Cl^-]' solution that contained (in mM) 121.1 K-gluconate, 1 $CaCl_2$, 1 $MgCl_2$, 10 HEPES, 11 EGTA, 6 TEA-Cl and 2 MgATP (both with pH 7.2, adjusted with KOH). The osmolarity of the intracellular solution was adjusted with 20-40 mM sucrose so that it was equal or higher than of the bath solution. When the 'low [Cl^-]' solution was used, the silver chloride wire of the pipette holder was chlorinated prior to each experiment, to compensate for the increased flow of Cl^- ions from the wire to the solution. All outside-out recordings were performed at a holding potential of -100 mV. Correction for junction potential was not applied. During the 3-5 min intervals between different glycine concentrations the patch was held at -60 mV, to prolong the stability of the seal. Recordings were filtered at 5 kHz and digitized with a sampling rate of 20-50 kHz.

For each glycine concentration ~10-50 responses to individual sweeps were recorded. Sweeps were separated by at least 20 s to allow full recovery from desensitization (Gentet and Clements, 2002). All sweeps from each concentration were averaged for analysis, excluding failures or responses that contained patch breakdowns. Only experiments in which the rundown between the average current from the first and last three sweeps in a series was less than 5% were included in the analysis. The risetime for average currents and tip potentials was measured from 10-90% of the peak using Clampfit 9.2 software and experiments in which the open tip response had a 10-90% exchange time slower than 300 μs were rejected. Both the time course of desensitization at prolonged glycine applications and the time course of deactivation at long (1 s) and short applications (2 ms) were fitted with a sum of one or two exponentials. Data are expressed as averages ± SEM.

Simulations of the deactivation of macroscopic currents using single-channel kinetic models were performed in SCALCS software (http://www.ucl.ac.uk/Pharmacology/dc.html).

Average currents from 1 s concentration jumps to three different glycine concentrations (100 μM, 500 μM and 10 mM at high [Cl^-] pipette solution, equimolar to the bath) were used for obtaining a rough estimation of concentration-response curve parameters. For these patches the average responses were normalized to the fitted maximum (response at 10 mM glycine) and fitted to the Hill equation with CVFIT.

Rate constants corresponding to the desensitized states in scheme 7A were determined using ChanneLab software (Synaptosoft Inc.), which optimizes the rate constant values of a mechanism by a simplex algorithm. The open tip potential, measured at the end of each experiment, was used as input for the agonist concentration profile. Currents were usually fitted in steps. The average response to a long glycine application (200 ms) was fitted to the model leaving all desensitization entry and exit rates free. Initially, I fitted the first 100 ms of each current in order to get estimates for the slow desensitization and these were later on fixed for obtaining also the rates for the fast desensitization component (in patches where this was present). All other rate constants in the model were fixed to the values obtained from HJCFIT for model 7A. The same procedure was followed for all three glycine concentrations (500 μM, 1 mM, 10 mM) applied in each patch. As a last step I only fitted the rising phase of the glycine current by leaving the binding rate constant (k_+) free and fixing all other rates. These fits were performed for individual currents and also simultaneously for all three concentrations of each patch. When referred to rate constants, data are expressed as the average of all fits ± the % of coefficient of variation (CV).

2.4 Appendix A (protocols)

2.4.1 Transformation of chemically competent *E.coli* cells

- LB medium: For 1 liter of medium 20 g of LB Broth base (Invitrogen, UK) was diluted in water to a final volume of 1 liter; the solution was autoclaved for 2 hours and then stored at 4 °C for a maximum of a month to avoid contamination.
- Ampicillin-containing LB medium plates: 20 g of LB Broth base medium and 12 g of select agar (Gibco BRL, UK) were mixed in water at a final volume of 1 liter; the bottle was autoclaved for 2 hours. Ampicillin was added to a final concentration of 100 μg/ml (LB: antibiotic 1:1000). The final medium was poured in Petri plates (~25 ml per plate); the plates were stored at 4 °C for not more than one month.
- Transformation of DH5a *E.coli* cells: The Invitrogen Kit (#18258-012) contains DH5α competent *E.coli* cells for routine transformation of large plasmids (up to 30 kb). Before the reaction assembly, DH5α cells were removed from -80 ^{o}C and thawed on ice for 30 min. For the transformation reaction 2 μl of plasmid DNA were used for transfecting 100 μl of cells followed by incubation on ice for 30 min. The cells were then heat-shocked for exactly 45 s in

water bath at 37 ^{o}C and placed on ice for at least 2 min. 900 μl of SOC medium (at 37 ^{o}C) was added to a final volume of 1 ml and the mixture was placed in a thermomixer (at 37 ^{o}C) for 1 hour, mixing at the lowest speed. A volume of the transformation reaction was finally spread on separate, dry LB agar plates containing ampicillin and the plates were inverted and incubated overnight at 37 ^{o}C.

2.4.2 Plasmid purification – Maxiprep (QIAGEN Maxi Kit)

The HiSpeed QIAGEN Maxi Kit is used for the isolation and purification of high-yield plasmid DNA. A single, isolated colony from a selective plate was picked and inoculated in 5 ml LB medium containing 5 μl of ampicillin. The culture was then incubated in a shaking incubator at 37 ^{o}C and at maximum speed for 8 hours. The starter culture was later diluted into a flask containing 100 ml LB medium and 100 μl ampicillin and incubated overnight in a shaking incubator at 37 ^{o}C and at maximum speed. The following day the mixture was centrifuged at a maximum speed for 20 min at 4 ^{o}C, the supernatant was removed and the pellet was treated, following the manufacturer's protocol, so as to destroy the cells (lysis) and isolate and purify the plasmid DNA.

2.4.3 *In vitro* synthesis of capped RNA (AMBION – mMESSAGE mMACHINE Kit)

The kit is designed for the *in vitro* synthesis of large amounts of capped RNA, to be used for oocyte injection. The cap analog at the 5′ end of the RNA sequence (7-methyl guanosine) provides protection from ribonucleases (RNases) and gives stability to the molecule by mimicking most eukaryotic mRNAs *in vivo*.

- Linearization of the [insert]/pSP64T.GL construct: the enzyme used for linearization must have a unique restriction site in the construct and this should not be in the insert. For the pSP64T.GL vector a good candidate is XbaI (Figure 2.1), which cuts the construct downstream of the 3′ UTR. While assembling the reaction the enzyme was kept at -20 ^{o}C. Approximately 10 ng for each DNA sample was added in 4 μl of 10x Buffer (corresponding to the enzyme used) and 2 μl of the restriction enzyme. MilliQ water was added to a final volume of 40 μl. The samples were incubated for 2-3 hours at the optimal temperature for each enzyme (37 ^{o}C for XbaI). To check the success of the digestion 2 μl of each digest (diluted in 8 μl of MilliQ water and 1 μl of loading dye) were loaded on a 1% agarose gel containing 2 μl of ethidium bromide (in 1x TAE buffer, National Diagnostics, UK). The samples were separated at 110 V/cm for 1 hour. Additional confirmation of a single band with the correct size was given by

loading DNA molecular weight markers on the gel. The DNA bands were visualized by UV transillumination.

- Proteinase K treatment: this was done in order to destroy any contaminating RNases or other enzymes that may inhibit the transcription reaction. Hence, the linear DNA (38 µl) was mixed with 5 µl of 10x proteinase K buffer, 2.5 µl of 10% SDS, 4 µl of RNAse-free water and 0.5 µl of proteinase K (total 50 µl) and incubated for 1 hour at 37 ^{o}C.
- Phenol/Chloroform extraction: for purifying the linear DNA, 200 µl of equilibrated RNase-free phenol was added to the mixture and centrifuged for 10 min at 14000 rpm at ambient temperature. 200 µl of phenol-chloroform was then added to the aqueous phase and the mixture was centrifuged for 10 min at 14000 rpm at ambient temperature. The aqueous phase was again separated, RNase-free chloroform was added (200 µl) and centrifuged as before. The final aqueous phase contained the purified linear plasmid DNA.
- DNA precipitation: 15 µl of 3 M NaOAc and 3 volumes of ice-cold ethanol 100% (both RNase-free) were added to the aqueous solution and the mixture was placed at -20 ^{o}C overnight. The precipitate was centrifuged for 30 min at 4 ^{o}C and 14000 rpm, the supernatant was removed and the pellet was washed using 100 µl of 70% ethanol. The mixture was centrifuged (10 min at 14000 rpm), the supernatant was removed and the pellet was left to dry. Later it was dissolved in 10 µl RNase-free water, placed for 2 min in a heating block at 70 ^{o}C and afterwards for 2 min on ice.
- *In vitro* transcription reaction: The mMESSAGE mMACHINE Kit (Ambion) must correspond to the specific type of RNA polymerase (SP6; Figure 2.1) according to the promoter site upstream of the sequence to be transcribed. The procedure was done in an RNase-free environment and the enzymes were kept at -20 ^{o}C or in a cooler while assembling the reaction: the reagents (10x reaction buffer, 2x NTP/CAP ribonucleotides and RNase-free water) were thawed and centrifuged until being completely in solution; the ribonucleotides were kept on ice and the 10x reaction buffer at room temperature while assembling the reaction. All the reagents were added in the following order, in RNase-free tubes: 2 µl of 10x reaction buffer, 10 µl of 2x NTP/CAP, linearized DNA template corresponding to 1 µg, 2 µl of 10x enzyme mix and RNase-free water for a total volume of 20 µl; the sample was centrifuged and incubated for 2-3 hours at 37 ^{o}C. For removal of the DNA template the sample was centrifuged for 10 s and 1 µl of RNase-free DNase 1 (2 U/µl) was added; the mixture was incubated for 15 min at 37 ^{o}C and then left on ice.

- Recovery of the RNA: The MEGAclear Kit (Ambion) is developed for purification of RNA from high yield transcription reactions by removing nucleotides, oligonucleotides, proteins and salts from the RNA samples. An RNase-free environment is again essential for preserving the quality of the RNA. The procedure was done by following the protocol provided with the kit. The cRNA samples were stored at -80 ^{o}C.
- RNA electrophoresis: The cRNA samples, including also a 0.24–9.5 kb RNA ladder (Invitrogen, UK), were diluted in a 1:1 ratio with Glyoxal sample loading dye (Ambion) and incubated for ~30 min at 50 °C. The sample was loaded on a 1% agarose gel made from 1x Gel Prep/Running buffer (NorthernMax-Gly, Ambion), separated at 110 V for ~1 hour and the RNA band was visualized by UV transillumination. The lack of degradation is a sign of good cRNA quality.

2.4.4 Mammalian cell culture (HEK293 cells)

The old medium was removed from the flask and cells were washed with Hanks' balanced salt solution (HBSS; Invitrogen, UK) and were detached from the bottom of the flask after brief exposure (40-50 s) to trypsin (1 ml for a 25 cm^2 flask of ~70% confluence). Cells were collected in supplemented DMEM (4 ml), centrifuged at 1000 rpm for 2-4 min and resuspended in 5 ml of DMEM. This step was performed in order to remove any remaining trypsin from the culturing medium. A small quantity of the cell suspension was then transferred into a new flask containing DMEM, in the required dilution. The procedure was always performed under sterile conditions to avoid contamination; cells were passaged every 2-3 days and up to ~30 times.

2.5 Appendix B (calculations-data analysis)

2.5.1 Response rundown calculation

As previously mentioned, the concentration-response curves obtained from oocytes or HEK293 cells were corrected for response rundown. A standard concentration of glycine (~EC_{20}-EC_{30}) was applied at the start of each experiment and then after every third response (1st, 4th, 7th, 10th application etc). The responses to be used in the concentration-response curve (2nd and 3rd, 5th and 6th, 8th and 9th application etc) were therefore bracketed by two applications of standard. For the rundown calculation the response to each standard concentration was recorded and

expressed as a percentage (correction factor, X) of the response to the first standard. For example:

Current from 1st standard = 165 nA which is considered as a 100% response

Current from 3rd standard = 155 nA which represents 93.9% of the initial response.

The correction factor for all standard applications was calculated and used in the following equations in order to correct for rundown for the concentrations applied between standards:

$I_C = I_R \times 100 / [X_1 - (X_1 - X_2)/3]$ (eq.1) for the first data point following a standard and

$I_C = I_R \times 100 / [X_1 - 2(X_1 - X_2)/3]$ (eq.2) for the second data point following a standard.

I_R represents the recorded current response to a given concentration and I_C the current after the correction of the same response for rundown; X_1 and X_2 are the correction factors for the standards before and after the application of two data point concentrations of glycine, respectively. These equations assume that the degree of rundown is linear between two standard applications.

Chapter 3: Results

3.1 Stoichiometry of α1β GlyRs in *Xenopus* oocytes – 9´ mutations

3.1.1 Knowledge concerning the stoichiometry of heteromeric GlyRs

As mentioned previously, in the pLGIC family the functional agonist binding sites are located in the interfaces between α and non-α subunits (Brejc *et al*., 2001; Unwin, 2005). Because of that, knowing how many copies of the α subunit are in the heteromer pentamer is useful, as it sets the upper limit for the number of binding sites.

Several biochemical and electrophysiological studies have addressed the question of stoichiometry for many subtypes of LGICs, either in native tissues or in recombinant systems (Anand *et al.*, 1991; Boorman *et al.*, 2000; Chang *et al.*, 1996; Cooper *et al.*, 1991; Plazas *et al.*, 2005a, b; for reviews see Gotti and Clementi, 2004; Karlin, 2002; Sieghart *et al.*, 1999). The stoichiometry of heteromeric GlyRs remains a puzzle. Other channels in this superfamily, such as the muscle nicotinic and GABA receptors contain two copies of the main binding subunit (α-like) and therefore are thought to contain two ligand binding sites. In contrast to that, the long-held view for GlyRs is that they have a stoichiometry of 3α:2β. Evidence for this first came from the cross-linking experiments of Langosch and colleagues, performed on the purified native receptor from the spinal cord (Langosch *et al*., 1988). Chemical cross-linking with reagents of different lengths and specificities revealed products of up to 260 kDa that contained the 48 kDa (α1) and 58 kDa subunits (β) in varying ratios. The 260 kDa product (5 times the mean subunit size) corresponds to a subunit pentamer. The 48 kDa/58 kDa ratio (determined by densitometry of silver-stained NaDodSO /polyacrylamide gels) was compatible with a stoichiometry of either 3α:2β or 4α:1β. The first was considered to be more plausible since one intermediate of lower molecular weight was identified as a β-β dimer, indicating the presence of at least two copies of the β subunit (Langosch *et al*., 1988).

An indirect confirmation of the 3α:2β stoichiometry was also given by Kuhse and coworkers while studying the "assembly boxes" that determine the formation of heteromers (Kuhse *et al.*, 1993; see section 1.2.7ii). As one of their tools, the authors use chimeric α/β subunits that can only assemble into heteromeric receptors, hence behaving like wild-type β subunits. Co-expression in oocytes of the α1/β chimeric subunit with the α2 subunit that contains a reporter mutation ($\alpha2^{G167L}$ + α1/β chimera combination) showed that the effects of the mutation were stronger than those of a $\alpha2^{G167L}$/β + α1 combination, indicating that more copies of the

mutation are present in the receptor in the first case (Kuhse *et al.*, 1993). This is consistent with a stoichiometry of 3α:2β for the heteromers, in agreement with Langosch and coworkers (1988). The argument however is dependent on the linear behavior of the reporter mutation (the effect of the mutation being proportional to the number of subunits that carry it in the receptor) and also on the lack of homomeric $\alpha2^{G167L}$ contamination. Equally, the method relies on the appropriate behaviour of the chimeric subunit (i.e. that the transferred assembly cassette does not decrease the effects of the mutation).

An alternative approach to determine the stoichiometry of heteromeric GlyRs was used in my laboratory in human embryonic kidney cells (HEK293, Burzomato *et al.*, 2003). This used a reporter mutation (a hydrophilic substitution of the 9′ leucine residue in the TM2; Figure 3.1A) that is known to produce a leftward shift in the agonist concentration-response curve for all pLGICs tested so far (for examples see Boorman *et al.*, 2000; Chang *et al.*, 1996; Filatov and White, 1995; Groot-Kormelink *et al.*, 1998; Labarca *et al.*, 1995). Co-expression of a mutated α1 or β subunit with wild-type β or α1 subunit, respectively, resulted in a greater shift of the glycine concentration-response curve when the α1 subunit was mutated. The simplest explanation of this is that more copies of the α1 subunit are incorporated into the pentamer, being in favour of the previously suggested stoichiometry of 3α:2β (Burzomato *et al.*, 2003).

Despite of the evidence presented so far, there still remains some uncertainty concerning stoichiometry. A more recent paper (Grudzinska *et al.*, 2005) favors a subunit ratio of 2α:3β on the basis of results from tandem α1_β constructs in *Xenopus* oocytes and of metabolic labeling of oocyte α1β GlyRs with [^{35}S]-methionine (Grudzinska *et al.*, 2005). Two explanations can be given for the inconsistency between this study and those arguing a 3α:2β stoichiometry. Firstly, it is possible that tandem subunits do not incorporate efficiently into the receptor product. A similar problem was seen with tandem constructs for neuronal nicotinic receptors indicating that concatemeric dimers or trimers should not be considered as reliable tools for studying the stoichiometry of a recombinant receptor (Groot-Kormelink *et al.*, 2004; see also Nicke *et al.*, 2003). Secondly, even if tandems assemble correctly, it is very likely that the oocyte expression system differs from HEK293 cells in the way heteromeric glycine receptors are formed. This argument could reconcile the results of Grudzinska *et al.* (2005) from the [^{35}S]-methionine labeling experiments, that argue for a 2α:3β stoichiometry, with the results from HEK293 cells that are in favor of a 3α:2β assembly (Burzomato *et al.*, 2003).

3.1.2 Aim

For clarifying the above argument I tested in *Xenopus* oocytes the same experimental approach that Burzomato *et al.,* (2003) followed in HEK293 cells. I therefore expressed 9′ mutant α1β GlyRs in oocytes, with the mutation being present either on the α1 or the β subunit, and compared their glycine sensitivity with that of wild-type channels. Simply, if the GlyR channel has a stoichiometry of 3α1:2β then a 9′ mutation on the α1 subunit will cause a greater effect compared with inserting the mutation on the β subunit. The opposite should occur if the stoichiometry is 2α1:3β. The idea of this approach is driven from the fact that, according to Unwin's model for the channel pore, the 9′ leucine residue takes part in the hydrophobic girdle that keeps the channel closed. In agreement with this model, substitution of the conserved hydrophobic 9′ leucine (Figure 3.1*A*) with a hydrophilic residue (serine, S or threonine, T; Figure 3.1*B*) causes an increase in agonist sensitivity and a decrease in the agonist EC_{50}. Apparently, the disruption of the hydrophobic girdle by a polar residue makes the channel easier to open. This has been well demonstrated for the muscle AChR (Filatov and White, 1995; Labarca *et al*., 1995), for neuronal nicotinic receptors (Boorman *et al*., 2000; Groot-Kormelink *et al.*, 1998; Revah *et al.*, 1991), for GABA receptors (Chang and Weiss, 1998) and more recently for GlyRs (Burzomato *et al.*, 2003). In all the above studies, each substitution of a 9′ leucine caused an equivalent leftward shift in EC_{50}. The magnitude of this decrease is independent of which subunit carries the mutation and the total shift is proportional to the number of mutated subunits that form the receptor (Figure 3.1*C*). For the muscle nicotinic receptor (Labarca *et al*., 1995) each mutation caused a ~10 fold increase in agonist sensitivity. As well as an increase in agonist sensitivity, 9′ mutations have also been related to a decrease in the rate of desensitization (Revah *et al*., 1991; Yakel *et al*., 1993) and an increase in the number of spontaneous openings (Chang and Weiss, 1998). The magnitude of these effects is, in most cases examined, proportional to the number of mutations, though saturation might occur if 3 or more copies of the mutation are present (Chang and Weiss, 1998, 1999; Plazas *et al*., 2005a).

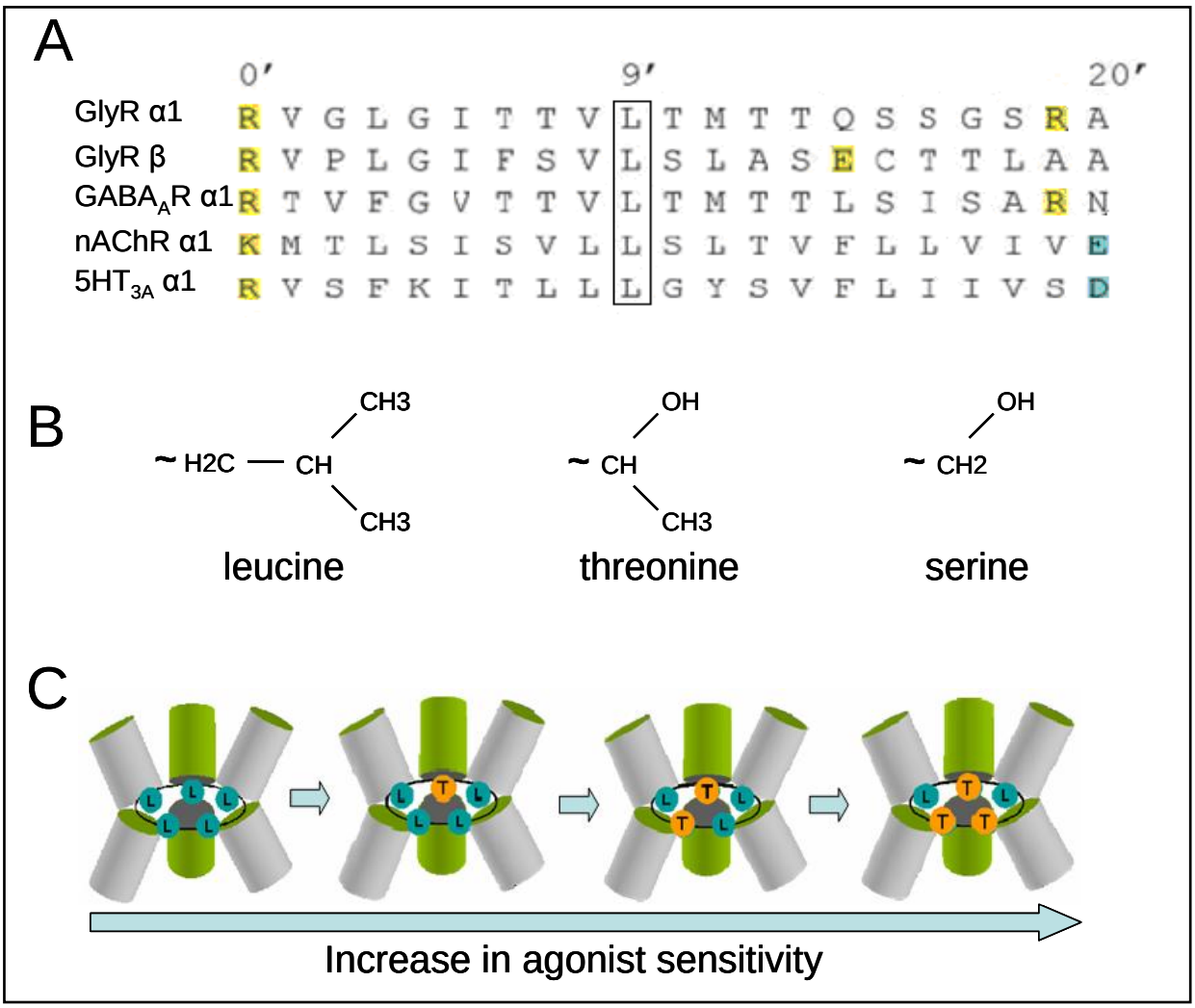

Figure 3.1 The reporter mutation approach at position 9′

A, Sequence alignment of the pore-lining TM2 domain for the different LGIC subunits. Note the conservation of the 9′ Leu (shown in the box) throughout the superfamily. Charged residues are highlighted in yellow (negative charge) and blue (positive charge). *B*, Structure of the amino-acid side-chains of threonine and serine used for the hydrophobic-to-hydrophilic mutation of 9′ leucine. *C*, Schematic representation of the effects of the reporter 9′LT mutation in a pLGIC (only three subunits are shown here). According to Unwin's model for the closed pore, hydrophobic interactions between the five leucines and surrounding residues (not shown) keep the channel closed. The introduction of a hydrophilic threonine disturbs the hydrophobic girdle, causing an increase in agonist sensitivity. This effect is proportional to the number of mutations inserted in the pentamer and is independent of subunit subtype.

The progressive effect of 9′ mutations in the agonist EC_{50} has proven very useful for stoichiometry studies of the nicotinic superfamily. Besides the Burzomato *et al*. (2003) study on GlyRs, which will be repeated here in oocytes, Boorman and co-workers used 9′ mutations on α3β4β3 neuronal nAChRs in *Xenopus* oocytes and came up with a stoichiometry of

2α3:2β4:1β3 for the triplet (Boorman *et al.*, 2000), Chang and colleagues deciphered the stoichiometry of α1β2γ2 $GABA_A$ receptors to being 2:2:1 (Chang *et al.*, 1996) and finally Plazas used 9′, 13′ and 17′ mutations in α9α10 receptors in oocytes and suggested a stoichiometry of 2α9:3α10 (Plazas *et al.*, 2005a, b).

3.1.3 Expression of heteromeric GlyRs in *Xenopus laevis* oocytes – Picrotoxin test

The first aim was to confirm that, in oocytes, most of the GlyRs expressed after co-injection of α1 and β cRNA are α1β heteromers. In order to do this, I tested the sensitivity of the receptors to the channel blocker picrotoxin (PTX). As mentioned previously (section 1.2.7), this alkaloid is a standard pharmacological tool for the discrimination between homomeric and heteromeric GlyRs, with homomers being much more sensitive to PTX inhibition than αβ heteromers (Pribilla *et al.*, 1992). Oocytes were therefore injected with α1+β GlyR subunit cRNA (1:40 ratio) and I compared concentration-inhibition curves to PTX with those obtained in oocytes expressing α1 homomeric receptors alone.

An example of the effect of PTX on homomeric and heteromeric receptors is shown in Figure 3.2. Homomeric receptors are clearly more sensitive to the blocker as shown by the traces in *A*: the current elicited by the application of 100 μM glycine (approximately EC_{50} for α1 and for α1β) on the homomer (top row) was clearly reduced by PTX concentrations greater than 0.5 μM and almost completely abolished by 100 μM PTX (from 335 nA to 3 nA). The same PTX concentrations caused a smaller reduction in glycine currents elicited in oocytes injected with α1+β (bottom row). Concentration-response curves from all experiments, fitted to the Hill equation, are shown in Figure 3.2*B*. As expected, the IC_{50} for homomeric receptors was very low, indicating their high sensitivity to picrotoxin, in agreement with Pribilla *et al.*, (1992); the average IC_{50} from four cells injected with α1+β was ~18-fold higher, suggesting the expression of α1β heteromers. The Hill slope coefficient was similar for both combinations and close to unity (Table 3.1).

Figure 3.2 and Table 3.1 summarise results from four oocytes that, when injected with α1+β cRNA, expressed heteromeric channels. Unexpectedly, two other oocytes (from a total of 6 cells) injected with the 1:40 subunit ratio (α1:β) gave a low picrotoxin IC_{50} (1.8 μM and 6.3 μM) when fitted with a single-component Hill equation, as if they were not expressing heteromeric receptors at all. In order to estimate the extent of homomeric contamination in

oocytes injected with α1+β, each of the remaining 4 experiments was refitted to a two-component Hill equation. I first fitted the data leaving all parameters free. In every experiment these fits were poorly defined. As a second step, I refitted the data by constraining the IC_{50} of the first component to be that of homomers and the two n_H to be equal 1. These fits were also poorly defined. The above would suggest that the α1 homomeric component is not large enough to be detected during a macroscopic experiment; for this reason I continued using the 1:40 ratio, for the expression of a predominant heteromeric receptor population that contributes to most of the agonist current.

Table 3.1 Mean concentration-inhibition curve parameters ± SEM obtained from one component Hill equation fits from oocytes injected with α1 or α1+β subunit cRNA.

	IC_{50} (μM) *	n_H	I_{max} (nA)	N
α1	5.3 ± 2.7	1.4 ± 0.4	340.2 ± 33.5	3
α1+β (1:40)	90.6 ± 17.4	0.9 ± 0.1	322.3 ± 69.6	4

Student's two-tailed *t* test:

- $p < 0.001$

3.1.4 Expression of L9′T mutant α1β GlyRs in oocytes

In order to test the effects of the 9′ LT mutation on the sensitivity of oocyte-expressed receptors, cells were injected with different subunit combinations (α1+β^{LT}, $\alpha1^{LT}$+β, $\alpha1^{LT}$+β^{LT} or $\alpha1^{LT}$ alone; 1:40 subunit ratio of α1 to β; see Methods) to obtain concentration-response curves to glycine. It was not possible to measure currents from the $\alpha1^{LT}$ and $\alpha1^{LT}$+β^{LT} combinations, as these oocytes appeared unhealthy, with an increased holding current that made voltage clamp difficult when the electrodes were inserted (this current is likely to arise from spontaneous openings of the all-mutant channels, see Chang and Weiss, 1998).

Representative responses to a range of glycine concentrations for the mutant and wild-type combinations are shown in Figure 3.3*A*. From the traces it is clear that the glycine sensitivity of either mutant is similar and does not differ much from the wild-type channels. This is more evident when all data are fitted to the Hill equation and the curve parameters are obtained from the fits (Figure 3.3B, Table 3.2).

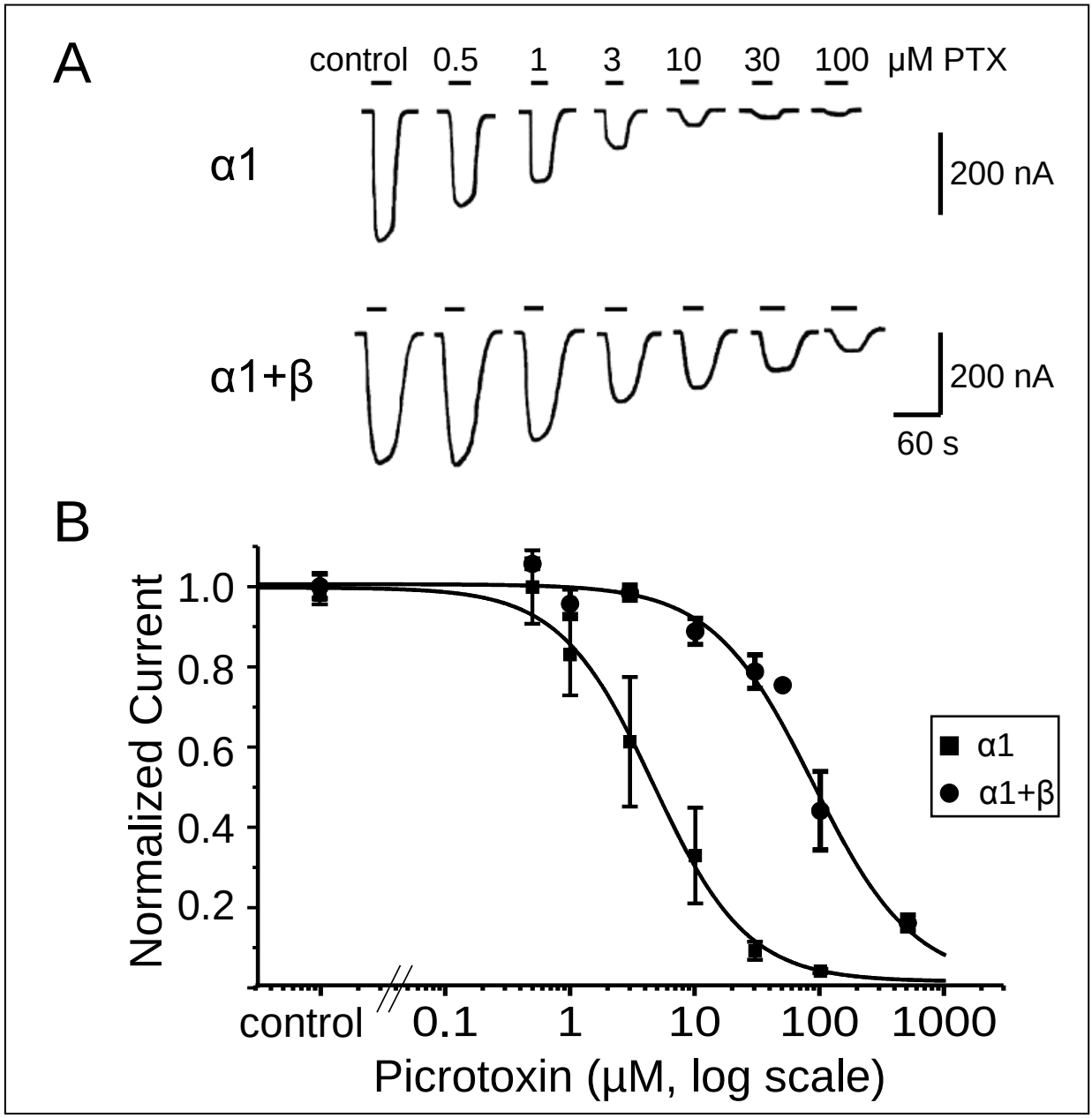

Figure 3.2 Picrotoxin sensitivity of oocyte-expressed receptors
A, Inward currents elicited by the co-application of a standard glycine concentration (100 μM; EC_{50} concentration of α1 GlyRs) with increasing concentrations of PTX to oocytes held at -70 mV. PTX concentrations are indicated above the traces; bars show the duration of each application. *B*, Pooled concentration-inhibition curves for homomeric and heteromeric receptors, taken from fitting the mean normalized responses with a one-component Hill equation. Note the higher sensitivity of homomeric receptors for PTX.

The average EC_{50} for α1β receptors was 81.5 ± 3.6 μM and only a very small reduction in EC_{50} was observed for the mutant receptors (61.7 ± 13.1 μM for $\alpha1\beta^{LT}$ and 50.1 ± 9.1 μM for $\alpha1^{LT}\beta$). This reduction was too small and inconsistent to reach statistical significance ($p > 0.05$ for both

mutant combinations compared with wild-type). This result is completely different from that of Burzomato *et al.* (2003) in HEK293 cells.

Given this lack of effect of co-expression of mutant subunits, it is reasonable to ask whether the mutant subunits incorporate into the receptor at all, particularly in the case of the β subunit (glycine receptors need α subunits to be functional). In other words, could the concentration-response curve of $\alpha1+\beta^{LT}$ be so similar to that of α1+β because both are mainly due to the activity of the homomer α1? As seen from the plots in Figure 3.3*B*, mutant receptors have an obvious reduction in the Hill slope (Table 3.2) and this is statistically significant. Also, if β incorporates poorly, $\alpha1^{LT}+\beta$ receptors would also be mainly homomers, and they would contain 5 copies of the mutation, so this does not explain the small change seen for the mutation. It is also to be noted that the maximum current elicited by glycine was somewhat lower for the mutant combinations ($p < 0.001$). These were indications that the mutant subunits take part in the receptors and that the presence of the mutation does cause some effect in receptor properties. Despite this however, no obvious differences exist between receptors with the α1 subunit mutated and those with the β mutated ($p > 0.05$). Hence these results cannot be interpreted in terms of stoichiometry, as done previously for HEK293 cells.

An explanation for these findings is that oocyte-expressed heteromeric receptors are a mixture of pentamers containing two and three alpha subunits. This would explain why the concentration-response curves for the mutants are so similar, irrespective of whether the mutation is in α1 or β, as effectively the receptor has on average 2.5 mutations in both cases.

Table 3.2 Mean concentration-response curve parameters ± SEM from separate fits of wild-type and L9′T mutation data, fitted with the Hill equation.

	EC_{50} (μM) *	n_H **	I_{max} (nA) ***	N
α1+β	81.5 ± 3.6	2.7 ± 0.3	717.0 ± 73.6	5
$\alpha1+\beta^{LT}$	61.7 ± 13.1	1.6 ± 0.1	346.5 ± 49.7	7
$\alpha1^{LT}+\beta$	50.1 ± 9.1	1.1 ± 0.1	203.9 ± 41.0	5

Bonferroni's multiple comparison tests:
* $p > 0.05$ for $\alpha1\beta$-$\alpha1\beta^{LT}$, $\alpha1\beta$-$\alpha1^{LT}\beta$ and $\alpha1\beta^{LT}$-$\alpha1^{LT}\beta$
** $p < 0.01$ for $\alpha1\beta$-$\alpha1\beta^{LT}$; $p < 0.001$ for $\alpha1\beta$-$\alpha1^{LT}\beta$; $p > 0.05$ for $\alpha1\beta^{LT}$-$\alpha1^{LT}\beta$
*** $p < 0.001$ for $\alpha1\beta$-$\alpha1\beta^{LT}$ and $\alpha1\beta$-$\alpha1^{LT}\beta$; $p > 0.05$ for $\alpha1\beta^{LT}$-$\alpha1^{LT}\beta$

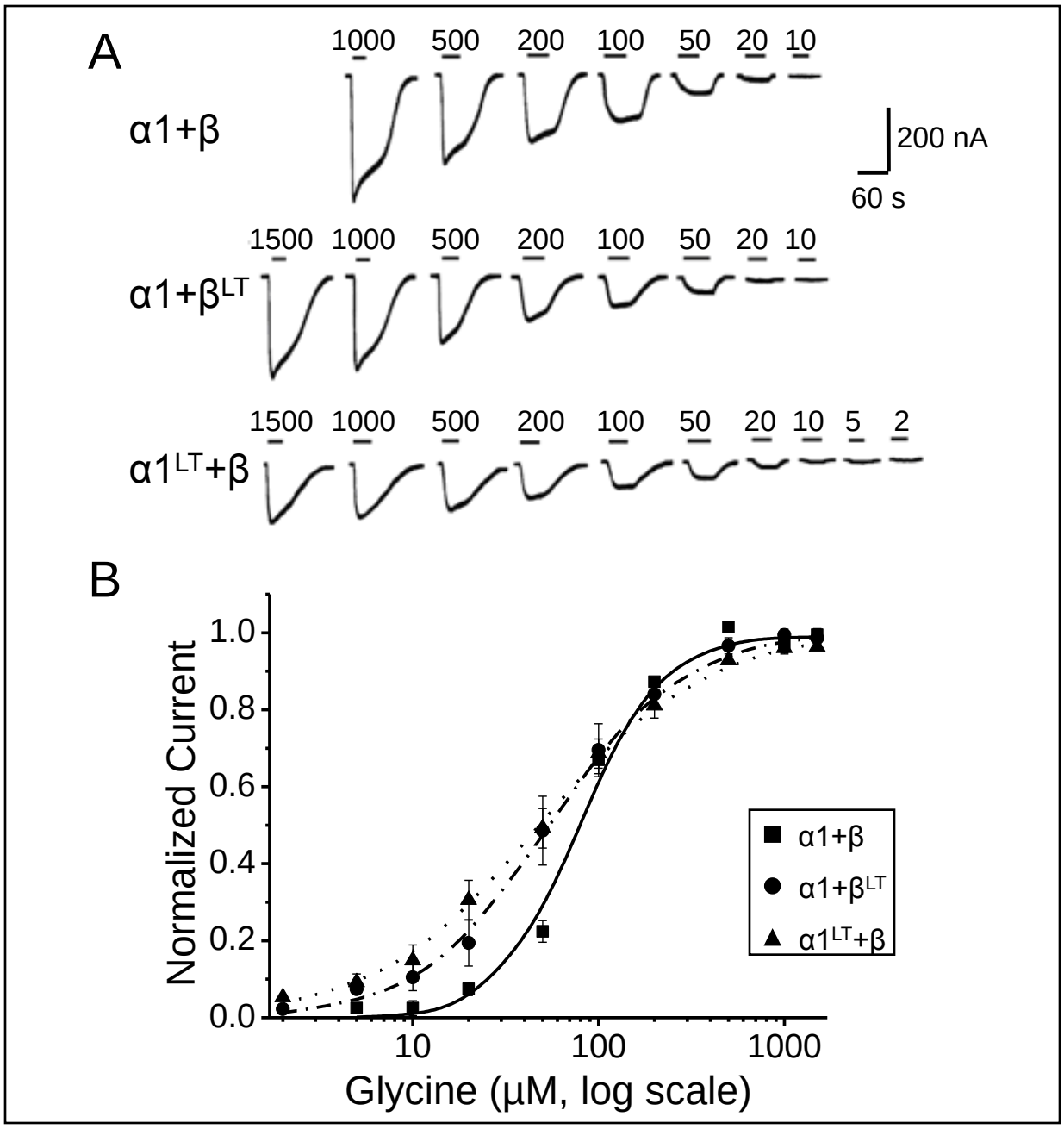

Figure 3.3 Effects of the L9´T mutation on oocyte-expressed receptors

A, Glycine responses from oocytes expressing wild-type and mutant receptors (-70 mV). The mutation causes a decrease in the current produced by different glycine concentrations (shown above the traces, in μM). The bars show the duration of each application. *B*, Average concentration-response curves, pooled to their fitted maxima for each combination. The mutation causes little decrease in the agonist EC_{50} ($p = 0.18$). The mutated receptors have a lower Hill slope compared with wild-type α1β but the difference between the two mutants is insignificant ($p > 0.05$).

3.1.5 Expression of L9´S mutant α1β GlyRs in oocytes

Due to the L9´T results being inconclusive, I made a further attempt and chose a different mutation (leucine, L to serine, S) at the same position. It has previously been shown that the L to S substitution has a greater effect in this position, compared with L to T (Chang and Weiss, 1998). The same approach of co-expressing L9´S mutant with wild-type subunits (1:40 ratio of α1:β) in oocytes was therefore used in order to compare mutant and wild-type concentration-response curves (Table 2.1, Methods). Again, it was impossible to record from oocytes expressing $\alpha1^{LS}\beta^{LS}$ receptors (the total holding current was more than 1 μA in all the cells tested). However, as seen from the traces in Figure 3.4*A*, I was able to record glycine responses from $\alpha1^{LS}$ receptors, though in this case the size of the responses was very much smaller (note the different scale for $\alpha1^{LS}$ traces). The sensitivity of this combination for glycine was ~30-fold higher than that of wild-type homomeric receptors with an EC_{50} value of 2.9 ± 0.7 μM (Table 3.3*A*). I was only able to record from 3 cells due to the increased vulnerability and low glycine-evoked current of this combination, indicative of high spontaneous activity of the all-mutant pentamers. The pooled data from the 3 cells, normalized to the maxima, are shown in Figure 3.4*B*, alongside data from wild-type α1 GlyRs for comparison.

As in the case of the L9´T, the glycine sensitivity of the two mutant heteromeric combinations was similar to wild-type α1β receptors with glycine EC_{50} of 81.2 ± 3.3 μM and 112.7 ± 10.0 μM for $\alpha1\beta^{LS}$ and $\alpha1^{LS}\beta$ respectively (Figure 3.5*A)*. Similarly, the effect of the mutation was apparent only as a Hill slope decrease, at least in the case of the $\alpha1^{LS}\beta$ combination (Figure 3.5*B*; Table 3.3*B*).

The data from the $\alpha1+\beta^{LS}$ combination question whether the mutant subunits actually incorporate to form heteromers. Receptors from these cells have EC_{50} and n_H values very similar to those of wild-type α1 GlyRs (Table 3.3). Similarly, application of PTX to $\alpha1+\beta^{LS}$ oocytes gave an IC_{50} of 7.42 ± 3.39 (n = 3) indicating a high sensitivity, as in the case of homomers (data not shown). Even if we assume, however, that β^{LS} fails to incorporate, this does not explain why $\alpha1^{LS}\beta$ receptors do not have an EC_{50} intermediate between that of α1β and $\alpha1^{LS}$ receptors.

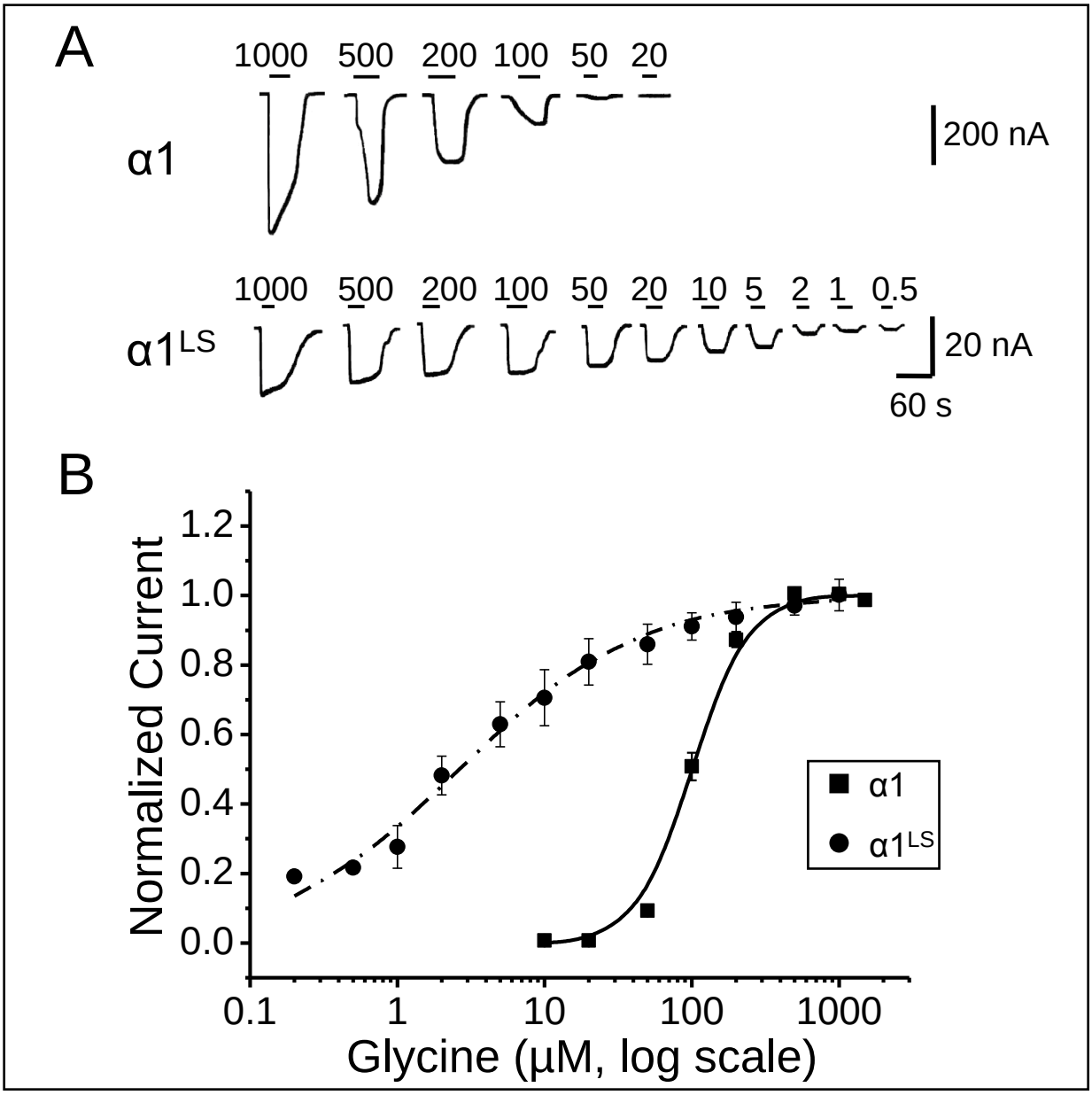

Figure 3.4 Effects of the L9´S mutation on homomeric GlyRs
A, The traces are inward currents elicited by the application of glycine (in μM) to oocytes (held at -70 mV) expressing wild-type and $\alpha1^{LS}$ receptors. Note the different scale for currents from $\alpha1^{LS}$-expressing oocytes. *B*, Average, normalized glycine responses, fitted to the Hill equation and pooled to their fitted maxima for the two receptor combinations.

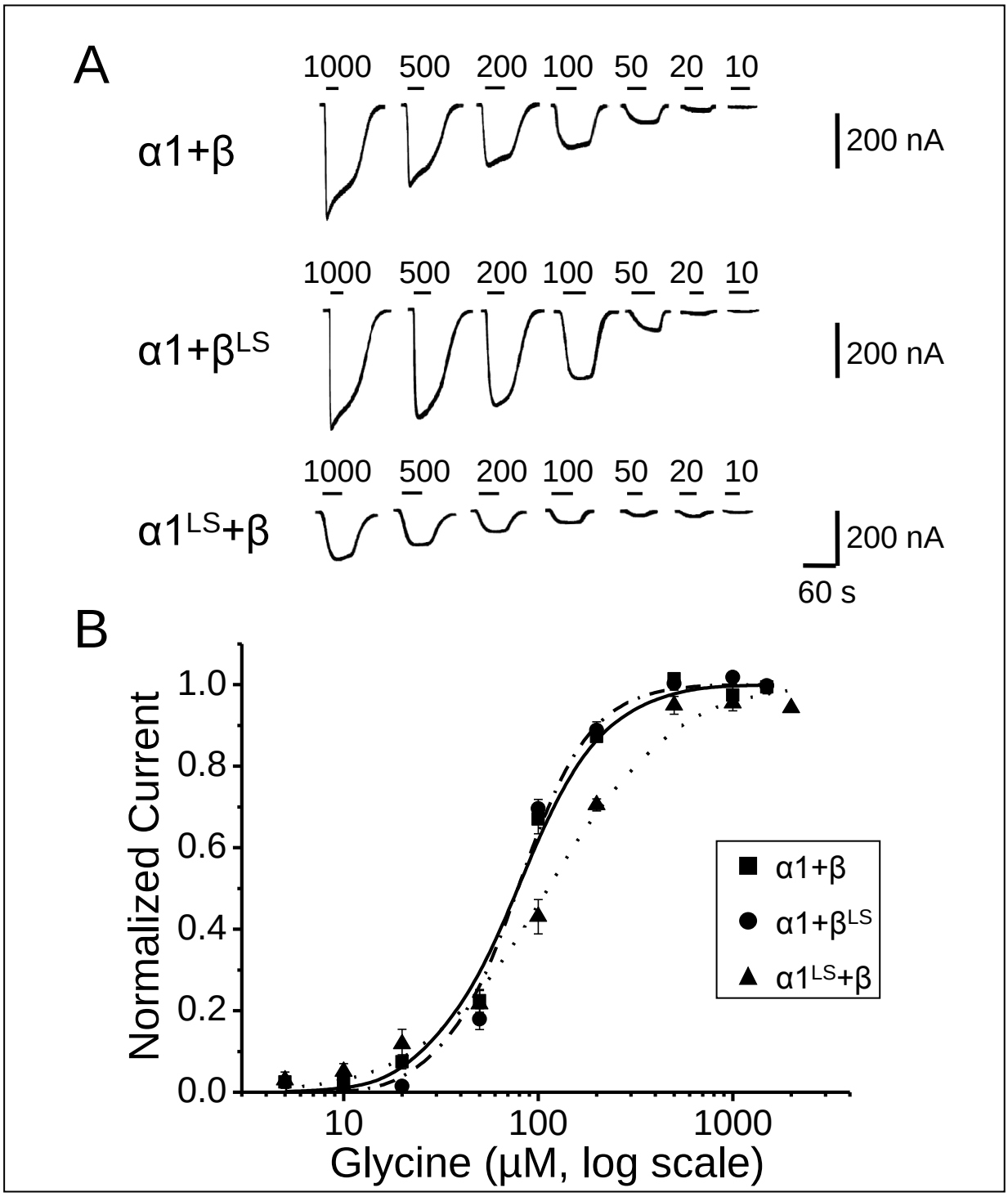

Figure 3.5 Effects of the L9´S mutation on heteromeric GlyRs

A, Glycine responses recorded from wild-type and mutant heteromeric receptors. The glycine concentrations above the traces are in μM. All cells were held at -70 mV. Note the reduction in the current from $\alpha1^{LS}\beta$ receptors. *B*, Average, normalized glycine responses, fitted to the Hill equation and pooled to their fitted maxima for each receptor combination. The β^{LS} mutation did not cause any obvious effect on the expressed receptors.

Table 3.3 Mean concentration-response curve parameters ± SEM from oocytes expressing wild-type and L9′S mutant receptors, fitted with a single-component Hill equation

		EC_{50} (μM) *	n_H **	I_{max} (nA) ***	N
A	**α1**	101.1 ± 3.8	3.31 ± 0.24	704.58 ± 86.11	5
	α1^{LS}	2.9 ± 0.7	0.79 ± 0.17	23.88 ± 6.76	3
B	**α1+β**	81.5 ± 3.6	2.7 ± 0.29	717.03 ± 73.60	5
	α1+β^{LS}	81.2 ± 3.3	3.07 ± 0.23	408.64 ± 52.73	7
	α1^{LS}+β	112.7 ± 10.0	1.56 ± 0.23	274.08 ± 22.02	4

A: Students' t test:
* $p < 0.0001$
** $p = 0.0004$
*** $p = 0.001$

B: Bonferroni's multiple comparison tests:
$p > 0.05$ for α1β-α1β^{LS}; $p < 0.01$ for α1β-α1^{LS}β and α1β^{LS}-α1^{LS}β
$p > 0.05$ for α1β-α1β^{LS}; $p < 0.05$ for α1β-α1^{LS}β; $p < 0.01$ for α1β^{LS}-α1^{LS}β
$p < 0.01$ for α1β-α1β^{LS}; $p < 0.001$ for α1β-α1^{LS}β; $p > 0.05$ for α1β^{LS}-α1^{LS}β

To summarize, both the 9′LT and the 9′LS mutation did not produce the expected results in oocytes: in both cases the agonist sensitivity of heteromeric mutant receptors does not differ much from the wild-type heteromer despite the fact that the incorporation into functional channels is evident (as a reduction in the Hill coefficient values for all mutant combinations, except the α1β^{LS}). This is different to what has seen in HEK293 cells for the GlyR (Burzomato *et al*., 2003) and also for other pLGICs. As a result I could not come to any conclusion concerning the stoichiometry of α1β channels in oocytes with this approach and hence had to resort to an alternative method.

3.2 Stoichiometry of α1β GlyRs – conductance mutations

3.2.1 Single-channel conductance of GlyRs

Two different domains have been shown to determine the single-channel conductance of nicotinic and 5-HT_3 channels (Peters *et al.,* 2006). One is the TM2 domain: this is known to be the main determinant of both conductance and ion selectivity in this receptor superfamily (Cohen *et al.,* 1992a, b; Imoto *et al.,* 1991; Labarca *et al.,* 1995; Villarroel *et al.,* 1991; see section 1.2.7.i). The second domain was originally identified in the cytoplasmic loop of 5-HT_3 channels, in a region that contains three conserved arginine residues in the 5-HT_3A subunit (R432, R436 and R440). These are partly responsible for the difference in conductance between homomeric 5-HT_3A and heteromeric 5-HT_3AB channels: mutations at these residues lead to a ~28 fold increase in single-channel conductance for the triple mutant (Davies *et al*., 1999; Kelley *et al*., 2003; Peters *et al*., 2004 and 2005). This latter region, within the MA stretch, was recently shown to control the ionic conductance of α1 homomeric glycine receptors, suggesting that the portals for ions accessing the channel from the cytoplasm are similar in cationic and anionic pLGICs (Carland *et al.*, 2009; Hales *et al*., 2006).

Extensive single-channel work on GlyRs has shown that the incorporation of the β subunit into heteromers leads to channels with approximately half the single-channel conductance of homomers. The residues that determine this difference in conductance were localized to the TM2 domain: expression of subunits with mutations in this domain was shown to alter the single-channel conductance of both homomeric and heteromeric glycine channels, in agreement with this region being the major determinant of single-channel conductance for glycine receptors (Bormann *et al.,* 1993; Carland *et al.,* 2009). Surprisingly, in the case of GlyRs, the number of different conductance levels that can be observed in a patch depends on the recording configuration. Cell-attached studies report the presence of only one conductance level, irrespective of receptor subtype (for examples see Beato *et al.,* 2004; Beato and Sivilotti, 2007; Burzomato *et al.,* 2004). The situation gets more complicated when recordings are performed in a cell-free configuration (i.e. excised patch) where GlyR channels open at different conductance levels. This was shown both for native (Bormann *et al.,* 1987; Takahashi and Momiyama, 1991; Twyman and MacDonald, 1991) and for recombinant GlyRs (Beato *et al.,* 2002; Bormann *et al.,* 1993). A detailed outside-out study on HEK293 cells reported five different conductance states for α1 GlyRs (ranging from 20-90 pS), six states for α2 and α3

GlyRs and 2-3 states for heteromeric channels (Bormann *et al.*, 1993). The reasons underlying the discrepancy between cell-attached and excised GlyRs are unclear though it is reasonable to assume that disruptions in the microenvironment of the channel, caused by the excision, may be relevant (see Fucile *et al.*, 2000).

3.2.2 Aim

Given that the work with the 9′ mutation did not allow coming to a conclusion on channel stoichiometry, I wanted to pursue the question of stoichiometry of α1β GlyRs in oocytes using a different approach which involves single-channel recordings from conductance mutants. Such an approach has been used by Cooper *et al*. (1991) for the investigation of the stoichiometry of chick α4β2 neuronal nicotinic receptors and by Béhé *et al*. (1995) for the determination of NR1 subunit copies in NMDA receptors expressed in *Xenopus* oocytes. The idea of the approach is simple: co-injection of the wild-type and the conductance mutant form of a given subunit leads to the expression of receptors with a mixture of wild-type, all-mutant and hybrid (intermediate) single-channel conductances. Based on the number of intermediate conductances one can determine the number of copies of the subunit in question in the receptor (i.e. its stoichiometry).

The selection of the appropriate conductance mutation is important and as mentioned above both the TM2 domain and the cytoplasmic loop are good candidate regions. Bormann and co-workers have already shown that substitution of β GlyR subunit residues within the TM2 with their corresponding residues in α1 and transfection of this chimeric subunit (β^{Ch}) together with α1 leads to the expression of $\alpha1\beta^{Ch}$ heteromeric channels with a homomer-like conductance (Bormann *et al*., 1993). This TM2-chimeric subunit is therefore a good candidate as a conductance mutant for my experiments.

The steps followed are, in brief:

i. Construction of the rat β^{Ch} (β subunit containing the α1 TM2, see Figure 2.3, Methods).
ii. Measure of the slope conductance of α1 and α1β GlyRs in oocytes. This was done in the cell-attached configuration in order to avoid the presence of multiple conductance levels for each receptor subtype. The subunit ratio of α1 to β was kept to 1:40.
iii. As a control I also injected oocytes with $\alpha1+\beta^{Ch}$ (to confirm a homomer-like conductance as Bormann *et al.*, 1993). The subunit ratio was 1:40.

iv. Finally, in order to determine the stoichiometry of the α1β GlyR, mutant and wild-type subunits were expressed together in the same cells (α1+β+β^{Ch}).

The rational for the latter is as follows: if both wild-type and mutant β subunits are expressed, it is likely that some receptors would incorporate them both. A mixture of different receptor types would then be assembled according to the stoichiometry of the channel (Table 3.4, second column). Each receptor type would have a different single-channel conductance. The total number of receptor types in a cell (i.e. the total number of different conductance levels) is equal to *N*+1 where *N* is the total number of the β subunits in a pentamer. Therefore, if the stoichiometry is 3α:2β, 3 different conductance levels would appear (*2*+1) whereas if the stoichiometry is 2α:3β I would expect to see 4 different conductance levels (*3*+1). The single-channel conductance of the all-wild-type and all-mutant receptor will be easily identified using the control injections mentioned above; the mixed receptors will give one or two intermediate single-channel conductances, depending on the stoichiometry (see the summary in Table 3.4).

Table 3.4 Possible subunit combinations for the two presumed stoichiometries when oocytes are co-injected with α1+β+β^{Ch} cRNA.

Presumed Stoichiometry	**Possible subunit combinations**	**Single-channel conductance levels**	**Conductances known from control injection**
3α:2β	α-α-α-β-β	3	α1+β
	α-α-α-β-β^{Ch}		-
	α-α-α-β^{Ch}-β^{Ch}		α1+β^{Ch}
2α:3β	α-α-β-β-β	4	α1+β
	α-α-β-β-β^{Ch}		-
	α-α-β-β^{Ch}-β^{Ch}		-
	α-α-β^{Ch}-β^{Ch}-β^{Ch}		α1+β^{Ch}

3.2.3 Single-channel conductance of α1 and α1β GlyRs in oocytes (1:40 ratio)

Before proceeding with the conductance mutant, I needed to measure the single-channel conductance of wild-type receptors. Single-channel recordings from α1 homomers would allow me to recognise homomeric openings occurring as "contaminants" (even when the extreme

ratio of 1:40 is used) and hence exclude them from the analysis. All recordings were performed in the cell-attached configuration and at a range of positive holding potentials (negative pipette potentials; see Methods) for obtaining I/V plots and the slope conductance of each channel. A high glycine concentration was used (1 mM); openings therefore occurred in clusters, each cluster representing events from one channel only.

A representative example of such an experiment is shown in Figure 3.6. The traces are obtained from a cell injected with rat α1 cRNA and represent continuous recordings at each holding potential from a single patch. Openings occur in clusters (up to ~10 s long), separated by long shut times likely to correspond to desensitized states of the channel. Note that although channel openings are downwards, the current is outward. This is due to the composition of the solutions and because at positive holding potentials chloride is flowing from the pipette to the cell. Only one conductance level was seen, in agreement with other cell-attached data in HEK293 cells (Beato *et al.*, 2004). For each patch I plotted the average amplitude at each holding potential and the I/V plot was fitted with a linear fit to obtain the slope conductance of the channel. For the experiment in Figure 3.6 the slope conductance was 72 pS. The I/V plot in Figure 3.6 was plotted from the average amplitude values pooled from all patches (n = 5) and had a slope of 68 pS. This was consistent with the average value obtained from individual fits to the same experiments (69 ± 1 pS; n = 5).

Figure 3.7 shows the same experiment performed on an oocyte injected with the rat α1+β cRNA at a ratio of 1:40. The range of holding potentials is the same used for the α1 experiments (from 0 mV to +60 mV). As before, openings at this concentration occur in clusters and only one main amplitude level is detected at each holding potential. As seen from the scale bar, the average amplitude of heteromeric channels, at equivalent holding potentials, is almost half of the amplitude of the homomeric channel in Figure 3.6 (2.1 pA and 4.6 pA respectively, +50 mV). This α1β channel has a slope conductance of 32 pS; the average value from individual fits of all patches with this combination was 33 ± 2 pS (n = 5). Similarly, the linear fit of the pooled I/V plot in Figure 3.7 (containing the average amplitude values from all patches) gave a slope conductance of 32 pS. The slope conductance values for the homomeric (69 ± 1 pS) and heteromeric (33 ± 2 pS) channels in oocytes are consistent with those previously reported for cell-attached recordings from recombinant GlyRs in HEK293 cells (Beato *et al.*, 2004; Burzomato *et al.*, 2003).

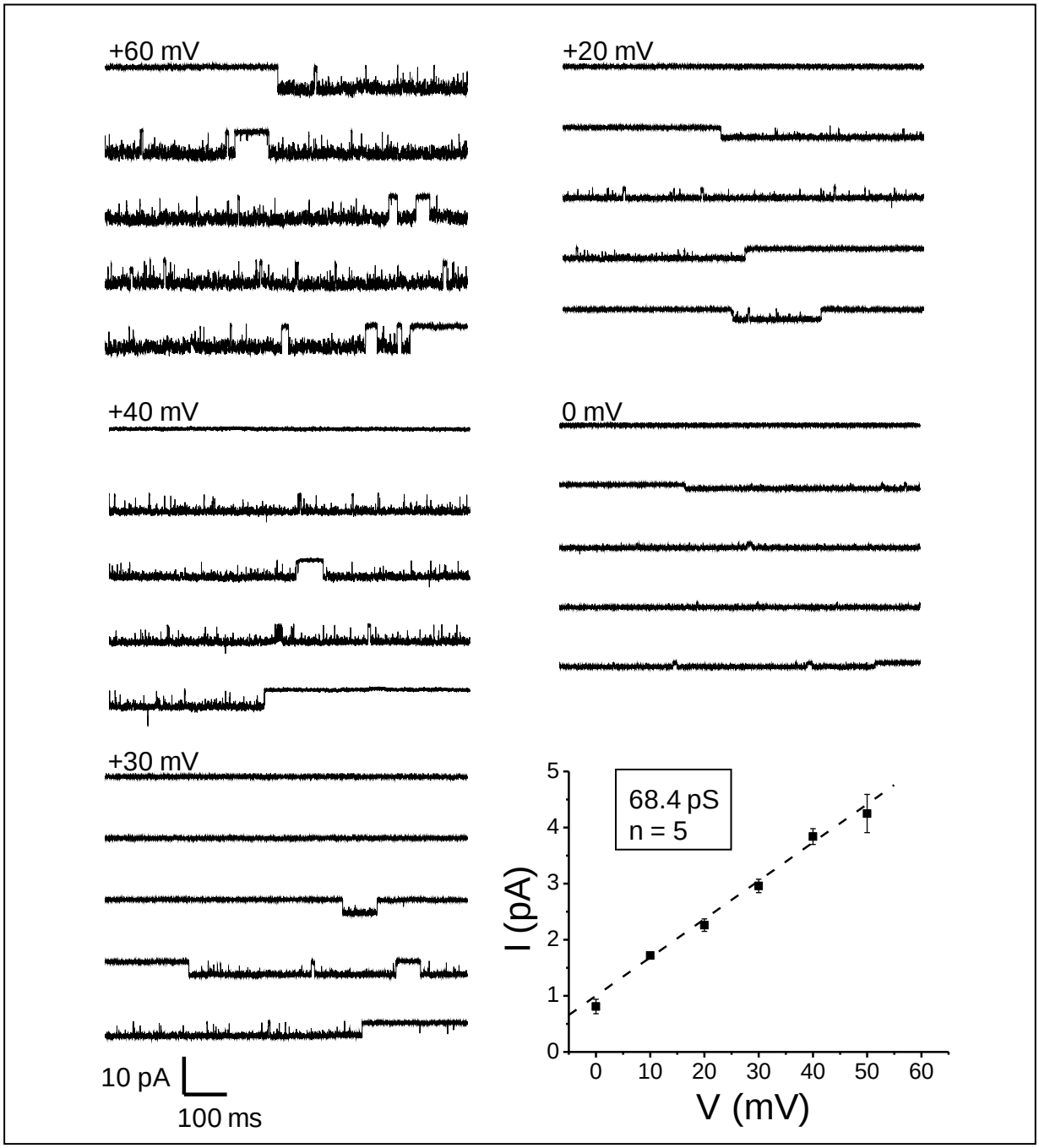

Figure 3.6 Slope conductance of α1 GlyRs

Continuous cell-attached recordings (4 s) of outward currents obtained at the specified holding potentials from an oocyte expressing α1 GlyRs. Openings are downwards. All traces are from the same patch with 1 mM glycine in the pipette. Only one amplitude level is observed. The average amplitudes at each holding potential from all patches were used to give rise to the I/V plot shown below. The plot was fitted with a straight line to estimate the average slope conductance for this receptor subtype.

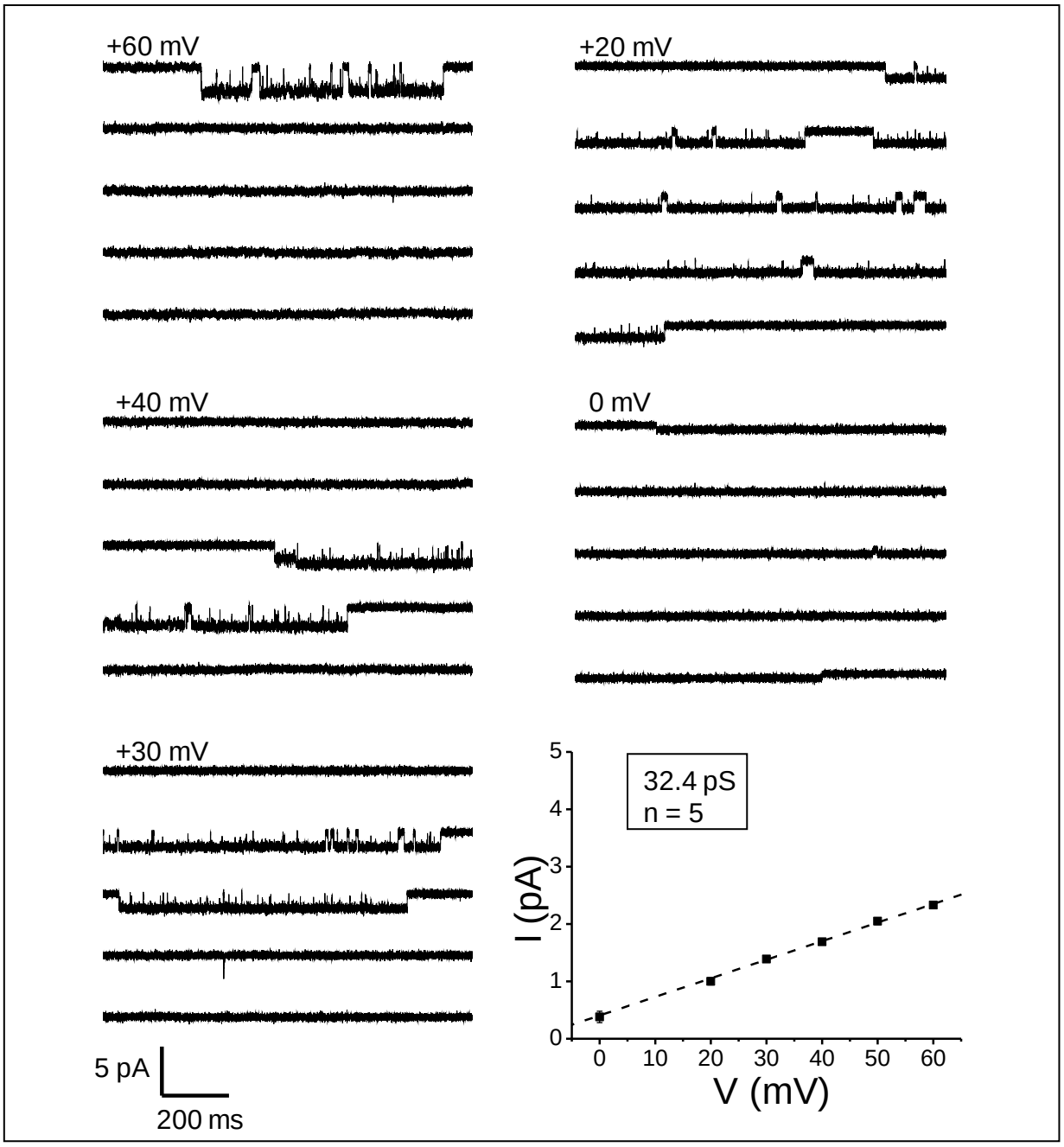

Figure 3.7 Slope conductance of heteromeric α1β GlyRs

Continuous cell-attached recordings (5 s) of outward currents obtained at different holding potentials from a single patch on an oocyte expressing α1β GlyRs (1:40) using 1 mM glycine. The pooled data from all patches are plotted against the holding potential and the I/V plot is fitted with a straight line to obtain the slope conductance for heteromeric receptors. Note that the conductance of these channels is half of that of homomers (compare with Figure 3.6).

3.2.4 Homomeric contamination of α1+β injected oocytes (1:40 ratio)

What the experiments with wild-type receptors show is that, as previously reported by Bormann and colleagues, the incorporation of the β subunit leads to α1β heteromers with single-channel conductance which is half that of α1 homomers (Bormann *et al*., 1993). In order to avoid the formation of α1 homomers, oocytes were injected with α1+β cRNA using an excess of β subunit (ratio of 1:40). Burzomato *et al.* (2003) showed that this ratio is sufficient for the expression of a predominant heteromeric population of channels in HEK293 cells: only 1 out of 19 cell-attached patches had homomeric openings when 1 mM glycine was used (Burzomato *et al*., 2003). The situation was very different in oocytes, as I observed homomeric openings in most of the patches obtained from α1+β injected oocytes, despite the subunit ratio of 1:40. Out of the total of 9 patches (recorded from 4 different oocytes), five patches showed homomeric openings. For two patches these occurred together with heteromeric openings (traces in a, b and c of Figure 3.8*A*) whereas in the other three patches I could only observe homomeric openings; an example of such a recording is shown in Figure 3.8*A* (d).

In order to confirm that the high amplitude channels correspond to homomers contaminating α1+β injected cells, I calculated their slope conductance from the I/V plots (these were obtained in 8 out of the 9 patches and the summary is shown in Figure 3.8*B*. The high amplitude channels have an average slope conductance of 64 ± 3 pS (n = 4), a value which is similar to what was observed for homomers from oocytes injected only with α1. Importantly, the summary shows that ~50% of patches contain a homomeric channel, indicating that an α:β ratio of 1:40 in oocytes is not as efficient in eliminating homomeric channels in oocytes as it is in HEK293 cells (Burzomato *et al*., 2003).

3.2.5 α1β^{Ch} channels have a homomer-like conductance in oocytes

After measuring the slope conductance of wild-type channels I went on to test the TM2-chimeric subunit. Despite the high contamination by homomers I continued to use the 1:40 ratio for the heteromeric combinations hoping to be able to distinguish homomeric channels if they appeared in a patch. First, oocytes were injected with the α1+β^{Ch} combination (1:40) or the β^{Ch} subunit cRNA alone, and I tested their level of expression by acquiring macroscopic currents using TEVC recording (1 mM glycine; see Table 2.2 in Methods). This was done in order to check that: (1) the α1+β^{Ch} combination gives sufficient current for single-channel recordings and (2) that the β^{Ch} subunit alone does not form functional receptors.

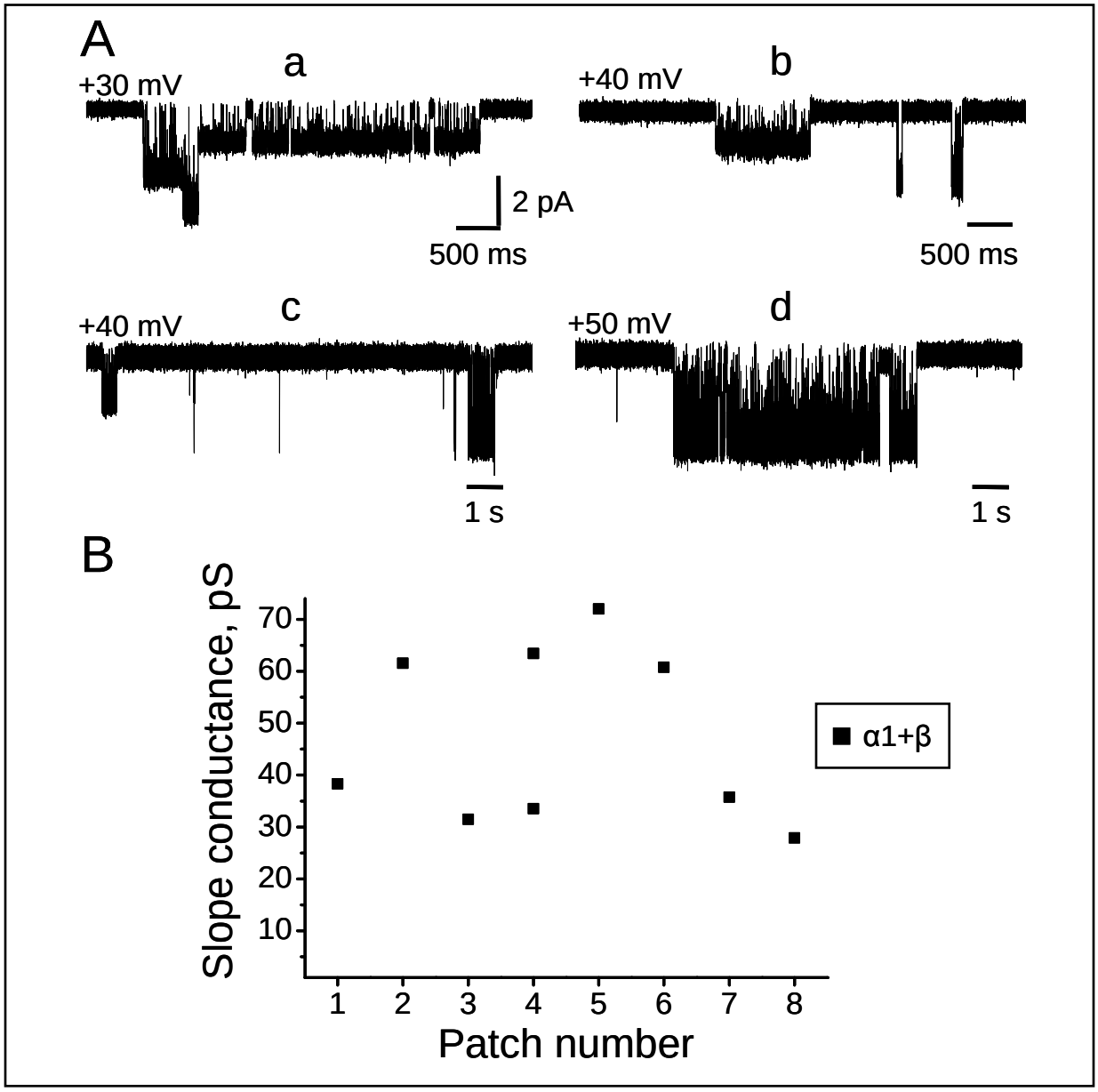

Figure 3.8 Homomeric contamination in oocytes injected with α1+β cRNA
A, Cell-attached traces in which homomeric openings are detected. Currents were obtained with 1 mM glycine from cells injected with α1+β (1:40). In the first three traces (a, b, c) the patches contained both heteromeric and homomeric channels, the latter having higher amplitude. The patch in d contained only homomeric openings. The traces in a and b are from the same patch. The summary from all experiments for this combination is shown in *B.*

As expected I could not record any current from β^{Ch}-injected cells. On the other hand, the current produced by α1+β^{Ch} cells was comparable with that from control α1+β injections (ranging from 100-400 nA, -70 mV; data not shown), reassuring me that I could proceed to single-channel recordings from this combination.

Cell-attached recordings from α1+β^{Ch} oocytes were performed similarly to the wild-type combinations, using 1 mM glycine and a range of positive holding potentials to obtain I/V plots. An example is shown in Figure 3.9. The traces represent continuous 5 s recordings at each holding potential from an individual patch. At this concentration and similarly to wild-type channels, openings occur in clusters. The behaviour of these channels is different from wild-type ones: as seen from the traces, at each holding potential the openings occur at more than one amplitude levels. These subconductances are always directly connected to the openings of the full conductance and are therefore produced by the same channel. The main amplitude of the channel in Figure 3.9 gave a slope conductance of 64 pS. Similarly, the average from 11 patches was 65 ± 1 pS, very similar to the slope obtained by pooling all patches into the I/V plot in Figure 3.9 which gave a conductance of 61 pS.

These values show that the main conductance of channels recorded from oocytes expressing the α1+β^{Ch} combination is similar to that of homomers. Considering that in oocytes injected with α1+β there was ~50% contamination by homomers, there is the possibility that the patches recorded from α1+β^{Ch} oocytes have channels that are mostly, or only, α1 homomers. In at least 6 out of the 11 patches however it is obvious that the β^{Ch} subunit is indeed incorporated into functional α1β^{Ch} heteromers: channels from these patches have a very long duration of clusters (more than 40 s) and the openings occur at more than one amplitude levels. These characteristics do not appear in α1-injected cells (see Figure 3.6). I was therefore confident that at least in these six 6 patches I have been recording from α1β^{Ch} heteromers. The average slope conductance for these was 62 ± 1 pS; these data are consistent with data from HEK293 cells where this chimeric combination was first tested (Bormann *et al*., 1993).

3.2.5 The α1+β+β^{Ch} combination gives a mixture of single-channel conductances

After confirming the formation of α1β^{Ch} channels with a 2-fold difference in the slope conductance compared with α1β, I went on to co-inject both wild-type and mutant β subunits in the same cells. This difference of ~30 pS, between the all-mutant (α1β^{Ch}) and the wild-type channels (α1β), should be enough for recognising one, or two, intermediate conductances, which would mean a 3α:2β or a 2α:3β stoichiometry of α1β GlyRs, respectively (Table 3.4). Oocytes were injected with the α1+β+β^{Ch} combination and I recorded single channels. As before, recordings were performed in the cell-attached configuration and at positive holding potentials to obtain I/V plots. The pipette contained 1 mM glycine.

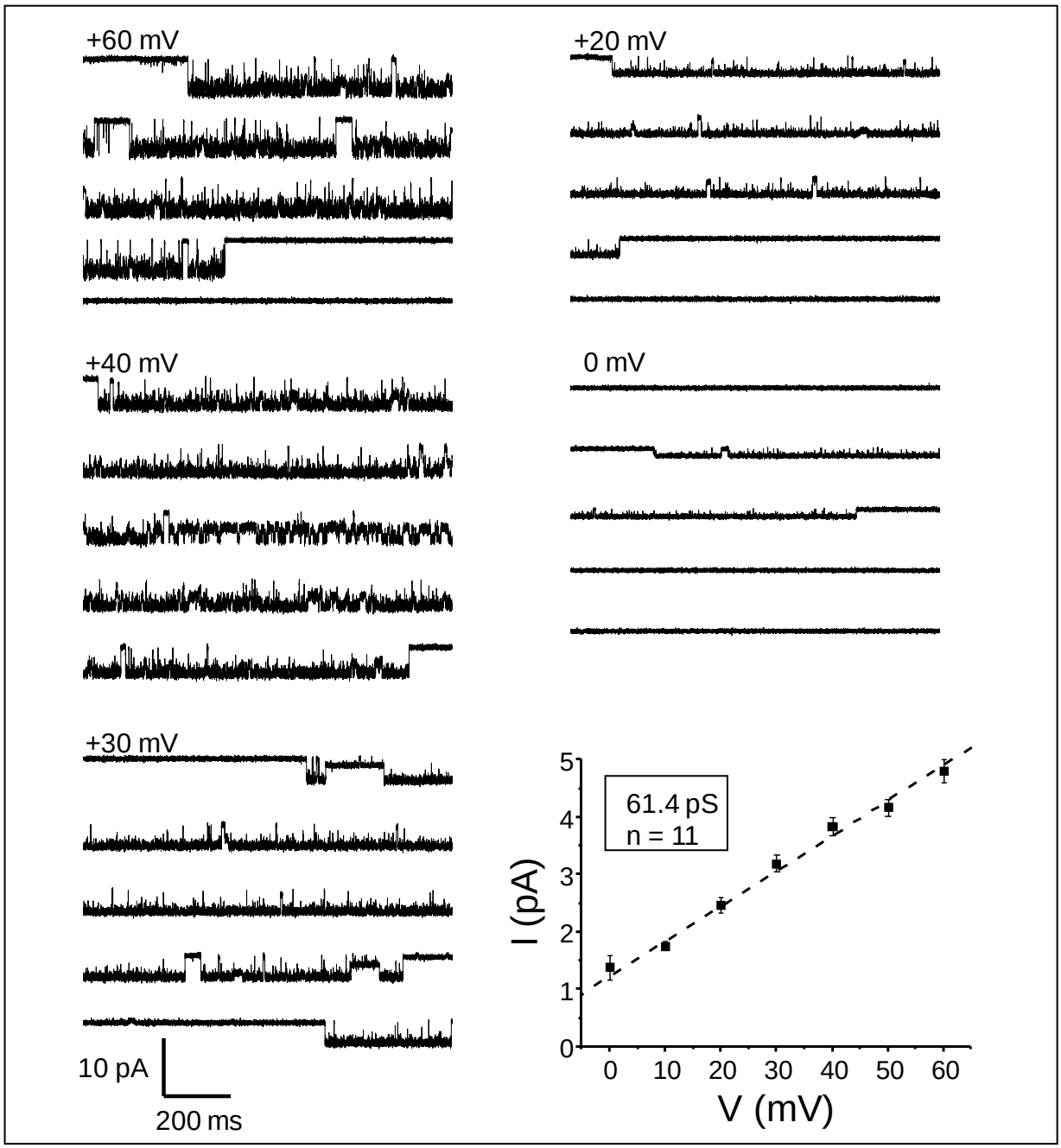

Figure 3.9 Properties of $\alpha1\beta^{Ch}$ channels in oocytes

Cell-attached recordings (5 s sweeps) from oocytes injected with the $\alpha1+\beta^{Ch}$ combination (1:40). All traces are from the same patch, held at the specified potentials, with 1 mM glycine in the pipette. With this combination openings occur at multiple conductance levels with direct links to the highest amplitude level. A maximum of two sublevels are detected for all concentrations. The highest (main) amplitudes at each potential were pooled for all patches to obtain the I/V plot at the bottom. The linear fit of the plot gave a homomer-like slope conductance.

As expected, this combination expressed channels that differed in their single-channel conductance. Figure 3.10 shows an example of a cell from which I was able to record openings at two different amplitude levels in the same patch. There are never direct transitions between the two levels suggesting that the openings derive from two different channels. Confirming this, the points of the average amplitude at each holding potential, for this patch, can be fitted with two linear fits, giving the I/V plot below the trace. The slopes correspond to conductances of 67.5 pS for the high-amplitude points and 45.7 pS for the low-amplitude points. The high-conductance channel is likely to be a α1 GlyR homomer since it does not appear to have the features of the $\alpha1\beta^{Ch}$ heteromers mentioned before.

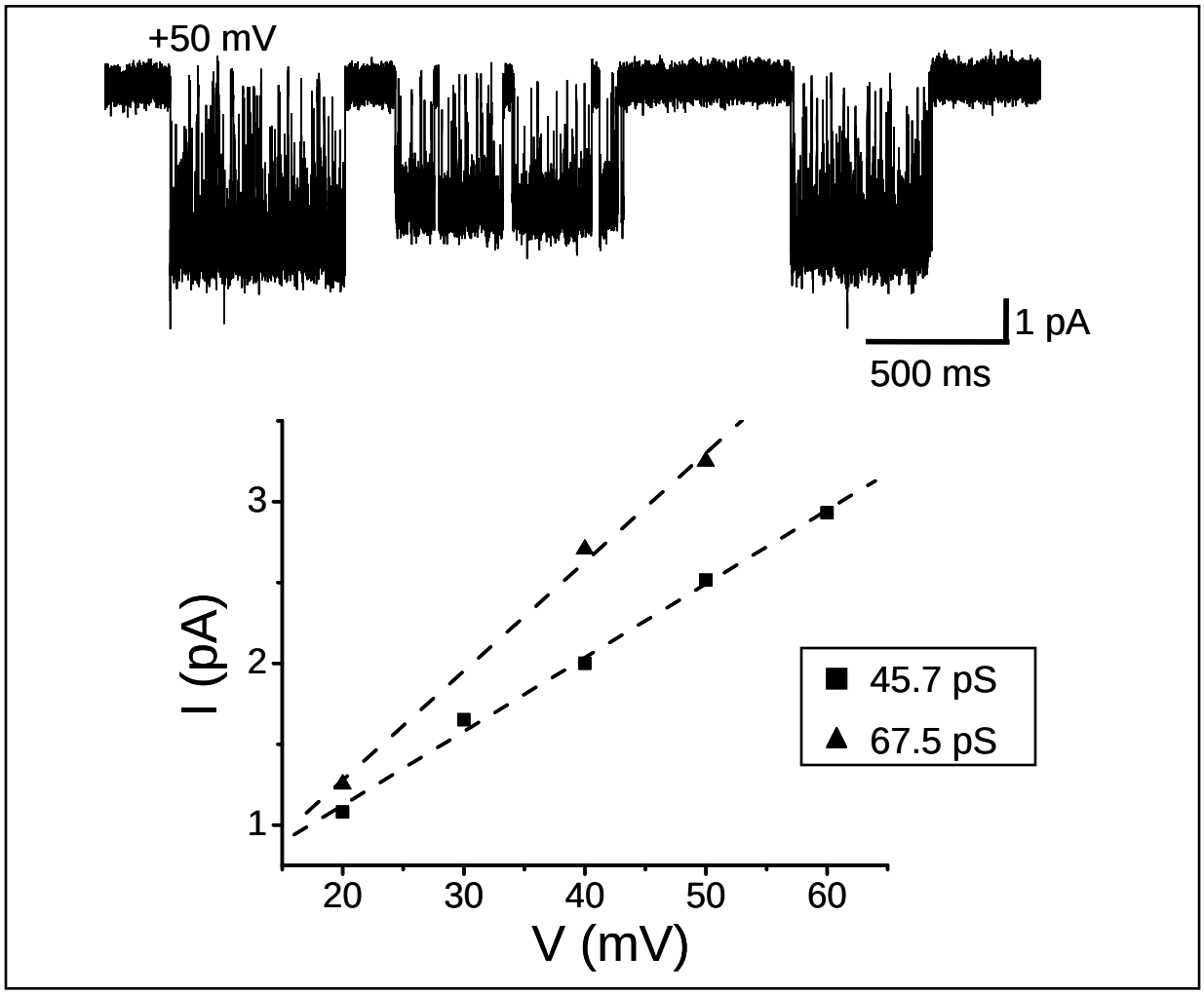

Figure 3.10 Mixture of conductances with the $\alpha1+\beta+\beta^{Ch}$ combination
Example of a cell-attached patch in which two channels with different conductances are detected, obtained from an oocyte injected with the above combination. Glycine was 1 mM. The patch was held at different holding potentials and the fits to the I/V plots for the two channels are shown below.

Figure 3.11*A* shows a summary of all the patches obtained with the α1+β+β^{Ch} combination, comparing the channels' slope conductance with that of channels in the control experiments. With this combination I expected to see at least one group of channels with an intermediate single-channel conductance between the homomer-like α1β^{Ch} (62 ± 1 pS) and the wild-type α1β conductance (33 ± 2 pS). A total of 10 different patches were obtained, out of which: one patch (#30) had two different channels (with two different conductances, see Figure 3.10) and three other patches (#25, 27 and 34) had only one type of channel whose properties suggested that they were α1β^{Ch} heteromers (i.e. homomer-like conductance, with sublevels (66 ± 2 pS). The remaining 7 patches had only one conductance, clearly lower than the homomer level. If considered as one group, these 7 patches (#26, 28, 29, 30, 31, 32 and 33) have channels with a mean slope conductance of 41 ± 2 pS. This average value is higher than the highest-conducting α1β channel (dash line in Figure 3.11; p = 0.016). This difference of ~7 pS however, is not big enough to allow us to group these channels as separate from α1β channels.

In other words, based on these 7 patches alone, I cannot conclude on the presence of channels with an intermediate conductance. More patches are needed in order to clarify how many classes there are in this group. Unfortunately, the α1+β+β^{Ch} combination resulted in a low yield of recordings. As shown in Figure 3.11*B*, the vast majority of the cell-attached patches I obtained had no channel activity and only 10 patches out of approximately 700 had some detectable channel openings. These were results from 6 different oocyte batches. I therefore tested a lower concentration of glycine (50 μM) in order to eliminate the possibility that the lack of channel activation is a result of intense desensitization of the channels at 1 mM. Decreasing the agonist concentration however did not increase success. I managed to record from only 1 patch (out of 40 'empty' ones) in which the slope conductance was 37 pS. This value is close to the average value of 41 ± 2 pS, obtained from the 1 mM traces. The low number of events observed with the low concentration suggests that the low activity I encountered is not a result of desensitization, but may be due to poor expression.

From the above, it was obvious that I could not continue with this combination. I therefore tested two alternatives: (1) repeat the same recordings in the outside-out configuration (2) test a different chimeric subunit.

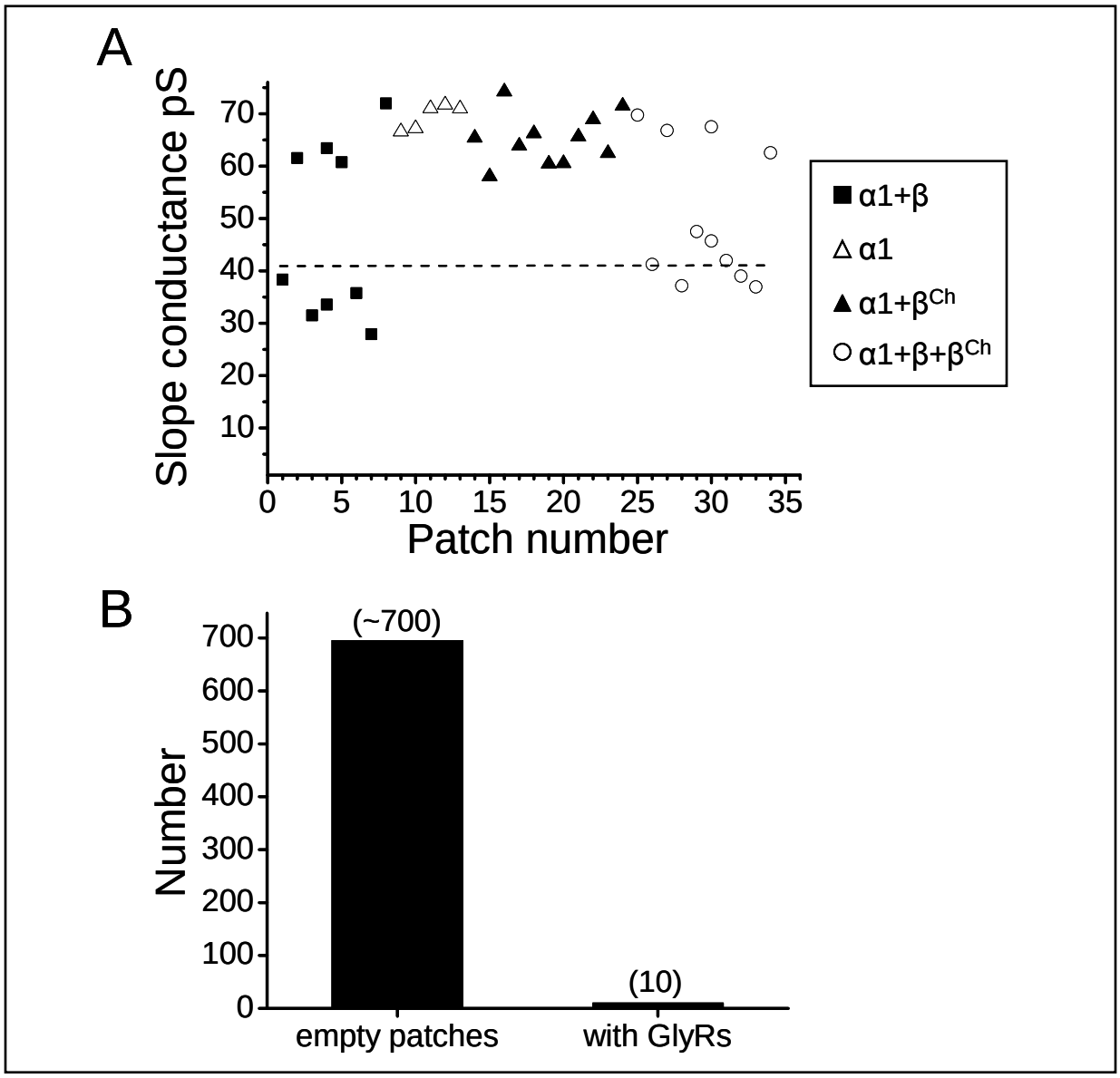

Figure 3.11 Summary for the α1+β+β^{Ch} combination in oocytes
A, Slope conductances of all channels recorded from oocytes injected with the α1+β+β^{Ch} mixture alongside data from the control injections for comparison. All recordings are from cell-attached patches with 1 mM glycine. The two points for patch 30 correspond to the two channels in Figure 3.10. The dash horizontal line represents the average of the 7 patches with the low-conducting channels from this combination (41 ± 2 pS). *B*, Total number of cell-attached patches (in brackets) in which GlyR activations were detected, compared with empty patches, for oocytes injected with the α1+β+β^{Ch} combination.

3.2.6 Chord conductances of oocyte-expressed GlyRs in the outside-out configuration

I switched to the outside-out configuration because of the low success in detecting channel openings in the cell-attached patches. The success rate should increase, because excised patches have a larger surface area (Ogden and Stanfield, 1987). The problem is that wild-type

GlyRs open in several conductance levels when recorded in this configuration (Beato and Sivilotti, 2007; Bormann *et al*., 1987, 1993; Takahashi and Momiyama, 1991; Twyman and MacDonald, 1991). That of course makes the interpretation of the results in terms of stoichiometry difficult since the aim is to measure different conductance levels that appear in the patch.

Recordings were performed with 1 mM glycine applied via bath, at -100 mV. Glycine was only applied to patches where no channel activations were detected for at least 1 min. As expected, the properties of the channels in the outside-out configuration differed from the cell-attached recordings due to the presence of more than one different amplitude levels. This is shown in Figures 3.12 and 3.13 where representative currents from the control injections are shown. From the traces it is evident that: (i) in some cases there are direct transitions between different amplitude levels, suggesting that they can be attributed to the same channels, but most commonly all openings occur independently, (ii) channels from α1-injected oocytes open at 4 different amplitude levels with the predominant level being that of 8.8 ± 0.1 pA (Figure 3.12*A*; Table 3.5), (iii) the data from the homomeric channels are identical to those from $\alpha1+\beta^{Ch}$ injected cells, indicating the homomer-like behaviour of $\alpha1\beta^{Ch}$ heteromers (Figure 3.12*B*), (iv) the presence of the wild-type β subunit decreases the single-channel conductance to a predominant value of 43 ± 1 pS (assuming a chloride reversal potential of 0 mV), almost half that of homomers (Figure 3.13) and finally (v) the contamination by homomers in α1+β injected cells is high, with at least 20% of openings deriving from α1 channels (in 12 out of 12 patches; first trace in Figure 3.13; Table 3.5). These results are in agreement with the cell-attached experiments. The exception is that in the cell-attached configuration the frequency of sublevels is much higher for $\alpha1+\beta^{Ch}$ recordings compared with α1.

The big number of different conductance states I observed from the controls makes it impossible to deduce any reliable conclusions concerning the stoichiometry simply from the number of the different conductance states for the $\alpha1+\beta+\beta^{Ch}$ combination. On the other hand, the frequent appearance of different conductances with this configuration might answer the following question that was raised from the cell-attached data: does the mixed combination truly produce functional 'mixed' receptors (with both wild-type and mutant β)? This could be proved if we detected conductance levels additional to those measured for $\alpha1\beta$ and $\alpha1+\beta^{Ch}$ channels.

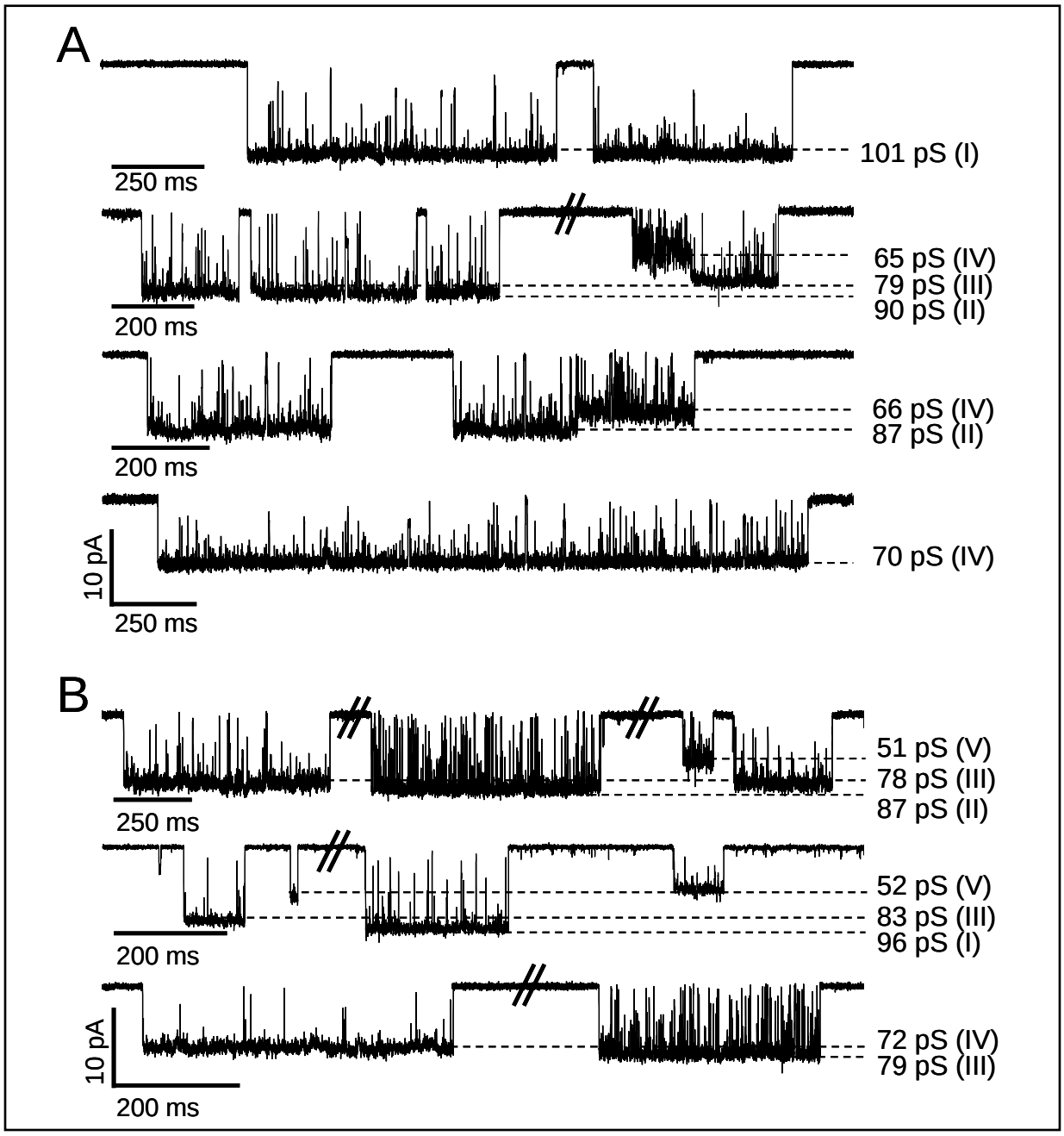

Figure 3.12 Conductance states of GlyRs in oocytes injected with α1 and α1+β^{Ch} cRNA
Recordings were performed in the outside-out configuration from oocytes injected with α1 (*A*) and α1+β^{Ch} cRNA (*B*). Channels were recorded at -100 mV with 1 mM glycine in the bath. The horizontal dash lines mark the different conductance levels, numbered with Roman numerals. Four different conductance levels appear for α1 homomers (A) and five for α1+β^{Ch} cells. Note how the conductance states I-IV are identical for the two combinations. Each line of traces is from a different patch.

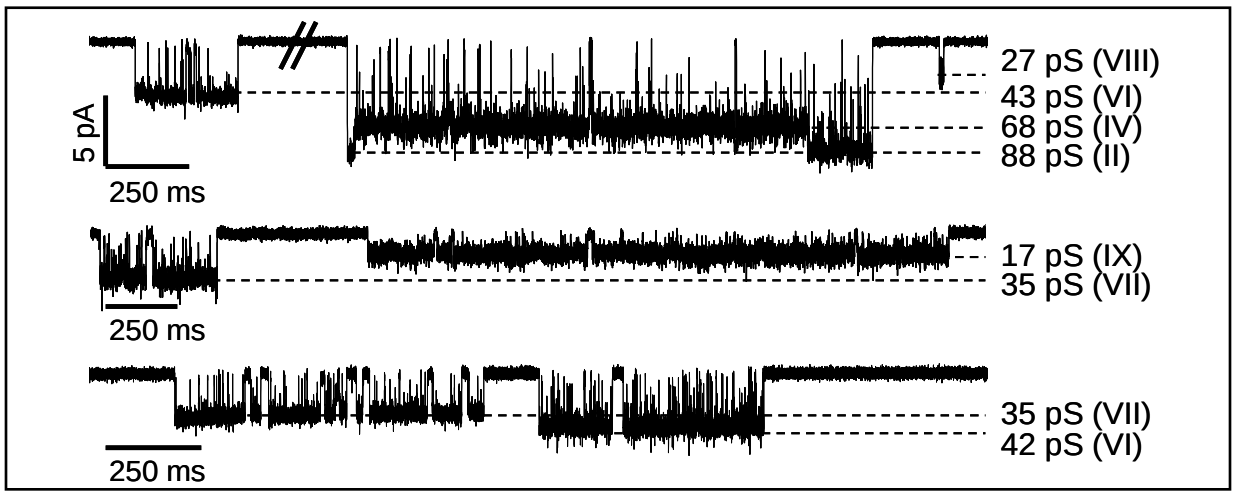

Figure 3.13 Conductance states of heteromeric α1β GlyRs
The traces (from three different patches) represent outside-out recordings from oocytes obtained at -100 mV with 1 mM glycine in the bath. Horizontal dash lines show the different conductance levels, numbered with Roman numerals. The first trace shows contamination by homomeric openings, appearing together with heteromers. Four conductance levels appear for α1β heteromers (VI-IX).

As expected, the greater patch surface in the outside-out configuration increased my recording success rate for the α1+β+β^{Ch} combination and glycine-evoked channel activations were observed in the majority of patches. As summarized in Table 3.5, I was able to identify at least 8 different conductance states. Examples of such channels from two different patches are shown in Figure 3.14. The majority of the channels from this combination open at α1β-like conductance states (VI-IX) with the predominant state being that of 45 ± 1 pS (~48% of openings), similar to the α1+β combination. The rest of openings were homomer-like, with the most common state being that of 90 ± 1 pS.

These results show that none of the conductance states was unique for the mixed combination. The presence of unique conductances would indicate the presence of functional 'mixed' receptor subtypes. Lack of intermediate states suggests that either these receptors are not formed or that their conductance states overlap with those from the control patches.

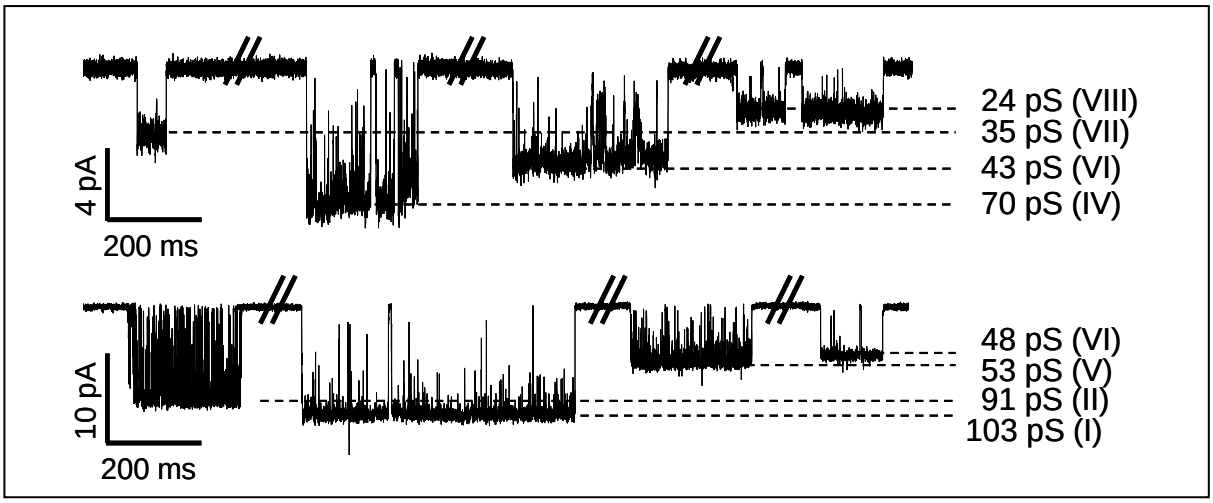

Figure 3.14 Conductance states from α1+β+β^{Ch} injected oocytes
Examples of outside-out recordings at -100 mV from oocytes injected with the mixture combination. Glycine was 1 mM. Horizontal dash lines show the observed conductance levels, numbered with Roman numerals.

Table 3.5 Chord conductance levels for the different cRNA combinations in oocytes.

	I (94-102)	**II** (84-91)	**III** (77-83)	**IV** (66-72)	**V** (51-57)	**VI** (40-46)	**VII** (33-39)	**VIII** (22-27)	**IX** (-17)
α1 N = 6	98 ± 2 n = 3 12%	88 ± 1 n = 4 31%	79 + 1 n = 2 27%	70 n = 1 30%					
α1+β^{Ch} N = 7	95 ± 1 n = 4 15%	87 ± 1 n = 6 39%	80 ± 1 n = 5 32%	69 ± 2 n = 3 10%	53 ± 2 n = 3 5%				
α1+β N = 12	96 ± 1 n = 2 1%	87 ± 1 n = 6 6%	78 ± 1 n = 4 3%	67 ± 1 n = 3 6%	56 ± 1 n = 3 4%	43 ± 1 n = 5 39%	37 ± 3 n = 4 11%	26 ± 1 n = 4 27%	17 n = 1 3%
α1+β+β^{Ch} N = 15	102 ± 1 n = 2 7%	90 ± 1 n = 5 9%		71 ± 1 n = 2 1%	54 ± 1 n = 4 4%	45 ± 1 n = 14 47%	35 ± 1 n = 9 25%	26 ± 1 n = 4 5%	17 n = 1 2%

The conductance levels are numbered with Roman numerals (I to IX); the range for each state is denoted in brackets. Average values ± SEM are in pS, n is the number of patches where each state is observed, % is the frequency of openings at each state; N is the total number of patches for each cRNA combination.

3.2.7 The α1+β+β^{Ch} combination gives only two conductance states in HEK293 cells

To distinguish between the two possibilities I tested the mixed α1+β+β^{Ch} combination in HEK293 cells. The advantage of using these cells is that the stoichiometry of α1β GlyRs is already established as 3α:2β using the 9′LT mutation and that homomer contamination can be reduced with the appropriate α:β ratio (Burzomato *et al.*, 2003). Hence, with this information at hand, any data from HEK293 cells might be useful in interpreting the oocyte data.

Cells were transfected with α1+β+β^{Ch} cDNA and recordings were performed in the cell-attached configuration using 1 mM or 200 μM glycine in the pipette. I recorded channels at a range of holding potentials (typically between 0 mV and -100 mV) and fitted the I/V plots with a linear fit to get the slope conductance. Figure 3.15*A* shows example traces from such an experiment. This patch was held at holding potentials ranging from -100 mV to +40 mV, with 1 mM glycine in the pipette. As for oocytes, at this concentration channel openings occur in clusters. This patch was idealised by time course fitting with SCAN and EKDIST was used for the distributions of fitted amplitudes. From the distributions it was evident that only one main amplitude level appears at each holding potential. For example, the distribution for fitted amplitudes at a holding potential of -100 mV can be well fitted by a single Gaussian curve, giving a peak at 3.22 pA and a standard deviation value of 0.32 pA (Figure 3.15*B*). All fitted amplitude values for this patch are shown in the stability plot in Figure 3.15*C*. For the I/V plot shown below (Figure 3.15*D*) the mean fitted amplitudes taken from the Gaussian fits were plotted against the holding potentials, giving a slope conductance of 31.9 pS for this channel. The chloride reversal potential was ~0 mV. This value of 31.9 pS, obtained from the idealised record, is identical to the value of 31.1 pS, obtained by analysing the same patch with cursor measurements in Clampfit. This confirms the validity of the oocyte data, which were all analysed by Clampfit.

The average slope conductance from all α1+β+β^{Ch} transfected HEK293 cells was 30 ± 1 pS (n = 27) for 1 mM patches and 31 ± 3 pS (n = 6) for 200 μM patches. A summary of all data is shown in Figure 3.16. As mentioned previously, the stoichiometry of α1β channels in HEK293 cells is 3α:2β which means that the α1+β+β^{Ch} combination is expected to produce 3 different receptor types, distinguished by different single-channel conductances. From the summary it is obvious that only two different conductance levels appear: one with an overall average of 30 ± 1 pS (both concentrations, 33 patches) and a homomer-like conductance of 66 ± 2 (n = 3).

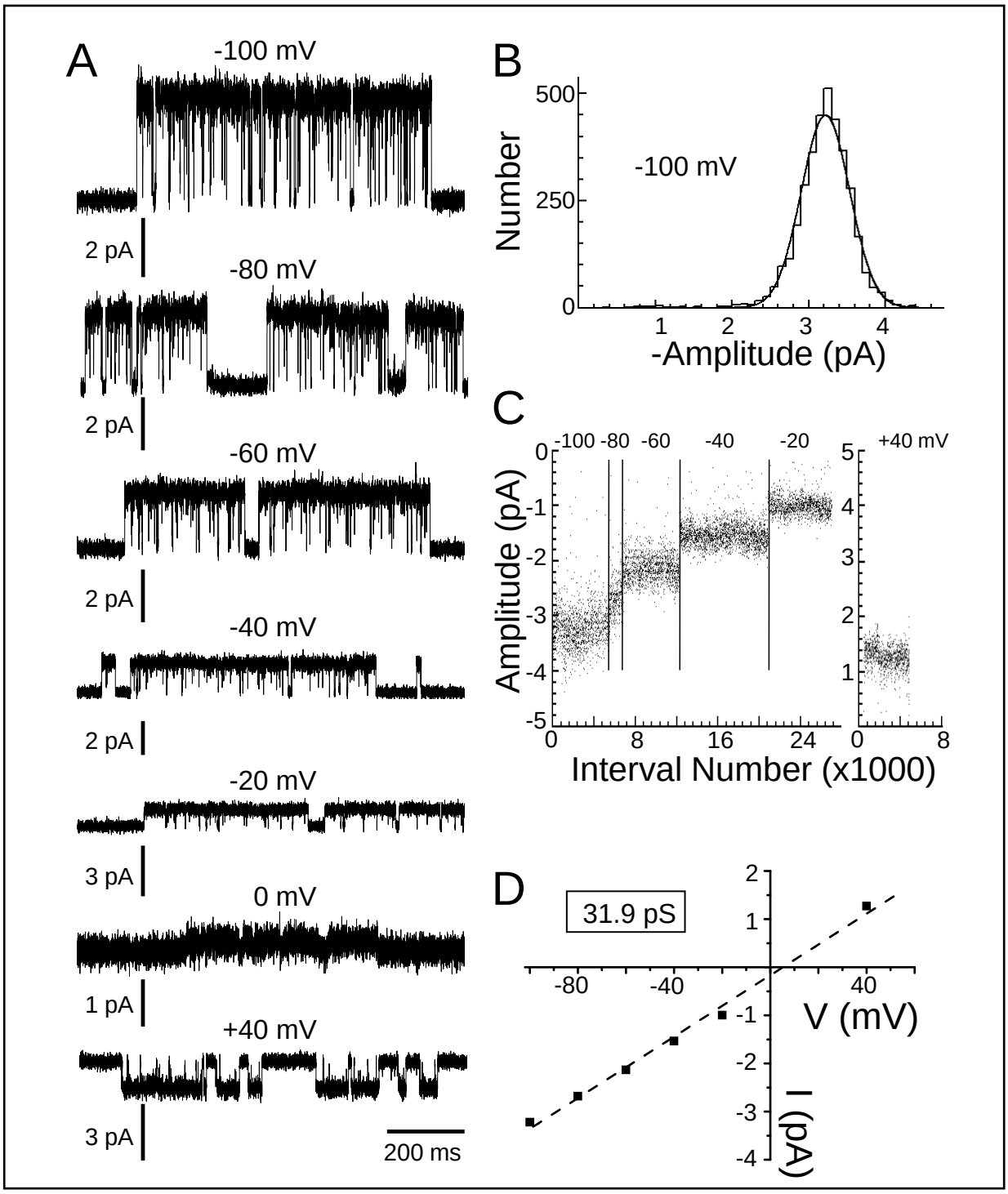

Figure 3.15 Conductance of GlyRs in HEK293 cells transfected with $\alpha1+\beta+\beta^{Ch}$

A, Cell-attached traces of GlyRs expressed in HEK293 with the mixture combination. All traces are from the same patch, held at a range of holding potentials. Glycine was 1 mM. This patch was idealised by time course fitting using SCAN. The distribution of fitted amplitudes at -100 mV is shown in *B*. The distribution is fitted with a single Gaussian component. In *C* is the stability plot of fitted amplitudes for the entire patch. The numbers on top are the corresponding holding potentials (in mV). Note that only one amplitude level is detected for cell-attached recordings. The I/V plot for this patch is in *D*.

The data from HEK293 cells are similar to what was observed for the same combination in oocytes. To summarise, the HEK293 cell data confirm the cell-attached and outside-out experiments of oocytes: the mixed combination of $\alpha1+\beta+\beta^{Ch}$ does not give intermediate conductance levels. Based on this, I cannot conclude on the stoichiometry of oocyte expressed $\alpha1\beta$ channels using this approach.

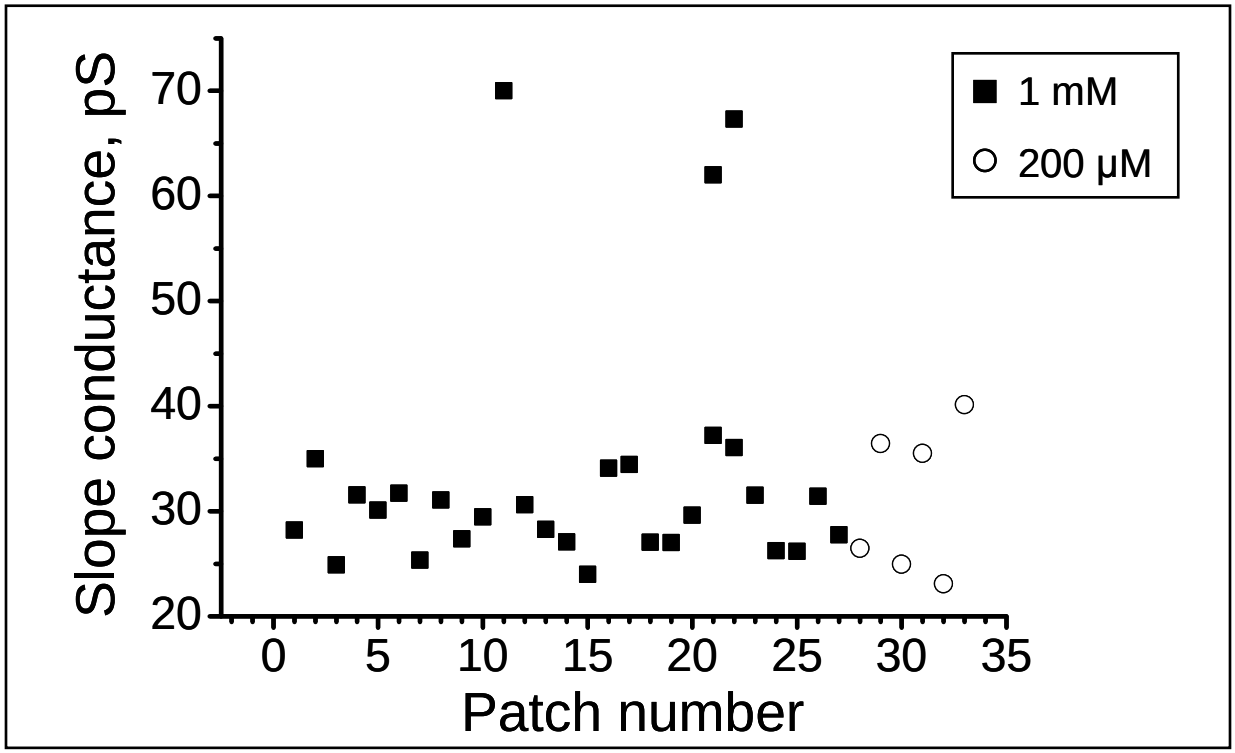

Figure 3.16 Summary of experiments in HEK293 cells transfected with $\alpha1+\beta+\beta^{Ch}$
The plot summarises all data obtained from HEK293 cells transfected with this combination. All recordings were performed in cell-attached with either 1 mM (squares) or 200 µM Gly (circles) in the pipette. Only two conductance levels were detected for this combination.

As a last alternative the $\alpha1^{Ch}$ subunit was constructed: this is the α1 subunit that carries the TM2 domain of the β subunit (see Figure 2.3, Methods). The rational of this is the same as with the β^{Ch} construct: a mixed $\alpha1+\beta+\alpha1^{Ch}$ combination injected into oocytes would produce an $N+1$ number of receptor subtypes, depending on the stoichiometry of the $\alpha1\beta$ heteromer. The subtypes would be distinguishable because of different single-channel conductances. Prior to proceeding to single-channel recording I tested whether injections into oocytes of the $\alpha1^{Ch}+\beta$ (1:40 ratio) and the $\alpha1^{Ch}$ combinations would produce enough current for single-channel recordings. TEVC recordings from $\alpha1^{Ch}+\beta$ injected cells using 1 mM glycine did not produce

any macroscopic current (n = 5), whereas cells injected with the $\alpha1^{Ch}$ subunit alone produced an average current of -11 nA (n = 4, data not shown). This amount of current is not sufficient for single-channel recordings. I therefore abandoned this approach.

Similarly to the 9′ mutation data, the conductance mutation approach I have followed for investigating the stoichiometry of α1β GlyRs in oocytes resulted in inconclusive data. Attempts to explain the data are considered in the Discussion section (Chapter 4).

3.3 Activation mechanism of α2 GlyRs

3.3.1 The α2 GlyR

In the immature nervous system the reversal potential for chloride is depolarizing and this means that the activation of a chloride-permeable channel such as the glycine receptor is effectively excitatory. The depolarization of immature neurons leads to the entry of calcium into the cells and finally to the modulation of processes such as proliferation, cell migration and differentiation. The α2 subunit is likely to play a major role in the embryonic form of GlyRs (Legendre, 2001); α2 transcripts are abundant in the embryonic and neonatal rat but are gradually replaced by the α1 subunit (Akagi and Miledi, 1988; Akagi *et al.*, 1991; Malosio *et al.*, 1991a; Watanabe and Akagi, 1995). Also, Takahashi *et al.* (1992) showed that the single-channel properties of embryonic (E20) and adult (P22) rat spinal GlyRs correspond better to recombinant α2 and α1 receptors, respectively (Takahashi *et al.*, 1992). The developmental switch of GlyRs is completed at approximately P20 in the rat, so in the early postnatal period, both α1 and α2 subunits may be present (Legendre, 2001; Bowery and Smart, 2006). The consensus view is that GlyRs on embryonic and neonatal neurons are predominantly homomers of α2, whereas adult receptors are α1β heteromers (Akagi and Miledi, 1988; Becker *et al.*, 1988; Hoch *et al.*, 1989; Pfeiffer *et al.*, 1982).

Despite the abundance of the α2 subunit in the embryonic brain, it is unclear whether α2 homomeric receptors are involved in glycinergic synaptic transmission. This is because: firstly, homomeric GlyRs cannot cluster at the synapse because only β subunits can interact with gephyrin (Meyer *et al.*, 1995; see section 1.2.7ii). Secondly, α2 is expressed in neuronal regions where no glycine-mediated synaptic transmission has been detected and in non-neuronal cells such as glial cells or progenitor cells (Belachew *et al.*, 1998; Flint *et al.*, 1998; Mangin *et al.*, 2002; Nguyen *et al.*, 2002). Finally, Legendre and colleagues have shown that α2 homomeric receptors have kinetic properties that make them unsuitable to mediate fast synaptic transmission: they activate and deactivate slowly and have a low probability of opening in response to the rapid application of brief pulses of glycine (Mangin *et al.*, 2003). It has been suggested that α2 homomeric receptors may be extrasynaptic channels that can be activated by a paracrine-like release of glycine or taurine, even at low concentrations, making

them potential players for neuronal development (Legendre, 2001; Mangin *et al.,* 2003; see also Clements, 2002).

3.3.2 Aim

A detailed description of receptor behaviour both at steady-state and in response to non-equilibrium conditions (i.e. at the synapse) consists of a scheme that links together all the functional states of the channel (open, closed, desensitized) together with the rate constants for the reactions that link the states. Such a kinetic mechanism also allows some understanding of the role of specific residues in the channel molecule: if for example a mutation in a specific position alters the gating but not the binding rates then it stands to reason that this residue forms part of the channel gate, or is indirectly involved in gating. Hence, kinetic modeling provides a link between structure and function, allowing conclusions to be drawn concerning the role of particular channel domains.

The aim of this section was to establish a quantitative activation mechanism for the kinetic behaviour of recombinant α2 GlyRs. The goal is to find the simplest model that can describe the data. The model has of course to be consistent with the available information on biochemical, pharmacological, and structural properties of the channel.

3.3.3 General features of α2 GlyR channel openings

Single-channel recordings from HEK293 cells transfected with rat α2 GlyR cDNA were performed in the cell-attached configuration, at -100 mV (pipette potential of +100 mV). Representative recordings at different glycine concentrations, ranging from 20 μM to 10 mM are shown in Figure 3.17. The first thing to be noted was that the success rate in obtaining patches with channel activity was low (~1 in 5 patches) at all concentrations. In the case of α1 (Beato *et al.,* 2004) and α1β GlyRs (Burzomato *et al.,* 2004), at low agonist concentrations openings occur in short bursts which, at high concentrations, become grouped into long clusters of openings, separated by long shut periods. Bursts within the clusters get closer and closer as the glycine concentration increases, and because of that the proportion of open time within the cluster steadily grows. For the α2 receptors, on the other hand, it was impossible to distinguish between bursts and clusters as channel activity presented a very similar appearance at all concentrations.

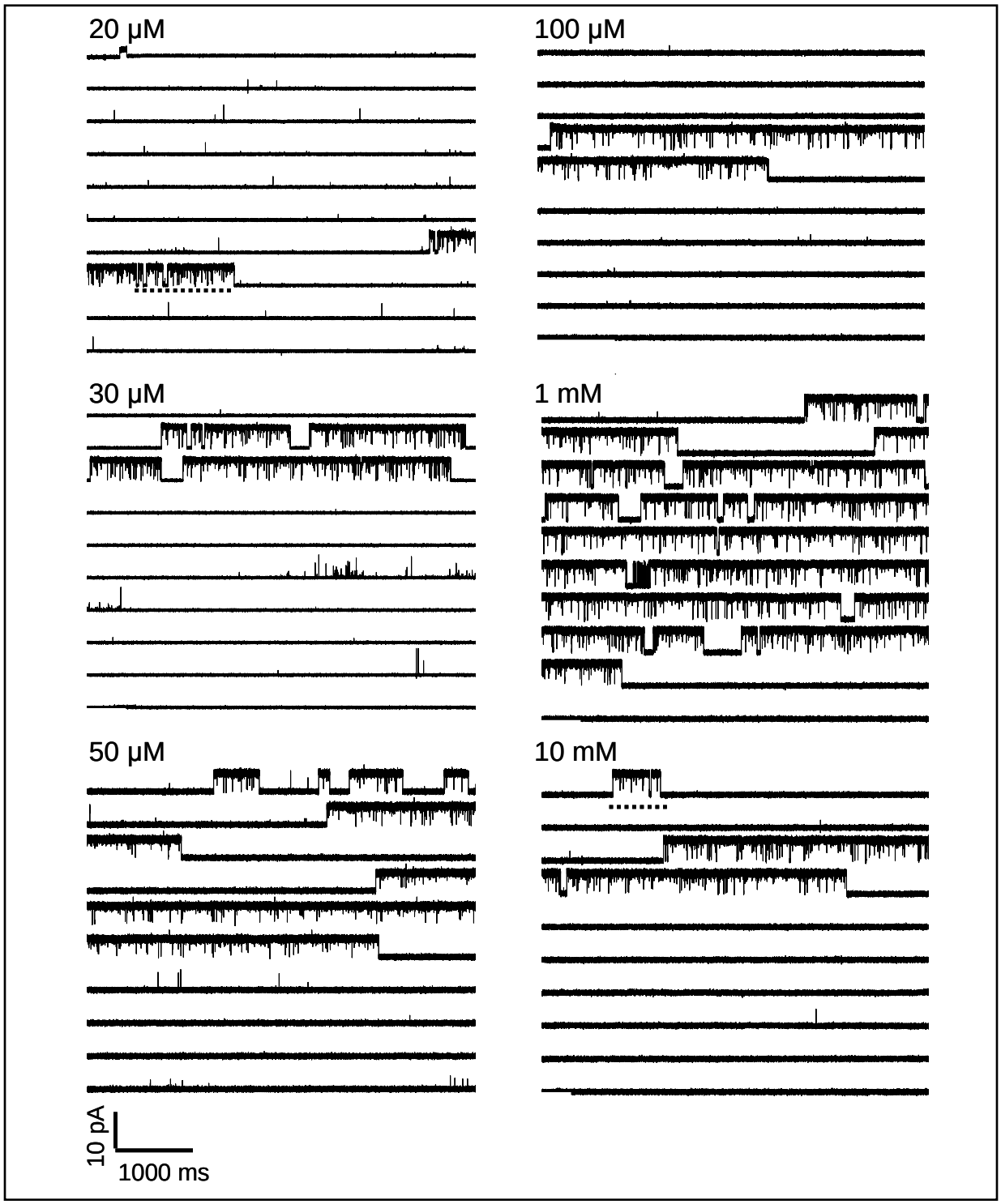

Figure 3.17 Activation of α2 GlyRs in HEK293 cells
Continuous (50 s) sweeps of single-channel recordings of α2 homomeric receptors evoked by different concentrations of glycine. Patches were obtained from HEK293 cells in the cell-attached configuration at a pipette potential of 100 mV. Traces were filtered at 5-7 kHz. The dotted lines under the 20 µM and 10 mM traces represent the regions expanded in Figure 3.18.

I never saw short bursts, and even at the low glycine concentrations groups of channel openings were long and separated by long shuttings (usually lasting for minutes). Each recording contained a relatively small number of these groups of openings. This is evident in Figure 3.18*A* where channel activity at 20 μM (lowest concentration) and 10 mM glycine (saturating concentration) are shown on an expanded time scale. Both traces have a high P_{open} and contain few short shuttings, unlike α1 and α1β channels in which the P_{open} is concentration dependent (Figure 3.18*B*). Despite the high P_{open} observed at 20 μM glycine I was never able to observe channel openings in patches exposed to lower glycine concentrations (n = 10).

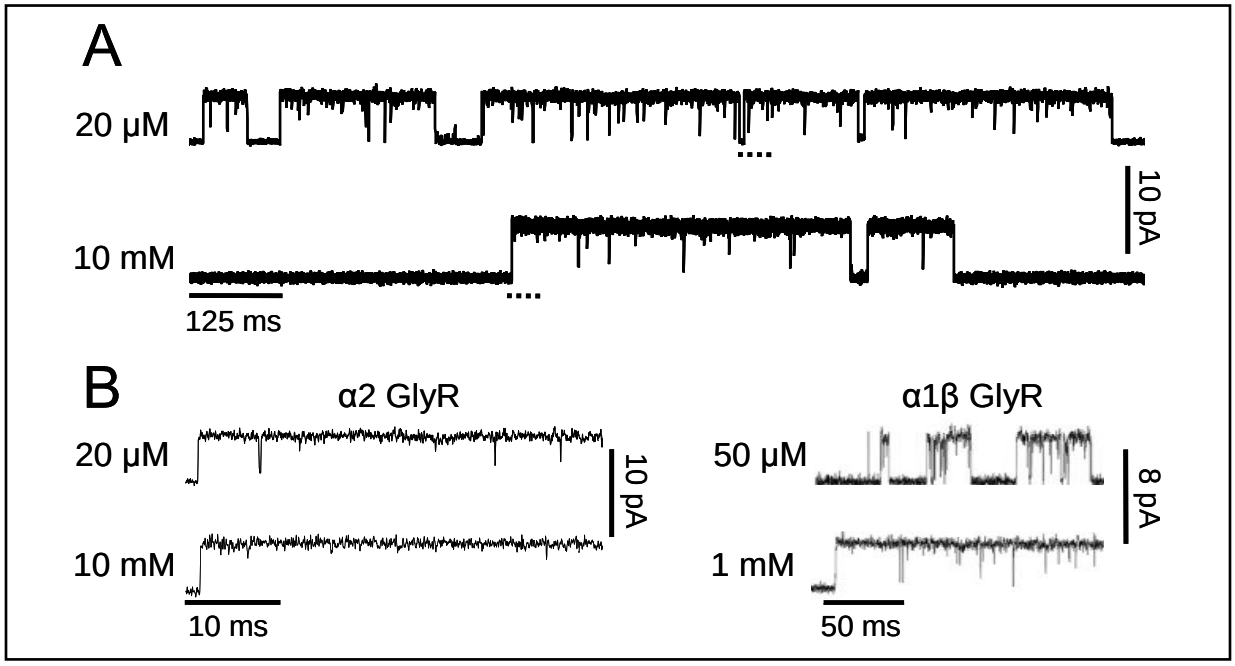

Figure 3.18 α2 GlyR clusters
A, The displays are parts of the clusters shown in Figure 3.17 (dotted lines) for the lowest (20 μM) and highest (10 mM) glycine concentration, expanded on the same time scale for comparison. Note how the open probability is similar for both concentrations, with few shut times within the cluster. The same traces are more expanded in the left panel of *B* (50 ms sweeps; dotted lines in *A*) and are shown against parts of α1β GlyR clusters for comparison (right panel). The lack of concentration dependence in the P_{open} is evident for α2 receptors. The α1β traces are reproduced from Burzomato *et al.* (2004).

Only one channel amplitude was detected in each patch. This is shown from the amplitude distributions in Figure 3.19 which are all fitted with a single Gaussian curve. The average amplitude from a total of 25 patches was 5.9 ± 0.2 pA. The mean fitted amplitude varied considerably between the 25 patches, ranging from 4.5 to 9.1 pA. This was expected for cell-

attached recordings since the amplitude of channel openings depends on both the intracellular chloride ion concentration and the resting membrane potential, both of which vary from cell to cell.

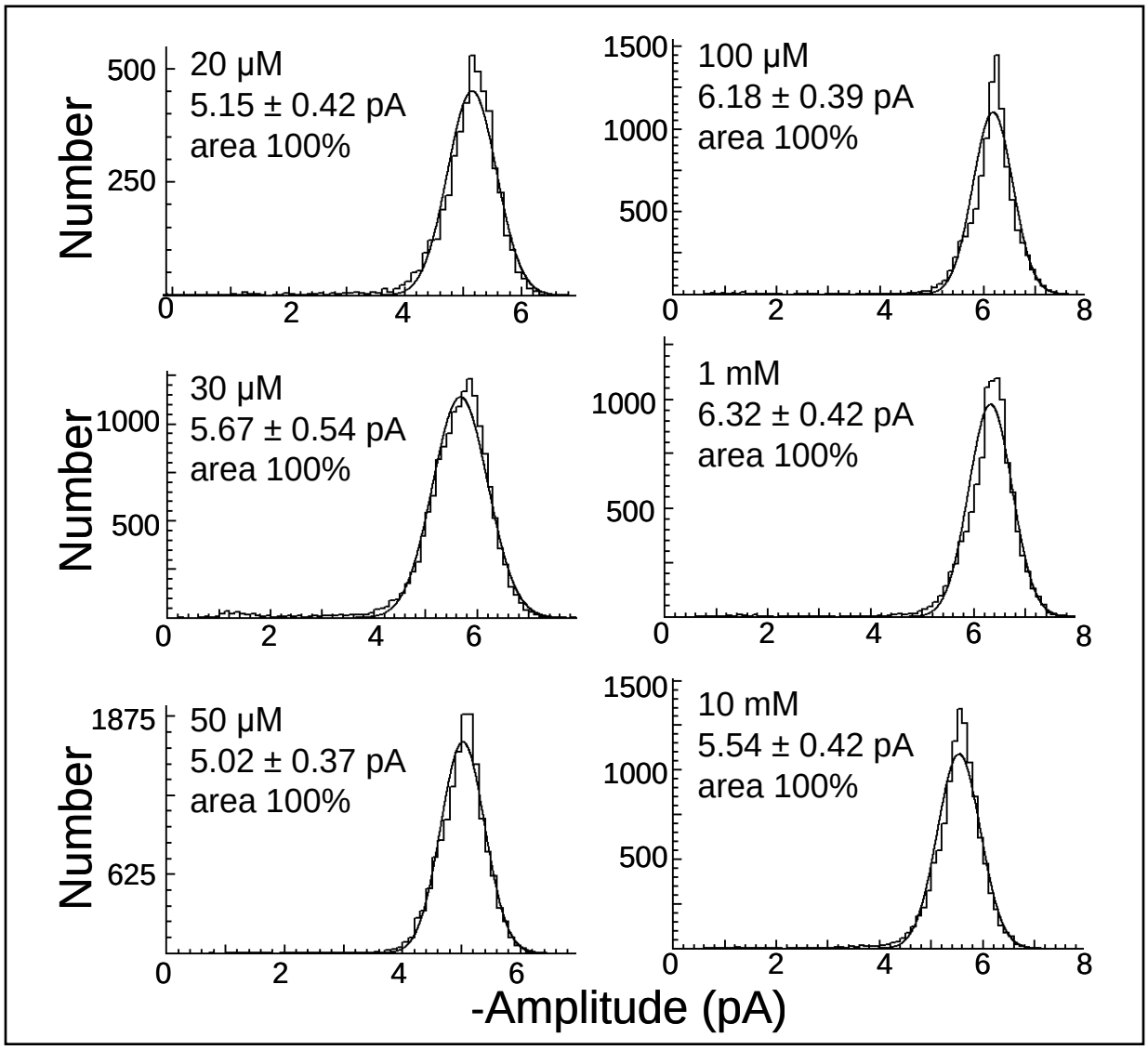

Figure 3.19 Fitted amplitude distributions for α2 GlyRs

The fitted amplitude distributions correspond to the traces in Figure 3.17. All distributions are fitted with a single Gaussian component, indicative of only one amplitude level for these channels and this configuration. Only openings that are longer than two filter risetimes are included.

3.3.4 Dwell-time distributions

In ideal conditions, the number of components in the open or shut-time distributions is equal to the number of open or shut states in the activation scheme. It is likely however that, in real data, one or more components will be undetectable. Therefore, fitting real distributions provides information about the *minimum* number of open or shut states needed.

Open-period distributions, examples of which are shown in Figure 3.20 for the six concentrations, have up to three exponential components (fitted using EKDIST, see Methods). The summary in Table 3.6 shows that a fast component (ranging from 8 to 51 μs) is almost always present in the distributions. The mean lifetime of this component is often faster than the resolution (20 μs) and only few events can be resolved in each patch. When fitted with EKDIST this component reached an area of up to 12% at low concentrations but gradually decreased to only 2% at 10 mM. The slowest component was predominant in all concentrations with an average area of 82-98%. An intermediate component of 0.2-0.5 ms is sometimes detected, but its contribution is minimal.

In other channels which can open at different levels of liganding, it is common to see that the mean open time increases with agonist concentration, as the longer open components (corresponding to the higher levels of ligation) increase in frequency. This is seen with α1 and α1β glycine receptors (Beato *et al.*, 2002; Burzomato *et al.*, 2004) but, as Table 3.6 shows, there is very little sign of this for the α2 channel. There is a shift to more prolonged openings as the glycine concentration increases from 20 to 30 μM, but the mean open period is similar for all concentrations above 30 μM (ranging from 27 to 34 ms).

Apparent shut-time distributions were fitted with three or four components (Figure 3.21, see Table 3.6). For all concentrations most shuttings belong to a very fast component which is predominant irrespective of glycine concentration. This component, with average time constants of 5-10 μs, is faster than the experimental resolution of 20 μs and most events in this component will be missed. Inspection of the values in Table 3.6 shows that the time constants for the first three components are similar across concentrations. On the other hand, the last component (τ4) becomes shorter at higher concentration (from 6 to 1 ms).

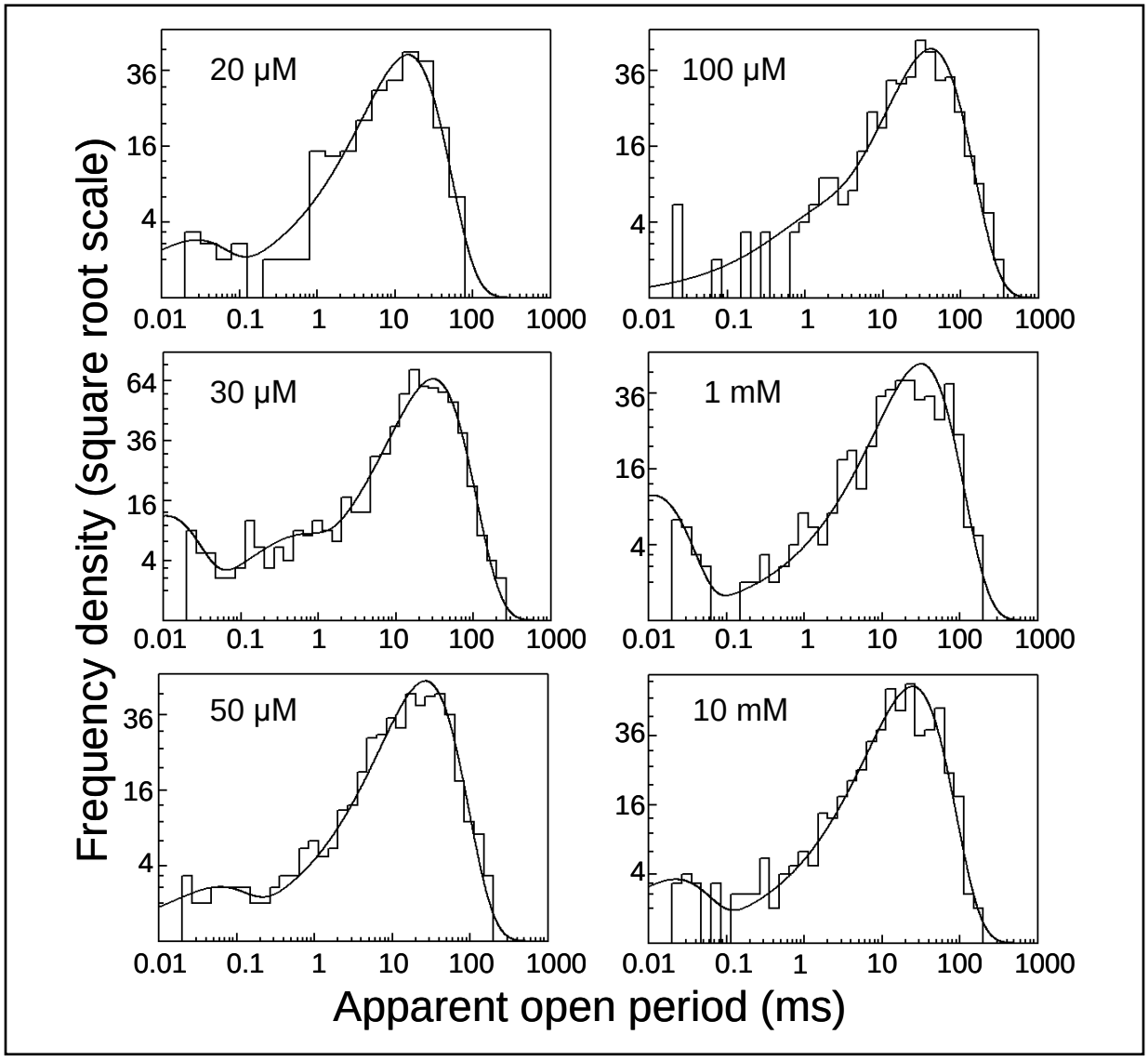

Figure 3.20 Open-period distributions for α2 GlyRs
The distributions, corresponding to the traces in Figure 3.17, are fitted with mixtures of exponential probability density functions. Open periods denote the time duration that the channel is continuously open, irrespective of amplitude level, between adjacent shut times that are longer than the resolution. Up to three exponential components were needed for these distributions (Table 3.6).

Given the aim of fitting a mechanism to the data, examining the concentration dependence of the shut-time distributions should help to understand which events are bursts and which are clusters of bursts and to set t_{crit} values to divide the low concentration records into bursts and the high concentration records into clusters. For the α2 data, the concentration dependence of the longest shut time is rather small, making the task of determining a t_{crit} for bursts very difficult and somewhat arbitrary.

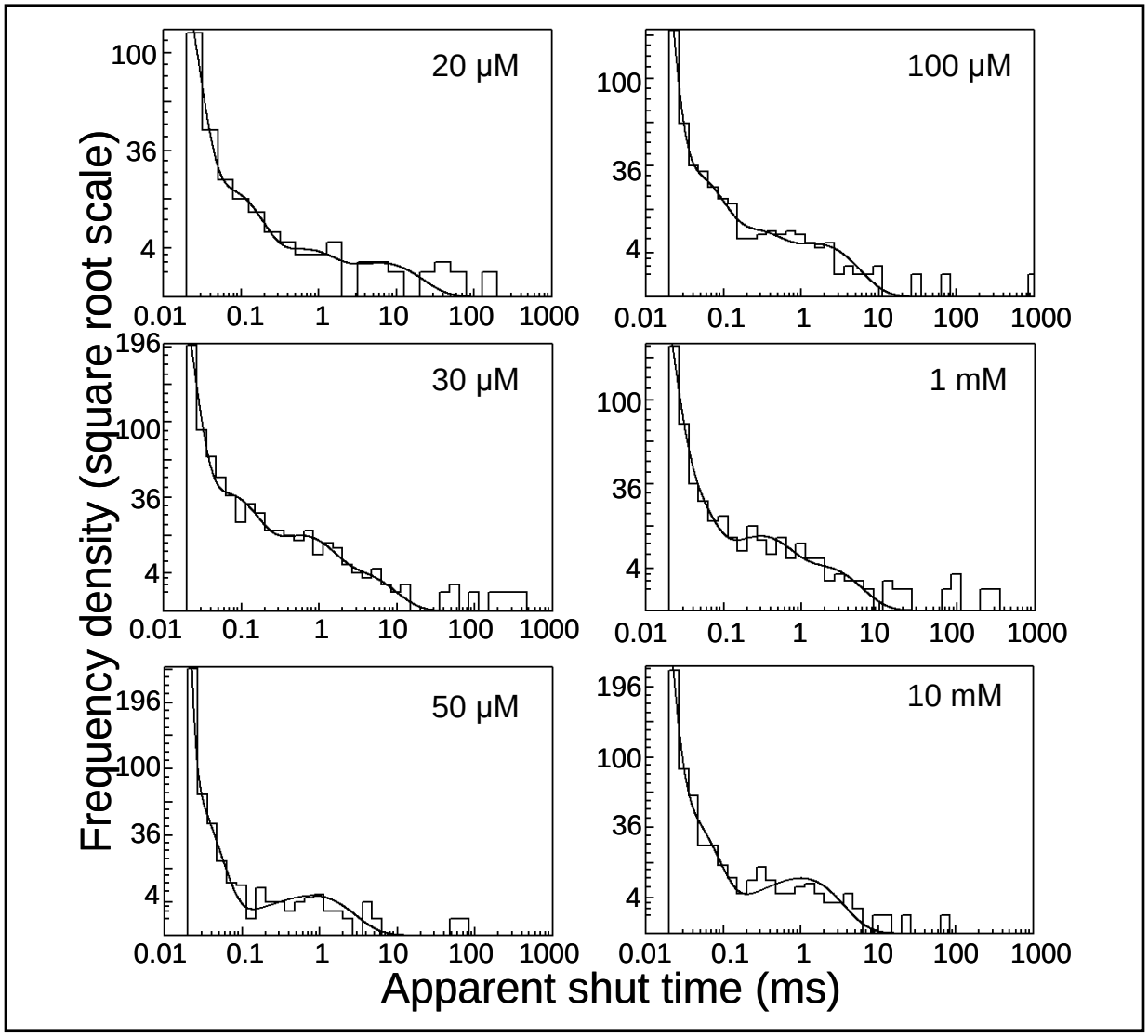

Figure 3.21 Shut-time distributions for α2 GlyRs
The shut-time distributions corresponding to the patches in Figure 3.17 were fitted with a mixture of up to four exponential probability density functions (Table 3.6).

In the first instance, I decided to divide all records (even those at low concentrations) into clusters and I have chosen a t_{crit} value of 7-10 ms for classifying events as being within clusters. In the distributions in Figure 3.21 there are only a few shuttings longer than 10 ms at all concentrations. These may be due to desensitization and therefore be the reflection of shuttings that occur between clusters (Colquhoun and Ogden, 1988). The same value was used for determining the P_{open} (see below). In the mechanism fits I also tested the effect of using different values of t_{crit}, (lower than 7 ms) and of classifying as bursts the groups of openings at the lower concentrations (20-100 μM, see below).

Table 3.6 Dwell-time distributions for α2 GlyRs.

Apparent open periods				
[Gly]	**τ1 (ms)** **Area (%)**	**τ2 (ms)** **Area (%)**	**τ3 (ms)** **Area (%)**	**Mean (ms)**
20 μM	0.017 ± 0.009 (12 ± 8%)	0.200 (5%)	13.1 ± 1.5 (83 + 12%)	12.46 ± 1.82
30 μM	0.011 ± 0.001 (12 ± 2%)	0.521 ± 0.134 (6 ± 1%)	37.4 ± 7.3 (82 ± 3%)	34.39 ± 7.48
50 μM	0.051 (2%)	–	29.0 ± 2.6 (98 ± 2%)	28.68 ± 2.88
100 μM	–	0.562 ± 0.449 (4 ± 1%)	32.8 ± 8.3 (96 ± 1%)	31.59 ± 7.80
1 mM	0.023 ± 0.011 (11 ± 8%)	–	32.7 ± 1.3 (89 ± 8%)	31.89 ± 1.65
10 mM	0.012 (2%)	–	30.2 ± 0.1 (98 ± 2%)	27.05 ± 3.04
Apparent shut times				
[Gly]	**τ1 (ms)** **Area (%)**	**τ2 (ms)** **Area (%)**	**τ3 (ms)** **Area (%)**	**τ4 (ms)** **Area (%)**
20 μM	0.010 ± 0.002 (88 ± 3%)	0.092 ± 0.028 (8 ± 1%)	0.589 ± 0.027 (3 + 1%)	6.06 ± 0.01 (1 + 0.4%)
30 μM	0.006 ± 0.001 (89 ± 2%)	0.044 ± 0.014 (8 ± 2%)	0.479 ± 0.055 (2 ± 0.2%)	5.16 ± 2.54 (1 ± 0.2%)
50 μM	0.005 ± 0.003 (99 ± 1%)	0.085 ± 0.071 (0.8 ± 0.8%)	–	2.83 (0.2%)
100 μM	0.005 ± 0.001 (97 ± 1%)	0.034 (3%)	0.171 ± 0.027 (1.0 ± 0.3%)	1.38 ± 0.22 (0.7 ± 0.1%)
1 mM	0.007 ± 0.001 (91 ± 3%)	0.047 ± 0.025 (6 ± 2%)	0.262 (2%)	1.63 ± 0.01 (1.3 ± 0.3%)
10 mM	0.005 ± 0.000 (98 ± 1%)	0.029 ± 0.002 (2 ± 1%)	–	1.06 ± 0.07 (0.3 ± 0.2%)

Distributions were fitted with a mixture of exponential probability density functions. Two idealized patches were used for each concentration. Time constant value and area (in brackets) of each component are the average ± SEM for each concentration.

3.3.5 P_{open} for clusters

The P_{open} value for each patch was calculated from clusters (groups of bursts). The P_{open} (7-10 ms) was estimated as the ratio between the cluster's total open time and cluster length. Values of the total open time and cluster length were taken from the idealised records, using two idealised patches for each concentration.

As expected from the inspection of the records, the mean P_{open} is similar for low and high concentrations, being always close to unity (Table 3.7). P_{open} values are plotted against glycine concentrations in Figure 3.22. As mentioned above, channel openings were never observed for concentrations lower than 20 μM. It is obvious from Figure 3.22 that the P_{open} is not concentration dependent. This suggests that the channel can only give rise to one type of (high P_{open}) activation; either the channel opens only when saturated with agonist, or activations at lower states of ligation also have very high P_{open}.

Table 3.7 Mean P_{open} for clusters at different glycine concentrations.

[glycine]	Number of clusters	Cluster duration (ms)	P_{open}
20 μM	28	358.1 ± 44.2	0.977 ± 0.003
30 μM	33	2050.4 ± 308	0.992 ± 0.001
50 μM	29	791.0 ± 97.2	0.996 ± 0.001
100 μM	24	1558.1 ± 274.1	0.993 ± 0.001
1 mM	41	583.8 ± 59.9	0.992 ± 0.001
10 mM	31	692.9 ± 65.4	0.994 ± 0.001

The P_{open} for each cluster was calculated as the ratio between total open time and total cluster duration. All data are pooled for each concentration to give the average P_{open} ± SEM. Two idealised records were used for each concentration. The t_{crit} value, chosen from the shut-time distributions, was 7 ms (for 50 μM and 10 mM) and 10 ms for the other concentrations.

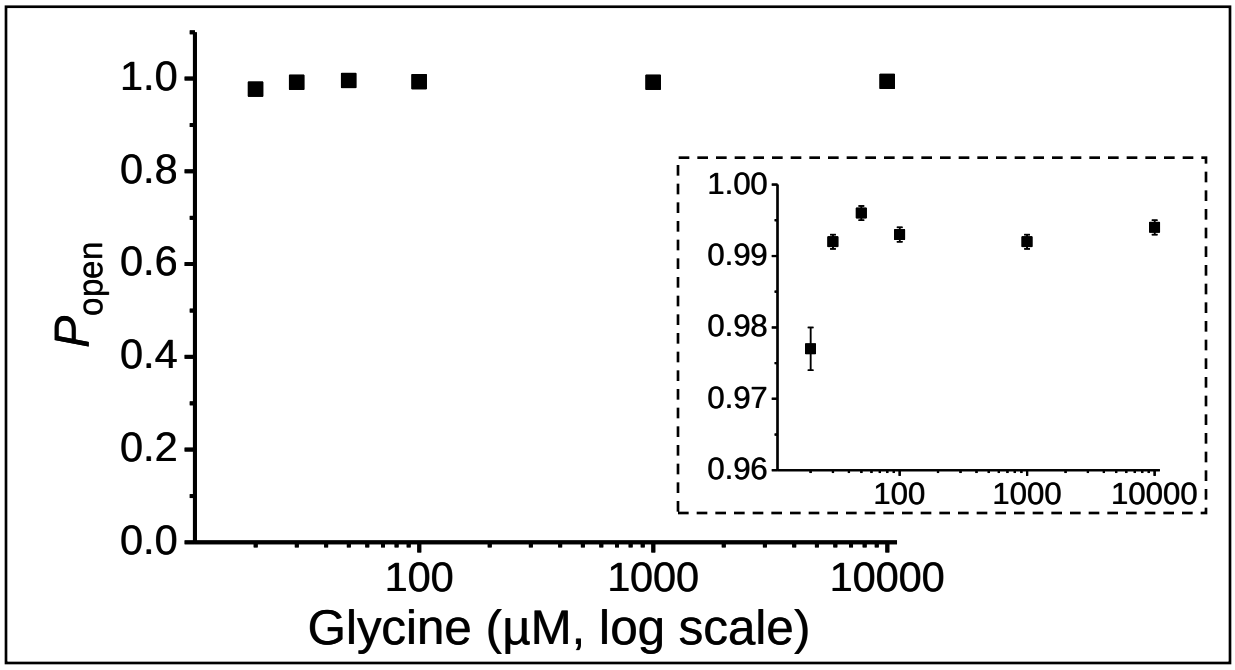

Figure 3.22 Open probability of α2 GlyR clusters
Each point in the plot represents the average P_{open} (± SEM) obtained after pooling the individual P_{open} values from all the clusters recorded at each glycine concentration. The P_{open} value for each cluster was obtained as the ratio between the cluster's total open time and total duration. Two idealised records were used for each concentration. Concentrations lower than 20 μM did not produce any channel activity. The insert shows the same plot rescaled.

3.3.6 Fits to putative mechanisms

For fitting putative mechanisms to the data using HJCFIT patches were grouped into sets, so that each set contained 2-3 patches spanning the range of glycine concentrations (see Methods). For the initial fits the t_{crit} was set to 7-10 ms for both the low and the high concentrations and data were fitted as clusters (steady-state vectors). Resolution was set to 20 μs. The following figures show the results of fitting different models to the same set of two patches (30 μM and 1 mM glycine). Similar results were obtained for other sets, tables of which are in Appendix C. For testing the quality of a model the predictions from a fit are compared with the experimental data (shut-time and open-period distributions). The quality of a mechanism is also evaluated based on how physically plausible and consistent the rate constant values are. The predicted P_{open} curve was compared with the experimental P_{open} values from single-channel data (i.e. maximum P_{open} close to unity and EC_{50} lower than 20 μM) and also from macroscopic recordings (see section viii).

i. Models of sequential binding steps

Given that α2 GlyRs are homomers of five α subunits, the maximum number of binding sites they might have is five. However, it has been shown that only three binding sites are required to maximally activate homomeric pLGICs (Beato *et al*. 2004; Rayes *et al.* 2009). To investigate the necessary number of α2 GlyRs binding sites I tested simple mechanisms with sequential binding steps and openings from all liganded resting states (for example see Figure 3.23), by varying the number of binding steps.

I tested different variations of these models, such as the presence of identical binding sites or the lack of interaction between binding sites. Lack of interactions means that binding and unbinding rate constants stay the same irrespective of how many sites are already occupied by glycine. This is done by fitting with the following constraints (see also Burzomato *et al*., 2004): $k_{(+1)} = k_{(+2)} = k_{(+3)} = k_{(+4)} = k_{(+5)}$ and $k_{(-1)} = k_{(-2)} = k_{(-3)} = k_{(-4)} = k_{(-5)}$.

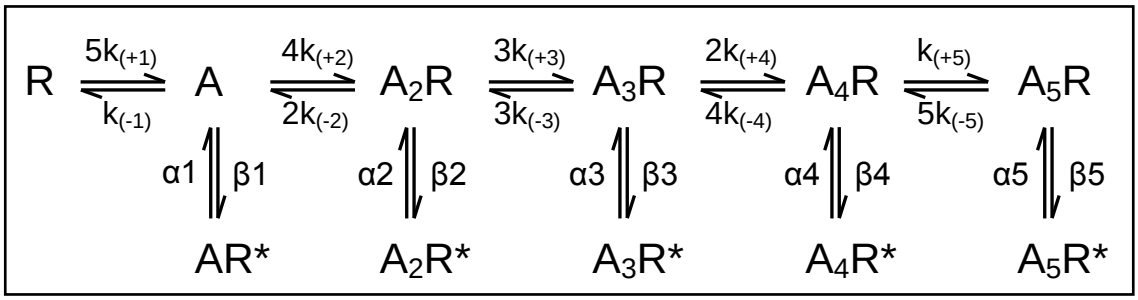

Figure 3.23 Sequential models with openings from all liganded states
This kinetic scheme (model 1) has five binding sites for glycine and openings can occur from any of the bound resting states. Variations of this model, with up to two binding sites (models 2-4) were tested. In all schemes the agonist is indicated by A, the resting states by R and the open states by R*. The names for all the different rate constants for the reaction steps are shown, also taking into account the statistical factors for the binding rate constants.

The first model tested was one with 5 binding steps and five open states (Figure 3.23). With or without the constraints for interacting binding sites, HJCFIT was unable to converge for any of the sets. Therefore I proceeded to fit data with a lower number of binding sites.

Fits of different data sets to a model of four binding sites and four open states were able to converge (scheme 2; Table A1, Appendix C). Although the major component of the open-period distributions is predicted well, the model failed to describe the smaller components. The predicted maximum of the P_{open} curve is close to the experimental observations (Table 3.8) but

the curve itself is not informative for any of the sets tested (Table A1, Appendix C). More importantly, this mechanism completely failed to predict the shut-time distributions. This model was not considered adequate to describe the data. Note that for the set in Table 3.8 the estimate for the fully liganded efficacy (*E*4) is zero, lower than any of the efficacy values at lower levels of ligation.

Table 3.8 Estimated parameters from fits of the same set of data with schemes 2-4

	Unit	**Scheme 2** 4 binding sites 4 open states	**Scheme 3** 3 binding sites 3 open states	**Scheme 4** 2 binding sites 2 open states
30 μM and 1 mM Vectors Free parameters		t_{crit} = 10 ms steady-state 10	t_{crit} = 10 ms steady-state 6	t_{crit} = 10 ms steady-state 4
α1	s^{-1}	56	877366	14116
β1	s^{-1}	17018	0.00	377
α2	s^{-1}	243804	14387	68
β2	s^{-1}	96801	375	37088
α3	s^{-1}	155	65	-
β3	s^{-1}	89179	34782	-
α4	s^{-1}	6	-	-
β4	s^{-1}	0.00	-	-
k_-	s^{-1}	439	688	1366
k_+	$M^{-1}s^{-1}$	$5.9x10^6$	$3.3x10^6$	$3.4x10^6$
E1		305	0.00	0.03
E2		0.40	0.03	549
E3		575	534	-
E4		0.00	-	-
K_R	μM	74	207	402
max P_{open}		0.993	0.998	0.998
EC_{50}	μM	undetermined	29	18
n_H		undetermined	2.64	1.92
L_{max} (log)		12262	11900	11939

Rate constant estimates for fits with models of simple sequential binding steps to the same set of data (set 1 with 30 μM and 1 mM glycine). Fits were done with constraints for non-interacting binding sites. The t_{crit} value, the type of vectors used for each patch and the number of free parameters are also shown. The efficacies ($E = \beta/\alpha$) and the dissociation equilibrium constant for the resting states ($K_R = k_-/k_+$) are calculated from the fitted rates. Also listed are the max P_{open}, EC_{50} and Hill slope predicted by HJCFIT. L_{max} is the maximum likelihood for each fit.

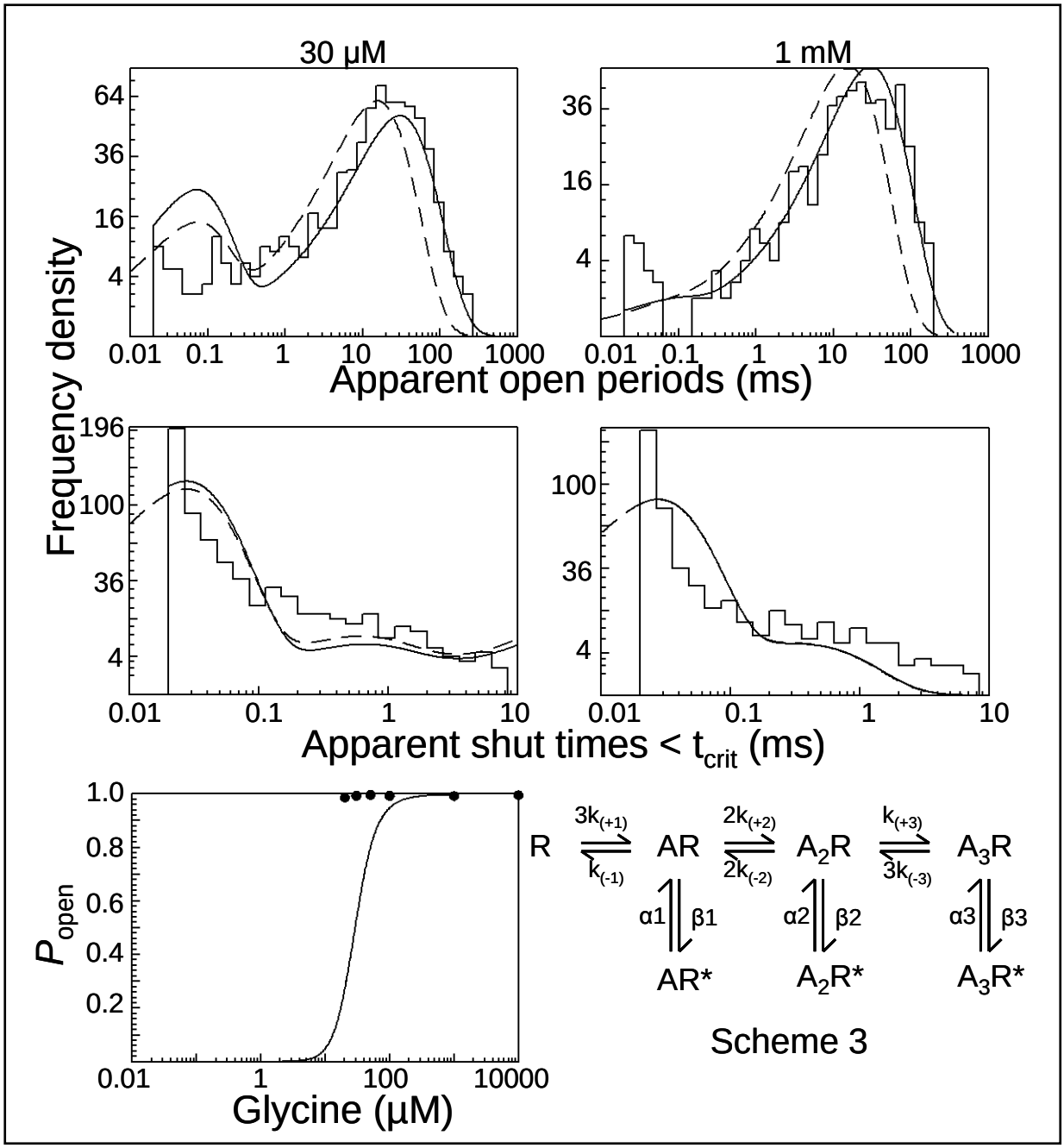

Figure 3.24 Fits of data with scheme 3

The first two rows show the comparison of the experimental data with the fit predictions for one set with two patches (at 30 μM and 1 mM). t_{crit} was 10 ms and steady-state vectors were used for both patches. Fits were performed with constraints for identical binding sites. The histograms are the experimental data, the solid lines are the calculated HJC distributions and the dash lines are the predicted fits at ideal resolution. The experimental P_{open} values (black circles) for all patches are plotted against glycine concentrations below. The solid line is the predicted P_{open}-concentration curve using this model and data set and the dash line (here overlapping the solid one) is the prediction at ideal resolution. The reaction rates for this fit are shown in Table 3.8.

This last finding suggests that better fits might be obtained if the number of binding sites is reduced further. Indeed, fits with a model with three binding steps and three open states (scheme 3) gave more reasonable rate constants for the sets tested (Table A2, Appendix C). Figure 3.24 shows the results of a fit with this model, using constraints for non-interacting binding sites. Not much difference was observed between these fits and those with four binding sites however: the major component of the open-period distributions is predicted reasonably well but the smaller components are overestimated for the low concentration. The predicted max P_{open} was reasonable (0.998). However, the model failed to describe the shut-time distributions, especially in the range of the short shut times. From the above, this model was also considered inappropriate for the data. Similar results were also obtained with a model of two binding sites and two open states (scheme 4, Table 3.8). The summary for fits to the same set of data with this group of schemes is shown in Table 3.8.

It is clear from Figure 3.24 that simple sequential binding site mechanisms are not suitable for the kinetics of α2 channels. From the above fits however it was evident that models with three or two binding sites gave more reasonable rate constants as the efficacy increased *with* the level of ligation. The same did not occur for scheme 2 (Table 3.8).

ii. The 'flip' mechanism

What else can we change in the model? Clearly the shut-time distribution is a problem, so adding more shut states may help. Both the homomeric and the heteromeric receptors containing the α1 subunit are well described by the 'flip' model (Burzomato *et al*., 2004), which introduces more shut states for each bound state of the receptor (Figure 1.8 in Chapter 1). A possible physical interpretation of these states is that they represent activation intermediates in which the extracellular domain has already changed its conformation in response to the binding of glycine, but the channel has not yet opened. I proceeded to test whether the same can occur for α2 receptors.

As shown in Figure 3.25, incorporation of flip states improves greatly the fits of the shut-time distributions. This model fitted very well both the shut-time and the open-period distributions and it predicted high P_{open} values, similar to the experimental observations. Also, the predicted EC_{50} was lower than the value of 20 μM expected from the experimental P_{open} values (Figure 3.22).

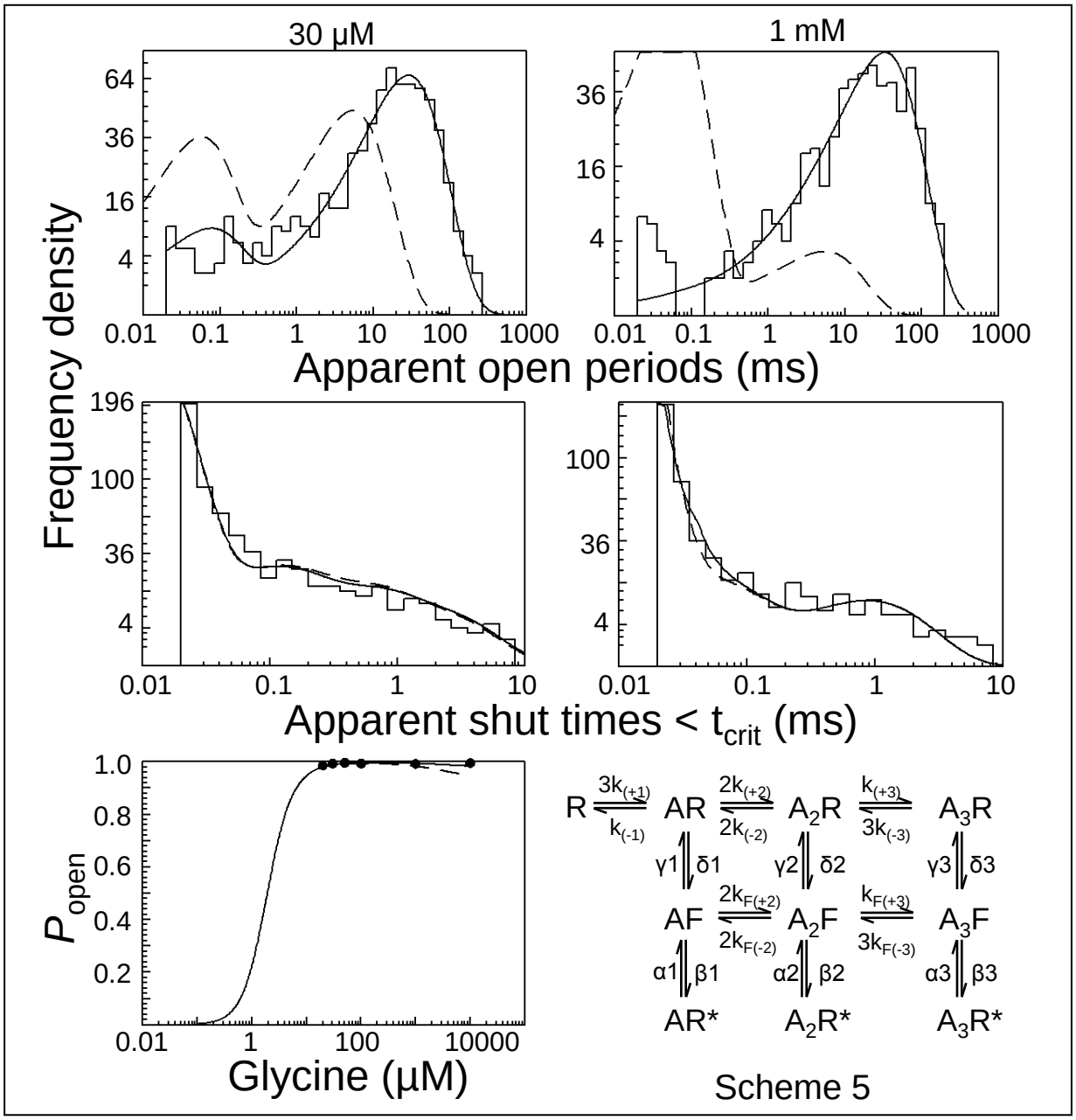

Figure 3.25 Fits of data with the 'flip' mechanism (scheme 5)

The introduction of additional shut states (flipped states, F) in scheme 5 ('flip' mechanism; Burzomato *et al.*, 2004), improves the fits to the experimental distributions for both shut times and open periods. The same set of data is shown as in Figure 3.24 for comparison. The t_{crit} was 10 ms and steady-state vectors were used for both patches. Fits were performed with constraints for all the binding steps for states R and F to have the same rate constants (same equilibrium dissociation constants K_R and K_F). Two rate constants (one for each cycle) were fixed to satisfy the requirements of microscopic reversibility. The predicted P_{open} curve is also shown. The solid lines are the calculated HJC distributions (at the experimental resolution) and the dashed lines are the distributions that would be observed if no events were missed. The reaction rates are in Table 3.9.

Table 3.9 Estimated parameters from fits to set 1 with the 'flip' model.

	Unit	**Scheme 5** 'flip' model with 3 binding sites	
30 μM 1 mM Vectors		t_{crit} = 10 ms t_{crit} = 10 ms steady-state	t_{crit} = 0.1 ms t_{crit} = 2 ms CHS
α1	s^{-1}	14037	7705
β1	s^{-1}	1531	804
α2	s^{-1}	186	249
β2	s^{-1}	100624	114538
α3	s^{-1}	18244	53546
β3	s^{-1}	337120	374572
k_-	s^{-1}	813	0.243
k_+	$M^{-1}s^{-1}$	$9.8x10^6$	75600
k_{F-}	s^{-1}	1381	3876
k_{F+}	$M^{-1}s^{-1}$	$2.9x10^7$	$6.5x10^7$
γ1	s^{-1}	994919	3896
δ1	s^{-1}	728018	$4.3x10^6$
γ2	s^{-1}	7505	96
δ2	s^{-1}	9670	5640
γ3	s^{-1}	0.01	704
δ3	s^{-1}	0.03	2223
E1		0.11	0.10
E2		542	460
E3		19	7
F1		0.73	1102
F2		1.29	58.98
F3		2.27	3.16
K_R	μM	83	3.21
K_F	μM	47	60
max P_{open}		0.993	undetermined
EC_{50}	μM	2	undetermined
n_H		1.89	undetermined
L_{max} (log)		12382	11038

Fits were performed with constraints for equal binding sites, for all conformations. Two rates were set by microscopic reversibility. The t_{crit} values and the type of vectors used are shown. The efficacies ($E = \beta/\alpha$), the equilibrium constants for the flip states ($F = \delta/\gamma$) and the dissociation equilibrium constant for the resting ($K_R = k_-/k_+$) and flip states ($K_F = k_{F-}/k_{F+}$) are calculated from the fitted rates. Also listed are the predicted max P_{open}, EC_{50} and Hill slope. L_{max} is the maximum likelihood for each fit.

However, only two data sets could be fitted with this model and the fits were not consistent between them: specifically, the values of the gating rate constants for the monoliganded state

(α1, β1) varied considerably (14037 and 1531 for set 1, shown in Figure 3.25 vs. 0.3 and 3621 for set 3, see Table A3 in Appendix C). Furthermore the results of the fits suggest that opening was most efficacious when the channel is diliganded, rather than fully liganded. For this scheme I also tested the effect of lowering the t_{crit} value and classifying concentrations lower than 100 μM as 'burst concentrations'. This attempt resulted in very poor fits for the set shown in this chapter and HJCFIT could not predict a P_{open} curve. The rate constants for this fit are shown in Table 3.9.

iii. Variants of the 'flip' mechanism: two open states

Considering that the introduction of flip states improved the fits, I went on to test different variations of 'flip' models in order to achieve consistency between sets. Some of these schemes are shown in Figure 3.26, where the number of open states is gradually reduced to account for the low efficacy predicted for partially liganded states. Different t_{crit} values were also tested. Data at concentrations lower than 100 μM were analysed both as clusters and as bursts (i.e. in the latter case using CHS vectors; see Methods).

I tested whether model 6A (Figure 3.26) would fit better than model 5. For initial fits with this model I used the same value of t_{crit} (10 ms) and steady-state vectors, as with models 1-5. Figure 3.27 (left panel) shows an example of such a fit with model 6A, using the same set of data as before. Again, using flip states resulted in a very good agreement of the experimental data with the HJC fits. The model fitted well more than two data sets, making it a better candidate compared with scheme 5 (see Table A4, Appendix C). The presence of only two instead of three open states resulted in a higher efficacy for the fully liganded instead of the partially liganded state and overall this model produced more reasonable rate constants than model 5.

As a second step, I tested lower t_{crit} values. Figure 3.27 (right column) shows the effect of lowering the t_{crit} and fitting with model 6A (concentrations lower that 100 μM were classed as "burst" and CHS vectors were used; note that this also means that the cluster P_{open} curve can only include concentrations higher than 100 μM). As expected, decreasing the t_{crit} did not alter the fits of the open-period distributions but somewhat improved the shut-time distribution fits. The results of fits with the lower t_{crit} predicted a 10-fold lower potency of glycine (from 3.7 μM to 47 μM). This is a direct result of an increase in the equilibrium dissociation constant (K_R; see Table 3.10).

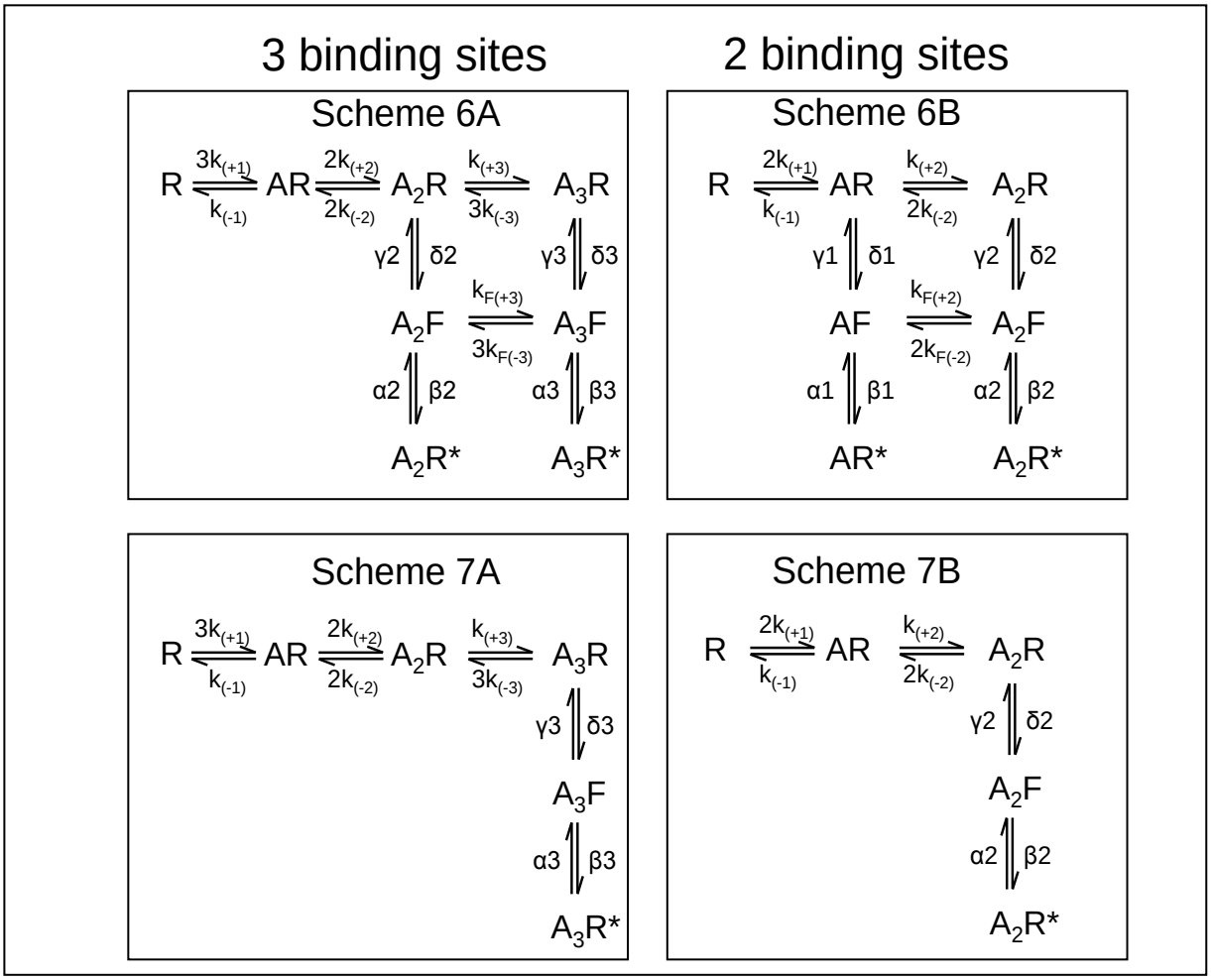

Figure 3.26 Different variations of 'flip' mechanisms used for fitting
Some of the kinetic mechanisms tested for α2 GlyRs. These models have either three (A) or two (B) binding sites and they all contain flip states. Fits to these models were performed with constraints for association and dissociation rate constants to be the same for all binding sites. For models 6A and 6B an additional rate ($k_{F(+)}$) was fixed for microscopic reversibility. Statistical factors in the binding rate constants are included.

These changes with low t_{crit} were similar across all data sets (Table A4, Appendix C). Despite the good fits produced by this scheme with the above conditions, I did not consider it appropriate for the data. The reason is that the values for α2 and β2 were not consistent across different sets of data, giving a big scatter in the values for *E*2, ranging from 0.6 to 24 (see Table A4, Appendix C). Also, in most sets (including the one shown here), the association rate constant for the flipped states, $k_{F(+)}$, had reached its diffusion limit of 10^9 $M^{-1}s^{-1}$, making it physically impossible, and these values unrealistic.

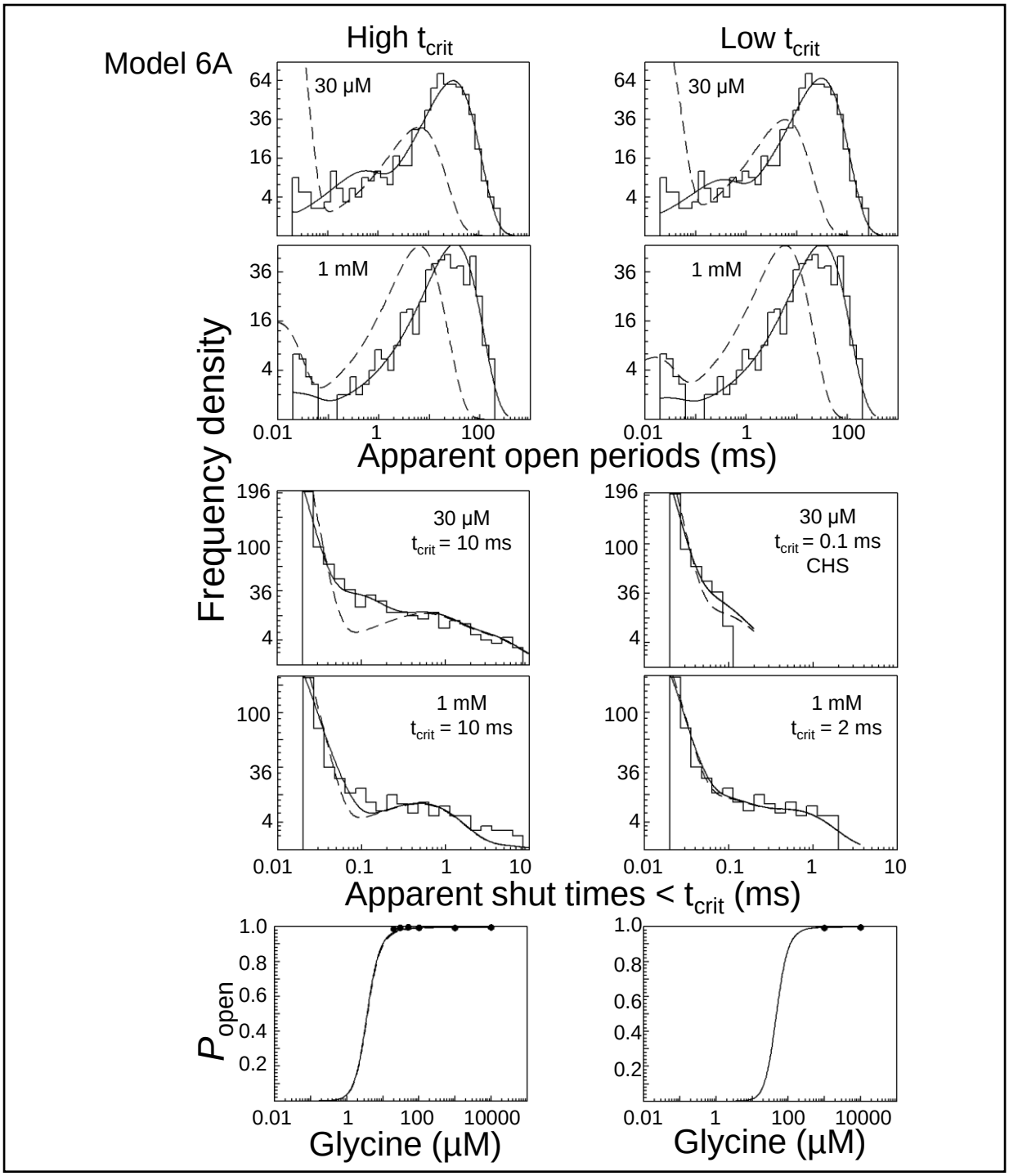

Figure 3.27 Effects of low t_{crit} values to fits with model 6A

Fits to the same data set using high (left) or low (right column) values for t_{crit}. The open-period distributions are unaffected but reducing t_{crit} improves the fit of the shut-time distribution for the 1 mM patch and shifts the P_{open} curve to the right. The fits were performed with constraints for identical binding sites. The solid lines are the calculated HJC distributions and the dash lines are the predicted fits at ideal resolution. In the P_{open} curves the experimental points correspond only to cluster concentrations (at which steady-state vectors were used). CHS vectors were used for concentrations lower than 100 μM (for t_{crit} < 7 ms). The rates for the fits can be found in Table 3.10.

iv. Variants of the 'flip' mechanism: one open state

Inspection of the *E* and *F* values in Table 3.10 shows that in all the fits of scheme 6A overall gating is much more efficacious for the tri- vs. the diliganded states (the product of *E* is at least 100-fold smaller for the diliganded openings and *F*2 is almost 0). I therefore chose to remove the first gating step from the scheme. The resulting model (7A) is shown in Figure 3.27.

Initial fits with high t_{crit} values provided very good agreement with the experimental data, as shown in Figure 3.28 (left). Due to the presence of only one open state in model 7A, the HJC fits of the open-period distributions do not fit the fastest component (compare with model 6, Figure 3.27) but this component only accounts for a very low number of events in each patch (see also Table 3.6). On the other hand, the predominant slow component is predicted extremely well (Figure 3.28). Again, reducing t_{crit} and using CHS vectors for the low concentrations profoundly improved the fits with scheme 7A, especially for the shut-time distributions (Figure 3.28). This improvement was not only evident for the slow shut-time components but also for the very fast component of 5-10 μs, which, as seen from the EKDIST distributions, represents ~90% of all shut times. This improvement was not observed for model 6A. Overall, the fits from model 7A provide the best agreement with the data. This is despite the fact that the free parameters in this model are fewer than in the previous models tested (n = 6 for model 7A). This scheme fitted three other sets of patches with equally good fits for the distributions and similar values for the fitted rate constants, showing its consistency between different sets (see Table A6, Appendix C). The predicted P_{open} curve gave a reasonable maximum P_{open} value (close to 1).

Model 7A denotes that the channel can only reach one single open state after three sequential (identical) agonist binding steps, implying that the binding sites do not interact. For the same model I also tested the effect of releasing the constraints of independence between the binding sites, meaning that the binding rate constants for one binding site might be affected by the binding of glycine to other binding sites. I therefore refitted all of the 10 rate constants as free parameters (four different sets; Table A8, Appendix C). The predicted distributions with the free fits were identical to those of model 7A with the constraints (Figure 3.28) though the release of the constraints resulted in a decrease in the slope and EC_{50} of the P_{open} curve.

Table 3.10 Effect of decreasing t_{crit} to fits of the same data set with models 6A and 7A

	Unit	**Scheme 6A**			**Scheme 7A**	
30 μM		t_{crit} = 10 ms	t_{crit} = 0.6 ms	t_{crit} = 0.1 ms	t_{crit} = 10 ms	t_{crit} = 0.1 ms
1 mM		t_{crit} = 10 ms	t_{crit} = 2 ms	t_{crit} = 2 ms	t_{crit} = 10 ms	t_{crit} = 2 ms
Vectors		steady-state	CHS	CHS	steady-state	CHS
Parameters		11	11	11	6	6
α2	s^{-1}	103496	97425	68266	-	
β2	s^{-1}	315032	324677	995366	-	
α3	s^{-1}	156	163	171	123	603
β3	s^{-1}	83917	87275	91679	71838	183984
k_-	s^{-1}	0.31	323	2133	143	4078
k_+	$M^{-1}s^{-1}$	14157	$3.9x10^6$	$5.4x10^6$	$2.6x10^7$	$6.7x10^6$
k_{F-}	s^{-1}	9980	10182	7462	-	-
k_{F+}	$M^{-1}s^{-1}$	$3.7x10^8$	$4.6x10^8$	$2.0x10^9$	-	-
γ2	s^{-1}	710	905	9460	-	-
δ2	s^{-1}	473	176	135	-	-
γ3	s^{-1}	4132	4948	6644	7833	8735
δ3	s^{-1}	2174	3659	10170	2248	23065
E2		3.04	3.33	14.58	-	-
E3		538	535	536	584	305
F2		0.67	0.19	0.01	-	-
F3		0.53	0.74	1.53	0.29	2.64
K_R	μM	22	83	395	5.6	610
K_F	μM	27	22	4	-	-
max P_{open}		0.996	0.997	0.998	0.993	0.998
EC_{50}	μM	4	13	47	1	73
n_H		2.41	2.56	2.68	2.47	2.68

Estimated rate constants for schemes 6A and 7A using high, intermediate and low t_{crit} values. The same set of data is used for both models. Fits were performed with constraints for non-interacting binding sites. k_{F-} was set by microscopic reversibility (scheme 6A). When stated, CHS vectors were used instead of steady-state vectors for the 30 μM patch, for separating openings into bursts. The efficacies, the equilibrium constants for entering a flip state and the dissociation equilibrium constants are calculated from the fitted rates. The fits with the high and low t_{crit} are shown in Figures 3.27 (scheme 6A) and 3.28 (scheme 7A).

The results of the fits suggest that the binding affinity is very high for the first binding step (K_{R1} ranges from 0.01 to 110), it decreases to more than 1000-fold for the second binding (K_{R2} is between 762 and 9523) and increases again after two agonist molecules are bound (Table A8, Appendix C). These fits suggest that the binding of one agonist molecule somehow prevents the binding of a second molecule but the binding of both finally allows for a third molecule to bind and the channel to open.

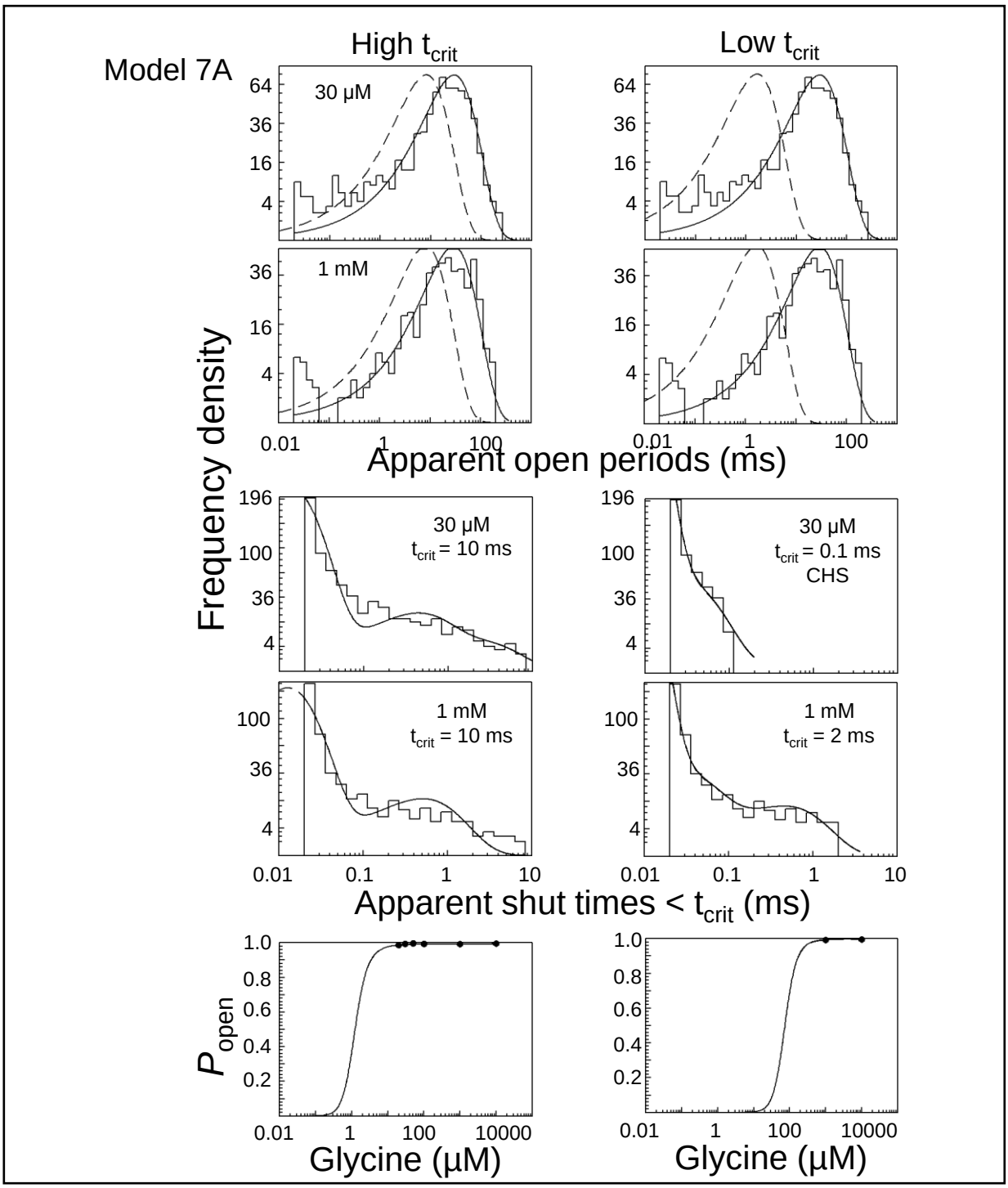

Figure 3.28 Effects of low t_{crit} values to fits with model 7A

Fits to the same data set (see Figure 3.27) using high and low t_{crit} values (both with constraints for equal, non-interacting binding sites). The solid lines are the calculated HJC distributions and the dash lines are the predicted fits at ideal resolution. Model 7A has one open state (A3R*) and open-period distributions are fitted with a single component. The fits of the shut-time distributions of both patches are very good with the low t_{crit}, including the predominant fast component (right column). The fits are very poor for high t_{crit} values (left column). As with model 6A, the P_{open} curve is shifted to the right. The rates for the fits are in Table 3.10.

The above interpretation of a negative interaction between binding sites and the big variability in the binding rate constants across sets do not make these free fits very reliable. Due to these, I continued fitting the data with constraints of non-interacting binding sites since the quality of the fits is good, even with fewer free parameters (n = 6 for model 7A with constraints).

v. Variants of the 'flip' mechanism: number of binding sites

It is obvious that the best fits are obtained with a model of only one open state, after flipping (scheme 7). Beato *et al.*, (2004) found that in α1 GlyRs maximum gating efficacy is reached when three molecules of glycine have bound. Model 7A, with three binding sites, agrees with the above, but I also tested the effect of changing the number of binding sites. The models ranged from one to five binding sites; an example of such a model, with two binding sites is shown in Figure 3.26 (scheme 7B). The same sets and settings (constraints and low t_{crit} values) were used for fitting. Surprisingly, the fitted rate constants for all schemes (and consequently the fits to the experimental distributions) were almost identical with those from scheme 7A (Table 3.11). Similar results were obtained with other data sets and also when a different pair of models was used (scheme 6A and 6B, Figure 3.26; see Tables A4-A7, Appendix C).

Table 3.11 Number of binding sites to models with 1 open state, after flipping.

	Unit	5 binding sites	4 binding sites	3 binding sites **(7A)**	2 binding sites **(7B)**	1 binding site
α	s^{-1}	606	604	603	598	572
β	s^{-1}	184268	184377	183984	183331	179904
k_-	s^{-1}	2477	3083	4078	6019	11462
k_+	$M^{-1}s^{-1}$	$7.5x10^6$	$7.2x10^6$	$6.7x10^6$	$5.8x10^6$	$3.7x10^6$
γ	s^{-1}	8740	8736	8735	8737	8792
δ	s^{-1}	23214	23171	23065	22822	21851
E		304	305	305	306	315
F		2.66	2.65	2.64	2.61	2.49
K_R	μM	330	429	610	1042	3131
max P_{open}		0.998	0.998	0.998	0.998	0.998
EC_{50}	μM	117	99	73	38	4
n_H		3.70	3.26	2.68	1.93	1.00
L_{max}		10922	10922	10922	10922	10922

Estimated rate constants for the same set, fitted with schemes containing up to five binding sites. Identical constraints are used (non-interacting binding sites) and also the same t_{crit} values (0.1 ms for 30 μM; 2 ms for 1 mM) for all models. CHS vectors were used for the 30 μM patch. The fits for the experimental distributions for all schemes are identical to those of model 7A (shown in Figure 3.28, right).

As shown in Table 3.11, in all cases the only effect of reducing the number of binding sites was a reduction in the EC_{50} and slope of the P_{open} curve. This is represented in Figure 3.29 for models 7A and 7B. A decrease in the binding affinity was also noticed (increase in K_R). From the above it is evident that the major determinant for choosing between the five different models was the P_{open} curve. Unfortunately, the experimental P_{open} values are all high and do not give any information on EC_{50} and slope (Figure 3.22). Because of that, we decided to obtain macroscopic responses from cells expressing α2 channels, using fast agonist application in order to minimise the effect of desensitization. Ideally, the information obtained from macroscopic concentration-response curves would help to choose between the models. Recordings of macroscopic currents were performed both in the whole-cell patch configuration by means of a U-tube system and in the outside-out configuration using a theta tube.

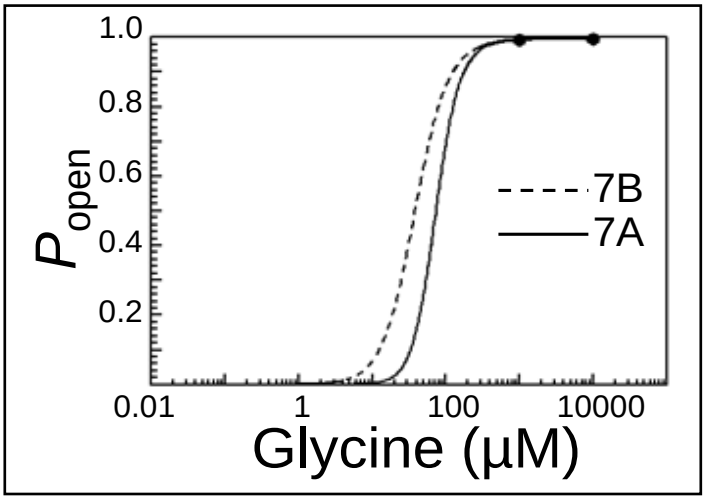

Figure 3.29 Two vs. three binding site models
P_{open}-concentration response curves calculated by the fits of the same data set with a model containing three (scheme 7A) and two (scheme 7B) binding sites. The models are shown in Figure 3.26. The set is the same used for Figures 3.27 and 3.28. Fits were performed with identical constraints for non-interacting binding sites and with the same low t_{crit} values. The rate constants for the two models are identical (see Table 3.11) and fits to the experimental data are shown in Figure 3.28 (right column). The two fits differ only in the predicted P_{open} curve, with an EC_{50} of 73 μM for model 7A and 38 μM for model 7B.

3.3.7 Properties of macroscopic currents from α2 GlyRs

Whole-cell currents from α2 GlyRs (examples of which are shown in Figure 3.30*A*) were recorded at -60 mV and individual concentration-response curves were fitted to the Hill equation. For 8 cells, the currents had an average fitted maximum of 8.96 ± 2.09 nA (range 2.8-22 nA), and EC_{50} and Hill coefficient of 379 ± 36 μM and 1.58 ± 0.09 respectively. These data were normalised and pooled to obtain the plot in Figure 3.30*C*; when fitted to the Hill equation, the curve gave an EC_{50} of 363 μM and a slope of 1.53, similar to the average values.

I also obtained responses to fast agonist application with a theta tube, recording from outside-out patches (in symmetrical chloride, 130 mM; see Methods). As shown in Figure 3.30*B,* I applied 1 s pulses of three different glycine concentrations (100 μM, 500 μM and 10 mM) and fitted the measured peak current responses (normalised to currents at 10 mM; -100mV) to the Hill equation, to characterize the concentration-response curve. These data are plotted with those obtained from the whole-cell recordings in Figure 3.30*C* for comparison. Note that even though only three concentrations are available for plotting, the data from concentration jumps are in agreement with those from whole-cell recordings. Individual fits with the Hill equation gave an average EC_{50} of 355 ± 72 μM and a slope of 1.23 ± 0.22 (n = 4).

The Hill slope values obtained from the whole-cell and outside-out recordings are in good agreement with the range of 1.6-1.9 reported in the literature for macroscopic α2 currents (see Mangin *et al.*, 2003; Han *et al*., 2004; Hawthorne *et al.*, 2006; Yang *et al.*, 2007). On the other hand, the EC_{50} values vary significantly between different studies, as observed for other GlyR subtypes (Beato *et al.*, 2002). This is expected, however, since both the speed of glycine application and the method of recording can affect EC_{50} values by altering the level of desensitization which, by definition, is a high affinity state (faster drug applications are expected to decrease desensitization and hence increase the EC_{50}).

The value of the Hill slope from macroscopic currents does not match, but is closer to two out of the five models of Table 3.11: the two binding site model (7B), which predicts n_H values of 1.93 ± 0.01, and the three binding site model (7A), with a slope of 2.68 ± 0.04 (average of 4 sets, shown in Tables A6 and A7, Appendix C). On the other hand, the observed EC_{50} value is much larger than the predictions of either of the two models (model 7A: 53 ± 15 μM; model 7B: 27 ± 7 μM).

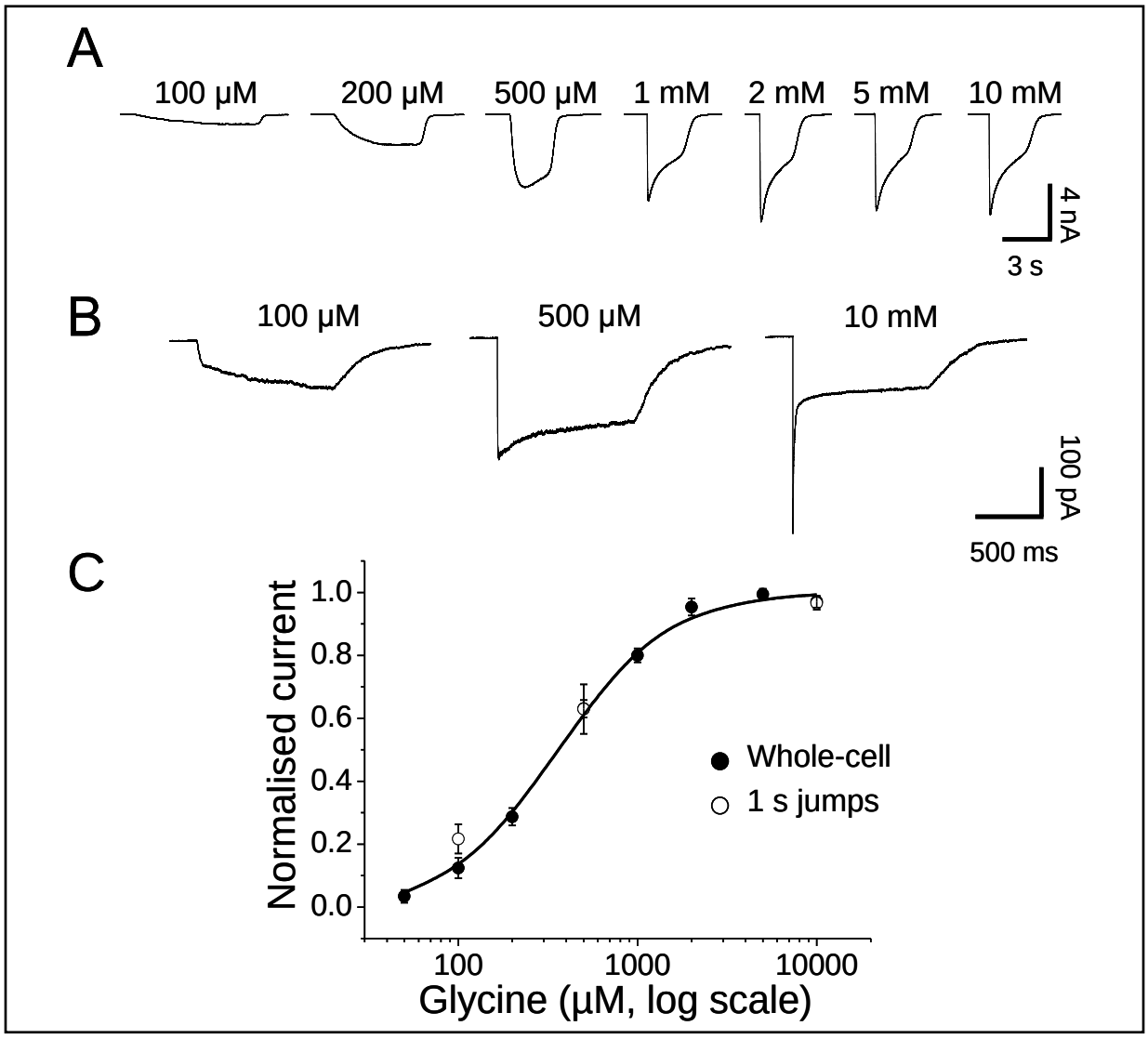

Figure 3.30 Concentration-response relations from macroscopic currents
Traces in *A* are representative glycine-evoked whole-cell currents from a HEK293 cell (held at -60 mV) expressing α2 GlyRs. The traces in *B* are average outside-out currents (at -100 mV) elicited by 1 s application of three different glycine concentrations on the same patch. Recordings for both *A* and *B* were performed with equimolar bath and pipette solutions (containing 130 mM chloride). *C*, Concentration-response curve for glycine obtained from pooled whole-cell data (filled circles) and fitted with the Hill equation (continuous line). The open circles are average data from 1 s concentration jumps, normalised to the 10 mM response for each patch.

Note that both the EC_{50} and the Hill slope predictions from kinetic models would be applicable to a P_{open} curve, not to one obtained from macroscopic data, as the latter is inevitably distorted by desensitization (which is not included in the models fitted to single-channels, as desensitized shut states cannot be analysed). For this reason, the macroscopic data alone are not sufficient for choosing the two binding site model (7B) over model 7A.

In addition to that, the macroscopic experiments described above were all completed before my colleagues identified internal chloride as a major determinant of α1β glycine channel kinetics (Pitt *et al*., 2008). The study shows that the deactivation of macroscopic currents predicted by cell-attached single-channel recordings is much faster than that observed with concentration jumps at high pipette chloride. The deactivation after jumps becomes faster (and similar to the single-channel model predictions) when low chloride is used in the pipette (resembling a more physiological intracellular chloride concentration). In the light of these results, it is now clear that the kinetic information from single-channel data can be combined with macroscopic data only if they are obtained in similar conditions and this means low internal chloride.

It is important to know whether intracellular chloride levels affect also the time course of macroscopic currents from α2 homomeric receptors. I compared the concentration jumps I had performed with high chloride in the pipette (130 mM; equimolar to the bath solution) with those using a low-chloride pipette solution (10 mM, also at -100 mV). I first examined responses to long (1 s) applications of saturating glycine (10 mM). The traces in Figure 3.31*A* show that the first noticeable difference is that at low chloride concentration in the pipette, glycine currents were much smaller (average of 83 ± 28 pA, n = 4 vs. 402 ± 11 pA, n = 6; see the calibration bars) because the driving force for chloride is smaller (100 mV in symmetrical chloride, ~35 mV in low chloride). More importantly, even with these long 1 s jumps (where desensitization is high) it is evident that reducing the pipette chloride concentration led to a ~3.5-fold decrease in the deactivation time constant, from an average of 383 ± 70 ms (n = 6) to 112 ± 26 ms (n = 4; see the inset with the scaled currents at the end of the pulse in Figure 3.31*A*). The use of more physiological intracellular chloride concentrations therefore speeds up the decay of both α1β and α2-mediated glycine currents.

When the application of agonist is short (1-2 ms jumps at saturating glycine), the decay of the current is thought to reflect the duration of the burst (Wyllie *et al.*, 1998). In these conditions, α1β channels deactivate with a time constant of ~10 ms (in low chloride; Pitt *et al.*, 2008). The deactivation of α2 currents elicited by a short glycine pulse is much slower than that of α1β channels. The off-current can be best fitted with two exponential components at saturating glycine (10 mM) and with either one or two exponentials at lower glycine concentrations (500 μM, 1 mM). Representative currents elicited by the three concentrations are shown in Figure 3.31*B*. The average time constants and areas for the exponential components are shown in

Table 3.12. The slow component, which is predominant at all concentrations, is ~8-11 times slower than the 10 ms decay of α1β channels. Note that the second, faster component is smaller at lower glycine concentrations, to a point where at some 500 μM patches it is rarely big enough to be detectable. These data differ from those of Mangin *et al.* (2003), who reported a single decay time constant of 153 ms for α2 channels in CHO cells. However, this discrepancy can be explained by the fact that the authors used a high chloride pipette solution for their outside-out experiments (~140 mM) which, as shown, would be expected to slow down the deactivation (Pitt *et al*., 2008; see also Figure 3.31*A*).

Table 3.12 Deactivation time constants from 2 ms concentration jumps.

[glycine]	τ1	τ2
10 mM	114.4 ± 12.9 ms 96 ± 1% (n = 8)	6.1 ± 1.4 ms 4 ± 1% (n = 7)
1 mM	85.8 ± 10.1 ms 97 ± 1% (n = 9)	5.4 ± 2.2 ms 5 ± 2% (n = 5)
500 μM	80.7 ± 8.8 ms 95 ± 4% (n = 6)	4.9 ± 1.8 ms 7 ± 5% (n = 4)

Data are average ± SEM from individual fits of average currents with exponential curves. The areas of each component and the number of patches are also shown. Recordings were performed with low (10 mM) chloride in the pipette and at -100 mV.

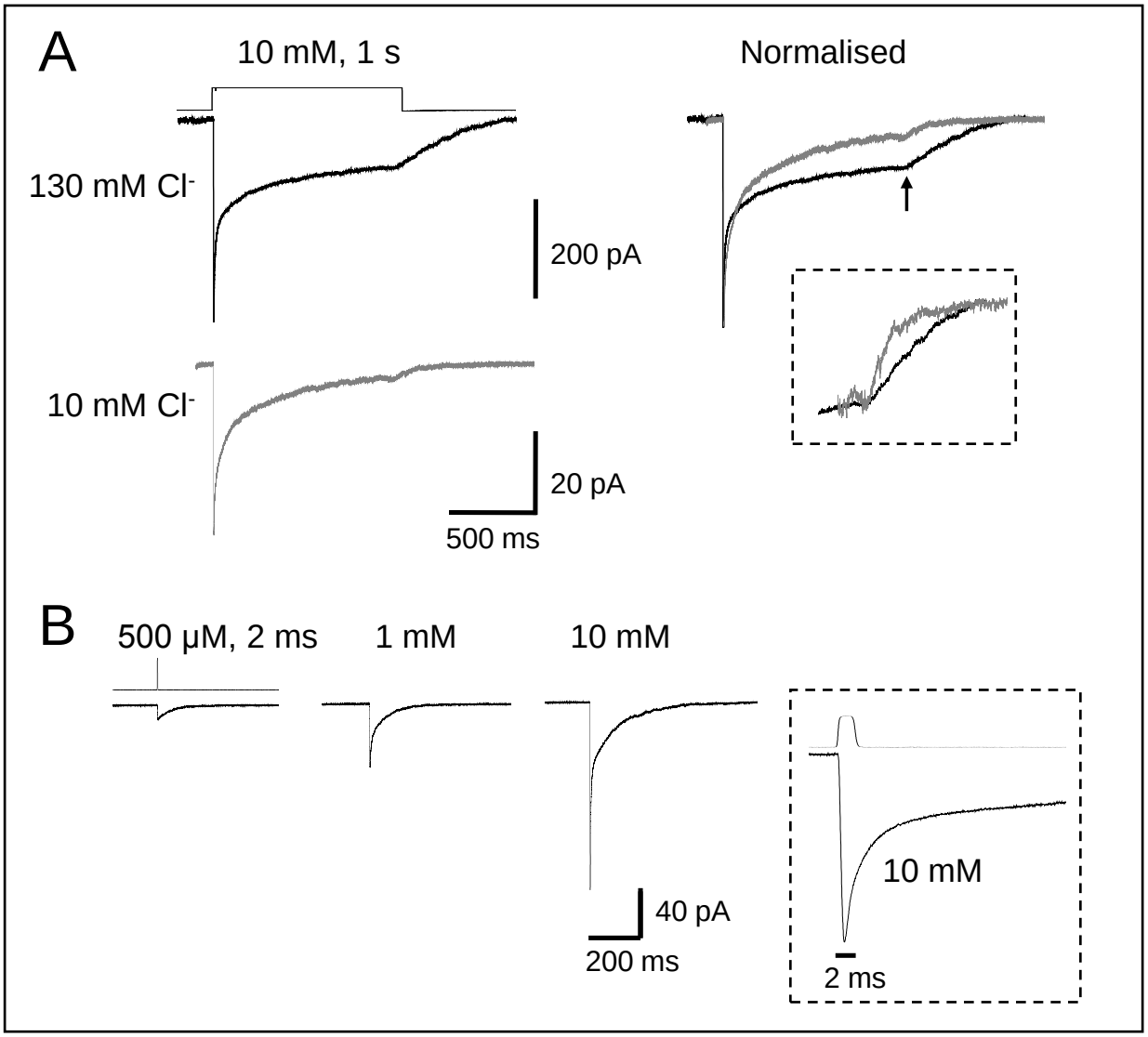

Figure 3.31 Deactivation time course of glycine-evoked currents

A, The traces on the left are average current responses to a 1 s pulse of saturating glycine (10 mM) to outside-out patches from HEK293 cells expressing rat α2 GlyRs. Recordings were performed at -100 mV with high (130 mM) or low (10 mM) chloride in the pipette solution (averages of 9 and 20 sweeps respectively). The time course of the glycine application, obtained by the open tip potential recorded at the end of the experiment, is shown above (here it corresponds to the 130 mM Cl^- patch). The two traces, normalised to their peak, are superimposed in the right panel of *A.* In the dashed box they are shown scaled to the beginning of deactivation (indicated by the arrow). Note the faster decay for the low chloride patch (grey trace). *B,* Average traces from a patch exposed to a brief (2 ms) pulse of glycine at the indicated concentrations, using the 10 mM chloride pipette solution. In the box is the 10 mM glycine trace expanded; note the biexponential decay ($\tau 1$ = 107 ms, $\tau 2$ = 3.4 ms, area1 = 96%).

For testing the two best kinetic models (7A and 7B) I calculated with the SCALCS program the decay expected for currents elicited by short pulses of 10 mM glycine. The program has the ability to simulate the relaxation of a macroscopic current after a concentration jump, using the rate constants of a kinetic scheme. Due to the fact that the rate constants between the two and three binding site schemes were almost identical, it was not surprising that the program gave similar predictions of the decay: 202.7 ms (7A) and 205.08 ms (7B) for a 1 s jump at 10 mM glycine. Identical values were predicted for faster applications. Note that four (7A) and three (7B) additional components are in theory predicted by the models but the areas of these exponentials are negligible. The value of ~200 ms, though not matching, is much closer to the decay of macroscopic currents obtained with low chloride in the pipette (112 ± 26 ms) than to the ~400 ms deactivation of currents recorded with high chloride. Because of that I continued using the low chloride solution for the rest of the concentration jump experiments.

Because we cannot distinguish between models 7A and 7B we proceeded in testing the quality of both against the macroscopic currents. The following paragraphs describe the testing of model 7A (three binding sites, 1 flip state, 1 open state) against the macroscopic data from concentration jumps.

In order to continue testing the validity of model 7A I needed to characterise desensitization for these receptors, as this process can affect the decay of macroscopic currents, even after brief agonist applications (Legendre *et al*., 2002). The single-channel analysis that resulted in schemes 7A and 7B cannot provide any information concerning this phenomenon since long sojourns in desensitized states were excluded from HJC fitting when shut times longer than t_{crit} were discarded. For the purpose of investigating the kinetics of desensitization of α2 receptors and, if possible, extending the mechanism to include appropriate desensitized states, I performed long (200 ms) concentration jumps at saturating glycine concentrations (10 mM) and recorded outside-out macroscopic currents at low pipette chloride.

Outside-out recordings revealed a large variability in the kinetics of desensitization between patches and this was correlated with differences in the amplitude and risetime of macroscopic currents. The larger currents had complex kinetics of desensitization that needed to be fitted with 2 exponentials ($\tau1 = 67 \pm 8$ ms, $\tau2 = 2.5 \pm 0.5$ ms; n = 8).

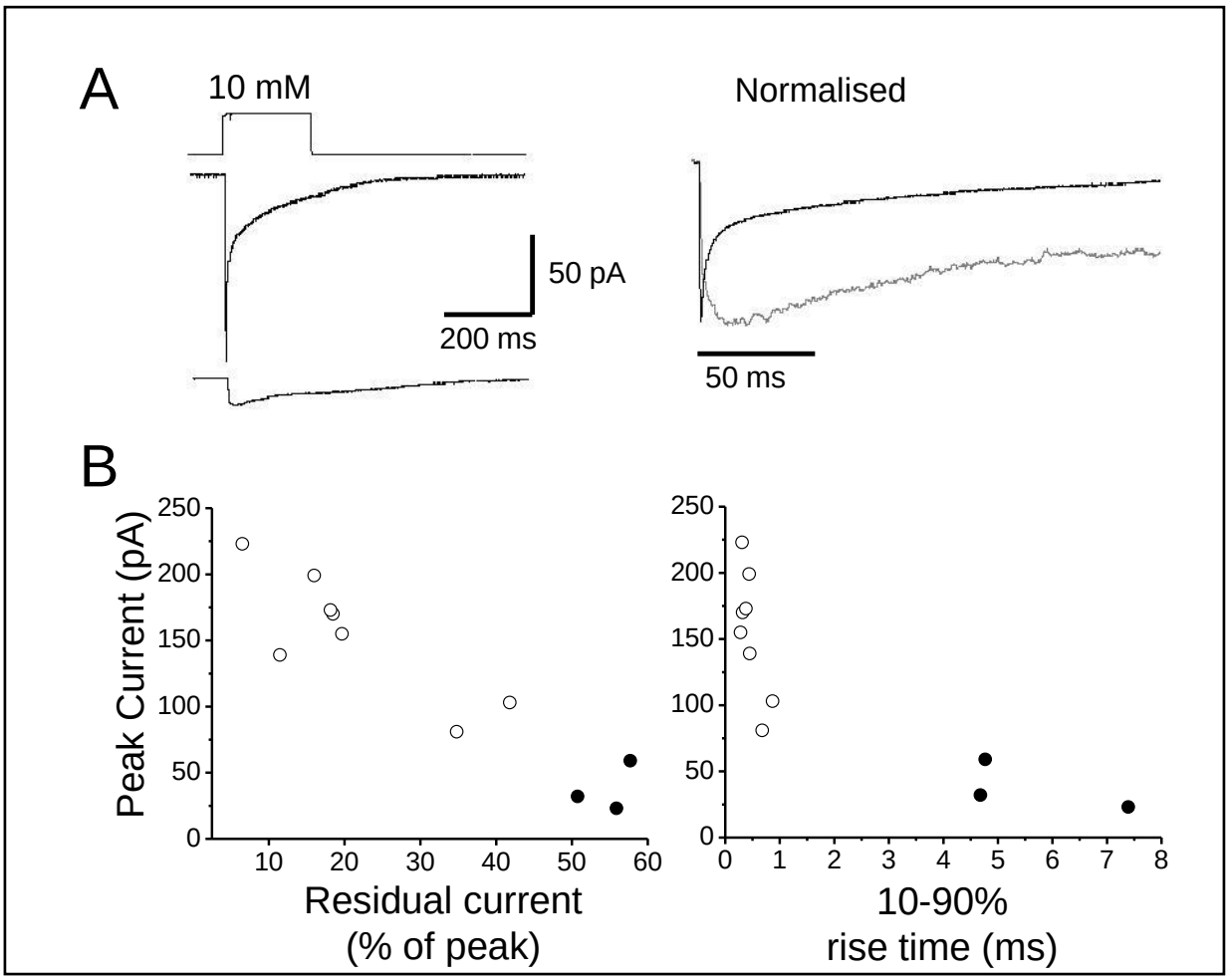

Figure 3.32 Desensitization of α2 glycine-evoked currents
A, The traces are average current responses to prolonged (200 ms) application of saturating glycine (10 mM) to outside-out patches. The top trace has a high current amplitude and high level of desensitization whereas the bottom trace has a low amplitude and little desensitization. Recordings were performed at -100 mV with a low chloride pipette solution. The two traces, normalised to their peak and with their desensitization phase (200 ms) expanded, are superimposed in the right panel of *A*. The plots in *B* show the inverse relationship between the current amplitude and the extent of desensitization (left) or the 10-90% risetime (right) for all 200 ms patches with 10 mM glycine. Note that low-amplitude currents have little desensitization and a slow onset (black circles). The extent of desensitization was taken as the residual current at the end of the 200 ms jump.

An example of such a trace is shown in Figure 3.32*A* (top trace). This current had peak amplitude of 139 pA and two desensitization exponential components with time constants of 3.8 ms and 86 ms. On the other hand, currents with low amplitude, like the bottom trace in the same figure (23 pA, desensitization τ = 82 ms) desensitized to a lesser extent and their desensitization could be fitted by one exponential component ($\tau = 69 \pm 10$ ms; n = 3). Similar values were obtained with 1 mM and 500 μM glycine. The difference in the desensitization

kinetics between the two examples in Figure 3.32*A* is more pronounced when they are normalised to their peak and their desensitization phase (200 ms) is expanded (right panel in Figure 3.32*A*). The plot of Figure 3.32*B* (left) shows that the extent of desensitization of all patches is inversely correlated with the current amplitude. In addition to that, only the larger currents had the fast desensitization component. Both observations are similar to published reports for α1 (Legendre *et al*., 2002) and α1β GlyRs (Pitt *et al.*, 2008). The currents that had a low current amplitude (38 ± 11 pA, n = 3) and lacked the fast desensitization component also had a slower rising phase with an average 10-90% risetime of 5.61 ± 0.89 ms (filled circles in Figure 3.32*B*, right) compared with the rest of the patches (average amplitude of 163 ± 17 pA and risetime less than 1 ms; open circles in Figure 3.32*B*).

3.3.8 Fits to macroscopic currents with scheme 7A

In order to describe the time course of a macroscopic glycine-evoked current, including the observed fast and slow desensitization, I introduced into scheme 7A two additional desensitized states ($A3D_{slow}$ and $A3D_{fast}$, see Figure 3.33*A*). The new model, 7A-d (with the rate constants fixed to those obtained from single-channel data), was introduced into ChanneLab software in order to estimate the rate constants for entry and exit from desensitization from fits to macroscopic currents (see Methods). When currents with high amplitude were fitted, both desensitized states were kept in the model; only the slow desensitized state was used for patches with low current. Macroscopic currents evoked by a long (200 ms) application of glycine were fitted well by model 7A-d and with the rates obtained from the single-channel data. Examples of such fits are shown in Figures 3.33*B* and *C* for a high- and a low-amplitude patch respectively. The average rate constants for entry and exit from slow desensitization were 202 s^{-1} ± 56% and 56 s^{-1} ± 44% for the 10 mM traces and similar values were obtained for the 1 mM and 500 μM traces (n = 6 for each concentration). The fast desensitization of the 10 mM traces had average rates of 337 s^{-1} ± 66% for entry and 248 s^{-1} ± 37% for exit but these values varied between concentrations and between patches. Low-amplitude currents, as noted before (see Figure 3.32*B*), had a much more modest desensitization with rate constants that were similar for the entry and exit from the single desensitized state (17-38 s^{-1} for the 10 mM traces and 15-80 s^{-1} for the 1 mM traces).

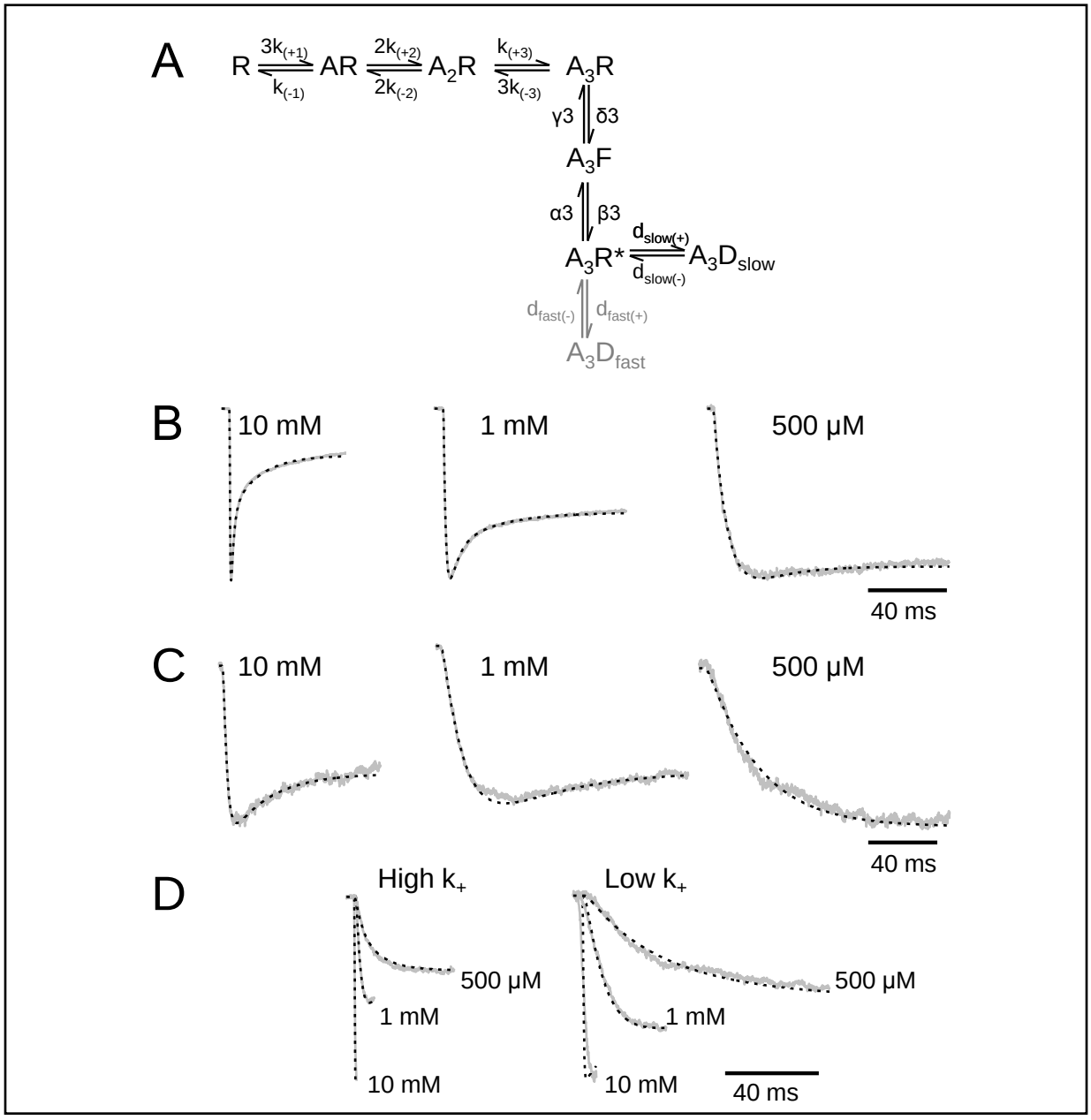

Figure 3.33 Fits of macroscopic currents with model 7A and desensitized states (7A-d)
A, The model has two desensitized states to account for the intense desensitization of high-amplitude currents. Fits were performed in ChanneLab to estimate the rate constants for desensitization and the association rate constant (k_+) after a 200 ms jump. All other rate constants were fixed to values obtained from HJCFIT (Table 3.11). For currents with low amplitude only one desensitized state was kept in the model. The traces are average currents with high (*B*) and low (*C*) amplitude fitted to the model. The fits are shown as black dash lines superimposed to the traces (continuous grey lines). Three glycine concentrations are applied on each patch. Currents are normalised to their peak prior to fitting. Records were obtained at -100 mV (10 mM chloride in the pipette). *D*, Simultaneous fits of the onset of glycine-evoked currents for a patch with fast (left) and slow risetime (right). Currents are normalised to the peak of the 10 mM response for each patch. The high- and low-amplitude currents (in *B, C, D*) correspond to the groups of patches in Figure 3.32*B* (white and black circles respectively).

It is interesting to note that single-channel dwells in the desensitized states that are needed in order to fit macroscopic current responses would have been excluded from the kinetic analysis with HJCFIT since their lifetime (4 ms for the fast desensitized state and 17.8 ms for the slow desensitized state with 10 mM glycine and high current patches; 35.7 ms for the desensitized state in low current patches) is longer than the highest t_{crit} chosen for the HJC fits (3 ms).

Using the rates obtained from fitting the desensitization and also the rates from HJCFIT, I proceeded to refine the value of the agonist association rate constant (k_{+3} in Figure 3.33*A*) by fitting only the onset of macroscopic currents. Similar to single-channel data, fits were performed with the constraint of identical, non-interacting binding sites, taking into account the available sites for each binding event (i.e. $k_{+1} = k_{+2} = k_{+3}$). As previously mentioned, the time course of the risetime for macroscopic responses was dependent on the receptor density with high-amplitude patches having a faster onset (see Figure 3.32*B*, right panel). It was therefore expected that the value of k_+ would also depend on the current amplitude. As a first step, the onset of each current from 200 ms jumps was fitted separately, by fixing all rate constants and leaving only k_+ free. The results for these fits, averaged for each concentration, are shown in Table 3.13. There are slight differences in the estimates across concentrations but the only meaningful difference seems to be between patches with high and with low current. The data in Table 3.13 summarize the results from patches in which all three concentrations were applied successfully (6 high-current and 2 low-current patches). The overall average value from all individual fits was 2.8×10^6 $M^{-1}s^{-1}$ ± 47% (n = 18) for the high-current patches and 1.0×10^6 $M^{-1}s^{-1}$ ± 47% (n = 6) for the low-amplitude patches. As a second step, I selected 2 high- and 1 low-current patch and fitted all the three responses to the different concentrations simultaneously for each patch, in order to estimate a 'patch' k_+. The latter did not differ from the average values mentioned above (Table 3.13; Figure 3.33*D*).

The k_+ values obtained from ChanneLab are somewhat lower than the value of 6.23×10^6 $M^{-1}s^{-1}$ ± 52% obtained from the single-channel data in HJCFIT (4 different data sets, see Table A9, Appendix C). The determination of the binding rate constant from single-channel data may be the weakest point in the global mechanism fits, given the lack of knowledge about the true number of channels in a patch (Colquhoun *et al*., 2003) and the arbitrariness in the choice of the t_{crit} in the case of the α2 data.

Table 3.13 Fits of the onset of macroscopic currents to scheme 7A-d.

[Gly]	**High k_+**		**Low k_+**	
10 mM	$2.2x10^6$ ± 58%	(6)	$0.5x10^6$ ± 56%	(2)
1 mM	$3.0x10^6$ ± 31%	(6)	$1.3x10^6$ ± 62%	(2)
500 μM	$3.3x10^6$ ± 49%	(6)	$1.3x10^6$ ± 18%	(2)
Simultaneous fits	$2.5x10^6$ ± 17%	(2)	$1.3x10^6$	(1)

The first three rows represent the average binding rate constant ± CV for individual fits of the rising phase to model 7A-d for currents evoked by 200 ms application of glycine. Patches were separated according to receptor density and correspond to the data in the right panel of Figure 3.32*B*. The number of patches is shown in brackets. The last row is the result from simultaneous fits of the three agonist responses of each patch, to the model. Only one (low k_+) or both desensitization states (high k_+) were included in the model, as in Figure 3.33*A*.

As a last test of the credibility of scheme 7A I proceeded to re-fit the single-channel data with HJCFIT, by fixing the k_+ value to either the high or the low solution obtained from the macroscopic jumps and tested again the quality of the fits. When the k_+ was fixed to the high value from the jumps, the HJC fits for 4 different sets did not differ much from the initial fits to model 7A. The average estimates of rate constants from fits to four sets (summarised in Table A8, Appendix C) with free and fixed k_+ are shown in Table 3.14. When the low k_+ was used however, the fits to the distributions were not as good and this value was discarded. It is reasonable to assume that the cell-attached single-channel recordings were performed in patches that had similar channel density as the high-amplitude patches from which the high k_+ value was obtained.

In summary, the combination of the results from the concentration jumps and the single-channel data agree that model 7A is a good candidate for the kinetic mechanism of α2 GlyRs: it describes well the behaviour of single channels with good predictions of the experimental open-period and shut-time distributions, it gives reasonable estimates for the maximum P_{open} and can also describe the time course of macroscopic currents after the model is extended to include desensitization. The behaviour of these channels however appears to be more complicated than what the model suggests: for example, model 7 does not explain the presence of two deactivation components after a brief exposure to saturating glycine, or the lack of any concentration dependence in the P_{open} values.

Table 3.14 Average estimates of rate constants from fits to four data sets with model 7A.

	Unit	**Model 7A Free k_+**		**Model 7A Fixed $k_{+(high)}$**		**Model 7A Fixed $k_{+(low)}$**	
α	s^{-1}	410	(40%)	312	(28%)	204	(14%)
β	s^{-1}	161763	(15%)	142415	(12%)	110141	(8%)
γ	s^{-1}	6226	(18%)	6218	(14%)	6365	(8%)
δ	s^{-1}	15699	(20%)	10414	(15%)	5067	(18%)
k_-	s^{-1}	2434	(22%)	1250	(18%)	373	(34%)
k_+	$M^{-1}s^{-1}$	$6.23x10^6$	(52%)	$2.80x10^6$	(fixed)	$1.00x10^6$	(fixed)
E		412	(27%)	469	(23%)	623	(39%)
F		2.28	(42%)	1.66	(60%)	0.83	(23%)
K_R	μM	501	(60%)	447	(61%)	373	(38%)
max P_{open}		0.998	(0.16%)	0.997	(0.17%)	0.997	(0.15%)
EC_{50}	μM	53	(55%)	52	(42%)	40	(62%)
n_H		2.68	(3%)	2.65	(3%)	2.49	(12%)
$d_{slow(+)}$	s^{-1}			202	(56%)	28	(54%)
$d_{slow(-)}$	s^{-1}			56	(44%)	28	(8)
$d_{fast(+)}$	s^{-1}			337	(66%)	-	
$d_{fast(-)}$	s^{-1}			248	(37%)	-	

Average rate constants (and % coefficient of variation of the mean) from four different sets of cell-attached patches (2 patches per set), fitted in HJCFIT with either all parameters free (first column) or with the binding rate constant (k_+) fixed to the high and low value obtained from the 200 ms concentration jumps. The desensitization rate constants were obtained from fits of 200 ms jumps to 10 mM glycine with low chloride in the pipette, from high- and low-amplitude currents (second and third column respectively).

3.4 Appendix C (HJC fitting to additional α2 single-channel data sets)

The following tables show results of fits to sets of single-channel data using the models described in Chapter 3.3. These data are complementary to set 1 (30 μM and 1 mM patches) shown in the chapter and are provided for a more detailed description of the quality of each kinetic scheme. Each table column includes information for each set, such as the glycine concentration of the patches, the t_{crit} used for each patch/fit and the type of vector (steady-state vector for a 'cluster' concentration or a CHS vector for a 'burst' concentration). In most cases the fits were performed with constraints for identical, non-interacting binding sites, (i.e. $k_{+1} = k_{+2} = k_{+3}$; $k_{-1} = k_{-2} = k_{-3}$). Model 7A was also fitted to sets of data without this constraint (Table A8). The tables also include the number of free parameters fitted for each model/fit and, where applicable, the number of parameters set by microscopic reversibility (MR).

The last table (Table A9) summarizes the results of fits to model 7A (3 binding sites, 1 flipped state, 1 open state) using the high and low values of the binding rate constant (k_+) obtained from ChanneLab. These values, fixed for each fit, are shown in bold numerals. Fits were performed with the low values of t_{crit}, as shown for each set. The average of these four sets is in Table 3.14.

Table A1 Fits to scheme 2 (4 binding sites, 4 open states).

	Units	**Set 1** 30 μM, 10 ms 1 mM, 10 ms steady-state constraints*	**Set 6** 30 μM, 10 ms 1 mM, 10 ms steady-state constraints*	**Set 9** 20 μM, 0.6 ms 1 mM, 10 ms CHS for 20 μM constraints*
α1	s^{-1}	56	39	131
β1	s^{-1}	17018	25480	32022
α2	s^{-1}	243804	58233	134192
β2	s^{-1}	96801	975	18267
α3	s^{-1}	155	134	215
β3	s^{-1}	89179	89829	107461
α4	s^{-1}	6	0.30	4
β4	s^{-1}	0.00	30	0.00
k_-	s^{-1}	439	402	442
k_+	$M^{-1}s^{-1}$	$5.9x10^6$	$6.5x10^6$	$3.1x10^6$
E1		305	650	244
E2		0.40	0.02	0.14
E3		575	669	501
E4		0.00	110	0.00
K_R	μM	74	61	141
max P_{open}		0.993	0.996	0.995
EC_{50}	μM	undetermined	undetermined	undetermined
n_H		undetermined	undetermined	undetermined
L_{max} (log)		12262	18140	7873
Free parameters		10	10	10

* $k_{-1} = k_{-2} = k_{-3} = k_{-4}$ and $k_{+1} = k_{+2} = k_{+3} = k_{+4}$

Table A2 Fits to scheme 3 (3 binding sites, 3 open states).

	Units	**Set 1**		**Set 3**			**Set 10**
		30 μM, 10 ms 1 mM, 10 ms	30 μM, 0.6 ms 1 mM, 10 ms	20 μM, 0.6 ms 50 μM, 3ms 1 mM, 10 ms	20 μM, 1 ms 1 mM, 3 ms	20 μM, 0.1 ms 1 mM, 3 ms	30 μM, 0.6 ms 100 μM, 10 ms 10 mM, 10 ms
		steady-state constraints*	CHS constraints*	CHS < 50 μM constraints*	CHS (20 μM) constraints*	CHS (20 μM) constraints*	CHS (30 μM) constraints*
α1	s^{-1}	877366	637362	2002	800777	775223	981220
β1	s^{-1}	0.00	48	0.00	998848	$1.0x10^6$	126
α2	s^{-1}	14387	14318	71	180392	126349	11306
β2	s^{-1}	375	80	546	467	65	212
α3	s^{-1}	65	67	111	72	85	39
β3	s^{-1}	34782	36768	25050	64406	74551	17872
k_{-1}	s^{-1}	688	1305	2698	1571	1772	1223
k_{+3}	$M^{-1}s^{-1}$	$3.3x10^6$	$3.2x10^6$	$1.9x10^6$	$4.5x10^6$	$4.3x10^6$	$2.3x10^7$
E1		0.00	0.00	0.00	1.25	1.29	0.00
E2		0.03	0.01	8	0.00	0.00	0.02
E3		534	550	225	890	876	458
K_R	μM	207	413	1382	350	414	52
max P_{open}		0.998	0.999	0.950	0.999	0.999	0.998
EC_{50}	μM	29	57	223	45	54	8
n_H		2.64	2.64	2.20	2.26	2.25	2.62
L_{max} (log)		11900	11617	12766	8087	7956	14262
Free parameters		6	6	6	6	6	6

* $k_{-1} = k_{-2} = k_{-3}$ and $k_{+1} = k_{+2} = k_{+3}$

Table A3 Fits to scheme 5 ('flip' model: 3 binding sites, 3 flipped states, 3 open states).

	Units	**Set 1**		**Set 3**	
		30 μM, 10 ms 1 mM, 10 ms steady-state constraints*	30 μM, 0.1 ms 1 mM, 2 ms CHS (30 μM) constraints*	20 μM, 10 ms 1 mM, 10 ms steady-state constraints*	20 μM, 1 ms 1 mM, 3 ms CHS (20 μM) constraints*
α1	s^{-1}	14037	7705	0.30	87
β1	s^{-1}	1531	804	3621	3
α2	s^{-1}	186	249	275	249
β2	s^{-1}	100624	114538	72877	111487
α3	s^{-1}	18244	53546	33510	1070
β3	s^{-1}	337120	374572	401860	912166
γ1	s^{-1}	994919	3896	226248	360035
δ1	s^{-1}	728018	$4.29x10^{6}$	998	553649
γ2	s^{-1}	7507	96	4200	6488
δ2	s^{-1}	9670	5640	2894	8479
γ3	s^{-1}	0.01	704	7711	0.00
δ3	s^{-1}	0.03	2223	830029	0.00
k_-	s^{-1}	813	0.24	1.46	1398
k_+	$M^{-1}s^{-1}$	$9.8x10^{6}$	75600	1039	$2.2x10^{6}$
k_{F-}	s^{-1}	1381	3876	723	84
k_{F+}	$M^{-1}s^{-1}$	$2.9x10^{7}$	$6.5x10^{7}$	$8.0x10^{7}$	113485
E1		0.11	0.10	13106	0.03
E2		542	460	265	448
E3		19	7	12	852
F1		0.73	1102	0.00	1.54
F2		1.29	58	0.69	1.31
F3		2.27	3.16	107	1.11
K_R	μM	83	3.21	1405	629
K_F	μM	47	60	13106	0.03
max P_{open}		0.993	undetermined	0.994	0.999
EC_{50}	μM	2	undetermined	8	16
n_H		1.89	undetermined	1.04	1.84
L_{max} (log)		12382	11038	8702	8550
Free parameters		14	14	14	14
MR rates		2	2	2	2

* $k_{-1} = k_{-2} = k_{-3}$ and $k_{+1} = k_{+2} = k_{+3}$

Table A4 Fits to scheme 6A (3 binding sites, 2 flipped states, 2 open states).

	Units	**Set 2** 20 μM, 10 ms 100 μM, 10 ms 1 mM, 10 ms steady-state* constraints	 20 μM, 0.1 ms 100 μM, 0.2 ms 1 mM, 2 ms CHS <100 μM* constraints	**Set 3** 20 μM, 1 ms 1 mM, 3 ms CHS for 20 μM* constraints	 20 μM, 0.1 ms 1 mM, 3 ms CHS for 20 μM* constraints	**Set 4** 50 μM, 0.5 ms 10 mM, 0.2 ms CHS for 50 μM* constraints	**Set 5** 30 μM, 0.1 ms 10 mM, 0.2 ms CHS for 30 μM* constraints	**Set 6** 30 μM, 0.3 ms 1 mM, 3 ms CHS for 30 μM* constraints
α2	s^{-1}	45690	41707	66476	61754	12417	59438	118664
β2	s^{-1}	277381	245405	79824	122536	298494	998777	71687
α3	s^{-1}	344	421	390	674	354	373	132
β3	s^{-1}	127798	161238	186360	225781	113902	124573	114958
γ2	s^{-1}	514	884	5714	3349	216	12436	4487
δ2	s^{-1}	2748	358	496	331	4621	1178	85
γ3	s^{-1}	1816	3674	3945	4039	4864	4321	5052
δ3	s^{-1}	1052	8947	14573	26749	29818	28048	7682
k_-	s^{-1}	160	1633	854	2521	2302	1005	803
k_+	$M^{-1}s^{-1}$	$1.1x10^7$	$4.4x10^6$	$2.0x10^6$	$3.4x10^6$	$6.8x10^6$	$4.6x10^6$	$2.2x10^6$
k_{F-}	s^{-1}	326640	$5.4x10^9$	333331	331131	20366	14221	6347
k_{F+}	$M^{-1}s^{-1}$	$2.5x10^9$	330055	$3.3x10^{10}$	$3x10^{10}$	$1.7x10^7$	$4.5x10^9$	$1.4x10^9$
E2		6.07	5.88	1.20	1.98	24.04	16.80	0.60
E3		372	383	479	335	322	334	871
F2		5.34	0.41	0.09	0.10	21.43	0.09	0.02
F3		0.58	2.44	3.69	6.62	6.13	6.49	1.52
K_R	μM	14	367	435	742	341	216	361
K_F	μM	129	61	10	11	1191	3	4
max P_{open}		0.995	0.998	0.999	0.999	0.998	0.999	0.999
EC_{50}	μM	1	41	39	62	9	18	36
n_H		1.73	2.62	2.75	2.77	1.89	2.74	2.73
L_{max} (log)		17923	16166	8340	8142	11640	12052	17140
Free parameters		11	11	11	11	11	11	11
MR rates		1	1	1	1	1	1	1

Fits to set 1 with model 6A are shown in Table 3.10

* $k_{-1} = k_{-2} = k_{-3}$ and $k_{+1} = k_{+2} = k_{+3}$

Table A5: Fits to scheme 6B (2 binding sites, 2 flipped states, 2 open states).

	Units	**Set 2**		**Set 3**	
		20 μM, 10 ms 100 μM, 10 ms 1 mM, 10 ms steady-state constraints*	20 μM, 0.1 ms 100 μM, 0.2 ms 1 mM, 2 ms CHS <100 μM constraints*	20 μM, 1 ms 1 mM, 3 ms CHS for 20 μM constraints*	20 μM, 0.1 ms 1 mM, 3 ms CHS for 20 μM constraints*
α1	s^{-1}	49419	43326	67282	63316
β1	s^{-1}	251669	142716	82427	115068
α2	s^{-1}	397	443	396	646
β2	s^{-1}	150280	186380	187420	222394
γ1	s^{-1}	429	3434	5448	3647
δ1	s^{-1}	530	272	422	284
γ2	s^{-1}	3088	5895	3959	3994
δ2	s^{-1}	3256	14836	14808	25037
k_-	s^{-1}	0.32	2806	1367	3436
k_+	$M^{-1}s^{-1}$	3285	$3.8x10^6$	$1.8x10^6$	$2.7x10^6$
k_{F-}	s^{-1}	427033	499739	498467	362728
k_{F+}	$M^{-1}s^{-1}$	$3.7x10^9$	$2.1\ x10^{10}$	$3.2x10^{10}$	$2.3x10^{10}$
E1		5.09	3.29	1.23	1.82
E2		378	421	474	344
F1		1.24	0.08	0.08	0.08
F2		1.05	2.52	3.74	6.27
K_R	μM	99	743	748	1263
K_F	μM	116	23	15	16
max P_{open}		0.997	0.999	0.999	0.999
EC_{50}	μM	4	24	18	28
n_H		1.40	1.92	1.95	1.95
L_{max} (log)		17930	16165	8341	8142
Free parameters		11	11	11	11
MR rates		1	1	1	1

* $k_{-1} = k_{-2}$ and $k_{+1} = k_{+2}$

Table A6 Fits to scheme 7A (3 binding sites, 1 flipped state, 1 open state).

	Units	**Set 3** 20 μM, 1 ms 1 mM, 3 ms CHS (20 μM) constraints*	20 μM, 0.1 ms 1 mM, 3 ms CHS (20 μM) constraints*	**Set 4** 50 μM, 10 ms 10 mM, 10 ms steady-state constraints*	50 μM, 3 ms 10 mM, 3 ms CHS (50 μM) constraints*	**Set 7** 100 μM, 3 ms 1 mM, 3 ms CHS (100 μM) constraints*	100 μM, 0.2 ms 1 mM, 3 ms CHS (100 μM) constraints*
α	s^{-1}	140	308	286	353	96	376
β	s^{-1}	105742	159609	104838	117107	95607	186353
γ	s^{-1}	6496	7178	2724	2904	6913	6086
δ	s^{-1}	6622	19399	1373	2509	4038	17822
k_{-1}	s^{-1}	1027	2707	100	578	623	2373
k_{+3}	$M^{-1}s^{-1}$	$2.9x10^6$	$3.9x10^6$	$1.6x10^7$	$1.1x10^7$	$4.1x10^6$	$3.7x10^6$
E		753.04	517.76	366.42	331.69	996.97	495.38
F		1.02	2.70	0.50	0.86	0.58	2.93
K_R	μM	357	691	6	54	153	650
max P_{open}		0.998	0.999	0.994	0.996	0.998	0.999
EC_{50}	μM	44	68	1	10	21	63
n_H		2.68	2.73	2.49	2.56	2.65	2.74
L_{max}(log)		8179	7979	11955	11888	9795	9486
Free parameters		6	6	6	6	6	6

For Set 1 see Table 3.10

* $k_{-1} = k_{-2} = k_{-3}$ and $k_{+1} = k_{+2} = k_{+3}$

Table A7 Fits to scheme 7B (2 binding sites, 1 flipped state, 1 open state).

	Units	**Set 3** 20 μM, 1 ms 1 mM, 3 ms CHS (20 μM) constraints*	20 μM, 0.1 ms 1 mM, 3 ms CHS (20 μM) constraints*	free	**Set 4** 50 μM, 10 ms 10 mM, 10 ms steady-state constraints*	50 μM, 3 ms 10 mM, 3 ms CHS (50 μM) constraints*	free	**Set 7** 100 μM, 3 ms 1 mM, 3 ms CHS (100 μM) constraints*	100 μM, 0.2 ms 1 mM, 3 ms CHS (100 μM) constraints*	free
α	s^{-1}	145	275	1297	286	353	357	105	372	375
β	s^{-1}	107734	151523	255267	104836	117083	117815	101484	185525	186116
γ	s^{-1}	6558	7208	4389	2725	2904	2910	7031	6107	6101
δ	s^{-1}	7058	17438	36044	1373	2509	2628	4818	17654	17913
k_{-1}	s^{-1}	1627	3673	5685	148	838	910	1156	3494	10544
k_{+1}	$M^{-1}s^{-1}$	$2.7x10^6$	$3.2x10^6$	$1.4x10^6$	$1.5x10^7$	$8.7x10^6$	$4.8x10^4$	$3.9x10^6$	$3.1x10^6$	$2.4x10^6$
k_{-2}	s^{-1}	1627	3673	5599	148	838	1406	1156	3494	3773
k_{+2}	$M^{-1}s^{-1}$	$2.7x10^6$	$3.2x10^6$	$7.7x10^6$	$1.5x10^7$	$8.7x10^6$	$3.0x10^7$	$3.9x10^6$	$3.1x10^6$	$7.2x10^6$
E		744	552	197	366	332	330	966	499	497
F		1.08	2.42	8.21	0.50	0.86	0.90	0.69	2.89	2.94
K_{R1}	μM	612	1144	4205	10	96	19117	300	1122	4444
K_{R2}	μM	612	1144	725	10	96	46	300	1122	524
max P_{open}		0.998	0.999	0.999	0.994	0.996	0.996	0.998	0.999	0.999
EC_{50}	μM	22	32	44	1	6	54	12	30	40
n_H		1.93	1.95	1.98	1.86	1.89	1.99	1.93	1.95	1.98
L_{max}(log)		8179	7978	7980	11955	11888	11890	9798	9486	9486
Free parameters		6	6	8	6	6	8	6	6	8

Set 1 see Table 3.11

* $k_{-1} = k_{-2}$ and $k_{+1} = k_{+2}$

Table A8 Scheme 7A (free fits vs. constraints for non-interacting binding sites).

	Units	**Set 1** 30 μM, 0.1 ms, CHS 1 mM, 2 ms, steady-state		**Set 3** 20 μM, 0.1 ms, CHS 1 mM, 3 ms, steady-state		**Set 4** 50 μM, 3 ms, CHS 10 mM, 3 ms, steady-state		**Set 7** 100 μM, 0.2 ms, CHS 1 mM, 3 ms, steady-state	
		constraints*	free	constraints*	free	constraints*	free	constraints*	free
α	s^{-1}	603	615	308	1302	353	357	376	375
β	s^{-1}	183984	185559	159609	255474	117107	117810	186353	186222
γ	s^{-1}	8735	8760	7178	4380	2904	2910	6086	6096
δ	s^{-1}	23065	23813	19399	36065	2509	2628	17822	17920
k_{-1}	s^{-1}	4078	15435	2707	295	578	72	2373	10
k_{+1}	$M^{-1}s^{-1}$	$6.7x10^6$	$1.4x10^8$	$3.9x10^6$	$1.7x10^8$	$1.1x10^7$	$3.7x10^7$	$3.7x10^6$	$1.3x10^9$
k_{-2}	s^{-1}	4078	2176	2707	2838	578	455	2373	5268
k_{+2}	$M^{-1}s^{-1}$	$6.7x10^6$	$2.9x10^6$	$3.9x10^6$	$1.4x10^6$	$1.1x10^7$	47807	$3.7x10^6$	$2.4x10^6$
k_{-3}	s^{-1}	4078	4243	2707	3732	578	937	2373	2516
k_{+3}	$M^{-1}s^{-1}$	$6.7x10^6$	$7.2x10^6$	$3.9x10^6$	$7.7x10^6$	$1.1x10^7$	$3.0x10^7$	$3.7x10^6$	$7.2x10^6$
E		305	302	518	196	332	330	495	496
F		2.64	2.72	2.70	8.23	0.86	0.90	2.93	2.94
K_{R1}	μM	610	110	691	2	54	2	650	0.01
K_{R2}	μM	610	762	691	2100	54	9523	650	2223
K_{R3}	μM	610	593	691	484	54	31	650	349
max P_{open}		0.998	0.998	0.999	0.999	0.996	0.996	0.999	0.999
EC_{50}	μM	73	54	68	44	10	55	63	40
n_H		2.68	2.35	2.73	1.99	2.56	2.01	2.74	1.98
L_{max}(log)		10922	10923	7979	7980	11888	11888	9486	9486
Free parameters		6	10	6	10	6	10	6	10

* $k_{-1} = k_{-2} = k_{-3}$ and $k_{+1} = k_{+2} = k_{+3}$

Table A9 Scheme 7A (with fixed k_+ values as obtained from ChanneLab).

	Units	**Set 1** 30 μM, 0.1 ms, CHS 1 mM, 2 ms, steady-state constraints*			**Set 3** 20 μM, 0.1 ms, CHS 1 mM, 3 ms, steady-state constraints*			**Set 4** 50 μM, 3 ms, CHS 10 mM, 3 ms, steady-state constraints*			**Set 7** 100 μM, 0.2 ms, CHS 1 mM, 3 ms, steady-state constraints*		
		free k_+	**$k_{+(high)}$**	**$k_{+(low)}$**	**free k_+**	**$k_{+(high)}$**	**$k_{+(low)}$**	**free k_+**	**$k_{+(high)}$**	**$k_{+(low)}$**	**free k_+**	**$k_{+(high)}$**	**$k_{+(low)}$**
α	s^{-1}	603	266	188	308	231	146	353	347	354	376	403	130
β	s^{-1}	183984	124069	99983	159609	139206	108215	117107	116109	117256	186353	190305	115109
γ	s^{-1}	8735	9132	8986	7178	7043	6476	2904	2899	2906	6086	5796	7090
δ	s^{-1}	23065	8439	5041	19399	13625	6498	2509	2387	2538	17822	17206	6192
k_-	s^{-1}	4078	939	190	2707	1699	447	578	336	344	2373	2027	511
k_+	$M^{-1}s^{-1}$	$6.7x10^6$	**$2.8x10^6$**	**$1.0x10^6$**	$3.9x10^6$	**$2.8x10^6$**	**$1.0x10^6$**	$1.1x10^7$	**$2.8x10^6$**	**$1.0x10^6$**	$3.7x10^6$	**$2.8x10^6$**	**$1.0x10^6$**
E		305	466	533	518	603	741	332	335	331	495	472	888
F		2.64	0.92	0.56	2.70	1.93	1.00	0.86	0.82	0.87	2.93	2.97	0.87
K_R	μM	610	335	190	691	607	447	54	120	344	650	724	511
max P_{open}		0.998	0.997	0.996	0.999	0.999	0.998	0.996	0.995	0.996	0.999	0.999	0.998
EC_{50}	μM	73	51	33	68	64	55	10	22	8	63	71	62
n_H		2.68	2.61	2.56	2.73	2.72	2.67	2.56	2.55	2.04	2.74	2.73	2.68
L_{max}(log)		10922	10912	10898	7979	7976	7959	11888	11886	11887	9486	9483	9452
Free parameters		6	5	5	6	5	5	6	5	5	6	5	5

* $k_{-1} = k_{-2} = k_{-3}$ and $k_{+1} = k_{+2} = k_{+3}$

Chapter 4: Discussion

4.1 Stoichiometry of α1β GlyRs in *Xenopus* oocytes

The first of the two aims of my work was to identify the stoichiometry of heteromeric α1β GlyRs expressed in *Xenopus* oocytes. For this purpose two different methods were employed, which involved either the use of a reporter mutation that alters the receptors' sensitivity to glycine or the use of a mutation that alters single-channel conductance. Both these techniques were proven useful in the past for the identification of the stoichiometry of a given ligand-gated ion channel.

4.1.1 The 9′ mutation in oocyte-expressed receptors

Since the aim was to study heteromeric receptors, it was essential first to test whether co-injection of α1 and β subunit cRNA into oocytes effectively produces a predominantly heteromeric population. As a precaution the α:β subunit ratio of 1:40 was chosen because this ratio produces very little contamination by α1 homomeric channels in HEK293 cells (Burzomato *et al*., 2003). My experiments with the 9′ mutation involved obtaining macroscopic responses to glycine; hence, at that point, performing single-channel recordings to test the validity of the 1:40 ratio in oocytes was not considered (see Burzomato *et al.*, 2003). The only test performed was that of picrotoxin applied on α1+β injected oocytes: if the expressed receptors are heteromers then their sensitivity to the alkaloid should be lower than that of homomers (α1-injected cells; Pribilla *et al*., 1992). For four out of six oocytes injected with the α1+β combination the high picrotoxin IC_{50} confirmed the expression of heteromers, but this does not exclude the presence of a small proportion of homomers also. With the glycine concentration used (100 μM; ~EC_{50} for homomers) a number of α1 homomeric receptors could be activated too. Indeed, in the remaining two cells the picrotoxin IC_{50} was as low as that of homomers suggesting that in these cells the α1 receptor was predominant. I therefore tried to re-fit the four experiments that gave a heteromer-like IC_{50}, this time with two components, to see if I could achieve a reliable fit that would describe the extent of contamination. Free fits of each curve were poorly defined, probably due to the large number of parameters fitted. When I repeated the fits with the parameters of the first component (representing current from α1 homomers) fixed to the values from α1-injected oocytes and with the Hill slopes for both components fixed to 1, fits were again poorly defined. The poor fits to two components and the low sensitivity to picrotoxin suggested that the level of contamination

was low and that the 1:40 ratio was sufficient for the production of a predominant heteromeric population in oocytes. It was only when cell-attached single-channel recordings were performed that the true extent of contamination became evident, and homomers were detected in ~50% of patches. The single-channel data therefore confirmed that the PTX experiments underestimate the presence of homomers.

Glycine concentration-response curves from the different 9′ mutant combinations in oocytes revealed, in most cases, small changes in agonist sensitivity and in Hill slopes, which confirmed that the mutant subunits were incorporated in the receptors. The only exception was the $\alpha1+\beta^{LS}$ combination, for which glycine EC_{50} and n_H and picrotoxin IC_{50} were almost identical to those of α1 homomers. Thus, introducing the 9′LS (but not the 9′LT) mutation on the β subunit either prevents its incorporation into heteromers or somehow increases picrotoxin sensitivity of $\alpha1\beta^{LS}$ receptors while failing to change agonist sensitivity. One way of testing this would be to record from $\alpha1^{LS}\beta^{LS}$ mutants and see whether they differ in glycine sensitivity compared with $\alpha1^{LS}$ homomers. However, it was impossible to record from $\alpha1^{LS}\beta^{LS}$ mutants (or from $\alpha1^{LT}$ and $\alpha1^{LT}\beta^{LT}$) due to an increased death rate and increased holding current, consistent with the fact that when many 9′ mutations are incorporated, channels can open spontaneously (Chang and Weiss, 1998, 1999).

In all other combinations the presence of the mutation did change the sensitivity to glycine, but these changes were small (less than 2-fold) and similar for receptors in which the α1 subunit is mutated and receptors in which the β is mutated. The latter does not give any indication on the stoichiometry of the heteromers. My results are in contrast to those from muscle nicotinic receptors (Labarca *et al.,* 1995; Filatov and White, 1995) and from other pLGIC family members (neuronal nAChRs and GABARs) in which the shift is such that obvious differences appear between receptors with mutant α and mutant non-α subunits (for examples see Boorman *et al.,* 2000; Chang *et al.,* 1996; Moroni *et al.,* 2006; Plazas *et al.,* 2005a, b;). More importantly, my results from oocytes do not agree with data from α1β glycine receptors expressed in HEK293 cells, in which the same receptor subtype and same subunit constructs were studied (Burzomato *et al.,* 2003). In the HEK293 cell study the dose ratios (calculated as the horizontal distance between the wild-type and the mutant concentration-response curve) were ~10-fold when β was mutated ($\alpha1\beta^{LT}$) and ~74-fold when α1 was mutated ($\alpha1^{LT}\beta$),

suggesting a stoichiometry of 3α:2β (Burzomato *et al.,* 2003). The strongest effect of the mutations in oocytes, on the other hand, was only a decrease in the Hill slope and in the maximum current produced by glycine. These were more obvious for receptors with a mutated α1 subunit ($\alpha1^{LS}\beta$, $\alpha1^{LT}\beta$). An effect on the Hill slope coefficient has also been reported for $GABA_A$ receptors (Chang *et al.,* 1996) and also for HEK293-expressed GlyRs (Burzomato *et al.,* 2003); in the latter, the reduction was also proportional to the number of mutations in the receptor. Given that 9′ mutations increase the probability of channel opening, these reductions in the Hill slope of mutant receptors have been interpreted as an indication that partially liganded states of the receptor contribute to the agonist current.

The strong evidence from the Burzomato study and the discrepancy with my data raises some questions: why, since the same receptors and mutations were studied, is this discrepancy observed? Or, to be more precise, what are the differences between the two expression systems that are responsible for the dissimilar results between the two studies? Some ideas are considered below:

A simple explanation for these findings may be that oocyte-expressed α1β receptors are a mixture of pentamers, some containing two and some containing three copies of the alpha subunit. Effectively, the average number of both subunits in each receptor would be the same, which would explain why the concentration-response curves for the mutant receptors are so similar, irrespective of whether the mutation is in the α1 or the β subunit. In simple words, the receptor has on average 2.5 mutations in both cases.

Another thing to be considered is also that the interpretations of the results from 9′ mutations relies on the assumption that the effect of the mutation is the same irrespective of which subunit carries it. This holds roughly true for muscle nicotinic receptors (Labarca *et al.,* 1995) but not for $GABA_A$Rs, suggesting that channel asymmetry is much greater in the latter (Chang *et al.,* 1996; Chang and Weiss, 1998). It is possible that such an asymmetry also appears in oocyte-expressed glycine receptors: it might be that β subunits are produced, or assembled, in such a way that they contribute to receptor gating in an asymmetric, non-equivalent manner, compared with α1 subunits. If indeed the conformational changes that lead to channel gating are asymmetrical and subunit-specific, then a gating mutation such as the 9′LT would also

result in subunit-specific changes to occur in EC_{50} values (see also Shan *et al.*, 2003). This of course does not explain why such 'irregularities' in receptor symmetry appear only in oocyte-expressed receptors and not in HEK293 cells.

In addition, there is extensive contamination by homomeric channels in oocytes. In the cRNA combinations where the α1 subunit was mutated (i.e. $\alpha1^{LT}$+β and $\alpha1^{LS}$+β) it is reasonable to assume that the contamination by homomers is insignificant because I could detect little, or no, current from $\alpha1^{LS}$ and $\alpha1^{LT}$ homomers respectively. Therefore, the EC_{50} obtained from such combinations truly represents the glycine sensitivity of a pure population of only α1-mutant heteromers. On the other hand, in the combination where the β subunit is mutated (α1+β^{LT} injections), one can argue that the EC_{50} value I obtained (from one-component fits) is in reality the result of a two-component curve, one component corresponding to α1 homomers and the other to $\alpha1\beta^{LT}$ heteromers. In such a case the EC_{50} I calculated could be higher than the one truly corresponding to $\alpha1\beta^{LT}$ heteromers, due to the high EC_{50} of homomers (~100 μM). An effort to fit the α1+β^{LT} data with a two-component Hill equation (either with all parameters free or with the values of the first component fixed to those from the α1 data) resulted in poor fits, indicating that the homomeric component could not be detected. Similar results were obtained for two-component fits of α1+β data. Poor fits, of course, do not exclude the fact that the formation of homomers does indeed distort the values I obtained from the heteromeric combinations. The contamination however cannot explain why, when the α1 subunit is mutated (in $\alpha1^{LS}\beta$ and $\alpha1^{LT}\beta$ channels), I see little effect in the sensitivity to glycine. An additional confounding factor is that, in oocytes, agonist EC_{50} values for glycine receptors may be affected by the level of expression. This was reported for α1 homomers by Taleb and Betz (1994).

As a last point, the physical differences between oocytes and HEK293 cells should also be taken into account. Oocytes are large cells, clearly visible by eye, with a diameter of ~1 mm. Though their size makes them ideal for two-electrode voltage clamp it also has a downside, in that it increases the thickness of the unstirred layer that the agonist has to diffuse through to reach the receptors. This means that the actual time course for the concentration of agonist at the receptors is slower than in a HEK293 cell or in a patch. Furthermore, the oocyte membrane has extensive invaginations. Because of these, the agonist responses recorded in oocytes are

more distorted by desensitization which in turn influences the shape and position of the agonist concentration-response curve. The EC_{50} therefore can be lower in oocytes than in cell lines for the same receptor. The problem arises when a mutation is introduced, like a 9′ mutation which has more than one effect: besides reducing the EC_{50} (by facilitating gating), 9′ mutations are known also to decrease the rate of desensitization (Revah *et al*., 1991; Yakel *et al.*, 1993). Reducing the impact of desensitization is expected to *increase* the EC_{50} and in cells with substantial agonist desensitization, like oocytes, this effect could be large enough to counterbalance the effect on gating. In other words, the two effects would cancel each other. Such an effect was shown for α5-containing neuronal nAChRs, channels with fast desensitization, in which the effect of 9′ mutations on the EC_{50} appeared to be attenuated or abolished, reducing their usefulness in determining receptor stoichiometry (Groot-Kormelink *et al.*, 2001).

To summarise, the data from 9′ mutations in oocytes cannot provide any conclusions concerning the stoichiometry of α1β heteromeric GlyRs, unlike what occurs in HEK293 cells (Burzomato *et al.*, 2003). We do not know the precise reason for this discrepancy but the problem of homomeric receptor contamination is by itself a disadvantage in using oocytes to study glycine heteromeric channels.

4.1.2 The use of the conductance mutation

Because of the inconclusive results of the 9′ mutation experiments, I tested an alternative way to assess stoichiometry. This method was used successfully by Cooper and colleagues (1991) for chick α4β2 neuronal nicotinic receptors and by Béhé *et al*. (1995) for the determination of NR1 subunit copies in NMDA receptors expressed in *Xenopus* oocytes. The method requires the use of a mutation that alters the single-channel conductance of glycine receptors and the TM2 domain is a good candidate for such a mutation: this region was shown to be the main determinant of single-channel conductance of both homomeric and heteromeric glycine channels (Bormann *et al*., 1993; Carland *et al.*, 2009). The task of selecting a single point mutation within this region is difficult so I chose the creation of chimeric subunits instead, with the β subunit containing the entire TM2 sequence of the α1 subunit and *vice versa*. Using the β-chimera (β^{Ch}) had an advantage: it has already been shown that when β^{Ch} is co-expressed with

α1 in HEK293 cells, it produces channels with a homomer-like conductance (Bormann *et al.*, 1993).

My cell-attached data from oocytes confirm this, as co-injection of this subunit with α1 in oocytes resulted in heteromeric channels with main slope conductance of approximately 70 pS. This is close to the conductance of α1 homomers, but the presence of subconductance levels and the long duration of clusters distinguish these $\alpha1\beta^{Ch}$ channels from α1 homomers. Single-channel data in oocytes also confirmed that wild-type heteromeric channels (α1β) have a conductance which is approximately half that of the mutant ones (33 pS). This mutation therefore provides, in principle, a good separation in slope conductance between receptors that incorporate only mutant and only wild-type β subunits. For investigating the stoichiometry, this ~35 pS difference should allow the detection of at least one intermediate conductance (from mixed receptors that incorporate both mutant and wild-type β subunits), when both the wild-type and the mutant subunits are injected in the same cell.

Unfortunately, an intermediate conductance could not be detected in my cell-attached data from either oocytes, or HEK293 cells, transfected with the $\alpha1+\beta+\beta^{Ch}$ combination. In HEK293 cells the slope conductances of the expressed receptors clearly fall into two groups, one corresponding to wild-type heteromers and the other one to homomer-like channels. In oocytes, the low-conductance group of 7 patches has a higher average conductance than wild-type α1β channels but this difference is too small (7 pS) to be sure that these channels are truly different from α1β. The low expression of this combination did not allow the collection of more data. Results from the outside-out experiments in oocytes also point towards the lack of unique conductance levels for the $\alpha1+\beta+\beta^{Ch}$ combination. Possible explanations that can account for the lack of any intermediate states are discussed below.

First of all, it could be that a mixed receptor containing both mutant and wild-type subunits does not assemble or cannot reach the cell membrane. This may also explain the low success rate in obtaining cell-attached patches containing channels, using the $\alpha1+\beta+\beta^{Ch}$ combination. However, the successful expression of the $\alpha1+\beta^{Ch}$ combination suggests that the β^{Ch} subunit preferentially assembles only with α1 but not with wild-type β subunits. One could argue that the mutation somehow alters the structure of the subunit, forbidding it to assemble with wild-

type β subunits. However, this is a completely *ad hoc* explanation, as there are no indications that the TM2 domain is involved in assembly of GlyRs and also there is no reason to assume that only the β-β^{Ch} interactions are affected.

For understanding better the behaviour of the β^{Ch} subunit we have to take into consideration the mutation I have used. In the swapping of the TM2 domain between the two subunits I included residue 21′, in agreement with Bormann and colleagues (1993), who showed that inclusion of this residue is essential for the homomer-like behaviour of the β^{Ch} subunit. This residue, a serine (S) for α1 and a glutamate (E) for β, lies immediately after the TM2 and at the beginning of the TM2-TM3 loop. Evidence from cationic pLGICs suggest that the TM2-TM3 loop is one of three regions involved in the wave of conformations that lead from agonist binding to channel gating (see for examples Lee and Sine, 2005; Lummis *et al.,* 2005; see Figure 1.6) and it is reasonable to assume that TM2-TM3 loop residues of GlyRs (such as residue 21′) are also involved in gating. For the α1 subunit this is demonstrated by the use of alanine and cysteine substitution mutants (Lynch *et al.,* 1997, 2001) and also from the fact that mutations in this region are linked to hyperekplexia cases with impaired gating (Lewis *et al.,* 1998). This may apply only to the α1 subunit, as there is evidence to suggest that the β subunit TM2-TM3 loop is either not involved in gating or that the structure of the loop is quite different from that of α1 subunits, making it less effective in gating (Shan *et al.,* 2003). The latter might explain the appearance of subconductance levels for α1β^{Ch} heteromers: these channels have a pore of α1 homomers (due to the presence of five α1-like TM2) but the five TM2-TM3 loops of α1β heteromers, and this asymmetry is likely to give rise to abnormal conformations during gating. A mixed α1+β+β^{Ch} receptor, if it does assemble, may be even more asymmetrical, as some of the β subunits would have in the 21′ position either glutamate (wild-type) or serine (chimeras). Could that impair the gating of such mixed channels so much that it would explain the failure to record any intermediate conductance states?

Another possible explanation for the lack of any intermediate conductance levels in oocytes injected with the α1+β+β^{Ch} combination is that all the expressed α1 subunit is used to form homomers. This combination was injected in oocytes in a ratio of 1:40 of α1 over the total β subunit, meaning that the expressed α1 will be 40 times less than β and β^{Ch}, assuming an equal efficiency in the production of all subunits. However, two points argue against this hypothesis.

First, even if the expression of heteromers is low, the rate of production of all-mutant heteromers ($\alpha1\beta^{Ch}$) should be the same as that for the production of the mixed combination. My data, on the other hand, argue that although the expression of $\alpha1\beta^{Ch}$ is successful, that of the mixed combination is not. Second, in HEK293 cells transfected with the $\alpha1+\beta+\beta^{Ch}$ combination, the homomeric contamination is minimal (only three patches contained a homomer-like conductance) and yet I did not observe any intermediate conductances. From the above it is evident that the formation of homomers is not sufficient for explaining the lack of intermediate conductances but it can justify the low success rate in obtaining patches with channels in oocytes.

So far we have considered the possibility that the mixed $\alpha1+\beta+\beta^{Ch}$ receptors are not formed, or that they are formed but do not gate. Another possible explanation is that their conductance is too close to that of the "control" $\alpha1\beta$ and $\alpha1\beta^{Ch}$ channels and they cannot be recognised as mixed channels. This experimental approach assumes that the mixed receptor (containing both β and β^{Ch}) would have a single-channel conductance that is intermediate between the controls. Eliminating one-by-one the β subunits in the channel (by replacing them with β^{Ch}) would increase the single-channel conductance to an extent proportional to the number of replaced β subunits. On the other hand, if the conductance of a mixed channel coincides with the controls, it would follow that one, or two, copies of β^{Ch} subunit(s) together with β is not enough to change the conductance, but all the β have to be replaced for this to occur. However, even if the two, or three, β subunits in the heteromer are not equivalent (indicative of some asymmetry in the channel), it is very unlikely that their substitution would not cause some alteration in conductance. This is because the mutation of all β subunits causes a massive increase (~35 pS) in the conductance of the channels. One could argue that the slight increase (~7 pS) in the conductance of the group of the 7 $\alpha1+\beta+\beta^{Ch}$ patches in oocytes, compared with the wild-type $\alpha1\beta$, is an indication of the presence of the mutation in these channels. However, none of these patches had the features of β^{Ch}-containing channels (long clusters and subconductance levels). Also, this increase was not observed in HEK293 cells. All the above make this explanation somewhat unconvincing.

To summarize, I have used two alternative approaches for studying the stoichiometry of $\alpha1\beta$ glycine receptors in *Xenopus* oocytes, in an effort to shed some light on the discrepancy

between studies that argue in favour of a 3α:2β or a 2α:3β stoichiometry. Both these techniques are reliable and established ways for studying the stoichiometry of a ligand-gated channel. However, with the results I obtained it was not possible to reach to a concrete conclusion concerning stoichiometry. On the other hand, these data provide indications that the oocyte is not a reliable expression system for heteromeric glycine receptors, mainly due to the heavy contamination by homomers. The latter is supported by studies showing that the properties of a given channel are dependent on the expression system (for examples see Farroni and McCool, 2004; Lewis *et al.,* 1997), raising a new challenge of establishing which expression system is the closest to each native receptor subtype. Therefore, to conclude, oocytes (unlike HEK293 cells) should not be considered for the study of heteromeric glycine receptors.

4.2 Activation mechanism of α2 GlyRs

4.2.1 Maximum likelihood fitting

The aim of the last part of my work was to determine a kinetic mechanism for the α2 homomeric glycine receptor.

There are different ways to deduce the kinetic mechanism of a given channel. The approach followed in the early 80's involved fitting mixtures of exponential probability density functions to single-channel dwell-time distributions. Counting the number of components needed to fit open and shut-time distributions gives a (minimum) number for open and shut states in the mechanism, and some information on their connectivity can be extracted by analysing correlations. Having drawn a putative activation mechanism, the rate constants for the different steps have to be estimated from the time constants of the different components. The process is somewhat complicated and suffers from several limitations. First of all, as it is the *distributions* of dwell times that are analysed, the information contained in the *order* of events is lost. Secondly, only approximate correction for missed events is possible, given that an exact correction is mechanism-dependent and can only be done if a mechanism is postulated (for a review see Colquhoun, 2006b). More recently, theoretical advances led to a more precise method of analysis, which involves analysing the whole of the idealised sequence of events. This means that, in principle, all the information contained in a single-channel record is used, including relationships between adjacent open and shut times through correlations (Colquhoun and Hawkes, 1987; Colquhoun *et al.*, 2003). In this global fit, rate constants are optimised to maximize their likelihood (i.e. to increase the probability of the sequence of events in a single-channel record). In this way the postulated mechanism is introduced in advance, initial guesses are given to the rate constants and their values are changed until a maximum for the likelihood is reached. As a mechanism is postulated at the start of the process, it is possible to implement an exact correction to missed events (Hawkes *et al.*, 1992). These advantages finally allow the calculation of the exact values of the rate constants and more complicated mechanisms can be tested (Colquhoun *et al.*, 2003).

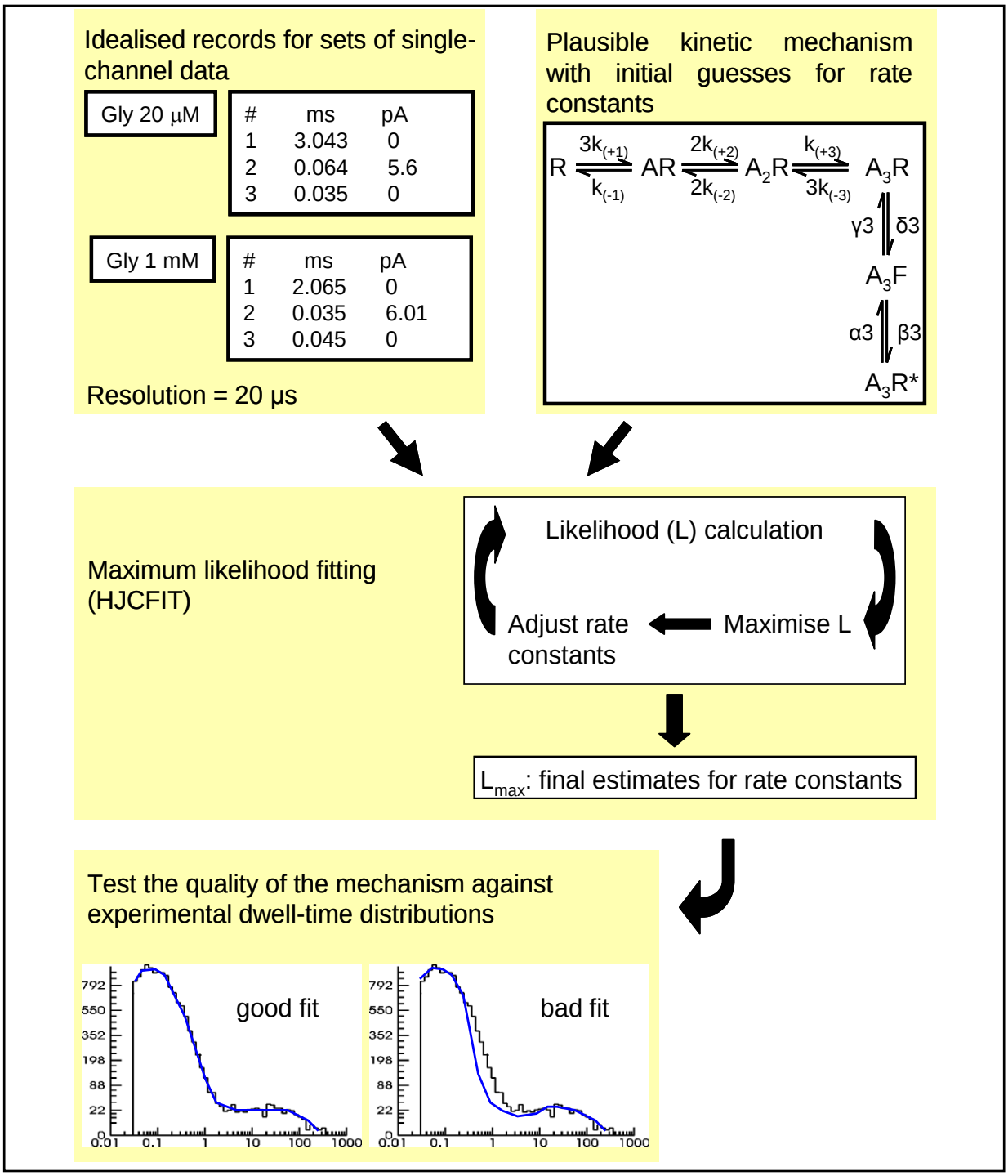

Figure 4.1 Direct maximum likelihood fitting to idealised single-channel data
The rate constants of a postulated mechanism are adjusted until the likelihood of the whole sequence of events in the experimental single-channel records is maximised. The validity of the final calculated rate constants is tested against the experimental observations, usually these being the shut times (as in the figure), the open times (or open periods) and the P_{open} curve. The scheme is considered satisfactory if the predicted distributions are in agreement with the experimental ones.

I used the method of maximum likelihood fitting of kinetic mechanisms to idealised single-channel data for the α2 glycine receptor, similarly to what was previously performed for other pLGICs (see Beato *et al.*, 2004; Burzomato *et al*., 2004; Hatton *et al*., 2003; Lape *et al*., 2008; Plested *et al*., 2007). The procedure is as described in Figure 4.1 (see also Colquhoun *et al*., 2003). Briefly: (i) single-channel data are idealised by time course fitting and recordings at different agonist concentrations are grouped into sets, (ii) a kinetic mechanism is postulated (usually taking into account exponential fits to experimental dwell-time distributions) and initial guesses are given to the rate constants, (iii) appropriate stretches from the idealised records, the appropriate resolution and the postulated mechanism are all input into a programme (HJCFIT) that can calculate the likelihood of the data given the reaction rates and maximise it and finally, (iv) the validity of the model and of the final rate constants are checked by looking at the experimental data (dwell-time histograms) and the predictions from the model superimposed. A good fitting scheme is not necessarily unique. If more than one mechanism fit the data equally well, it may not be possible to choose between the two on the basis of quality of fit. In such a case the plausibility of each mechanism has to be considered, taking also into account the physical interpretations deriving from each scheme (for example see Burzomato *et al.*, 2004).

4.2.2 Features of single-channels from α2 receptors

The first kinetic analysis on native GlyRs, performed on cultures of spinal motoneurons, showed that the relative frequency of long openings increases with agonist concentration (Twyman and MacDonald, 1991). Specifically, the analysis of open periods showed that, although the time constants of the different components were unaffected by the concentration of glycine, the area of each component was not (Twyman and MacDonald, 1991). The same phenomenon was subsequently shown to occur in recombinant homomeric and heteromeric receptors containing the α1 subunit (Beato *et al*., 2002, 2004; Burzomato *et al.*, 2004; Fucile *et al.*, 1999).

A striking feature of single-channels from α2 glycine receptors is that this concentration dependence is never observed. At all agonist concentrations channel activity occurs in long activations, which resemble what in an α1 channel we would consider a cluster of bursts. The lowest concentration at which openings are detected is 20 μM and already at this concentration

openings occur in prolonged group of openings. The number of these groups of openings in each patch was usually low and the groups were separated by very long shut times which usually lasted for minutes. In a few patches initially more than one channel could be simultaneously open but the onset of desensitization finally allowed the separation of individual groups of openings. In general, very few events could be detected in each patch, suggesting the presence of a low number of channels. Another thing to be noted is the low success rate in obtaining records with any openings at all. It is difficult to be sure whether one should classify these groups of openings as bursts, or as clusters (of bursts). The long gaps between groups of openings, the low number of these groups and the low number of transitions within the groups meant that the number of records that had enough transitions to be used for a kinetic analysis was small.

A characteristic of all patches was that the distributions of fitted amplitude histograms could be well described with a single Gaussian component. The finding of a single amplitude value (5.9 ± 0.2 pA) differs in principle from other single-channel studies on α2 GlyRs that showed multiple conductance states for this subtype, ranging from 20 to 110 pS (Bormann *et al.,* 1993; Mangin *et al*., 2003; Takahashi *et al.,* 1992). These studies agree on a main conductance state of 90-110 pS (which represents 60-90% of the total open time). This difference can be explained by the different patch clamp configuration that was used for recordings. The studies mentioned above were performed in the outside-out configuration whereas I was recording in the cell-attached configuration. The same difference in the number of conductance states between cell-attached and outside-out patches was also observed for α1 and α1β channels (see Chapter 3.2). The reasons underlying the discrepancy between cell-attached and excised GlyRs conductance is unclear although excision and differences in ionic concentrations in the different recording configurations are known to have a variety of effects on the channel kinetics (Fucile *et al.,* 2000; Pitt *et al*., 2008).

It is worth noting that the fitted amplitude showed considerable variation between the different cell-attached patches (from 4.5 to 9.1 pA). A similar situation was observed for other native or recombinant glycine receptors recorded in this configuration (see Beato and Sivilotti, 2007; Plested *et al.,* 2007) although it was shown that, despite the differences in amplitude, all patches had a similar slope conductance (Beato and Sivilotti, 2007). Differences in channel

amplitude might be due to differences in the internal chloride concentration, which affects the conductance of the channel (Bormann *et al.*, 1987), or in the resting membrane potential which determines the driving force for chloride through the channel (together with the pipette holding potential which was +100 mV for all patches).

4.2.3 Dwell-time distributions and the P_{open}

Open-period and shut-time distributions for α2 channels were fitted with mixtures of exponential probability density functions (the resolution was set at 20 μs for all patches). An open period is defined as the duration between two resolvable adjacent shut times, irrespective of transitions between different amplitude levels. In theory, at ideal resolution, the number of exponential components needed for fitting an open-period, or a shut-time, distribution would represent the exact number of open and shut states that the channel can access in a kinetic scheme. However, in real experiments one or more components might be missed, and the distributions provide us with a *minimum* number of shut and open states that might exist in the scheme. Other information can also be obtained from the analysis of distributions, such as the concentration dependence (if any) of the time constants, or of the areas of the different exponential components. Nevertheless, information extracted from such empirical fits is only descriptive and was not used for determining any of the rate constants of a kinetic model; the open-period and shut-time histograms are only used for testing the validity of a fit after a model has already been used for fitting the data (Figure 4.1).

The open-period distributions were best fitted with a maximum of three exponential components, in agreement with single-channel data from oocytes and embryonic spinal neurons (Takahashi *et al.,* 1992). Although the first and second components were not always present, the third (slowest) component was observed in all patches and concentrations and was always predominant. The differences between my study and that of Takahashi and colleagues (who reported slower time constants) is likely to be due to differences in configuration, and expression system and to the better resolution of my experiments, which implies that fewer shut times are missed and therefore results in shorter open periods. Analysis of the open periods showed very little difference between the time constants of different glycine concentrations. A closer inspection of these components indicates an increase in the mean open period (from 12.5 ± 1.8 to 34.4 ± 7.5 ms) as the concentration increases from 20 to 30 μM.

This concentration dependence is very mild compared with α1β and α1 channels (Beato *et al.*, 2004; Burzomato *et al.*, 2004; see also Twyman and MacDonald, 1991). The absence of concentration dependence is obvious at higher concentrations (from 30 μM to 10 mM) for which the time constants of the three components, their areas and also the mean open periods are almost identical. The values for the mean open period at concentrations higher than 30 μM (27-34 ms) are similar to that of ~50 ms reported by Mangin *et al.*, (2003). The small difference in this value, compared with my data, and also the fact that the authors only identify one component in their distribution can be explained by the different method of analysis and the configuration. Note also that their value of ~50 ms was obtained at saturating glycine (30 mM) and my data from 10 mM identify a small second component (0.012 ms) with an area of only 2% which could easily be missed during a 'manual' idealisation as the one performed by Mangin *et al.*, (2003).

Shut-time distributions were fitted with a maximum of four exponential components, similarly to data from α1 homomeric receptors (Beato *et al*., 2004). The time constants of the first three components were the most consistent across different patches and concentrations. The majority of events belonged to the shortest component (with areas ranging from 88 to 98%) which predominated irrespective of concentration, with time constants of 5-10 μs. Note that such time constants are faster than the resolution of 20 μs, suggesting that many such gaps would be missed, though in an idealised record of more than 10000 transitions, the number of the resolved fast shut times is still sufficient for kinetic analysis.

For an accurate description of the kinetic mechanism it is important to include in the analysis only stretches of data that are likely to occur from one channel molecule. For this purpose, a critical shut time should be chosen (t_{crit}) in a way that shut times longer than t_{crit} could be classified as between clusters (at high concentrations) or between bursts (at low concentrations). In the case of the α2 receptor, for which the discrimination between burst and cluster concentrations is not at all obvious, the selection of t_{crit} from the shut-time distributions 'by eye' was difficult. Having a look at the distributions, one could confidently say that the t_{crit} should be smaller than 10 ms for all concentrations, since events longer than 10 ms are very scarce. Additionally, the time constants of the forth component are the most variable across concentrations (ranging from 1.1 to 6.1 ms). Despite these two 'criteria' however, there is a

large margin of uncertainty in deciding what the t_{crit} should be for each concentration and, for this reason, different values of t_{crit} were used during the process of fitting a mechanism. Note however that during the idealisation of α2 records I selected stretches of data with consistent high P_{open} (i.e. clusters): at such high channel activity, the lack of double openings increases the confidence that the openings occur from only one channel, however ambiguous the choice of t_{crit} was.

The t_{crit} of 7-10 ms was chosen for calculating the P_{open} of the clusters at the different glycine concentrations. The definition of a cluster is any group of openings that is ended by a gap longer than t_{crit}; the P_{open} for each cluster was the ratio between the cluster's total open time and its length, both obtained from the idealised trace. Therefore, the precision of the estimation is effectively dependent on the duration of each cluster, with longer clusters resulting in more accurate estimates. As mentioned above, the value of 10 ms is the highest possible from the shut-time distributions, and it was chosen for calculating the P_{open} in order to avoid overestimations: a lower t_{crit} value, if incorrect, would result in breaking up a true cluster into several smaller ones, which would lead to overestimation of the P_{open} (due to a decrease in the cluster's length). Due to the lack of concentration dependence in the open periods, it was not surprising that the calculated P_{open} was similar for all concentrations and with values close to 1. These values provide a rough estimate of the maximum P_{open} (close to 1) in agreement with outside-out data from Mangin and colleagues, who reported a maximum P_{open} of 0.996 (Mangin *et al.*, 2003), and also suggest that the EC_{50} for α2 channels should be lower than 20 μM. The high P_{open} value across all concentrations suggests that the channel can give rise to only one type of activation: this would be consistent with the channel opening only at saturating agonist concentrations or, alternatively, that activations at lower states of ligation also have very high P_{open}.

4.2.4 The kinetic mechanism of α2 GlyRs using maximum likelihood fitting

For the purpose of characterising the kinetic behaviour of homomeric α2 GlyRs, steady-state single-channel data were fitted to 15 different kinetic schemes, most of which are described in Chapter 3.3. During this analysis it became evident that to get good fits the mechanisms had to: (i) include only one open state, (ii) contain flipped states to improve the quality of the fits to shut-time distributions and (iii) be fitted to the data choosing low values of t_{crit} (0.1-0.3 ms for

burst and 1-3 ms for cluster concentrations). Kinetic models with the above characteristics gave plausible estimates for the rate constant values if the fits were done with constraints for identical, non-interacting binding sites. Both model 7A and 7B (with three and two binding sites, respectively) gave excellent fits and converged to very similar values for the gating rate constants.

i. Introduction of flipped states improves the fits

From the initial fits with models 1-4 (with direct openings from each liganded state) it was obvious that more shut states were needed for a good fit. As in the case of α1-containing glycine receptors (Burzomato *et al.*, 2004), extra shut states can be added distal to the open states (see Jones and Westbrook, 1995) or, like in the 'flip' mechanism, between the resting and the open states. For α1β glycine receptors both approaches resulted in very good fits to the single-channel data (Burzomato *et al.*, 2004). Unlike the first approach, the shut flipped states in the 'flip' mechanism have an obvious plausible physical interpretation (i.e. the conformational changes after the agonist is bound and before the channel opens). For this reason, the 'flip' mechanism is more appealing (Burzomato *et al.*, 2004).

Fitting the α2 single-channel data with variations of the 'flip' mechanism profoundly improved the predictions from the shut-time distributions compared with simple sequential mechanisms. This observation was evident for all the models that included flipped states (schemes 5-7) irrespective of the number of binding sites, or open states in each model. Note that it was not the *number* of shut states in a model that improved the shut-time distribution fits but, rather, the *presence* of flipped state(s): for example, the best-fitting model (7B; with 2 binding sites, 1 flipped and 1 open state) has a total of 4 shut states, fewer than the sequential models of five, or four, binding sites (without flip, models 1 and 2), that could not converge, or could not fit well the data.

ii. Number of open states

Kinetic analysis of homomeric α1 and heteromeric α1β GlyRs suggests that openings can occur from any of the liganded shut states, after flipping. Both receptor types are fitted with the 'flip' mechanism, which contains three open states (Burzomato *et al.*, 2004). The 'flip' model can describe the behaviour of the channels over a wide range of agonist concentrations and the

openings from any liganded shut state can account for the observation of short bursts at low concentrations, or clusters of bursts at higher concentrations. This model is in line with initial studies on native and recombinant receptors that argue in favour of at least three distinguishable open states (Beato *et al*., 2002, 2004; Lewis *et al*., 2003, Twyman and MacDonald, 1991).

Homomeric α2 receptors were different from the α1-containing channels in that they were best fitted with a 'flip' model that contains only one open state (model 7). This was not surprising, as there were no apparent monoliganded openings in the single-channel records: it reflects the lack of any concentration dependence in the duration of channel openings, as all openings occur in groups of high P_{open} values at all glycine concentrations. The need for fewer open states was already obvious when I tried to fit the 'flip' model of Burzomato and colleagues (model 5) and obtained for monoliganded openings an efficacy of ~0. Similarly, fits with model 6 (6A and 6B), with two open states, had very low values of *E* for the partially liganded open state, with ill-defined gating rates across different sets. Model 6 predicts a mean lifetime of 16.6 μs for the partially liganded open state (calculated as 1/α2 for model 6A; α2 = 60374 ± 14272 s^{-1}, n = 6 sets). Even if these openings truly occurred, most of them would be missed with a resolution of 20 μs. For the above reasons I considered it more sensible to remove this gating step from the mechanism.

Even though model 7 (with one open state) predicts very accurately the single-channel and macroscopic data, there are some drawbacks to be considered. The experimental open-period distributions were best fitted with a mixture of at least two exponential components, suggesting that the channels can access at least two open states, one of which is not visited frequently (due to the very few events that were detected and correspond to the small component in the open-period distributions). Because of that a second open state should be added to model 6, for a more accurate description, but in a manner different to model 7. A recent study on the kinetics of nicotinic receptors describes a model of two sequential flipped states (instead of one shown in my study), with openings occurring from any of the two flipped states: the first flipped-to-open transition accounts for the observed brief openings and the second to more prolonged openings (Mukhtasimova *et al.,* 2009). It would be interesting to see whether the addition of a

second (or more) flipped-to-open transition to model 7 would improve the fits of the α2 data further.

iii. Binding sites

A homomeric pentamer, such as the α2 GlyR, has up to 5 binding sites, but we do not know how many of these are functional (i.e. can be occupied by an agonist) and whether the channel can open from states that are partially liganded. As seen with model 7, only one open state, linked to the fully-liganded shut state after flipping, is sufficient for fitting well the data. Fitting this type of model with a different number of binding sites (from one to five) resulted in very similar values for the rate constants and therefore identical predictions for the experimental distributions. Note that these predictions provide the best fits for the α2 data but, as their quality is equally high, the fits of the five models are not informative. The only difference in the rates between these five different models was a decrease in the binding affinity (increase in K_R) as the number of binding sites decreased, which is expected since fewer sites are available for the agonist to bind. This had a direct effect on the predicted P_{open} curve, with the EC_{50} and the slope of the curve decreasing as the number of the binding sites decrease.

For α2 GlyRs we do not really have a well-defined experimental P_{open} curve; all we know is that the maximum P_{open} is nearly 1 and the EC_{50} is below 20 μM, and this information *per se* is not at all useful. Because of that, I had to use macroscopic data for choosing between the models. The Hill slopes from concentration-response curves obtained from whole-cell recordings and outside-out concentration jumps range between 1.2 and 1.9. These values are very close to the Hill slope value predicted from fits with model 7B, which has two binding sites. That would make model 7B the best-fitting model from the ones tested.

Scheme 7B (and also 7A) was initially fitted with the constraints of no cooperativity, i.e. that the equilibrium dissociation constant (K_R) was the same for all binding steps. For both models these fits were satisfactory. When the constraints were removed and the fits were performed with all parameters free to test for co-operativity in binding, the predicted distributions and P_{open} curves were unchanged, and so were the values of the gating rate constants. When the three binding site model (7A) was fitted, affinity decreased (by ~1000-fold) for the second binding step and then increased in the third. These changes were however inconsistent across

the four sets fitted. Free fits with model 7B (two binding sites) predicted marked positive cooperativity in binding, with a ~13-fold increase in the affinity of the receptor for glycine from the first to the second agonist binding step. While the effect on the equilibrium constant was clear and consistent, in some sets this effect originated from a change in association rate constants and in others from a change in dissociation rate constant. Overall, the results from both models show that the fits are more reliable and consistent when the constraints are included in the models; this does not affect the quality of the predicted fits, even if there are fewer free parameters with the constraints.

iv. Fits to macroscopic currents

Agonist concentration jumps aim to reproduce the fast and brief exposure of the receptors to saturating concentrations of neurotransmitter during synaptic transmission (Clements *et al*., 1992). However, these experiments have to be in the outside-out configuration which changes the single-channel properties of GlyRs (Fucile *et al*., 2000; see also Chapter 3.2), so it is not surprising that macroscopic glycine currents obtained with concentration jumps usually have a deactivation time course slower than that of glycinergic IPSCs (Singer and Berger, 1999). Much of the discrepancy may be due to differences in the intracellular chloride concentration, as shown for α1β glycine receptors by Pitt *et al.* (2008), who found that the deactivation of macroscopic currents becomes faster, and resembles the fast decay predicted from cell-attached based kinetic models, when the pipette contains low chloride, mimicking more physiological chloride concentrations.

In view of the above, I needed to compare the predictions of the cell-attached kinetic models with macroscopic outside-out recordings obtained with low intracellular chloride. I found that deactivation after long concentration jumps (1 s) of saturating glycine became 3-fold faster when the pipette chloride is low. When shorter jumps (2 ms) to three different glycine concentrations were applied, two different deactivation components were identified. The faster component appears to be concentration dependent as it becomes faster and more difficult to detect when glycine concentration is reduced from 10 mM to 500 μM. The slow component is the main one (area > 95%) at all concentrations and does not show signs of concentration dependence. It is this component that defines the deactivation of α2 currents, ~10-fold slower than that of α1β channels. This difference may make α2 homomers unsuitable for fast synaptic

transmission, as pointed out by Mangin and colleagues (2003). The authors reported an even slower decay for α2 currents but this was probably because they used high intracellular chloride (Mangin *et al.*, 2003).

Simulations of the relaxation after a brief jump to saturating agonist, using models 7B (and 7A), predict a somewhat slower deactivation than that observed experimentally in low chloride. The presence of 5 or 6 states in these models implies that the decay should have four, or five, components, but the small areas of most of these components calculated from our estimates for the rate constants mean that only one of these components would be detectable, with a time constant of about 200 ms. This is faster than the main time constant from the experiments using symmetrical 130 mM chloride (383 ± 70 ms), but is broadly comparable with the main time constant of deactivation in low intracellular chloride (112 ± 26 ms).

The desensitization properties of α2 channels are similar to α1-containing receptors with more than one components usually being detected (Gentet and Clements, 2002; Legendre, 1998; Legendre *et al*., 2002; Pitt *et al*., 2008). Hence, two desensitized states were added to model 7A to account for the presence of a fast and a slow desensitization component detected in responses to long glycine applications. Both states are connected to the single open state in the model. Fast desensitization is only observed in patches with high current amplitude, in a manner similar to that described for α1 and α1β GlyRs (Legendre *et al*., 2002; Pitt *et al.*, 2008). The identification of a fast and a slow component for α2 receptors in my study is in contrast with concentration jump experiments performed by Mangin and colleagues that identify only one slow desensitization component in CHO cells (Mangin *et al*., 2003). Despite this, the authors proposed a model of two desensitized states, each linked to a liganded shut state (Mangin *et al.*, 2003). It is worth noting that preliminary fits with the model of Mangin *et al*., using my α2 single-channel data, showed that although the model can predict well the experimental distributions, it resulted in a very shallow P_{open} curve with a slope of ~1, much lower than what the macroscopic data have shown and what the authors show themselves (n_H of 1.8; Mangin *et al.*, 2003).

Legendre and colleagues (2002) have shown that the desensitization of α1 GlyRs was fast enough to occur during a brief (1 ms) application of saturating glycine, shaping the decay of

the macroscopic current. Specifically, the authors showed that in high-current patches, which have a prominent fast desensitization, the deactivation had an additional exponential component which was likely to correspond to desensitization. Is it possible that the second component I observed in the deactivation of α2 currents (after a 2 ms application of glycine) corresponds to desensitization? Two points are in favour of this hypothesis: (i) the time constant of this deactivation component (6.1 ± 1.4 ms, 10 mM glycine) is similar to the time constant of the fast desensitization component (2.5 ± 0.5 ms, 10 mM glycine, 200 ms) and (ii) in some patches the onset of the deactivation phase starts prior to the end of the 2 ms pulse of glycine (see for example the inset in Figure 3.31*B*). Additionally, the small deactivation component appears to be concentration dependent, which would argue in favour of being the result of desensitization. This last argument is not very strong however, due to the small number of patches and the small range of concentrations tested. All the above argue that it is likely that fast desensitization can shape the decay of α2 currents, as in the case of α1 GlyRs, but more experiments are needed to confirm this.

The model 7A-d, with the desensitized states linked to the open state, could fit very well the macroscopic currents from 200 ms jumps to three different glycine concentrations, both from high and from low-amplitude patches, though the quality of the fits is slightly better for the high amplitude currents. This is in line with the fact that the model is a good candidate for the kinetic mechanism of α2 channels. Preliminary fits using model 7B-d (with two instead of three binding sites and desensitized states) can also describe equally well the macroscopic currents (data not shown). This situation was expected since the two models have almost identical rate constants. As previously noted, the mean lifetime of any of the desensitized states, as predicted by the model 7A-d, is longer than the 3 ms limit set by the highest t_{crit} chosen, meaning that desensitization would have been excluded from the single-channel analysis performed with HJCFIT. This confirms that low values of t_{crit} were necessary for high quality analysis of α2 single-channels, not only for improving the fits but also for avoiding interference by desensitization.

The rate constant of entry into fast desensitization for high-amplitude patches, predicted by model 7A-d ($d_{fast(+)}$ = 337 s^{-1}), is faster than the closing rate constant (α = 312 s^{-1}) of fits in which the k_{on} was constrained. According to model 7A, when the channel is open (A_3R^*) it can

either enter a short-lived shut state (A_3F), from which the burst can terminate because of dissociation, or enter the longer-lived desensitized state (A_3D_{fast}). The fact that the rate of entry into desensitization is comparable with the closing rate constant suggests that bursts (transitions between open and short-lived shut states) can be terminated also by desensitization. That is supported by the fact that the low value of α roughly corresponds to a τ_{decay} value of ~3 ms though the experimental value is much higher. The latter indicates that deactivation could be prolonged due to dwells into desensitization prior to finally entering a resting state. The above speculations might explain why we cannot observe any openings at concentrations lower than 20 μM (i.e. 'burst' concentrations) and also why the 'patch' P_{open} (i.e. the total open time/total duration of the recording) is very low for these channels. Other cases in which the entry into desensitization appears to contribute to the time course of deactivation have also been reported for gain-of-function muscle nAChRs (Elenes *et al.*, 2006) and, as mentioned above, for α1 GlyRs (Legendre *et al.*, 2002).

To summarise my findings on recombinant α2 GlyRs, I propose a kinetic scheme that contains a single, fully-liganded open state and two, or three, sequential agonist binding steps together with a pre-opening conformational change (flip). Additional data from macroscopic concentration-response curves favour two rather than three binding steps. Although the model can describe adequately the single-channel and macroscopic data I have obtained, there are nevertheless limitations which suggest future experimental directions. For example, an improvement in recording resolution might help to reveal more exponential components in the shut-time and open-period distributions that would allow a more accurate determination of a t_{crit} value for bursts. In addition, a more thorough investigation of the properties of desensitization is needed, in order to clarify its contribution, if any, in shaping deactivation. Revisions of the model will have to be done, to account for the more complicated nature of these channels. Yet, despite the above considerations, this model is a good starting candidate for the kinetics of these channels.

Bibliography

- Akabas, M. H., Kaufmann, C., Archdeacon, P., & Karlin, A. (1994). Identification of acetylcholine receptor channel-lining residues in the entire M2 segment of the α subunit. *Neuron* **13**, 919-927.
- Akagi, H. & Miledi, R. (1988). Heterogeneity of glycine receptors and their messenger RNAs in rat brain and spinal cord. *Science* **242**, 270-273.
- Akagi, H., Hirai, K., & Hishinuma, F. (1991). Cloning of a glycine receptor subtype expressed in rat brain and spinal cord during a specific period of neuronal development. *FEBS Lett.* **281**, 160-166.
- Akopian, A. N., Sivilotti, L., & Wood, J. N. (1996). A tetrodotoxin-resistant voltage-gated sodium channel expressed by sensory neurons. *Nature* **379**, 257-262.
- Albarran, F. A., Roa, J. P., Navarrete, R., Castillo, R., Nualart, F., & Aguayo, L. G. (2001). Effect of protein kinase C activation on the glycine evoked Cl^- current in spinal cord neurons. *Brain Res.* **902**, 1-10.
- Ali, D. W., Drapeau, P., & Legendre, P. (2000). Development of spontaneous glycinergic currents in the Mauthner neuron of the zebrafish embryo. *J.Neurophysiol.* **84**, 1726-1736.
- Amin, J. & Weiss, D. S. (1993). $GABA_A$ receptor needs two homologous domains of the beta-subunit for activation by GABA but not by pentobarbital. *Nature* **366**, 565-569.
- Amiri, S., Tai, K., Beckstein, O., Biggin, P. C., & Sansom, M. S. (2005). The α7 nicotinic acetylcholine receptor: molecular modelling, electrostatics, and energetics. *Mol.Membr.Biol.* **22**, 151-162.
- Anand, R., Conroy, W. G., Schoepfer, R., Whiting, P., & Lindstrom, J. (1991). Neuronal nicotinic acetylcholine receptors expressed in *Xenopus* oocytes have a pentameric quaternary structure. *J.Biol.Chem.* **266**, 11192-11198.
- Aprison, M. H. & Werman, R. (1965). The distribution of glycine in cat spinal cord and roots. *Life Sci.* **4**, 2075-2083.
- Arias, H. R. (2000). Localization of agonist and competitive antagonist binding sites on nicotinic acetylcholine receptors. *Neurochem.Int.* **36**, 595-645.
- Baccei, M. L. & Fitzgerald, M. (2004). Development of GABAergic and glycinergic transmission in the neonatal rat dorsal horn. *J.Neurosci.* **24**, 4749-4757.
- Baev, K. V., Rusin, K. I., & Safronov, B. V. (1992). Primary receptor for inhibitory transmitters in lamprey spinal cord neurons. *Neuroscience* **46**, 931-941.
- Baker, E., Sutherland, G. R., & Schofield, P. R. (1994). Localization of the glycine receptor α1 subunit gene (*GLRA1*) to chromosome 5q32 by FISH. *Genomics* **22**, 491-493.
- Bakker, M. J., van Dijk, J. G., van den Maagdenberg, A. M., & Tijssen, M. A. (2006). Startle syndromes. *Lancet Neurol.* **5**, 513-524.
- Bali, M. & Akabas, M. H. (2007). The location of a closed channel gate in the $GABA_A$ receptor channel. *J.Gen.Physiol* **129**, 145-159.
- Balse, E., Tessier, L. H., Forster, V., Roux, M. J., Sahel, J. A., & Picaud, S. (2006). Glycine receptors in a population of adult mammalian cones. *J.Physiol* **571**, 391-401.
- Bardoni, R., Ghirri, A., Salio, C., Prandini, M., & Merighi, A. (2007). BDNF-mediated modulation of GABA and glycine release in dorsal horn lamina II from postnatal rats. *Dev.Neurobiol.* **67**, 960-975.
- Beato, M., Groot-Kormelink, P. J., Colquhoun, D., & Sivilotti, L. G. (2002). Openings of the rat recombinant α1 homomeric glycine receptor as a function of the number of agonist molecules bound. *J.Gen.Physiol* **119**, 443-466.
- Beato, M., Groot-Kormelink, P. J., Colquhoun, D., & Sivilotti, L. G. (2004). The activation mechanism of α1 homomeric glycine receptors. *J.Neurosci.* **24**, 895-906.
- Beato, M. & Sivilotti, L. G. (2007). Single-channel properties of glycine receptors of juvenile rat spinal motoneurones in vitro. *J.Physiol* **580**, 497-506.

- Beato, M., Burzomato, V., & Sivilotti, L. G. (2007). The kinetics of inhibition of rat recombinant heteromeric α1β glycine receptors by the low-affinity antagonist SR-95531. *J.Physiol* **580**, 171-179.
- Beato, M. (2008). The time course of transmitter at glycinergic synapses onto motoneurons. *J.Neurosci.* **28**, 7412-7425.
- Becker, C. M., Hoch, W., & Betz, H. (1988). Glycine receptor heterogeneity in rat spinal cord during postnatal development. *EMBO J.* **7**, 3717-3726.
- Beg, A. A. & Jorgensen, E. M. (2003). EXP-1 is an excitatory GABA-gated cation channel. *Nat.Neurosci.* **6**, 1145-1152.
- Béhé, P., Stern, P., Wyllie, D. J., Nassar, M., Schoepfer, R., & Colquhoun, D. (1995). Determination of NMDA NR1 subunit copy number in recombinant NMDA receptors. *Proc.Biol.Sci.* **262**, 205-213.
- Belachew, S., Rogister, B., Rigo, J. M., Malgrange, B., Mazy-Servais, C., Xhauflaire, G., Coucke, P., & Moonen, G. (1998). Cultured oligodendrocyte progenitors derived from cerebral cortex express a glycine receptor which is pharmacologically distinct from the neuronal isoform. *Eur.J.Neurosci.* **10**, 3556-3564.
- Betz, H. & Laube, B. (2006). Glycine receptors: recent insights into their structural organization and functional diversity. *J.Neurochem.* **97**, 1600-1610.
- Betz, H., Gomeza, J., Armsen, W., Scholze, P., & Eulenburg, V. (2006). Glycine transporters: essential regulators of synaptic transmission. *Biochem.Soc.Trans.* **34**, 55-58.
- Bloomenthal, A. B., Goldwater, E., Pritchett, D. B., & Harrison, N. L. (1994). Biphasic modulation of the strychnine-sensitive glycine receptor by Zn^{2+}. *Mol.Pharmacol.* **46**, 1156-1159.
- Bocquet, N., Nury, H., Baaden, M., Le Poupon, C., Changeux, J. P., Delarue, M., & Corringer, P. J. (2009). X-ray structure of a pentameric ligand-gated ion channel in an apparently open conformation. *Nature* **457**, 111-114.
- Boorman, J. P., Groot-Kormelink, P. J., & Sivilotti, L. G. (2000). Stoichiometry of human recombinant neuronal nicotinic receptors containing the β3 subunit expressed in *Xenopus* oocytes. *J.Physiol* **529 Pt 3**, 565-577.
- Bormann, J., Hamill, O. P., & Sakmann, B. (1987). Mechanism of anion permeation through channels gated by glycine and gamma-aminobutyric acid in mouse cultured spinal neurones. *J.Physiol* **385**, 243-286.
- Bormann, J., Rundström, N., Betz, H., & Langosch, D. (1993). Residues within transmembrane segment M2 determine chloride conductance of glycine receptor homo- and hetero-oligomers. *EMBO J.* **12**, 3729-3737.
- Borst, J. G. & Sakmann, B. (1996). Calcium influx and transmitter release in a fast CNS synapse. *Nature* **383**, 431-434.
- Bowery, N. G. & Smart, T. G. (2006). GABA and glycine as neurotransmitters: a brief history. *Br.J.Pharmacol.* **147 Suppl 1**, S109-S119.
- Breitinger, H. G. & Becker, C. M. (2002). The inhibitory glycine receptor-simple views of a complicated channel. *Chembiochem.* **3**, 1042-1052.
- Brejc, K., van Dijk, W. J., Klaassen, R. V., Schuurmans, M., van Der, O. J., Smit, A. B., & Sixma, T. K. (2001). Crystal structure of an ACh-binding protein reveals the ligand-binding domain of nicotinic receptors. *Nature* **411**, 269-276.
- Buckwalter, M. S., Cook, S. A., Davisson, M. T., White, W. F., & Camper, S. A. (1994). A frameshift mutation in the mouse α1 glycine receptor gene (*Glra1*) results in progressive neurological symptoms and juvenile death. *Hum.Mol.Genet.* **3**, 2025-2030.
- Burzomato, V., Groot-Kormelink, P. J., Sivilotti, L. G., & Beato, M. (2003). Stoichiometry of recombinant heteromeric glycine receptors revealed by a pore-lining region point mutation. *Receptors.Channels* **9**, 353-361.

- Burzomato, V., Beato, M., Groot-Kormelink, P. J., Colquhoun, D., & Sivilotti, L. G. (2004). Single-channel behavior of heteromeric α1β glycine receptors: an attempt to detect a conformational change before the channel opens. *J.Neurosci.* **24**, 10924-10940.
- Caraiscos, V. B., Mihic, S. J., MacDonald, J. F., & Orser, B. A. (2002). Tyrosine kinases enhance the function of glycine receptors in rat hippocampal neurons and human α1β glycine receptors. *J.Physiol* **539**, 495-502.
- Carland, J. E., Cooper, M. A., Sugiharto, S., Jeong, H. J., Lewis, T. M., Barry, P. H., Peters, J. A., Lambert, J. J., & Moorhouse, A. J. (2009). Characterization of the effects of charged residues in the intracellular loop on ion permeation in α1 glycine receptor channels. *J.Biol.Chem.* **284**, 2023-2030.
- Cascio, M. (2004). Structure and function of the glycine receptor and related nicotinicoid receptors. *J.Biol.Chem.* **279**, 19383-19386.
- Cascio, M. (2006). Modulating inhibitory ligand-gated ion channels. *AAPS.J.* **8**, E353-E361.
- Chakrapani, S., Bailey, T. D., & Auerbach, A. (2004). Gating dynamics of the acetylcholine receptor extracellular domain. *J.Gen.Physiol* **123**, 341-356.
- Chang, Y., Wang, R., Barot, S., & Weiss, D. S. (1996). Stoichiometry of a recombinant $GABA_A$ receptor. *J.Neurosci.* **16**, 5415-5424.
- Chang, Y. & Weiss, D. S. (1998). Substitutions of the highly conserved M2 leucine create spontaneously opening ρ1 γ-Aminobutyric acid receptors. *Mol.Pharmacol.* **53**, 511-523.
- Chang, Y. & Weiss, D. S. (1999). Allosteric activation mechanism of the α1β2γ2 γ-aminobutyric acid type A receptor revealed by mutation of the conserved M2 leucine. *Biophys.J.* **77**, 2542-2551.
- Chaudhry, F. A., Reimer, R. J., Bellocchio, E. E., Danbolt, N. C., Osen, K. K., Edwards, R. H., & Storm-Mathisen, J. (1998). The vesicular GABA transporter, VGAT, localizes to synaptic vesicles in sets of glycinergic as well as GABAergic neurons. *J.Neurosci.* **18**, 9733-9750.
- Chen, Z., Dillon, G. H., & Huang, R. (2004). Molecular determinants of proton modulation of glycine receptors. *J.Biol.Chem.* **279**, 876-883.
- Chen, Z., Dillon, G. H., & Huang, R. (2006). Identification of residues critical for Cu^{2+}-mediated inhibition of glycine α1 receptors. *Neuropharmacology* **51**, 701-708.
- Chen, Z. & Huang, R. (2007). Identification of residues mediating inhibition of glycine receptors by protons. *Neuropharmacology* **52**, 1606-1615.
- Chéry, N. & de Koninck, Y. (1999). Junctional versus extrajunctional glycine and $GABA_A$ receptor-mediated IPSCs in identified lamina I neurons of the adult rat spinal cord. *J.Neurosci.* **19**, 7342-7355.
- Clements, J. D., Lester, R. A., Tong, G., Jahr, C. E., & Westbrook, G. L. (1992). The time course of glutamate in the synaptic cleft. *Science* **258**, 1498-1501.
- Clements, J. D. (1996). Transmitter timecourse in the synaptic cleft: its role in central synaptic function. *Trends Neurosci.* **19**, 163-171.
- Clements, J. D. (2002). Glycine receptor maturation: no experience required. *J.Physiol* **542**, 665.
- Cohen, B. N., Labarca, C., Czyzyk, L., Davidson, N., & Lester, H. A. (1992a). $Tris^+/Na^+$ permeability ratios of nicotinic acetylcholine receptors are reduced by mutations near the intracellular end of the M2 region. *J.Gen.Physiol* **99**, 545-572.
- Cohen, B. N., Labarca, C., Davidson, N., & Lester, H. A. (1992b). Mutations in M2 alter the selectivity of the mouse nicotinic acetylcholine receptor for organic and alkali metal cations. *J.Gen.Physiol* **100**, 373-400.
- Colquhoun, D. & Hawkes, A. G. (1987). A note on correlations in single ion channel records. *Proc.R.Soc.Lond B Biol.Sci.* **230**, 15-52.
- Colquhoun, D. & Ogden, D. C. (1988). Activation of ion channels in the frog end-plate by high concentrations of acetylcholine. *J.Physiol* **395**, 131-159.
- Colquhoun, D. (1998). Binding, gating, affinity and efficacy: the interpretation of structure-activity relationships for agonists and of the effects of mutating receptors. *Br.J.Pharmacol.* **125**, 924-947.

- Colquhoun, D., Hatton, C. J., & Hawkes, A. G. (2003). The quality of maximum likelihood estimates of ion channel rate constants. *J.Physiol* **547**, 699-728.
- Colquhoun, D. (2006a). The quantitative analysis of drug-receptor interactions: a short history. *Trends Pharmacol.Sci.* **27**, 149-157.
- Colquhoun, D. (2006b). Agonist-activated ion channels. *Br.J.Pharmacol.* **147 Suppl 1**, S17-S26.
- Connolly, C. N. (2008). Trafficking of 5-HT_3 and $GABA_A$ receptors. *Mol.Membr.Biol.* **25**, 293-301.
- Cooper, E., Couturier, S., & Ballivet, M. (1991). Pentameric structure and subunit stoichiometry of a neuronal nicotinic acetylcholine receptor. *Nature* **350**, 235-238.
- Corringer, P. J., Le Novère, N., & Changeux, J. P. (2000). Nicotinic receptors at the amino-acid level. *Annu.Rev.Pharmacol.Toxicol.* **40**, 431-458.
- Corry, B. (2006). An energy-efficient gating mechanism in the acetylcholine receptor channel suggested by molecular and Brownian dynamics. *Biophys.J.* **90**, 799-810.
- Crawford, D. K., Perkins, D. I., Trudell, J. R., Bertaccini, E. J., Davies, D. L., & Alkana, R. L. (2008). Roles for loop 2 residues of α1 glycine receptors in agonist activation. *J.Biol.Chem.* **283**, 27698-27706.
- Crook, J., Hendrickson, A., & Robinson, F. R. (2006). Co-localization of glycine and GABA immunoreactivity in interneurons in *Macaca* monkey cerebellar cortex. *Neuroscience* **141**, 1951-1959.
- Cummings, C. J., Dahle, E. J., & Zoghbi, H. Y. (1998). Analysis of the genomic structure of the human glycine receptor α2 subunit gene and exclusion of this gene as a candidate for Rett syndrome. *Am.J.Med.Genet.* **78**, 176-178.
- Curtis, D. R., Hosli, L., & Johnston, G. A. (1967). Inhibition of spinal neurons by glycine. *Nature* **215**, 1502-1503.
- Curtis, D. R., Hosli, L., Johnston, G. A., & Johnston, I. H. (1968). The hyperpolarization of spinal motoneurones by glycine and related amino acids. *Exp.Brain Res.* **5**, 235-258.
- Cymes, G. D., Grosman, C., & Auerbach, A. (2002). Structure of the transition state of gating in the acetylcholine receptor channel pore: a Φ-value analysis. *Biochemistry* **41**, 5548-5555.
- Czajkowski, C. (2005). Neurobiology: triggers for channel opening. *Nature* **438**, 167-168.
- Dahan, M., Levi, S., Luccardini, C., Rostaing, P., Riveau, B., & Triller, A. (2003). Diffusion dynamics of glycine receptors revealed by single-quantum dot tracking. *Science* **302**, 442-445.
- David-Watine, B., Goblet, C., de Saint Jan, D., Fucile, S., Devignot, V., Bregestovski, P., & Korn, H. (1999). Cloning, expression and electrophysiological characterization of glycine receptor α subunit from zebrafish. *Neuroscience* **90**, 303-317.
- Davidoff, R. A., Shank, R. P., Graham, L. T., Jr., Aprison, M. H., & Werman, R. (1967). Association of glycine with spinal interneurones. *Nature* **214**, 680-681.
- Davies, P. A., Pistis, M., Hanna, M. C., Peters, J. A., Lambert, J. J., Hales, T. G., & Kirkness, E. F. (1999). The 5-HT_{3B} subunit is a major determinant of serotonin-receptor function. *Nature* **397**, 359-363.
- Davies, P. A., Wang, W., Hales, T. G., & Kirkness, E. F. (2003). A novel class of ligand-gated ion channel is activated by Zn^{2+}. *J.Biol.Chem.* **278**, 712-717.
- de Saint Jan, D., David-Watine, B., Korn, H., & Bregestovski, P. (2001). Activation of human α1 and α2 homomeric glycine receptors by taurine and GABA. *J.Physiol* **535**, 741-755.
- Devignot, V., Prado, d. C., Bregestovski, P., & Goblet, C. (2003). A novel glycine receptor αZ1 subunit variant in the zebrafish brain. *Neuroscience* **122**, 449-457.
- Diana, M. A. & Bregestovski, P. (2005). Calcium and endocannabinoids in the modulation of inhibitory synaptic transmission. *Cell Calcium* **37**, 497-505.
- Dugué, G. P., Dumoulin, A., Triller, A., & Dieudonné, S. (2005). Target-dependent use of co-released inhibitory transmitters at central synapses. *J.Neurosci.* **25**, 6490-6498.
- Dumba, J. S., Irish, P. S., Anderson, N. L., & Westrum, L. E. (1998). Electron microscopic analysis of gamma-aminobutyric acid and glycine colocalization in rat trigeminal subnucleus caudalis. *Brain Res.* **806**, 16-25.

- Dumoulin, A., Rostaing, P., Bedet, C., Lévi, S., Isambert, M. F., Henry, J. P., Triller, A., & Gasnier, B. (1999). Presence of the vesicular inhibitory amino acid transporter in GABAergic and glycinergic synaptic terminal boutons. *J.Cell Sci.* **112 (Pt 6)**, 811-823.
- Dupre, M. L., Broyles, J. M., & Mihic, S. J. (2007). Effects of a mutation in the TM2-TM3 linker region of the glycine receptor α1 subunit on gating and allosteric modulation. *Brain Res.* **1152**, 1-9.
- Elenes, S., Ni, Y., Cymes, G. D., & Grosman, C. (2006). Desensitization contributes to the synaptic response of gain-of-function mutants of the muscle nicotinic receptor. *J.Gen.Physiol* **128**, 615-627.
- Eulenburg, V., Armsen, W., Betz, H., & Gomeza, J. (2005). Glycine transporters: essential regulators of neurotransmission. *Trends Biochem.Sci.* **30**, 325-333.
- Eulenburg, V., Becker, K., Gomeza, J., Schmitt, B., Becker, C. M., & Betz, H. (2006). Mutations within the human *GLYT2* (SLC6A5) gene associated with hyperekplexia. *Biochem.Biophys.Res.Commun.* **348**, 400-405.
- Farroni, J. S. & McCool, B. A. (2004). Extrinsic factors regulate partial agonist efficacy of strychnine-sensitive glycine receptors. *BMC.Pharmacol.* **4**, 16.
- Feng, G., Tintrup, H., Kirsch, J., Nichol, M. C., Kuhse, J., Betz, H., & Sanes, J. R. (1998). Dual requirement for gephyrin in glycine receptor clustering and molybdoenzyme activity. *Science* **282**, 1321-1324.
- Filatov, G. N. & White, M. M. (1995). The role of conserved leucines in the M2 domain of the acetylcholine receptor in channel gating. *Mol.Pharmacol.* **48**, 379-384.
- Filippova, N., Wotring, V. E., & Weiss, D. S. (2004). Evidence that the TM1-TM2 loop contributes to the ρ1 GABA receptor pore. *J.Biol.Chem.* **279**, 20906-20914.
- Flint, A. C., Liu, X., & Kriegstein, A. R. (1998). Nonsynaptic glycine receptor activation during early neocortical development. *Neuron* **20**, 43-53.
- Fucile, S., de Saint Jan, D., David-Watine, B., Korn, H., & Bregestovski, P. (1999). Comparison of glycine and GABA actions on the zebrafish homomeric glycine receptor. *J.Physiol* **517 (Pt 2)**, 369-383.
- Fucile, S., de Saint Jan, D., de Carvalho, L. P., & Bregestovski, P. (2000). Fast potentiation of glycine receptor channels of intracellular calcium in neurons and transfected cells. *Neuron* **28**, 571-583.
- Fujita, M., Sato, K., Sato, M., Inoue, T., Kozuka, T., & Tohyama, M. (1991). Regional distribution of the cells expressing glycine receptor β subunit mRNA in the rat brain. *Brain Res.* **560**, 23-37.
- Gadea, A. & Lopez-Cólomé, A. M. (2001). Glial transporters for glutamate, glycine, and GABA III. Glycine transporters. *J.Neurosci.Res.* **64**, 218-222.
- Galzi, J. L., Devillers-Thiéry, A., Hussy, N., Bertrand, S., Changeux, J. P., & Bertrand, D. (1992). Mutations in the channel domain of a neuronal nicotinic receptor convert ion selectivity from cationic to anionic. *Nature* **359**, 500-505.
- Gao, B. X. & Ziskind-Conhaim, L. (1995). Development of glycine- and GABA-gated currents in rat spinal motoneurons. *J.Neurophysiol.* **74**, 113-121.
- Gao, B. X. & Ziskind-Conhaim, L. (1998). Development of ionic currents underlying changes in action potential waveforms in rat spinal motoneurons. *J.Neurophysiol.* **80**, 3047-3061.
- Gao, B. X., Cheng, G., & Ziskind-Conhaim, L. (1998). Development of spontaneous synaptic transmission in the rat spinal cord. *J.Neurophysiol.* **79**, 2277-2287.
- Gao, B. X., Stricker, C., & Ziskind-Conhaim, L. (2001). Transition from GABAergic to glycinergic synaptic transmission in newly formed spinal networks. *J.Neurophysiol.* **86**, 492-502.
- García-Alcocer, G., Mejía, C., Berumen, L. C., Miledi, R., & Martinez-Torres, A. (2008). Developmental expression of glycine receptor subunits in rat cerebellum. *Int.J.Dev.Neurosci.* **26**, 319-322.
- Gasnier, B. (2000). The loading of neurotransmitters into synaptic vesicles. *Biochimie* **82**, 327-337.

- Gee, V. J., Kracun, S., Cooper, S. T., Gibb, A. J., & Millar, N. S. (2007). Identification of domains influencing assembly and ion channel properties in α7 nicotinic receptor and 5-HT_3 receptor subunit chimaeras. *Br.J.Pharmacol.* **152**, 501-512.
- Gentet, L. J. & Clements, J. D. (2002). Binding site stoichiometry and the effects of phosphorylation on human alpha1 homomeric glycine receptors. *J.Physiol* **544**, 97-106.
- Gisselmann, G., Pusch, H., Hovemann, B. T., & Hatt, H. (2002). Two cDNAs coding for histamine-gated ion channels in *D. melanogaster*. *Nat.Neurosci.* **5**, 11-12.
- González-Forero, D. & Alvarez, F. J. (2005). Differential postnatal maturation of $GABA_A$, glycine receptor, and mixed synaptic currents in Renshaw cells and ventral spinal interneurons. *J.Neurosci.* **25**, 2010-2023.
- Gotti, C. & Clementi, F. (2004). Neuronal nicotinic receptors: from structure to pathology. *Prog.Neurobiol.* **74**, 363-396.
- Graham, B. A., Schofield, P. R., Sah, P., Margrie, T. W., & Callister, R. J. (2006). Distinct physiological mechanisms underlie altered glycinergic synaptic transmission in the murine mutants spastic, spasmodic, and oscillator. *J.Neurosci.* **26**, 4880-4890.
- Graham, D., Pfeiffer, F., Simler, R., & Betz, H. (1985). Purification and characterization of the glycine receptor of pig spinal cord. *Biochemistry* **24**, 990-994.
- Grenningloh, G., Rienitz, A., Schmitt, B., Methfessel, C., Zensen, M., Beyreuther, K., Gundelfinger, E. D., & Betz, H. (1987). The strychnine-binding subunit of the glycine receptor shows homology with nicotinic acetylcholine receptors. *Nature* **328**, 215-220.
- Grenningloh, G., Pribilla, I., Prior, P., Multhaup, G., Beyreuther, K., Taleb, O., & Betz, H. (1990a). Cloning and expression of the 58 kD beta subunit of the inhibitory glycine receptor. *Neuron* **4**, 963-970.
- Grenningloh, G., Schmieden, V., Schofield, P. R., Seeburg, P. H., Siddique, T., Mohandas, T. K., Becker, C. M., & Betz, H. (1990b). Alpha subunit variants of the human glycine receptor: primary structures, functional expression and chromosomal localization of the corresponding genes. *EMBO J.* **9**, 771-776.
- Griffon, N., Büttner, C., Nicke, A., Kuhse, J., Schmalzing, G., & Betz, H. (1999). Molecular determinants of glycine receptor subunit assembly. *EMBO J.* **18**, 4711-4721.
- Groc, L. & Choquet, D. (2008). Measurement and characteristics of neurotransmitter receptor surface trafficking. *Mol.Membr.Biol.* **25**, 344-352.
- Groot-Kormelink, P. J. & Luyten, W. H. (1997). Cloning and sequence of full-length cDNAs encoding the human neuronal nicotinic acetylcholine receptor (nAChR) subunits β3 and β4 and expression of seven nAChR subunits in the human neuroblastoma cell line SH-SY5Y and/or IMR-32. *FEBS Lett.* **400**, 309-314.
- Groot-Kormelink, P. J., Luyten, W. H., Colquhoun, D., & Sivilotti, L. G. (1998). A reporter mutation approach shows incorporation of the "orphan" subunit β3 into a functional nicotinic receptor. *J.Biol.Chem.* **273**, 15317-15320.
- Groot-Kormelink, P. J., Boorman, J. P., & Sivilotti, L. G. (2001). Formation of functional α3β4α5 human neuronal nicotinic receptors in *Xenopus* oocytes: a reporter mutation approach. *Br.J.Pharmacol.* **134**, 789-796.
- Groot-Kormelink, P. J., Beato, M., Finotti, C., Harvey, R. J., & Sivilotti, L. G. (2002). Achieving optimal expression for single channel recording: a plasmid ratio approach to the expression of α1 glycine receptors in HEK293 cells. *J.Neurosci.Methods* **113**, 207-214.
- Groot-Kormelink, P. J., Broadbent, S. D., Boorman, J. P., & Sivilotti, L. G. (2004). Incomplete incorporation of tandem subunits in recombinant neuronal nicotinic receptors. *J.Gen.Physiol* **123**, 697-708.
- Grosman, C., Zhou, M., & Auerbach, A. (2000). Mapping the conformational wave of acetylcholine receptor channel gating. *Nature* **403**, 773-776.

- Grudzinska, J., Schemm, R., Haeger, S., Nicke, A., Schmalzing, G., Betz, H., & Laube, B. (2005). The β subunit determines the ligand binding properties of synaptic glycine receptors. *Neuron* **45**, 727-739.
- Hales, T. G., Dunlop, J. I., Deeb, T. Z., Carland, J. E., Kelley, S. P., Lambert, J. J., & Peters, J. A. (2006). Common determinants of single channel conductance within the large cytoplasmic loop of 5-hydroxytryptamine type 3 and α4β2 nicotinic acetylcholine receptors. *J.Biol.Chem.* **281**, 8062-8071.
- Hamill, O. P., Marty, A., Neher, E., Sakmann, B., & Sigworth, F. J. (1981). Improved patch-clamp techniques for high-resolution current recording from cells and cell-free membrane patches. *Pflugers Arch.* **391**, 85-100.
- Hamill, O. P., Bormann, J., & Sakmann, B. (1983). Activation of multiple-conductance state chloride channels in spinal neurones by glycine and GABA. *Nature* **305**, 805-808.
- Han, N. L., Haddrill, J. L., & Lynch, J. W. (2001). Characterization of a glycine receptor domain that controls the binding and gating mechanisms of the beta-amino acid agonist, taurine. *J.Neurochem.* **79**, 636-647.
- Han, N. L., Clements, J. D., & Lynch, J. W. (2004). Comparison of taurine- and glycine-induced conformational changes in the M2-M3 domain of the glycine receptor. *J.Biol.Chem.* **279**, 19559-19565.
- Handford, C. A., Lynch, J. W., Baker, E., Webb, G. C., Ford, J. H., Sutherland, G. R., & Schofield, P. R. (1996). The human glycine receptor β subunit: primary structure, functional characterisation and chromosomal localisation of the human and murine genes. *Brain Res.Mol.Brain Res.* **35**, 211-219.
- Harvey, R. J., Thomas, P., James, C. H., Wilderspin, A., & Smart, T. G. (1999). Identification of an inhibitory Zn^{2+} binding site on the human glycine receptor α1 subunit. *J.Physiol* **520 Pt 1**, 53-64.
- Harvey, R. J., Schmieden, V., Von Holst, A., Laube, B., Rohrer, H., & Betz, H. (2000). Glycine receptors containing the α4 subunit in the embryonic sympathetic nervous system, spinal cord and male genital ridge. *Eur.J.Neurosci.* **12**, 994-1001.
- Harvey, R. J., Depner, U. B., Wässle, H., Ahmadi, S., Heindl, C., Reinold, H., Smart, T. G., Harvey, K., Schütz, B., Abo-Salem, O. M., Zimmer, A., Poisbeau, P., Welzl, H., Wolfer, D. P., Betz, H., Zeilhofer, H. U., & Müller, U. (2004). GlyR α3: an essential target for spinal PGE2-mediated inflammatory pain sensitization. *Science* **304** , 884-887.
- Hatton, C. J., Shelley, C., Brydson, M., Beeson, D., & Colquhoun, D. (2003). Properties of the human muscle nicotinic receptor, and of the slow-channel myasthenic syndrome mutant εL221F, inferred from maximum likelihood fits. *J.Physiol* **547**, 729-760.
- Hawkes, A. G., Jalali, A., & Colquhoun, D. (1992). Asymptotic distributions of apparent open times and shut times in a single channel record allowing for the omission of brief events. *Philos.Trans.R.Soc.Lond B Biol.Sci.* **337**, 383-404.
- Hawthorne, R. & Lynch, J. W. (2005). A picrotoxin-specific conformational change in the glycine receptor M2-M3 loop. *J.Biol.Chem.* **280**, 35836-35843.
- Hawthorne, R., Cromer, B. A., Ng, H. L., Parker, M. W., & Lynch, J. W. (2006). Molecular determinants of ginkgolide binding in the glycine receptor pore. *J.Neurochem.* **98**, 395-407.
- Hilf, R. J. & Dutzler, R. (2008). X-ray structure of a prokaryotic pentameric ligand-gated ion channel. *Nature* **452**, 375-379.
- Hoch, W., Betz, H., & Becker, C. M. (1989). Primary cultures of mouse spinal cord express the neonatal isoform of the inhibitory glycine receptor. *Neuron* **3**, 339-348.
- Horikoshi, T., Asanuma, A., Yanagisawa, K., Anzai, K., & Goto, S. (1988). Taurine and β-alanine act on both GABA and glycine receptors in *Xenopus* oocytes injected with mouse brain messenger RNA. *Brain Res.* **464**, 97-105.
- Imboden, M., de Saint Jan, D., Leulier, F., Korn, H., Goblet, C., & Bregestovski, P. (2001a). Isolation and characterization of an alpha 2-type zebrafish glycine receptor subunit. *Neuroscience* **103**, 799-810.

- Imboden, M., Devignot, V., & Goblet, C. (2001b). Phylogenetic relationships and chromosomal location of five distinct glycine receptor subunit genes in the teleost *Danio rerio*. *Dev.Genes Evol.* **211**, 415-422.
- Imboden, M., Devignot, V., Korn, H., & Goblet, C. (2001c). Regional distribution of glycine receptor messenger RNA in the central nervous system of zebrafish. *Neuroscience* **103**, 811-830.
- Imoto, K., Busch, C., Sakmann, B., Mishina, M., Konno, T., Nakai, J., Bujo, H., Mori, Y., Fukuda, K., & Numa, S. (1988). Rings of negatively charged amino acids determine the acetylcholine receptor channel conductance. *Nature* **335**, 645-648.
- Imoto, K., Konno, T., Nakai, J., Wang, F., Mishina, M., & Numa, S. (1991). A ring of uncharged polar amino acids as a component of channel constriction in the nicotinic acetylcholine receptor. *FEBS Lett.* **289**, 193-200.
- Imoto, K. (1993). Molecular aspects of ion permeation through channels. *Ann.N.Y.Acad.Sci.* **707**, 38-50.
- Jang, I. S., Jeong, H. J., Katsurabayashi, S., & Akaike, N. (2002). Functional roles of presynaptic $GABA_A$ receptors on glycinergic nerve terminals in the rat spinal cord. *J.Physiol* **541**, 423-434.
- Jensen, M. L., Timmermann, D. B., Johansen, T. H., Schousboe, A., Varming, T., & Ahring, P. K. (2002). The β subunit determines the ion selectivity of the $GABA_A$ receptor. *J.Biol.Chem.* **277**, 41438-41447.
- Jensen, M. L., Schousboe, A., & Ahring, P. K. (2005). Charge selectivity of the Cys-loop family of ligand-gated ion channels. *J.Neurochem.* **92**, 217-225.
- Jeong, H. J., Jang, I. S., Moorhouse, A. J., & Akaike, N. (2003). Activation of presynaptic glycine receptors facilitates glycine release from presynaptic terminals synapsing onto rat spinal sacral dorsal commissural nucleus neurons. *J.Physiol* **550**, 373-383.
- Jonas, P., Bischofberger, J., & Sandkühler, J. (1998). Co-release of two fast neurotransmitters at a central synapse. *Science* **281**, 419-424.
- Jones, M. V. & Westbrook, G. L. (1995). Desensitized states prolong $GABA_A$ channel responses to brief agonist pulses. *Neuron* **15**, 181-191.
- Jursky, F. & Nelson, N. (1995). Localization of glycine neurotransmitter transporter (GLYT2) reveals correlation with the distribution of glycine receptor. *J.Neurochem.* **64**, 1026-1033.
- Karlin, A. & Akabas, M. H. (1998). Substituted-cysteine accessibility method. *Methods Enzymol.* **293** , 123-145.
- Karlin, A. (2002). Emerging structure of the nicotinic acetylcholine receptors. *Nat.Rev.Neurosci.* **3**, 102-114.
- Kash, T. L., Jenkins, A., Kelley, J. C., Trudell, J. R., & Harrison, N. L. (2003). Coupling of agonist binding to channel gating in the $GABA_A$ receptor. *Nature* **421**, 272-275.
- Kash, T. L., Kim, T., Trudell, J. R., & Harrison, N. L. (2004). Evaluation of a proposed mechanism of ligand-gated ion channel activation in the $GABA_A$ and glycine receptors. *Neurosci.Lett.* **371**, 230-234.
- Katsurabayashi, S., Kubota, H., Moorhouse, A. J., & Akaike, N. (2004). Differential modulation of evoked and spontaneous glycine release from rat spinal cord glycinergic terminals by the cyclic AMP/protein kinase A transduction cascade. *J.Neurochem.* **91**, 657-666.
- Katz, B. & Miledi, R. (1965a). The effect of calcium on acetylcholine release from motor nerve terminals. *Proc.R.Soc.Lond B Biol.Sci.* **161**, 496-503.
- Katz, B. & Miledi, R. (1965b). Propagation of electric activity in motor nerve terminals. *Proc.R.Soc.Lond B Biol.Sci.* **161**, 453-482.
- Kelley, S. P., Dunlop, J. I., Kirkness, E. F., Lambert, J. J., & Peters, J. A. (2003). A cytoplasmic region determines single-channel conductance in $5\text{-}HT_3$ receptors. *Nature* **424**, 321-324.

- Keramidas, A., Moorhouse, A. J., French, C. R., Schofield, P. R., & Barry, P. H. (2000). M2 pore mutations convert the glycine receptor channel from being anion- to cation-selective. *Biophys.J.* **79**, 247-259.
- Keramidas, A., Moorhouse, A. J., Pierce, K. D., Schofield, P. R., & Barry, P. H. (2002). Cation-selective mutations in the M2 domain of the inhibitory glycine receptor channel reveal determinants of ion-charge selectivity. *J.Gen.Physiol* **119**, 393-410.
- Keramidas, A., Moorhouse, A. J., Schofield, P. R., & Barry, P. H. (2004). Ligand-gated ion channels: mechanisms underlying ion selectivity. *Prog.Biophys.Mol.Biol.* **86**, 161-204.
- Keramidas, A., Kash, T. L., & Harrison, N. L. (2006). The pre-M1 segment of the α1 subunit is a transduction element in the activation of the $GABA_A$ receptor. *J.Physiol* **575**, 11-22.
- Kingsmore, S. F., Giros, B., Suh, D., Bieniarz, M., Caron, M. G., & Seldin, M. F. (1994). Glycine receptor β-subunit gene mutation in spastic mouse associated with LINE-1 element insertion. *Nat.Genet.* **7**, 136-141.
- Kirsch, J., Langosch, D., Prior, P., Littauer, U. Z., Schmitt, B., & Betz, H. (1991). The 93-kDa glycine receptor-associated protein binds to tubulin. *J.Biol.Chem.* **266**, 22242-22245.
- Kirsch, J., Wolters, I., Triller, A., & Betz, H. (1993a). Gephyrin antisense oligonucleotides prevent glycine receptor clustering in spinal neurons. *Nature* **366**, 745-748.
- Kirsch, J., Malosio, M. L., Wolters, I., & Betz, H. (1993b). Distribution of gephyrin transcripts in the adult and developing rat brain. *Eur.J.Neurosci.* **5**, 1109-1117.
- Kirsch, J. & Betz, H. (1993). Widespread expression of gephyrin, a putative glycine receptor-tubulin linker protein, in rat brain. *Brain Res.* **621**, 301-310.
- Kirsch, J. & Betz, H. (1995). The postsynaptic localization of the glycine receptor-associated protein gephyrin is regulated by the cytoskeleton. *J.Neurosci.* **15**, 4148-4156.
- Kiyosawa, A., Katsurabayashi, S., Akaike, N., Pang, Z. P., & Akaike, N. (2001). Nicotine facilitates glycine release in the rat spinal dorsal horn. *J.Physiol* **536**, 101-110.
- Kling, C., Koch, M., Saul, B., & Becker, C. M. (1997). The frameshift mutation oscillator (Glra1(spd-ot)) produces a complete loss of glycine receptor alpha1-polypeptide in mouse central nervous system. *Neuroscience* **78**, 411-417.
- Kneussel, M. & Betz, H. (2000). Receptors, gephyrin and gephyrin-associated proteins: novel insights into the assembly of inhibitory postsynaptic membrane specializations. *J.Physiol* **525 Pt 1**, 1-9.
- Kneussel, M. & Loebrich, S. (2007). Trafficking and synaptic anchoring of ionotropic inhibitory neurotransmitter receptors. *Biol.Cell* **99**, 297-309.
- Konno, T., Busch, C., Von Kitzing, E., Imoto, K., Wang, F., Nakai, J., Mishina, M., Numa, S., & Sakmann, B. (1991). Rings of anionic amino acids as structural determinants of ion selectivity in the acetylcholine receptor channel. *Proc.Biol.Sci.* **244**, 69-79.
- Kontro, P. & Oja, S. S. (1987). Glycinergic systems in the brain stem of developing and adult mice: effects of taurine. *Int.J.Dev.Neurosci.* **5**, 461-470.
- Kuhse, J., Schmieden, V., & Betz, H. (1990a). A single amino acid exchange alters the pharmacology of neonatal rat glycine receptor subunit. *Neuron* **5**, 867-873.
- Kuhse, J., Schmieden, V., & Betz, H. (1990b). Identification and functional expression of a novel ligand binding subunit of the inhibitory glycine receptor. *J.Biol.Chem.* **265**, 22317-22320.
- Kuhse, J., Kuryatov, A., Maulet, Y., Malosio, M. L., Schmieden, V., & Betz, H. (1991). Alternative splicing generates two isoforms of the α2 subunit of the inhibitory glycine receptor. *FEBS Lett.* **283**, 73-77.
- Kuhse, J., Laube, B., Magalei, D., & Betz, H. (1993). Assembly of the inhibitory glycine receptor: identification of amino acid sequence motifs governing subunit stoichiometry. *Neuron* **11**, 1049-1056.
- Kwok, J. B., Raskin, S., Morgan, G., Antoniuk, S. A., Bruk, I., & Schofield, P. R. (2001). Mutations in the glycine receptor α1 subunit (*GLRA1*) gene in hereditary hyperekplexia pedigrees: evidence for non-penetrance of mutation Y279C. *J.Med.Genet.* **38**, E17.

- Labarca, C., Nowak, M. W., Zhang, H., Tang, L., Deshpande, P., & Lester, H. A. (1995). Channel gating governed symmetrically by conserved leucine residues in the M2 domain of nicotinic receptors. *Nature* **376**, 514-516.
- Langosch, D., Thomas, L., & Betz, H. (1988). Conserved quaternary structure of ligand-gated ion channels: the postsynaptic glycine receptor is a pentamer. *Proc.Natl.Acad.Sci.U.S.A* **85**, 7394-7398.
- Langosch, D., Becker, C. M., & Betz, H. (1990). The inhibitory glycine receptor: a ligand-gated chloride channel of the central nervous system. *Eur.J.Biochem.* **194**, 1-8.
- Langosch, D., Laube, B., Rundström, N., Schmieden, V., Bormann, J., & Betz, H. (1994). Decreased agonist affinity and chloride conductance of mutant glycine receptors associated with human hereditary hyperekplexia. *EMBO J.* **13**, 4223-4228.
- Lape, R., Colquhoun, D., & Sivilotti, L. G. (2008). On the nature of partial agonism in the nicotinic receptor superfamily. *Nature* **454**, 722-727.
- Laube, B., Kuhse, J., Rundström, N., Kirsch, J., Schmieden, V., & Betz, H. (1995). Modulation by zinc ions of native rat and recombinant human inhibitory glycine receptors. *J.Physiol* **483 (Pt 3)**, 613-619.
- Laube, B., Kuhse, J., & Betz, H. (2000). Kinetic and mutational analysis of Zn^{2+} modulation of recombinant human inhibitory glycine receptors. *J.Physiol* **522 Pt 2**, 215-230.
- Laube, B., Maksay, G., Schemm, R., & Betz, H. (2002). Modulation of glycine receptor function: a novel approach for therapeutic intervention at inhibitory synapses? *Trends Pharmacol.Sci.* **23**, 519-527.
- Le Novère , N. & Changeux, J. P. (1999). The Ligand Gated Ion Channel Database. *Nucleic Acids Res.* **27**, 340-342.
- Lee, W. Y. & Sine, S. M. (2005). Principal pathway coupling agonist binding to channel gating in nicotinic receptors. *Nature* **438**, 243-247.
- Legendre, P. & Korn, H. (1994). Glycinergic inhibitory synaptic currents and related receptor channels in the zebrafish brain. *Eur.J.Neurosci.* **6**, 1544-1557.
- Legendre, P. & Korn, H. (1995). Voltage dependence of conductance changes evoked by glycine release in the zebrafish brain. *J.Neurophysiol.* **73**, 2404-2412.
- Legendre, P. (1998). A reluctant gating mode of glycine receptor channels determines the time course of inhibitory miniature synaptic events in zebrafish hindbrain neurons. *J.Neurosci.* **18**, 2856-2870.
- Legendre, P. (2001). The glycinergic inhibitory synapse. *Cell Mol.Life Sci.* **58**, 760-793.
- Legendre, P., Muller, E., Badiu, C. I., Meier, J., Vannier, C., & Triller, A. (2002). Desensitization of homomeric α1 glycine receptor increases with receptor density. *Mol.Pharmacol.* **62**, 817-827.
- Lévi, S., Schweizer, C., Bannai, H., Pascual, O., Charrier, C., & Triller, A. (2008). Homeostatic regulation of synaptic GlyR numbers driven by lateral diffusion. *Neuron* **59**, 261-273.
- Lewis, C. A., Ahmed, Z., & Faber, D. S. (1991). A characterization of glycinergic receptors present in cultured rat medullary neurons. *J.Neurophysiol.* **66**, 1291-1303.
- Lewis, T. M., Harkness, P. C., Sivilotti, L. G., Colquhoun, D., & Millar, N. S. (1997). The ion channel properties of a rat recombinant neuronal nicotinic receptor are dependent on the host cell type. *J.Physiol* **505 (Pt 2)**, 299-306.
- Lewis, T. M., Sivilotti, L. G., Colquhoun, D., Gardiner, R. M., Schoepfer, R., & Rees, M. (1998). Properties of human glycine receptors containing the hyperekplexia mutation α1 (K276E), expressed in *Xenopus* oocytes. *J.Physiol* **507 (Pt 1)**, 25-40.
- Lewis, T. M., Schofield, P. R., & McClellan, A. M. (2003). Kinetic determinants of agonist action at the recombinant human glycine receptor. *J.Physiol* **549**, 361-374.
- Li, Y. F., Wu, L. J., Li, Y., Xu, L., & Xu, T. L. (2003). Mechanisms of H^+ modulation of glycinergic response in rat sacral dorsal commissural neurons. *J.Physiol* **552**, 73-87.

- Liu, Q. R., López-Corcuera, B., Nelson, H., Mandiyan, S., & Nelson, N. (1992). Cloning and expression of a cDNA encoding the transporter of taurine and β-alanine in mouse brain. *Proc.Natl.Acad.Sci.U.S.A* **89**, 12145-12149.
- Lu, T., Rubio, M. E., & Trussell, L. O. (2008). Glycinergic transmission shaped by the co-release of GABA in a mammalian auditory synapse. *Neuron* **57**, 524-535.
- Lummis, S. C. (2004). The transmembrane domain of the 5-HT_3 receptor: its role in selectivity and gating. *Biochem.Soc.Trans.* **32**, 535-539.
- Lummis, S. C., Beene, D. L., Lee, L. W., Lester, H. A., Broadhurst, R. W., & Dougherty, D. A. (2005). Cis-trans isomerization at a proline opens the pore of a neurotransmitter-gated ion channel. *Nature* **438**, 248-252.
- Lynch, J. W., Rajendra, S., Barry, P. H., & Schofield, P. R. (1995). Mutations affecting the glycine receptor agonist transduction mechanism convert the competitive antagonist, picrotoxin, into an allosteric potentiator. *J.Biol.Chem.* **270**, 13799-13806.
- Lynch, J. W., Rajendra, S., Pierce, K. D., Handford, C. A., Barry, P. H., & Schofield, P. R. (1997). Identification of intracellular and extracellular domains mediating signal transduction in the inhibitory glycine receptor chloride channel. *EMBO J.* **16**, 110-120.
- Lynch, J. W., Jacques, P., Pierce, K. D., & Schofield, P. R. (1998). Zinc potentiation of the glycine receptor chloride channel is mediated by allosteric pathways. *J.Neurochem.* **71**, 2159-2168.
- Lynch, J. W., Han, N. L., Haddrill, J., Pierce, K. D., & Schofield, P. R. (2001). The surface accessibility of the glycine receptor M2-M3 loop is increased in the channel open state. *J.Neurosci.* **21**, 2589-2599.
- Lynch, J. W. (2004). Molecular structure and function of the glycine receptor chloride channel. *Physiol Rev.* **84**, 1051-1095.
- Ma, D., Liu, Z., Li, L., Tang, P., & Xu, Y. (2005). Structure and dynamics of the second and third transmembrane domains of human glycine receptor. *Biochemistry* **44**, 8790-8800.
- Maksay, G., Laube, B., & Betz, H. (2001). Subunit-specific modulation of glycine receptors by neurosteroids. *Neuropharmacology* **41**, 369-376.
- Maksay, G., Nemes, P., & Bíro, T. (2004). Synthesis of tropeines and allosteric modulation of ionotropic glycine receptors. *J.Med.Chem.* **47**, 6384-6391.
- Malosio, M. L., Marquèze-Pouey, B., Kuhse, J., & Betz, H. (1991a). Widespread expression of glycine receptor subunit mRNAs in the adult and developing rat brain. *EMBO J.* **10**, 2401-2409.
- Malosio, M. L., Grenningloh, G., Kuhse, J., Schmieden, V., Schmitt, B., Prior, P., & Betz, H. (1991b). Alternative splicing generates two variants of the alpha 1 subunit of the inhibitory glycine receptor. *J.Biol.Chem.* **266**, 2048-2053.
- Mangin, J. M., Guyon, A., Eugène, D., Paupardin-Tritsch, D., & Legendre, P. (2002). Functional glycine receptor maturation in the absence of glycinergic input in dopaminergic neurones of the rat substantia nigra. *J.Physiol* **542**, 685-697.
- Mangin, J. M., Baloul, M., Prado de Carvalho, L., Rogister, B., Rigo, J. M., & Legendre, P. (2003). Kinetic properties of the α2 homo-oligomeric glycine receptor impairs a proper synaptic functioning. *J.Physiol* **553**, 369-386.
- Matzenbach, B., Maulet, Y., Sefton, L., Courtier, B., Avner, P., Guénet, J. L., & Betz, H. (1994). Structural analysis of mouse glycine receptor α subunit genes. Identification and chromosomal localization of a novel variant. *J.Biol.Chem.* **269**, 2607-2612.
- McDearmid, J. R., Liao, M., & Drapeau, P. (2006). Glycine receptors regulate interneuron differentiation during spinal network development. *Proc.Natl.Acad.Sci.U.S.A* **103**, 9679-9684.
- McIntire, S. L., Reimer, R. J., Schuske, K., Edwards, R. H., & Jorgensen, E. M. (1997). Identification and characterization of the vesicular GABA transporter. *Nature* **389**, 870-876.
- Meier, J., Meunier-Durmort, C., Forest, C., Triller, A., & Vannier, C. (2000). Formation of glycine receptor clusters and their accumulation at synapses. *J.Cell Sci.* **113 (Pt 15)** , 2783-2795.

- Meier, J., Vannier, C., Sergé, A., Triller, A., & Choquet, D. (2001). Fast and reversible trapping of surface glycine receptors by gephyrin. *Nat.Neurosci.* **4**, 253-260.
- Meier, J. C., Henneberger, C., Melnick, I., Racca, C., Harvey, R. J., Heinemann, U., Schmieden, V., & Grantyn, R. (2005). RNA editing produces glycine receptor α3 (P185L), resulting in high agonist potency. *Nat.Neurosci.* **8**, 736-744.
- Methfessel, C., Witzemann, V., Takahashi, T., Mishina, M., Numa, S., & Sakmann, B. (1986). Patch clamp measurements on *Xenopus laevis* oocytes: currents through endogenous channels and implanted acetylcholine receptor and sodium channels. *Pflugers Arch.* **407**, 577-588.
- Meyer, G., Kirsch, J., Betz, H., & Langosch, D. (1995). Identification of a gephyrin binding motif on the glycine receptor β subunit. *Neuron* **15**, 563-572.
- Mezler, M., Hornberger, W., Mueller, R., Schmidt, M., Amberg, W., Braje, W., Ochse, M., Schoemaker, H., & Behl, B. (2008). Inhibitors of GlyT1 affect glycine transport via discrete binding sites. *Mol.Pharmacol.* **74**, 1705-1715.
- Mihic, S. J., Ye, Q., Wick, M. J., Koltchine, V. V., Krasowski, M. D., Finn, S. E., Mascia, M. P., Valenzuela, C. F., Hanson, K. K., Greenblatt, E. P., Harris, R. A., & Harrison, N. L. (1997). Sites of alcohol and volatile anaesthetic action on $GABA_A$ and glycine receptors. *Nature* **389**, 385-389.
- Millar, N. S. & Harkness, P. C. (2008). Assembly and trafficking of nicotinic acetylcholine receptors. *Mol.Membr.Biol.* **25**, 279-292.
- Miller, C. (1989). Genetic manipulation of ion channels: a new approach to structure and mechanism. *Neuron* **2**, 1195-1205.
- Miller, P. S., Da Silva, H. M., & Smart, T. G. (2005a). Molecular basis for zinc potentiation at strychnine-sensitive glycine receptors. *J.Biol.Chem.* **280**, 37877-37884.
- Miller, P. S., Beato, M., Harvey, R. J., & Smart, T. G. (2005b). Molecular determinants of glycine receptor alphabeta subunit sensitivities to Zn^{2+}-mediated inhibition. *J.Physiol* **566**, 657-670.
- Miller, P. S., Topf, M., & Smart, T. G. (2008). Mapping a molecular link between allosteric inhibition and activation of the glycine receptor. *Nat.Struct.Mol.Biol.* **15**, 1084-1093.
- Mitchell, K. E., Iwamoto, T., Tomich, J., & Freeman, L. C. (2000). A synthetic peptide based on a glycine-gated chloride channel induces a novel chloride conductance in isolated epithelial cells. *Biochim.Biophys.Acta* **1466**, 47-60.
- Miyazawa, A., Fujiyoshi, Y., Stowell, M., & Unwin, N. (1999). Nicotinic acetylcholine receptor at 4.6 Å resolution: transverse tunnels in the channel wall. *J.Mol.Biol.* **288**, 765-786.
- Miyazawa, A., Fujiyoshi, Y., & Unwin, N. (2003). Structure and gating mechanism of the acetylcholine receptor pore. *Nature* **423**, 949-955.
- Mori, M., Gahwiler, B. H., & Gerber, U. (2002). β-alanine and taurine as endogenous agonists at glycine receptors in rat hippocampus in vitro. *J.Physiol* **539**, 191-200.
- Moroni, M., Zwart, R., Sher, E., Cassels, B. K., & Bermudez, I. (2006). α4β2 nicotinic receptors with high and low acetylcholine sensitivity: pharmacology, stoichiometry, and sensitivity to long-term exposure to nicotine. *Mol.Pharmacol.* **70**, 755-768.
- Mukhtarov, M., Ragozzino, D., & Bregestovski, P. (2005). Dual Ca^{2+} modulation of glycinergic synaptic currents in rodent hypoglossal motoneurones. *J.Physiol* **569**, 817-831.
- Mukhtasimova, N., Lee, W. Y., Wang, H. L., & Sine, S. M. (2009). Detection and trapping of intermediate states priming nicotinic receptor channel opening. *Nature* **459**, 451-454.
- Mülhardt, C., Fischer, M., Gass, P., Simon-Chazottes, D., Guénet, J. L., Kuhse, J., Betz, H., & Becker, C. M. (1994). The spastic mouse: aberrant splicing of glycine receptor β subunit mRNA caused by intronic insertion of L1 element. *Neuron* **13**, 1003-1015.
- Nevin, S. T., Cromer, B. A., Haddrill, J. L., Morton, C. J., Parker, M. W., & Lynch, J. W. (2003). Insights into the structural basis for zinc inhibition of the glycine receptor. *J.Biol.Chem.* **278**, 28985-28992.

- Nguyen, L., Malgrange, B., Belachew, S., Rogister, B., Rocher, V., Moonen, G., & Rigo, J. M. (2002). Functional glycine receptors are expressed by postnatal nestin-positive neural stem/progenitor cells. *Eur.J.Neurosci.* **15**, 1299-1305.
- Nicke, A., Rettinger, J., & Schmalzing, G. (2003). Monomeric and dimeric byproducts are the principal functional elements of higher order P2X1 concatamers. *Mol.Pharmacol.* **63**, 243-252.
- Nikolic, Z., Laube, B., Weber, R. G., Lichter, P., Kioschis, P., Poustka, A., Mülhardt, C., & Becker, C. M. (1998). The human glycine receptor subunit α3. *Glra3* gene structure, chromosomal localization, and functional characterization of alternative transcripts. *J.Biol.Chem.* **273**, 19708-19714.
- Ogden, D., & Stanfield, P., (1987). Chapter 4, Microelectrode Techniques – The Plymouth Workshop Handbook: Second Edition. The Company of Biologists Limited, Cambridge.
- Okamura, Y., Nishino, A., Murata, Y., Nakajo, K., Iwasaki, H., Ohtsuka, Y., Tanaka-Kunishima, M., Takahashi, N., Hara, Y., Yoshida, T., Nishida, M., Okado, H., Watari, H., Meinertzhagen, I. A., Satoh, N., Takahashi, K., Satou, Y., Okada, Y., & Mori, Y. (2005). Comprehensive analysis of the ascidian genome reveals novel insights into the molecular evolution of ion channel genes. *Physiol Genomics* **22**, 269-282.
- Ortells, M. O. & Lunt, G. G. (1995). Evolutionary history of the ligand-gated ion-channel superfamily of receptors. *Trends Neurosci.* **18**, 121-127.
- Ottersen, O. P., Storm-Mathisen, J., & Somogyi, P. (1988). Colocalization of glycine-like and GABA-like immunoreactivities in Golgi cell terminals in the rat cerebellum: a postembedding light and electron microscopic study. *Brain Res.* **450**, 342-353.
- Pan, Z. H. & Slaughter, M. M. (1995). Comparison of the actions of glycine and related amino acids on isolated third order neurons from the tiger salamander retina. *Neuroscience* **64**, 153-164.
- Peters, J. A., Kelley, S. P., Dunlop, J. I., Kirkness, E. F., Hales, T. G., & Lambert, J. J. (2004). The 5-hydroxytryptamine type 3 (5-HT_3) receptor reveals a novel determinant of single-channel conductance. *Biochem.Soc.Trans.* **32**, 547-552.
- Peters, J. A., Hales, T. G., & Lambert, J. J. (2005). Molecular determinants of single-channel conductance and ion selectivity in the Cys-loop family: insights from the 5-HT_3 receptor. *Trends Pharmacol.Sci.* **26**, 587-594.
- Peters, J. A., Carland, J. E., Cooper, M. A., Livesey, M. R., Deeb, T. Z., Hales, T. G., & Lambert, J. J. (2006). Novel structural determinants of single-channel conductance in nicotinic acetylcholine and 5-hydroxytryptamine type-3 receptors. *Biochem.Soc.Trans.* **34**, 882-886.
- Pfeiffer, F. & Betz, H. (1981). Solubilization of the glycine receptor from rat spinal cord. *Brain Res.* **226**, 273-279.
- Pfeiffer, F., Graham, D., & Betz, H. (1982). Purification by affinity chromatography of the glycine receptor of rat spinal cord. *J.Biol.Chem.* **257**, 9389-9393.
- Piechotta, K., Weth, F., Harvey, R. J., & Friauf, E. (2001). Localization of rat glycine receptor alpha1 and alpha2 subunit transcripts in the developing auditory brainstem. *J.Comp Neurol.* **438**, 336-352.
- Pitt, S. J., Sivilotti, L. G., & Beato, M. (2008). High intracellular chloride slows the decay of glycinergic currents. *J.Neurosci.* **28**, 11454-11467.
- Plazas, P. V., De Rosa, M. J., Gomez-Casati, M. E., Verbitsky, M., Weisstaub, N., Katz, E., Bouzat, C., & Elgoyhen, A. B. (2005a). Key roles of hydrophobic rings of TM2 in gating of the α9α10 nicotinic cholinergic receptor. *Br.J.Pharmacol.* **145**, 963-974.
- Plazas, P. V., Katz, E., Gomez-Casati, M. E., Bouzat, C., & Elgoyhen, A. B. (2005b). Stoichiometry of the α9α10 nicotinic cholinergic receptor. *J.Neurosci.* **25**, 10905-10912.
- Pless, S. A., Millen, K. S., Hanek, A. P., Lynch, J. W., Lester, H. A., Lummis, S. C., & Dougherty, D. A. (2008). A cation-π interaction in the binding site of the glycine receptor is mediated by a phenylalanine residue. *J.Neurosci.* **28**, 10937-10942.
- Plested, A. J., Groot-Kormelink, P. J., Colquhoun, D., & Sivilotti, L. G. (2007). Single-channel study of the spasmodic mutation α1A52S in recombinant rat glycine receptors. *J.Physiol* **581**, 51-73.

- Pribilla, I., Takagi, T., Langosch, D., Bormann, J., & Betz, H. (1992). The atypical M2 segment of the β subunit confers picrotoxinin resistance to inhibitory glycine receptor channels. *EMBO J.* **11**, 4305-4311.
- Prior, P., Schmitt, B., Grenningloh, G., Pribilla, I., Multhaup, G., Beyreuther, K., Maulet, Y., Werner, P., Langosch, D., Kirsch, J., & Betz, H. (1992). Primary structure and alternative splice variants of gephyrin, a putative glycine receptor-tubulin linker protein. *Neuron* **8**, 1161-1170.
- Purves, D., Augustine, G. J., Fitzpatrick, D., Hall, W. C., LaMantia, A-S., McNamara, J. O., & Williams, S. M. (2004). Neuroscience: Third Edition. Sinauer Associates, Inc.
- Racca, C., Gardiol, A., & Triller, A. (1997). Dendritic and postsynaptic localizations of glycine receptor alpha subunit mRNAs. *J.Neurosci.* **17**, 1691-1700.
- Racca, C., Gardiol, A., & Triller, A. (1998). Cell-specific dendritic localization of glycine receptor α subunit messenger RNAs. *Neuroscience* **84**, 997-1012.
- Ragozzino, D. & Eusebi, F. (1993). Inhibition of GABA and glycine responses by glutamate in rat hippocampal neurons. *Brain Res.* **628**, 115-120.
- Rajendra, S., Lynch, J. W., Pierce, K. D., French, C. R., Barry, P. H., & Schofield, P. R. (1994). Startle disease mutations reduce the agonist sensitivity of the human inhibitory glycine receptor. *J.Biol.Chem.* **269**, 18739-18742.
- Rajendra, S., Lynch, J. W., Pierce, K. D., French, C. R., Barry, P. H., & Schofield, P. R. (1995a). Mutation of an arginine residue in the human glycine receptor transforms β-alanine and taurine from agonists into competitive antagonists. *Neuron* **14**, 169-175.
- Rajendra, S., Vandenberg, R. J., Pierce, K. D., Cunningham, A. M., French, P. W., Barry, P. H., & Schofield, P. R. (1995b). The unique extracellular disulfide loop of the glycine receptor is a principal ligand binding element. *EMBO J.* **14**, 2987-2998.
- Rajendra, S., Lynch, J. W., & Schofield, P. R. (1997). The glycine receptor. *Pharmacol.Ther.* **73**, 121-146.
- Rayes, D., De Rosa, M. J., Sine, S. M., & Bouzat, C. (2009). Number and locations of agonist binding sites required to activate homomeric Cys-loop receptors. *J.Neurosci.* **29**, 6022-6032.
- Rees, M. I., Lewis, T. M., Kwok, J. B., Mortier, G. R., Govaert, P., Snell, R. G., Schofield, P. R., & Owen, M. J. (2002). Hyperekplexia associated with compound heterozygote mutations in the beta-subunit of the human inhibitory glycine receptor (GLRB). *Hum.Mol.Genet.* **11**, 853-860.
- Rees, M. I., Harvey, K., Ward, H., White, J. H., Evans, L., Duguid, I. C., Hsu, C. C., Coleman, S. L., Miller, J., Baer, K., Waldvogel, H. J., Gibbon, F., Smart, T. G., Owen, M. J., Harvey, R. J., & Snell, R. G. (2003). Isoform heterogeneity of the human gephyrin gene (*GPHN*), binding domains to the glycine receptor, and mutation analysis in hyperekplexia. *J.Biol.Chem.* **278**, 24688-24696.
- Reid, C. A., Bekkers, J. M., & Clements, J. D. (2003). Presynaptic Ca^{2+} channels: a functional patchwork. *Trends Neurosci.* **26**, 683-687.
- Ren, J. & Greer, J. J. (2006). Modulation of respiratory rhythmogenesis by chloride-mediated conductances during the perinatal period. *J.Neurosci.* **26**, 3721-3730.
- Revah, F., Bertrand, D., Galzi, J. L., Devillers-Thiéry, A., Mulle, C., Hussy, N., Bertrand, S., Ballivet, M., & Changeux, J. P. (1991). Mutations in the channel domain alter desensitization of a neuronal nicotinic receptor. *Nature* **353**, 846-849.
- Rosenberg, M., Meier, J., Triller, A., & Vannier, C. (2001). Dynamics of glycine receptor insertion in the neuronal plasma membrane. *J.Neurosci.* **21**, 5036-5044.
- Rundström, N., Schmieden, V., Betz, H., Bormann, J., & Langosch, D. (1994). Cyanotriphenylborate: subtype-specific blocker of glycine receptor chloride channels. *Proc.Natl.Acad.Sci.U.S.A* **91**, 8950-8954.
- Ryan, S. G., Buckwalter, M. S., Lynch, J. W., Handford, C. A., Segura, L., Shiang, R., Wasmuth, J. J., Camper, S. A., Schofield, P., & O'Connell, P. (1994). A missense mutation in the gene encoding the α1 subunit of the inhibitory glycine receptor in the spasmodic mouse. *Nat.Genet.* **7**, 131-135.

- Sagné, C., El Mestikawy, S., Isambert, M. F., Hamon, M., Henry, J. P., Giros, B., & Gasnier, B. (1997). Cloning of a functional vesicular GABA and glycine transporter by screening of genome databases. *FEBS Lett.* **417**, 177-183.
- Saransaari, P. & Oja, S. S. (2009). Mechanisms of glycine release in mouse brain stem slices. *Neurochem.Res.* **34**, 286-294.
- Sarto-Jackson, I. & Sieghart, W. (2008). Assembly of $GABA_A$ receptors. *Mol.Membr.Biol.* **25**, 302-310.
- Sato, K., Kiyama, H., & Tohyama, M. (1992). Regional distribution of cells expressing glycine receptor α2 subunit mRNA in the rat brain. *Brain Res.* **590**, 95-108.
- Saul, B., Schmieden, V., Kling, C., Mülhardt, C., Gass, P., Kuhse, J., & Becker, C. M. (1994). Point mutation of glycine receptor α1 subunit in the spasmodic mouse affects agonist responses. *FEBS Lett.* **350**, 71-76.
- Saul, B., Kuner, T., Sobetzko, D., Brune, W., Hanefeld, F., Meinck, H. M., & Becker, C. M. (1999). Novel *GLRA1* missense mutation (P250T) in dominant hyperekplexia defines an intracellular determinant of glycine receptor channel gating. *J.Neurosci.* **19**, 869-877.
- Schmieden, V., Grenningloh, G., Schofield, P. R., & Betz, H. (1989). Functional expression in *Xenopus* oocytes of the strychnine binding 48 kd subunit of the glycine receptor. *EMBO J.* **8**, 695-700.
- Schmieden, V., Kuhse, J., & Betz, H. (1992). Agonist pharmacology of neonatal and adult glycine receptor α subunits: identification of amino acid residues involved in taurine activation. *EMBO J.* **11**, 2025-2032.
- Schmieden, V., Kuhse, J., & Betz, H. (1993). Mutation of glycine receptor subunit creates β-alanine receptor responsive to GABA. *Science* **262**, 256-258.
- Schmitt, B., Knaus, P., Becker, C. M., & Betz, H. (1987). The Mr 93,000 polypeptide of the postsynaptic glycine receptor complex is a peripheral membrane protein. *Biochemistry* **26** , 805-811.
- Schneider, S. P. & Fyffe, R. E. (1992). Involvement of GABA and glycine in recurrent inhibition of spinal motoneurons. *J.Neurophysiol.* **68**, 397-406.
- Schofield, C. M., Jenkins, A., & Harrison, N. L. (2003). A highly conserved aspartic acid residue in the signature disulfide loop of the α1 subunit is a determinant of gating in the glycine receptor. *J.Biol.Chem.* **278**, 34079-34083.
- Schofield, C. M., Trudell, J. R., & Harrison, N. L. (2004). Alanine-scanning mutagenesis in the signature disulfide loop of the glycine receptor α1 subunit: critical residues for activation and modulation. *Biochemistry* **43**, 10058-10063.
- Schönrock, B. & Bormann, J. (1995). Modulation of hippocampal glycine receptor channels by protein kinase C. *Neuroreport* **6**, 301-304.
- Schumann, T., Grudzinska, J., Kuzmin, D., Betz, H., & Laube, B. (2009). Binding-site mutations in the α1 subunit of the inhibitory glycine receptor convert the inhibitory metal ion Cu^{2+} into a positive modulator. *Neuropharmacology* **56**, 310-317.
- Seitanidou, T., Triller, A., & Korn, H. (1988). Distribution of glycine receptors on the membrane of a central neuron: an immunoelectron microscopy study. *J.Neurosci.* **8**, 4319-4333.
- Shan, Q., Haddrill, J. L., & Lynch, J. W. (2001). A single β subunit M2 domain residue controls the picrotoxin sensitivity of αβ heteromeric glycine receptor chloride channels. *J.Neurochem.* **76**, 1109-1120.
- Shan, Q., Nevin, S. T., Haddrill, J. L., & Lynch, J. W. (2003). Asymmetric contribution of α and β subunits to the activation of αβ heteromeric glycine receptors. *J.Neurochem.* **86**, 498-507.
- Shiang, R., Ryan, S. G., Zhu, Y. Z., Hahn, A. F., O'Connell, P., & Wasmuth, J. J. (1993). Mutations in the α1 subunit of the inhibitory glycine receptor cause the dominant neurologic disorder, hyperekplexia. *Nat.Genet.* **5**, 351-358.

- Shoudai, K., Nonaka, K., Maeda, M., Wang, Z. M., Jeong, H. J., Higashi, H., Murayama, N., & Akaike, N. (2007). Effects of various K^+ channel blockers on spontaneous glycine release at rat spinal neurons. *Brain Res.* **1157**, 11-22.
- Sieghart, W., Fuchs, K., Tretter, V., Ebert, V., Jechlinger, M., Höger, H., & Adamiker, D. (1999). Structure and subunit composition of $GABA_A$ receptors. *Neurochem.Int.* **34**, 379-385.
- Sigel, E. & Minier, F. (2005). The *Xenopus* oocyte: system for the study of functional expression and modulation of proteins. *Mol.Nutr.Food Res.* **49**, 228-234.
- Sine, S. M. (2002). The nicotinic receptor ligand binding domain. *J.Neurobiol.* **53**, 431-446.
- Sine, S. M. & Engel, A. G. (2006). Recent advances in Cys-loop receptor structure and function. *Nature* **440**, 448-455.
- Singer, J. H., Talley, E. M., Bayliss, D. A., & Berger, A. J. (1998). Development of glycinergic synaptic transmission to rat brain stem motoneurons. *J.Neurophysiol.* **80**, 2608-2620.
- Singer, J. H. & Berger, A. J. (1999). Contribution of single-channel properties to the time course and amplitude variance of quantal glycine currents recorded in rat motoneurons. *J.Neurophysiol.* **81**, 1608-1616.
- Singer, J. H. & Berger, A. J. (2000). Development of inhibitory synaptic transmission to motoneurons. *Brain Res.Bull.* **53**, 553-560.
- Singer, J. H. (2008). GABA is an endogenous ligand for synaptic glycine receptors. *Neuron* **57**, 475-477.
- Sivilotti, L. & Colquhoun, D. (1995). Acetylcholine receptors: too many channels, too few functions. *Science* **269**, 1681-1682.
- Sixma, T. K. & Smit, A. B. (2003). Acetylcholine binding protein (AChBP): a secreted glial protein that provides a high-resolution model for the extracellular domain of pentameric ligand-gated ion channels. *Annu.Rev.Biophys.Biomol.Struct.* **32**, 311-334.
- Sixma, T. K. (2007). Nicotinic receptor structure emerging slowly. *Nat.Neurosci.* **10**, 937-938.
- Smart, T. G., Hosie, A. M., & Miller, P. S. (2004). Zn^{2+} ions: modulators of excitatory and inhibitory synaptic activity. *Neuroscientist.* **10**, 432-442.
- Smit, A. B., Syed, N. I., Schaap, D., van Minnen, J., Klumperman, J., Kits, K. S., Lodder, H., van der Schors, R. C., van Elk, R., Sorgedrager, B., Brejc, K., Sixma, T. K., & Geraerts, W. P. (2001). A glia-derived acetylcholine-binding protein that modulates synaptic transmission. *Nature* **411**, 261-268.
- Smith, K. E., Borden, L. A., Wang, C. H., Hartig, P. R., Branchek, T. A., & Weinshank, R. L. (1992). Cloning and expression of a high affinity taurine transporter from rat brain. *Mol.Pharmacol.* **42**, 563-569.
- Spier, A. D. & Lummis, S. C. (2000). The role of tryptophan residues in the 5-Hydroxytryptamine$_3$ receptor ligand binding domain. *J.Biol.Chem.* **275**, 5620-5625.
- Stein, V. & Nicoll, R. A. (2003). GABA generates excitement. *Neuron* **37**, 375-378.
- Steinbach, J. H. (2007). A slip 'twixt the cup and the lip': a new way to impair function of transmitter-gated channels. *J.Physiol* **581**, 3.
- Supplisson, S., & Roux, M. J. (2002). Why glycine transporters have different stoichiometries. *FEBS Lett.* **529**, 93-101.
- Suwa, H., Saint-Amant, L., Triller, A., Drapeau, P., & Legendre, P. (2001). High-affinity zinc potentiation of inhibitory postsynaptic glycinergic currents in the zebrafish hindbrain. *J.Neurophysiol.* **85**, 912-925.
- Takahashi, T. & Momiyama, A. (1991). Single-channel currents underlying glycinergic inhibitory postsynaptic responses in spinal neurons. *Neuron* **7**, 965-969.
- Takahashi, T., Momiyama, A., Hirai, K., Hishinuma, F., & Akagi, H. (1992). Functional correlation of fetal and adult forms of glycine receptors with developmental changes in inhibitory synaptic receptor channels. *Neuron* **9**, 1155-1161.

- Takeda, D., Nakatsuka, T., Papke, R., & Gu, J. G. (2003). Modulation of inhibitory synaptic activity by a non-α4β2, non-α7 subtype of nicotinic receptors in the substantia gelatinosa of adult rat spinal cord. *Pain* **101**, 13-23.
- Taleb, O. & Betz, H. (1994). Expression of the human glycine receptor α1 subunit in *Xenopus* oocytes: apparent affinities of agonists increase at high receptor density. *EMBO J.* **13**, 1318-1324.
- Tapia, J. C., Espinoza, F., & Aguayo, L. G. (1997). Differential intracellular regulation of cortical $GABA_A$ and spinal glycine receptors in cultured neurons. *Brain Res.* **769**, 203-210.
- Tapia, J. C., Mentis, G. Z., Navarrete, R., Nualart, F., Figueroa, E., Sanchez, A., & Aguayo, L. G. (2001). Early expression of glycine and $GABA_A$ receptors in developing spinal cord neurons. Effects on neurite outgrowth. *Neuroscience* **108**, 493-506.
- Todd, A. J. (1990). An electron microscope study of glycine-like immunoreactivity in laminae I-III of the spinal dorsal horn of the rat. *Neuroscience* **39**, 387-394.
- Todd, A. J., Watt, C., Spike, R. C., & Sieghart, W. (1996). Colocalization of GABA, glycine, and their receptors at synapses in the rat spinal cord. *J.Neurosci.* **16**, 974-982.
- Tokutomi, N., Kaneda, M., & Akaike, N. (1989). What confers specificity on glycine for its receptor site? *Br.J.Pharmacol.* **97**, 353-360.
- Triller, A., Cluzeaud, F., Pfeiffer, F., Betz, H., & Korn, H. (1985). Distribution of glycine receptors at central synapses: an immunoelectron microscopy study. *J.Cell Biol.* **101**, 683-688.
- Triller, A., Cluzeaud, F., & Korn, H. (1987). γ-Aminobutyric acid-containing terminals can be apposed to glycine receptors at central synapses. *J.Cell Biol.* **104**, 947-956.
- Triller, A., Sur, C., & Korn, H. (1993). Heterogeneous distribution of glycinergic and GABAergic afferents on an identified central neuron. *J.Comp Neurol.* **338**, 83-96.
- Triller, A., Rostaing, P., Korn, H., & Legendre, P. (1997). Morphofunctional evidence for mature synaptic contacts on the Mauthner cell of 52-hour-old zebrafish larvae. *Neuroscience* **80**, 133-145.
- Trombley, P. Q. & Shepherd, G. M. (1996). Differential modulation by zinc and copper of amino acid receptors from rat olfactory bulb neurons. *J.Neurophysiol.* **76**, 2536-2546.
- Turecek, R. & Trussell, L. O. (2001). Presynaptic glycine receptors enhance transmitter release at a mammalian central synapse. *Nature* **411**, 587-590.
- Turecek, R. & Trussell, L. O. (2002). Reciprocal developmental regulation of presynaptic ionotropic receptors. *Proc.Natl.Acad.Sci.U.S.A* **99**, 13884-13889.
- Twyman, R. E. & MacDonald, R. L. (1991). Kinetic properties of the glycine receptor main- and sub-conductance states of mouse spinal cord neurones in culture. *J.Physiol* **435**, 303-331.
- Ulens, C., Hogg, R. C., Celie, P. H., Bertrand, D., Tsetlin, V., Smit, A. B., & Sixma, T. K. (2006). Structural determinants of selective α-conotoxin binding to a nicotinic acetylcholine receptor homolog AChBP. *Proc.Natl.Acad.Sci.U.S.A* **103**, 3615-3620.
- Unwin, N. (1995). Acetylcholine receptor channel imaged in the open state. *Nature* **373**, 37-43.
- Unwin, N., Miyazawa, A., Li, J., & Fujiyoshi, Y. (2002). Activation of the nicotinic acetylcholine receptor involves a switch in conformation of the α subunits. *J.Mol.Biol.* **319**, 1165-1176.
- Unwin, N. (2005). Refined structure of the nicotinic acetylcholine receptor at 4Å resolution. *J.Mol.Biol.* **346**, 967-989.
- Vaello, M. L., Ruiz-Goméz, A., Lerma, J., & Mayor, F., Jr. (1994). Modulation of inhibitory glycine receptors by phosphorylation by protein kinase C and cAMP-dependent protein kinase. *J.Biol.Chem.* **269**, 2002-2008.
- Vafa, B., Lewis, T. M., Cunningham, A. M., Jacques, P., Lynch, J. W., & Schofield, P. R. (1999). Identification of a new ligand binding domain in the α1 subunit of the inhibitory glycine receptor. *J.Neurochem.* **73**, 2158-2166.
- van den Pol, A. N. & Gorcs, T. (1988). Glycine and glycine receptor immunoreactivity in brain and spinal cord. *J.Neurosci.* **8**, 472-492.

- Vandenberg, R. J., Handford, C. A., & Schofield, P. R. (1992a). Distinct agonist- and antagonist-binding sites on the glycine receptor. *Neuron* **9**, 491-496.
- Vandenberg, R. J., French, C. R., Barry, P. H., Shine, J., & Schofield, P. R. (1992b). Antagonism of ligand-gated ion channel receptors: two domains of the glycine receptor α subunit form the strychnine-binding site. *Proc.Natl.Acad.Sci.U.S.A* **89**, 1765-1769.
- Vandenberg, R. J., Rajendra, S., French, C. R., Barry, P. H., & Schofield, P. R. (1993). The extracellular disulfide loop motif of the inhibitory glycine receptor does not form the agonist binding site. *Mol.Pharmacol.* **44**, 198-203.
- Villarroel, A., Herlitze, S., Koenen, M., & Sakmann, B. (1991). Location of a threonine residue in the α-subunit M2 transmembrane segment that determines the ion flow through the acetylcholine receptor channel. *Proc.Biol.Sci.* **243**, 69-74.
- Wang, D. S., Xu, T. L., & Li, J. S. (1999). Modulation of glycine-activated chloride currents by substance P in rat sacral dorsal commissural neurons. *Sheng Li Xue.Bao.* **51**, 361-370.
- Wang, D. S., Zhu, H. L., Hong, Z., & Li, J. S. (2002). Cu^{2+} inhibition of glycine-activated currents in rat sacral dorsal commissural neurons. *Neurosci.Lett.* **328**, 117-120.
- Wang, D. S., Mangin, J. M., Moonen, G., Rigo, J. M., & Legendre, P. (2006). Mechanisms for picrotoxin block of α2 homomeric glycine receptors. *J.Biol.Chem.* **281**, 3841-3855.
- Wang, T. L., Hackam, A. S., Guggino, W. B., & Cutting, G. R. (1995). A single amino acid in γ-aminobutyric acid ρ1 receptors affects competitive and noncompetitive components of picrotoxin inhibition. *Proc.Natl.Acad.Sci.U.S.A* **92**, 11751-11755.
- Wang, Z. M., Katsurabayashi, S., Rhee, J. S., Brodwick, M., & Akaike, N. (2001). Substance P abolishes the facilitatory effect of ATP on spontaneous glycine release in neurons of the trigeminal nucleus pars caudalis. *J.Neurosci.* **21**, 2983-2991.
- Watanabe, E. & Akagi, H. (1995). Distribution patterns of mRNAs encoding glycine receptor channels in the developing rat spinal cord. *Neurosci.Res.* **23**, 377-382.
- Werman, R., Davidoff, R. A., & Aprison, M. H. (1967). Inhibition of motoneurones by iontophoresis of glycine. *Nature* **214**, 681-683.
- Wilkins, M. E., Hosie, A. M., & Smart, T. G. (2005). Proton modulation of recombinant $GABA_A$ receptors: influence of GABA concentration and the β subunit TM2-TM3 domain. *J.Physiol* **567**, 365-377.
- Wilson, G. G. & Karlin, A. (1998). The location of the gate in the acetylcholine receptor channel. *Neuron* **20**, 1269-1281.
- Wojcik, S. M., Katsurabayashi, S., Guillemin, I., Friauf, E., Rosenmund, C., Brose, N., & Rhee, J. S. (2006). A shared vesicular carrier allows synaptic co-release of GABA and glycine. *Neuron* **50**, 575-587.
- Wotring, V. E., Miller, T. S., & Weiss, D. S. (2003). Mutations at the GABA receptor selectivity filter: a possible role for effective charges. *J.Physiol* **548**, 527-540.
- Wu, F. S., Yang, Y. C., & Tsai, J. J. (2000). Noncompetitive inhibition of the glycine receptor-mediated current by melatonin in cultured neurons. *Brain Res.* **881**, 208-211.
- Wyllie, D. J., Béhé, P., & Colquhoun, D. (1998). Single-channel activations and concentration jumps: comparison of recombinant NR1a/NR2A and NR1a/NR2D NMDA receptors. *J.Physiol* **510 (Pt 1)**, 1-18.
- Xu, M., Covey, D. F., & Akabas, M. H. (1995). Interaction of picrotoxin with $GABA_A$ receptor channel-lining residues probed in cysteine mutants. *Biophys.J.* **69**, 1858-1867.
- Xu, M. & Akabas, M. H. (1996). Identification of channel-lining residues in the M2 membrane-spanning segment of the $GABA_A$ receptor α1 subunit. *J.Gen.Physiol* **107**, 195-205.
- Xu, T. L., Li, J. S., Jin, Y. H., & Akaike, N. (1999). Modulation of the glycine response by Ca^{2+}-permeable AMPA receptors in rat spinal neurones. *J.Physiol* **514 (Pt 3)**, 701-711.

- Xu, T. L., Dong, X. P., & Wang, D. S. (2000). N-methyl-D-aspartate enhancement of the glycine response in the rat sacral dorsal commissural neurons. *Eur.J.Neurosci.* **12**, 1647-1653.
- Xue, H. (1998). Identification of major phylogenetic branches of inhibitory ligand-gated channel receptors. *J.Mol.Evol.* **47**, 323-333.
- Yakel, J. L., Lagrutta, A., Adelman, J. P., & North, R. A. (1993). Single amino acid substitution affects desensitization of the 5-hydroxytryptamine type 3 receptor expressed in *Xenopus* oocytes. *Proc.Natl.Acad.Sci.U.S.A* **90**, 5030-5033.
- Yamashita, M., Ueno, T., Akaike, N., & Ikemoto, Y. (2001). Modulation of miniature inhibitory postsynaptic currents by isoflurane in rat dissociated neurons with glycinergic synaptic boutons. *Eur.J.Pharmacol.* **431**, 269-276.
- Yang, X. C. & Sachs, F. (1990). Characterization of stretch-activated ion channels in *Xenopu*s oocytes. *J.Physiol* **431**, 103-122.
- Yang, Z., Cromer, B. A., Harvey, R. J., Parker, M. W., & Lynch, J. W. (2007). A proposed structural basis for picrotoxinin and picrotin binding in the glycine receptor pore. *J.Neurochem.* **103**, 580-589.
- Ye, J. H. (2008). Regulation of excitation by glycine receptors. *Results Probl.Cell Differ.* **44**, 123-143.
- Yevenes, G. E., Peoples, R. W., Tapia, J. C., Parodi, J., Soto, X., Olate, J., & Aguayo, L. G. (2003). Modulation of glycine-activated ion channel function by G-protein βγ subunits. *Nat.Neurosci.* **6**, 819-824.
- Yevenes, G. E., Moraga-Cid, G., Guzmán, L., Haeger, S., Oliveira, L., Olate, J., Schmalzing, G., & Aguayo, L. G. (2006). Molecular determinants for G protein βγ modulation of ionotropic glycine receptors. *J.Biol.Chem.* **281**, 39300-39307.
- Young-Pearse, T. L., Ivic, L., Kriegstein, A. R., & Cepko, C. L. (2006). Characterization of mice with targeted deletion of glycine receptor α2. *Mol.Cell Biol.* **26**, 5728-5734.
- Young, A. B. & Snyder, S. H. (1973). Strychnine binding associated with glycine receptors of the central nervous system. *Proc.Natl.Acad.Sci.U.S.A* **70**, 2832-2836.
- Young, T. L. & Cepko, C. L. (2004). A role for ligand-gated ion channels in rod photoreceptor development. *Neuron* **41**, 867-879.
- Zafra, F., Gomeza, J., Olivares, L., Aragón, C., & Giménez, C. (1995a). Regional distribution and developmental variation of the glycine transporters GLYT1 and GLYT2 in the rat CNS. *Eur.J.Neurosci.* **7**, 1342-1352.
- Zafra, F., Aragón, C., Olivares, L., Danbolt, N. C., Giménez, C., & Storm-Mathisen, J. (1995b). Glycine transporters are differentially expressed among CNS cells. *J.Neurosci.* **15**, 3952-3969.
- Zarbin, M. A., Wamsley, J. K., & Kuhar, M. J. (1981). Glycine receptor: light microscopic autoradiographic localization with [^{3}H]strychnine. *J.Neurosci.* **1**, 532-547.
- Zhou, L., Chillag, K. L., & Nigro, M. A. (2002). Hyperekplexia: a treatable neurogenetic disease. *Brain Dev.* **24**, 669-674.
- Zita, M. M., Marchionni, I., Bottos, E., Righi, M., Del Sal, G., Cherubini, E., & Zacchi, P. (2007). Post-phosphorylation prolyl isomerisation of gephyrin represents a mechanism to modulate glycine receptors function. *EMBO J.* **26**, 1761-1771.

Acknowledgements

I would like to express my gratitude to Lucia Sivilotti for giving me the opportunity to work on this project and also for all the advice, criticism, help and knowledge that she has given me during these years of working with her. I would like to express my respect for her as a scientist, as an academic and as a woman.

I am grateful to Remi Lape, Marco Beato and Paul Groot-Kormelink for everything they have taught me, for sharing their exceptional skills with me and for all the advice and support the have given me. Also, I would like to thank Fe Abogadie and Steven Broadbent for making the lab a friendly place to work in.

Finally, my thanks to my family and to Massimiliano, for their love and sacrifices, their support and trust.